QUANTITATIVE RISK ASSESSMENT OF THERMAL HAZARDOUS REACTIONS WITH CASE STUDY

SAHEED ADEKUNLE BUSURA

QUANTITATIVE RISK ASSESSMENT OF THERMAL HAZARDOUS REACTIONS WITH CASE STUDY

BY

Saheed Adekunle BUSURA

A Thesis Submitted to the

School of Graduate Studies

In partial fulfillment of the requirements for the degree of

Master of Engineering

Faculty of Engineering and Applied Science

Memorial University of Newfoundland

August 2011

St. John's Newfoundland Canada

Abstract

Thermal hazards constitute menace to the exploration, processing and their allied industries. This work presents quantitative risk assessment of these thermal hazards via a simplified model, probability and severity determination with quantitative risk and proposed risk ranking for thermal runaway reactions using a case study of self-heating mineral ores.

A number of sulphide-containing mineral ores supplied by Vale Inco from Reid deposit were already investigated for self-heating thermal hazardous behaviour on the effect of mineralogy, particle size distribution and moisture contents using combined state-of-the-art instruments like Mineral Liberation Analysis, Thermal Gravimetric Analysis and Differential Scanning Calorimetry. The obtained results are then analyzed using AKTS software with the final data used for the risk assessment by first validating the developed kinetic model.

A continuous probability function, Gaussian probability distribution, is used to determine the associated chances of occurrence of the thermal hazards having fitted the representative data of thermal hazards into continuous distribution using Matlab. The probability of the hazards is determined under seven major classes of activation energy and Arrhenius' constant.

Similarly, severity of the defined thermal hazards is evaluated using the ratio of enthalpy of reaction of the ore under specific investigated effect to a referenced thermally hazardous material under four major categories of low, medium, high and extremely high risk classes using well-studies referenced materials. The associated risks are then determined as product of probability and consequences.

Finally, the numerical values of the associated risks are evaluated for consistency on a predefined scale with the risk ranked and coded by means of colour legend. The associated risk

with these mineral ores is found to be of medium class category and can be managed effectively. Recommendations are made for further work on the subject and approach for improvements.

Acknowledgements

I express my sincere gratitude to all my supervisors, Dr. AbdulJelil Iliyas, Dr. Faisal Khan and Dr. Kelly Hawboldt, for their immense efforts, assistance, support and uncompromising thorough drilling throughout the course of my M. Eng. Program without which the completion of this work would not have materialized.

Even at the face of keen struggle, few were still standing lending their unflinching supports. I hereby acknowledge men of courage and integrity ranging from Dr. Sayed Imtiaz and Dr. Shafiq Alam even to the associate friends and fellow colleagues for their supportive roles.

I thank my supervisors, Barrister S. A. Adenipekun (SAN) of Emmanuel Chambers, Pharmacist A. A. Adesina and the school of graduate studies, Memorial University of Newfoundland for their financial supports.

Kudos must be given to those who deserve it. I am highly indebted to my lecturers during both my undergraduate and postgraduate studies in Nigeria and Canada for their exemplary tutelage, modeling and all round development of the feeble soul. Worthy of mentioning is Dr. S. J. Akinbode who proofread this work.

I acknowledge my golden spectacles (my parents) for all they have put in to nurture this weaker vessel to fruition. May Almighty ALLAH in His infinite majesty reward you excellently.

Thesis Table of Contents

List of Figures

List of Tables

Nomenclature

A	Arrhenius' Constant
ASTM E698	American Society of Testing and Materials (Standard Test Method for Arrhenius kinetic constants for industrial Chemicals)
C or [ ]	Concentration of reactant or product species
C_f	Final Concentration of the chemical species
C_o	Initial Concentration of the chemical species
C_p	Specific heat capacity of chemical species
$C_p(T)$	Specific heat capacity of chemical species as function of Kelvin Temperature
c	Specific heat capacity of material
c_s	Specific heat capacity of a substance
c_c	Specific heat capacity of reacting vessel or reactor
D_e	Fick's Law diffusion constant or co-efficient
DeltaTad	Adiabatic temperature change for the reaction
DTBP	Di-tertiary butyl peroxide
dTad	Adiabatic temperature change for the reaction

$\frac{dT}{dt}$	Self-heat rate
$\frac{dT}{dt_{@\,Tonset}}$	Self-heat rate at the onset temperature of exothermic reaction
E	Power of 10
Ea	Activation energy of reaction
e	Exponentiation or Euler's Constant
$f(x)$	Kinetic function of reaction
$f(x)$	Probability mass function in term of variate
$f(z)$	Probability density function in term of standard or Z-score
H	Enthalpy of reaction
ΔH_R	Enthalpy change for reaction at any Kelvin temperature T
ΔH^o_R	Enthalpy change for reaction at standard condition
h	Planck's Constant
i	Counting index for 1,2,3,…or chemical species
j	Counting index for 1,2,3,…or chemical species
K_B	Boltzmann's Constant
k_{eff}	Effective specific rate constant of reaction
k_g	Specific rate constant with respect to diffusing gaseous reactant

k_s	Specific rate constant with respect to solid reactant through the ash formed.
MW(App)	Apparent molecular weight of the mineral ore.
m	Mass of the chemical species or vessel
m_s	Mass of the chemical substance
m_c	Mass of the reactor or vessel
$\dot{m}$	Mass flow rate
$\dot{m}_{in}$	Mass flow rate into the reactor
$\dot{m}_{out}$	Mass flow rate out of the reactor
N or N_i	Number of mole
n_o	Initial number of mole of feed or reactant
n_f	Final number of mole of product
P	Pressure
P_o	Initial Pressure of gas or vapour
Pr	Probability of an event occurring
p	Subscript referring to product
Q	Heat input or output from the reaction or reactor
Q_c or q_{ex}	Heat loss due to cooling

Q_{gen}	Heat energy generated due to chemical reaction
Q_{rxn} or q_{rx}	Heat of reaction
Q_{feed}	Sensible heat of feed
Q^{I}_{rxn}	Specific heat of reaction
R	Radius of spherical particle
R	Universal Gas Constant
r	Radius of gaseous plume or vapour or subscript referring to reactant
r_c	Spreading radius of solid reacting part or core
r_{crit}	Critical radius of gas or vapour plume
r_i	Rate of reaction of chemical species "i"
r_p	Rate of reaction of substance P with respect to concentration
r_{px}	Rate of reaction of substance P with respect to fractional conversion
SADT	Self Accelerating Decomposition Temperature
SH	Self-heating
SHR	Self-Heating Rate
T	Temperature
T_{am}	Ambient room temperature

T_c	Coolant temperature
T_i or T_o	Initial Temperature
T_{onset}	Onset temperature of exothermic reaction or self-heating
T_{ref}	Referenced initial room temperature
T(t)	Operational reaction temperature as a function of time
TMRad	Time to maximum rate under adiabatic condition
TNR	Temperature of no return for the reaction
TNT	Trinitrotoluene
t	Time
ΔT	Change in Temperature
ΔT_{ad}	Change in temperature under adiabatic condition with respect to fractional Conversion or accumulation
$\Delta T'_{ad}$	Change in temperature under adiabatic condition
Δt	Change in time
U	Overall heat transfer co-efficient for the reactor and reactants
V	Reactor or gas volume
υ	Volumetric flow rate for the reactant or product

$\dot{w}_s$	Work rate
x	Fractional conversion or variate whose probability is sought
Z	Gas z-factor
Z –Score	Standard score
z	Gas formation volume factor or standard score
α	Fractional conversion or progress of conversion
β	Consequence or severity value
ρ	Density of the ore
δ	Form factor
δ_{crit}	Critical form factor
ø	Phi-factor
σ	Standard deviation of the data distribution
τ	Residence time
μ	Mean of the data distribution
π	Product of probability numerical values or 3.142

Chapter 1

Introduction

Accidents do not just occur but are caused by acts of commission or omission on the part of operators or processing operations and equipment. In the Chemical processing industries, accidents are typically attributed to improper storage and handling of hazardous chemicals. Implementation of risk management strategies can decrease the occurrence and severity of these accidents. The process of risk analysis entails the following (Nolan, 1996):

- Hazard identification.
- What are the chances? (Probability assessment)
- Hazard quantification.
- Hazard prevention strategies implementation with emergency planning (Hazard mitigation).

1.1 Thermal Risk Assessment in Exploration, Manufacturing and Process Industries

Generally, risk assessment is a unique process of systematically qualifying or quantifying inherent hazards from processes, materials or substances and events involved in industries. The process industries are with huge inventories of stored chemicals, high temperature and pressure reactions and complex layout, control and instrumentation. Risk assessment of these industries is vital to their overall operations considering the huge investments involved and environmental issues.

Assessment of the associated risk with a recognized hazard involves determination of the precursors to the accident (Shah et al, 2003; Shah et al, 2005, Ozog & Bendizen, 1997). This is done by combination of the methods such as: hazard and operability study (HAZOP)

which identifies the hazards but not frequencies or chances of occurrence; hazard analysis (HAZAN) which estimates the frequencies of the occurrence and consequences to the employees, members of the public, industry and profits, and compares and contrasts the results of the associated frequencies and consequences with a target or criterion as to its acceptance or rejection of the hazards (Barton & Rogers, 1997). Hence, quantitative risk assessment (QRA) entails three major steps of hazard quantification, probability assessment and consequences assessment that are concurrently executed with risk estimation. HAZAN employs the use of fault tree analysis (FTA) (Hauptmans, 2004), event tree analysis (ETA), Markov modeling, etc. to obtain the probability assessment. Other methods employed include the use of probability functions (Srinivasan & Nhan, 2008). Risk is finally quantified as the product of the probability and consequences.

Various merits of QRA are the accurate cost-effective or cost-benefit engineering design, safe operations and maintenance, well informed process routes management and decision making for global excellent profit margin. The risk assessment process cuts across ecological, process and toxicological hazards identification, quantification and mitigation. In this work, the focus is to study risk assessment specific to exploration, process and manufacturing operations

1.2 Objectives of the Research

The main aims of this work include:

- To evaluate available methods and models for thermal hazards and risk assessment
- To develop and test a quantitative thermal risk model cum assessment methodology

Thermal hazards are very challenging to manage. Therefore, available technologies and models must be continuously modified to mitigate the new discoveries associated with these challenges. The available quantitative risk-based methods for thermal hazards are not only time consuming and laborious but also require specialized laboratories and equipment. The methods do not provide categorization of the chemicals nor do they characterize their hazardous activities.

In view of the above, a simple method of characterizing the chemicals and risk categorization will be developed to cater for these. This developed method will be used to quantify the thermal hazards alongside with the usual determinations of exothermicity and time of no return. Considering the amount of needed time to be invested in carrying out the experiments as well as the expensive costs and specialized laboratories with highly sensitive equipment to ascertain minute details, this simple method will give the same results at lesser cost and time with few experimental runs and data.

Quantum effect of scaling up from laboratory to industrial scale will be well accommodated within the developed methodology so that the portend hazards inherent in such operations can be diagnosed promptly. Also, the approach is aimed at incorporating the effect of interactions between multiple factors that are responsible for the thermal hazards within few experimental runs compactly so that comprehensive inference can be deduced.

The proposed approach can equally be used to identify and compare the chemical's thermal hazards, as well as estimating the magnitude of the hazards thereby providing various alternatives for mitigating them. It will equally serve as an oval window into ways of selecting and specifying safety measures. Such derived kinetic and risk- based models

should be able to confirm, corroborate and replicate experimental results obtained by the sophisticated instruments as well as yielding the same conclusions.

Runaway reaction of self-heating sulfide minerals will be used as case study for testing the new model to be developed.

1.3 Justification of the Work

It is imperative to assess the risks of runaway reactions due to the hazards associated with them such as explosion, loss of lives, industrial plants, environment and capital. Ranging from major industrial accidents in Germany OPPAU (1921), to a host of others, the material costs amount to the tune of millions of dollars e.g. $458m for La Medes (1992), France (Egidijus & Varmantas, 2008). The fatalities incurred in such accidents are very grave and irreparable as resources are lost in terms of quality personnel, experience and trainings. Therefore, proper identification and assessment of operating risks could decrease the frequency and severity of thermal accidents. It will also enhance superb handling and storage of these hazardous chemicals.

1.4 Thesis Layout

Layout analysis of this thesis has six major chapters. Chapter 1 reviews QRA from historical perspective to modern trends and some of the basic steps of thermal risk assessment in various industries. Also, the chapter outlines the objectives of this research work. A literature review of the state of knowledge on the subject is presented in chapter 2 with the background knowledge of thermal reaction hazards analysis. Chapter 3 is solely devoted to methodology with application of this methodology to a case study presented in chapter 4 portraying the self-heating phenomenon.

Every model and result is parametrically sensitive. Chapter 5 is concerned with this sensitivity analysis and discussion of the obtained results for the case studies. Conclusions and recommendations are in chapter 6. Organogram of the written epistle is diagrammatically represented in Figure 1.1.

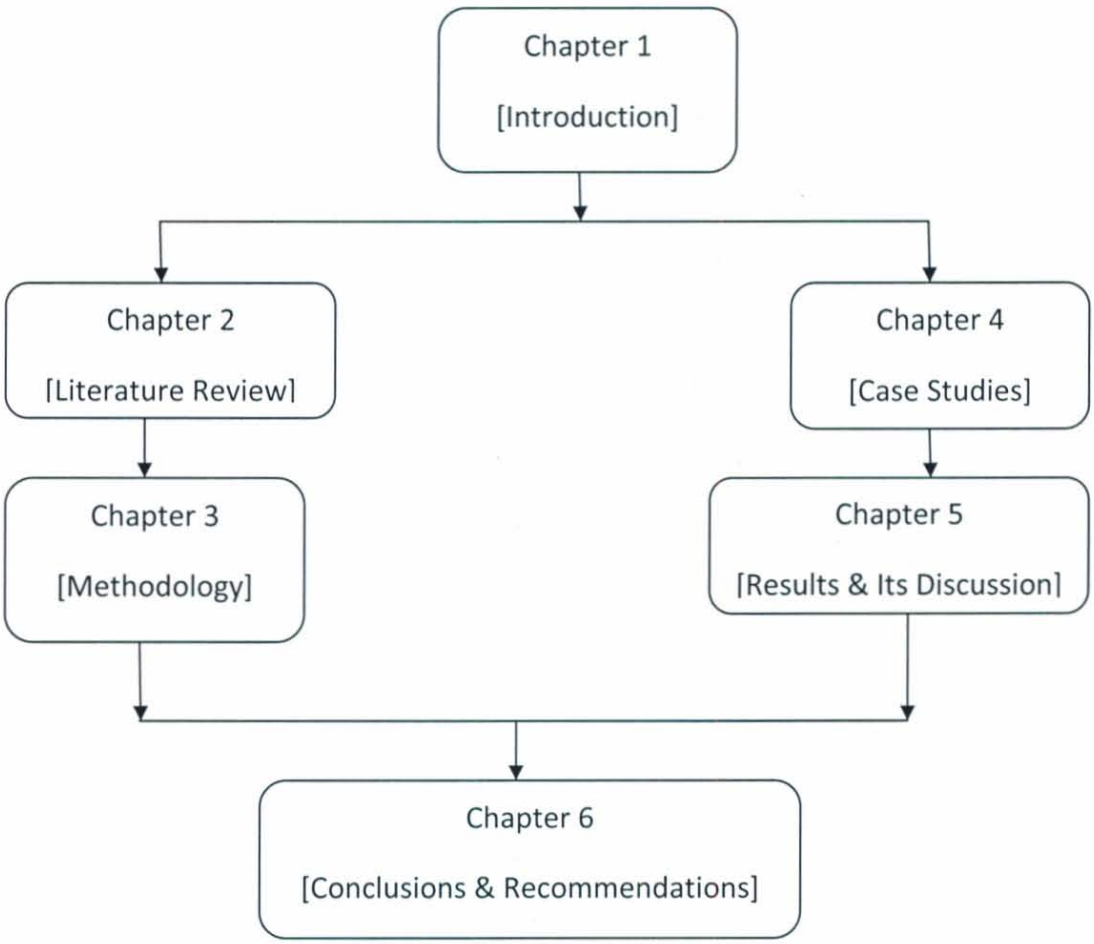

Figure 1.1: Organogram of the Thesis

Chapter 2

Literature Review

Risk is the potential loss (an undesirable outcome) that a chosen action or activity (including the choice of inaction) may lead to. The notion implies that the style one chooses to pursue an action has a great influence on the outcome of the action, and so the likely losses that may be encountered in the outcome can be referred to as "risks".

Alternatively, risk is the product of the impact of the severity (consequences) and impact of the likelihood (probability) of a hazardous event or phenomenon. The simplest definition was given in CMPT (1999) as "combination of likelihood and consequence of an accident". Kaplan and Garrick (1981) opined that risk is a set of phenomena- each with its own chance of occurrence and consequence. The most comprehensive one was presented by Covello and Merkhofer (1992) as: "Risk is, at minimum, a 2-D concept involving (1) the possibility of an adverse outcome, and (2) uncertainty over the occurrence, timing, or magnitude of that adverse outcome. If either of these attributes is absent, there is no risk constituted at all".

Risk can be assessed both quantitatively and qualitatively. The consequences and probability determination models for varieties of processes, events and scenarios are aptly and succinctly summarized in "Guidelines for Chemical Reactivity Evaluation & Application to Process Design, CCPS of AIChE, New York (1995)". Similarly, excellent work was done on numerous methodologies and techniques for risk assessment and safety management by various researchers since '70s (Khan & Abbassi, 1998; Shen and Wang, 2005; Venugopal & Kohn, 2005; Sears, 2006; Garrick et al, 2010; Markowski et al, 2010) which include "Design and evaluation of safety measures using newly proposed methodology "SCAP", 2002" and a

host of others. Equally, ample work has been done on the area of QRA for the thermal hazardous reactions and worthy of mention are the works of Ando, et al. (1991), Wang, et al. (2009) and Sanchirico, (2011).

Wang et al. (2009) did thermal risk assessment for reaction hazards by collecting data from previously published measurements of pressure DSC for 37 selected reactive hazards out of 820 spanning various functional groups undergoing decomposition reactions in conjunction with using Gaussian03 program to estimate those experimental values that were not available. Two basic criteria of onset temperature and TMRad were then established and justified for correlating onset temperatures with their corresponding activation energies and TMRad with onset temperature from the collected data *without recourse to the decrement in concentration during chemical reaction.* The obtained correlations having R^2 of 0.99 revealed the perfect concord among the chosen parameters and thus provided basis for drawing conclusion that reaction hazards with high activation energy during the decomposition reaction would have relatively high onset temperatures and TMRad. Finally, they used thermal risk index, a defined parameter connecting enthalpy of reaction and TMRad, to quantify the thermal hazard alongside with reaction hazard index.

Sanchiirico, (2011) delved into the minimum number of thermoanalytical experiments that should be deemed in arriving at complete and reliable kinetic analysis when using semi-empirical models. They drew inference by concluding that only two of such DSC experimental curves were sufficient to provide such complete analysis having made attempt at resolving the problem of gathering reliable thermokinetic information from non-isothermal techniques. They adopted Militky and Sestak approach of finding parametric vector used for the kinetic constant in the Arrhenius' type expression and lumped parameter $f(\alpha)$. This was

done via simulation of the analytically obtained model in conjunction with the DSC experimental runs discarding the redundant term as it was sufficient and adequate enough to model autocatalytic processes in Sestak-Berggren (SB) equation. This helped to solve problems associated with unknown detailed kinetic network characteristic of the thermally hazardous decomposition and oxidation reactions having several elementary reactions under a reasonable time scale. They submitted that the kinetic triplet of Arrhenius' constant, Activation energy and lumped parameter f(α) were crucial to the safety margin of such kinetic analysis having obtained global minimum function from the built models alongside with governing parametric vector. Complex thermally hazardous Cumene Hydroperoxide reaction was used as case study in DSC experiment with the numerical simulation done by Matlab. The problem of the kinetic triplet was addressed by using *"lsqnonlin subroutine"* in Matlab to solve the minimization problem either using the trust-region-reflective or Levenberg-Marquardt method for all the DSC data at different ramping rates for the objective function via reparametrized expression to reduce multicollinearity problem. Both experimental and simulated results were in absolute agreement which justified the use of semi-empirical model for the thermal hazardous risk assessment.

All the aforementioned approaches assert that the whole process plants or operations should have the following properties in view of safety required, (Pitblado, et al, 1990):

- It should be based on a thorough review of the role of safety management on the actual accident causation within the chemical process industries.
- The set questions must address all areas shown to be important in accident causation.
- It should confirm that the widely accepted principles of management "science" are suitably embedded in all key elements of the management system.

- The techniques should provide both a qualitative overview of site safety management and an indication of quantitative modification to generic failure frequencies.
- Although it is initially based on judgment, yet, it should be repeatable, checkable for quality assurance purposes and easily traceable to its effect on risk prediction.
- The resources required for the application should be commensurate with the needs of a subsidiary technique for application within Chemical Process Quantitative Risk Assessment (CPQRA).

All the above can be achieved for QRA of thermal hazards by integrating experimental and theoretical approaches to cater for risk reductions for any processing operations or industries.

Based on the existing state of knowledge on thermal hazardous reactions and materials, experiments are typically conducted on materials to ascertain their stability and reactivity (Ahonen, 1992; Asaki et al, 1984; Burelbach, 1999; Oba et al, 2002; Bach & Edward, 2003; Bowles et al, 2011; Baba & Adekola 2010, and Chirita et al, 2008). Instruments used for such experiments include the use of Advanced Reactive System Screening Tool (ARSST), Acceleration Reaction Calorimeter (ARC), Differential Scanning Calorimetry (DSC), Heat Flow Calorimetry, Thermo-Gravimetric Analysis (TGA) and Micro-reactors. The choice of these instruments and approaches depends on the sensitivity of each approach and equipment (Janzen et al 2000; Nandi et al, 2004; Ottaway 2004; Gunawan & Zhang, 2009; Jeong et al, 2010 and Carreto-Vasquez et al, 2010). Thermal hazards are also quantized by using numerical simulations and software (Roduit et al, 2008; Kuznetsov and Stizhak, 2009; Zhang et al, 2009 and Kumpinsky, 2008).

2.1 Background of Thermal Reaction Hazards Analysis

Thermal hazards analyses are classified into 3 major stages:

1. Initiation studies (process conceptualization) including characterization of process alternatives, choice and suitability of process and screening of chemical reaction hazards via experimental routes.
2. Pilot Plant studies where impact of plant selection on hazards are executed alongside with definition of safe procedures, effect of anticipated variations in process conditions and clear definition of critical limits (Kohlbrand, 1984).
3. Full Scale studies where chemical reaction hazards are re-evaluated and emphasis is placed on newly revealed reactivity hazards from plant operations, management of observed changes with updates of safety procedure based on process safety with engineering, production, economic and commercial aspects of the process.

Table 1 summarizes simple experimental testing procedures for thermal hazards as identified by the AIChE and Bretherick' s Handbook of Reactive Chemical Hazards (vol. 1&2, 2007) . Some of the parameters normally explored in the course of experiments are: onset temperature, real or apparent activation energy, Arrhenius' constant, adiabatic temperature rise, auto-ignition temperature, critical steady state temperature, self-accelerating decomposition temperature (SADT), time to maximum rate under adiabatic condition and adiabatic induction time of hazardous reaction for the exothermic reactions.

Usually data analysis is *simplified* on the basis of reaction rates, reaction stability and mass and energy balances. For the worst case scenario, the adiabatic condition is normally assumed to obtain a conservative safety margins. Analytical methods such as differential

method of Friedman, integral method of Flynn-Ozawa-Wall and the advanced integral methods of Vyazovkin are normally used for estimating many parameters from experimental results (Roduit et al, 2005; Roduit et al, 2008a, Roduit et al, 2008b, Roduit, et al, 2008c). The methods, among others, are based on isoconversional approaches. The isoconversional method is rooted in the assumption that reaction rate is solely a function of temperature which makes it possible for the dependence of activation energy on reaction progress, α, without detail explicit analysis of the kinetic parameters and order or molecularity of the reactions i.e. $f(\alpha)$ is a lumped parameter (Roduit et al, 2008).

Table 2.1: Thermal Hazards Chronological Testing Procedures

Subject	Property to Be Investigated	Typical Instrument Information
Identification of exothermic activity	Thermal Stability	DSC/DTA
Explosion of individual substances	Detonation	Chemical structure Tube test Card Gap Drop weight
	Deflagration	Oxygen balance High rate test Explosibility test
Compatibility	Reaction with common Contaminants (e.g. water)	Specialized tests
Normal Reaction	Reaction profile Effect of change Gas evolution	Bench-scale reactors (e.g. Reactor Calorimeter by Mettler-Toledo Inc.
Minimum exothermic runaway temperature	Establish minimum temperature	Adiabatic Dewar Adiabatic Calorimetry ARC
Consequence of runaway reaction	Temperature rise rates	Adiabatic Dewar Adiabatic Calorimetry Pressure ARC
	Gas evolution rates	VSP/ARSST or RSST Reactor Calorimeter pressure vessel

Source: Guidelines for Chemical Reactivity Evaluation and Application to Process Design CCPS AIChE

Any well defined system mimicking or modeling thermal hazardous reaction is generally of the simple form:

$$C_p \frac{dT}{dt} = Q_{in} - Q_{out} + Q_{rxn} \qquad \textbf{2.1}$$

Where: $C_p \frac{dT}{dt}$ = System's heat accumulation rate

Q_{in} = Heat rate associated with flow into the system

Q_{out} = Heat rate associated with flow out of the system

Q_{rxn} = Heating rate associated with reaction

Various terms incorporated into the heat balance expression are outlined below:

- *Heat rate of reaction:* heat from prevailing chemical reactions. It is a function of enthalpy and rate of reaction. It is denoted for substance "p" as:

$$Q_{rxn} = r_p V[-\Delta H_R] = kC_o^n(1-x)^n V[\Delta H_R]$$

Note: $k = k_{eff} = k(T) = k_o e^{-\frac{E}{RT}}$ *and for shrinking un-reacted core model, k is:* $\frac{1}{k_{eff}} = \frac{1}{k_s} + \frac{r_c}{R^2 k_g} + \frac{(R-r_c)r_c}{R\mathcal{D}_e}$

- *Heat removal term:* This deals with the cooling of the reaction system. For thermal safety purposes, overall heat transfer co-efficient is used thereby translating the expression for heat removal to the form:

$$Q_c = UA[T_c - T].$$

- *Sensible Heat of the feed:* The involved heat for the initial heating of the feed is called sensible heat. It is represented as: $Q_{feed} = C_{p,feed}\dot{m}_{feed}[T_{feed} - T]$.

- *Accumulation term:* It signifies and accounts for the variation of the system's energy content with temperature. It is normally depicted as:

$$Q_{acc} = \frac{d[m_i c_{p,i} T_i]}{dt} \text{ for all species "i" routed and equipment used.}$$

The enthalpy of reaction is calculated as:

$$-\Delta H_R = \Delta H_R^o + \int_{T_1}^{T_o} N_{i,r}\, C_{Pi,r}(T)dT + \int_{T_1}^{T_2} N_{i,p}\, C_{Pi,p}(T)dT = \Delta H_R^o + \int_{T_o}^{T_2} \Delta(N_i\, C_{Pi}(T))dT \qquad \textbf{2.2}$$

Where:

$-\Delta H_R$= Enthalpy of reaction at any temperature T, N_i=Number of mole of species "i",

$Cp_i(T)$ = Specific heat capacity of species "i" as a function of temperature T,

"r" and "p" are subscripts denoting reactants and products respectively.

The specific heat capacity,C_p, is a function of temperature and different correlations are used (Aylward & Findlay, 1971, Daubert & Danner, 1985 and Perry, 1999). Associated with the specific enthalpy of reaction is an important term called adiabatic temperature rise,$\Delta T'_{ad}$, and is used in measuring the thermal runaway behavior of reactants.

$$\Delta T'_{ad} = Q'_{rxn}/C_p = \frac{\Delta H_R C}{\rho C_p} \qquad \textbf{2.3}$$

It can also be expressed in terms of fractional conversion or accumulation of reactants as (Stoessel, 2008):

$$\Delta T_{ad} = x\Delta T'_{ad} = \frac{\Delta H_R x C}{\rho C_p} \qquad \textbf{2.4}$$

The above oversimplified expression for energy balance can be solved for any system on the basis of specific rate per kg, or globally with the inclusion of mass flow rate which is normally isolated later during derivations as "phi-factor,ø" given thus:

$$\emptyset = 1 + \frac{m_s c_s + m_c c_c}{m_c c_c} \quad \textbf{2.5}$$

Phi-factor is such an important parameter used to rectify many parameters like ΔT_{ad}, ΔH_R, TMR_{ad}, time of no return ($\boldsymbol{T_{NR}}$), self-heating time ($\boldsymbol{t_{\emptyset}}$), etc. obtained from experimental data:

$$\Delta H_R = \emptyset\, C_p\, \Delta T_{ad} \quad \textbf{2.6}$$

$$Power\ P_{ti} = \left[\frac{dT}{dt}\right]_{ti} C_p\, \emptyset \quad \textbf{2.7}$$

$$TMR_{ad}\ (corrected) = TMR_{ad} / \emptyset \quad \textbf{2.8}$$

$$T_{NR} = T_{onset} + \frac{RT^2}{E_a} \quad \textbf{2.9}$$

$$t_{\emptyset} = \int_{T_{\emptyset o}}^{T_{\emptyset f}} \left[\frac{1}{\left[\frac{dT}{dt}\right]_{\emptyset}}\right] dT \quad \textbf{2.10}$$

Chapter 3

Methodology

3.1 Model Development for Thermal Hazard Assessment

Runaway reactions are thermal hazards where "normal" temperature trend associated with a given reaction is exceeded. Generally, all chemical reactions are modeled from their kinetics and transport phenomena associated with the reactor and reaction (Lengke & Tempel, 2001; Lengke & Tempel, 2005 and Asay, 2010). The reactors in which such reactions occur play significant roles in the models. Many reaction mechanisms are complex and made up of parallel to multiple reactions. Derivation of these mechanisms is challenging due to limits in ability to analyze, detect species in experiments i.e. reaction pathways. In this work, a simplified methodology to determine thermal hazards associated with these reactions as verified by simulation and experiments are done. The model is based on the worst case scenario which is based on the use of adiabatic reactor. Consider an arbitrary runaway reaction

$$\boldsymbol{P} + \boldsymbol{Q} \rightarrow \boldsymbol{R} + \boldsymbol{S}$$

Initial [ ]	C_o	-	-
Change in [ ]	$-xC_o$	$+xC_o$	$+xC_o$
Final [ ]	C_f	$+xC_o$	$+xC_o$

For such a typical runaway reaction in which the most important reactant is "P", the final concentration C_f at any time t, can be expressed as:

$$C_f = C_o - xC_o = C_o[1-x] \qquad \textbf{3.1a}$$

Fractional conversion is written as $\frac{C_o - C_f}{C_o} = x$. If the rate of reaction of the reaction can be expressed with respect to the most important reactant **P** as in [3.1b] and in terms of conversion, this gives [3.1c]:

$$r_p = r = kC_f^n = k[C_o(1-x)]^n = kC_o^n(1-x)^n = \frac{-dC_f}{dt} = \frac{C_o dx}{dt} \qquad \textbf{3.1b}$$

$$r_{px} = \frac{dx}{dt} = kC_o^{n-1}(1-x)^n \qquad \textbf{3.1c}$$

But for simplicity, the specific rate constant "k" which is the effective reaction rate constant is temperature dependent as mentioned earlier (i.e. $k = k(T) = Ae^{-E_a/RT}$). Therefore, the kinetic model of the reaction which is based on the Arrhenius' equation can be written as:

$$r_{px} = Ae^{(-E_a/RT)}\{C_o^{n-1}(1-x)^n\} = Ae^{-E_a/RT}\{f(x)\} \qquad \textbf{3.2a}$$

$$r_p = Ae^{(-E_a/RT)}C_o^1\{C_o^{n-1}(1-x)^n\} = Ae^{(-E_a/RT)}C_o^1\{f(x)\} \qquad \textbf{3.2b}$$

Where: $f(x) = C_o^{n-1}(1-x)^n$ and $r_{px} = \frac{dx}{dt}$.

The term "$\boldsymbol{f(x)}$" is unknown prior to experimental determination. Once the involved parameters in this equation are known, the model can be executed. The rate of reaction for the various types of reactions that can lead to runaway reaction can be modeled depending on the type of reactions.

Energy Balance for the Thermal Reaction

The enthalpy balance for a reactor for the above reaction is (Figure 3.1a):

{Accumulation heat rate} = {rate of enthalpy in} - {rate of enthalpy out} + {Reaction heat generation rate}- {Cooling rate} + {Shaft work rate} + {work rate}.

Mathematically, this can be written as:

$$\frac{d[mC_p(T)T]}{dt} = \int_{T_{ref}}^{T_1} \dot{m}_{in} C_{p,in}(T)dT - \int_{T_1}^{T_2} \dot{m}_{out} C_{p,out}(T)dT + r_p(-\Delta H_R)V - UA_c(T_2 - T_c) + \dot{W}_s \quad \textbf{3.3}$$

Equation [3.3] can be solved for our worst case scenario with the following conditions or assumptions:

- The reactor is adiabatic (no exchange of heat with the surrounding).
- No work is exchanged with the surroundings.

This becomes;

$$\frac{d[mC_p(T)T]}{dt} = \int_{T_{ref}}^{T_1} \dot{m}_{in} C_{p,in}(T)dT - \int_{T_1}^{T_2} \dot{m}_{out} C_{p,out}(T)dT + r_p(-\Delta H_R)V \quad \textbf{3.4}$$

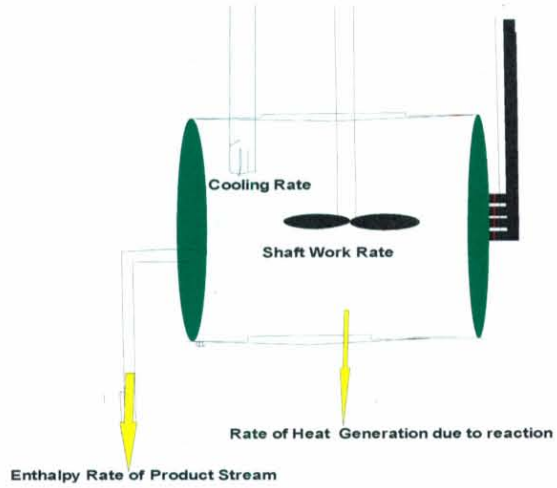

Figure 3.1a: Gross Overview of Energy Balance for the Model

In terms of reactor and feed variables, the expression becomes:

$$\frac{d[\rho V C_p(T)T]}{dt} = \int_{T_{ref}}^{T_1} \rho\nu C_{p,in}(T)dT - \int_{T_1}^{T_2} \rho\nu C_{p,out}(T)dT + r_p(-\Delta H_R)V \quad \textbf{3.5}$$

$$\frac{Vd[\rho C_p(T)T]}{dt} = \int_{T_{ref}}^{T_1} \rho\nu C_{p,in}(T)dT - \int_{T_1}^{T_2} \rho\nu C_{p,out}(T)dT + r_p(-\Delta H_R)V \quad \textbf{3.6}$$

Where: V = Reactor volume (m^3), C_p = Specific Heat capacity (J/kg K)

ρ= Density of feed (kg/m^3), ν= volumetric feed flow rate (m^3/s).

If the fluid or feed is incompressible and of constant flow rate, the expression becomes:

$$\frac{V\rho d[C_p(T)T]}{dt} = \rho\nu \int_{T_{ref}}^{T_1} C_{p,in}(T)dT - \rho\nu \int_{T_1}^{T_2} C_{p,out}(T)dT + r_p(-\Delta H_R)V \quad \textbf{3.7}$$

If the specific heat capacity $\boldsymbol{C_p(T)}$, is constant over the range of operating temperature, the expression reduces to:

$$V\rho C_p \frac{dT}{dt} = \rho\nu C_{p,in} \int_{T_{ref}}^{T_1} dT - \rho\nu C_{p,out} \int_{T_1}^{T_2} dT + r_p(-\Delta H_R)V \quad \textbf{3.8}$$

For the referenced reactant or product, this becomes;

$$V\rho C_p \frac{dT}{dt} = \rho\nu C_{p,in} \int_{T_{ref}}^{T_1} dT - \rho\nu C_{p,out} \int_{T_1}^{T_2} dT + r_p(-\Delta H_R)V \quad \textbf{3.9}$$

$$V\rho C_p \frac{dT}{dt} = \rho\nu C_p \int_{T_{ref}}^{T_2} dT + r_p(-\Delta H_R)V \quad \textbf{3.10}$$

$$V\rho C_p \frac{dT}{dt} = \rho\nu C_p[T - T_{ref}] + r_p(-\Delta H_R)V \quad \textbf{3.11}$$

Defining residence time as: τ =V/ν = $\frac{xC_o}{r_P}$ and dividing through [3.11] by "ρνC_p" yields;

$$\tau\frac{dT}{dt} = \mathrm{T} - T_{ref} + r_p\tau[(-\Delta H_R)/\rho C_p] \quad \textbf{3.12}$$

$$\frac{dT}{dt} = \frac{1}{\tau}[\mathrm{T} - T_{ref}] + r_p[(-\Delta H_R)/\rho C_p] \quad \textbf{3.13}$$

In term of semi-empirical model where experiments are performed, this becomes:

$$\frac{dT}{dt} = \frac{1}{\tau}[\mathrm{T} - T_{ref}] + \frac{r_p}{xC_o}[(-\Delta H_R x C_o)/\rho C_p] \quad \textbf{3.14}$$

Where:$\Delta T_{ad} = [(-\Delta H_R)C_o x/\rho C_p]$ & $r_p = \frac{xC_o}{\tau}$ from compositional balance in term of space time

$$\frac{dT}{dt} = \frac{1}{\tau}[T - T_{ref}] + [(\Delta T_{ad})/\tau] \quad \textbf{3.15}$$

$$\frac{dT}{dt} = \frac{1}{\tau}[(T - T_{ref}) + (\Delta T_{ad})] \quad \textbf{3.16}$$

Integrating the last expression above gives:

$$\int_{T_{ref}}^{T} \frac{dT}{T - T_{ref} + \Delta T_{ad}} = \int_0^t \frac{dt}{\tau} \quad \textbf{3.17}$$

$$ln[(T - T_{ref}) + (\Delta T_{ad})]_{T_{ref}}^{T} = \frac{1}{\tau}[t]_0^t \quad \textbf{3.18}$$

$$ln\left[\frac{(T - T_{ref}) + (\Delta T_{ad})}{\Delta T_{ad}}\right] = \frac{t}{\tau} \quad \textbf{3.19}$$

$$T = T_{ref} + \Delta T_{ad}(e^{\frac{t}{\tau}} - 1) \quad \textbf{3.20}$$

$$T = T_{ref} - \Delta T_{ad}[1 - e^{\frac{t}{\tau}}] \quad \textbf{3.21}$$

Note: $\Delta T_{ad} = T - T_{onset}$ with $T > T_{onset}$ for the thermal hazardous reaction which is only available from experiments after exotherm from instruments such as: ARC, ARSST, DSC,

HFC and TGA (McInttosh and Waldram, 2003). Equations [3.2a] & [3.13] are the required equations to be solved numerically for specified initial and boundary conditions to obtain the relationship between temperature, T(t) and time, t, with other parameters. If experiment data is available, only equation [3.16] can be used. For compressible systems, density is not constant. Hence, an EOS or other equations for compressible fluids is used in equation [3.6] before evaluating the function $\frac{dT}{dt}$ alongside with equation [3.2a].

Certain care must be exercised when coupling equations for numerical simulation for thermal runaway reaction of any kind (Fogler, 2006; Levenspiel, 1999 and Schmidt, 2005)

- Work rate is not negligible for compressible fluids that are sensitive to pressure change. Modified ideal gas and Clausius-Clapeyron equation relating pressure and temperature with heat of vapourization may be used in estimating corresponding gas and vapour pressure respectively, i.e.

  $P = \frac{zNRT}{V}$ & $ln\left[\frac{P}{P_o}\right] = \frac{-\Delta H_v}{R}\left[\frac{T_o - T}{TT_o}\right]$ *respectively*

  This is used for the shrinking un-reacted core or ash-layer control model as well as for compressible fluids.

- For n-multiple **known** reactions occurring together simultaneously, there is a change in heat generation term which is incorporated as follows:

$$\dot{Q}_g = Q_{rxn} = \tau \sum_{i=1}^{n} [\frac{-\Delta H_{Ri} C_{oi}}{\rho C_{pi}}][r_i(x_i, T)], \qquad Where: i = 1,2,3, \dots, n$$

3.1.1 Experimental Work

Ore samples were already investigated using DSC and ARSST for their thermal hazards by running repeated experiments under various conditions as discussed below:

Differential Scanning Calorimetric (DSC) Tests

DSC screening tests were carried out on the ore samples with onset temperatures and heat rates determined which were used to determine kinetic parameters using the advanced thermokinetic (AKTS) software. The DSC instrument has the ability to operate in both negative and positive temperature regimes depending on the experimental set-up and procedure.

For each investigated effect, 5-10mg ore sample was weighed out by Toledo Mettler Balance and loaded into the hermetic aluminum or high pressure gold pan-lid sealed assembly. A corresponding empty reference pan of the same material was weighed and simultaneously loaded having previously calibrated the instrument with indium and zinc prior to the commencement of the experiment to internally standardize it.

The experimental method was prepared on the DSC instrument under its own section and saved which could easily be loaded at the commencement of each experimental run. Various ramp rates were used from 0.5-8.0K/min and operating temperature 20 to 450°C in air (oxygen) environment. Air was admitted into the DSC at flow rate of 10ml/min as purge gas during each experimental run at constant pressure. Exothermic peaks were observed alongside with heat rate (Appendix D).

The raw experimental results are as shown in Appendix C for some of the ores. These were obtained from the DSC software. Further treatment of the results was done by importing the data to the AKTS software where various kinetic data was determined and further safety parameters could be predicted. Figure 3.1b shows the DSC experimental set-up. Mineralogy effect was investigated for the ores by masking the effect of moisture content and particle sizes holding them constant at 3% and 75μm respectively. Similarly, selected ore 05-

658(257m) was investigated for particle size effect by ramping each of the sorted distribution of <75μm, 75μm-180μm, >180μm and mixed particle sizes in the ratio 1:3 each at 0.5, 1, 2 and 4K/min rate in the DSC. This is to observe both the "within" and "across" the samples effect at constant 3% moisture content in high pressure gold pans. The effect of moisture content was investigated at the atmospheric baseline of 3% initially and later improved upon by saturating the ore 03-601(207m) at 8, 15 and 25%.

Figure 3.1b: Experimental Set-up for Ore's Thermal Hazards Investigation

Advanced Reactive System Screening Tool (ARSST)

The ARSST, another versatile instrument, was used in investigating thermal behaviour of ores and operated under pseudo-adiabatic condition. This was used to further ascertain the previous results obtained by the DSC screening experiments. 13g sample of each ore was loaded into the 10ml test cell containing magnetic stirring rod and immersed into the calorimeter. The oxygen and nitrogen purge gases were used for the experiments. The typical

set-up is shown in Figure 3.1c. Ores were ramped at ramping rate of 2°C/min from near room temperature to 500°C. The pressure range was 0-60psig depending on the experiments and test cell used. The process of data collection during experimental procedure was started by launching the ARSST 4.1 software. The circuitry was completed by turning on the ARSST control panel, the magnetic stirrer, the heaters on feeding in the experimental data on the Graphical Unit interface (GUI) and having checked the pressure regulator with admittance of the purge gas either oxygen(air) or nitrogen. Finally, the experiment was commenced by clicking on the start button on the GUI after pre-setting the automatic termination conditions for the experiment.

The acquisition stage commenced once the exotherm was detected with the heating rate greater than the preset ramp rate by 0.1°C/min. The final temperature was 500°C, which is the maximum temperature of the instrument. At the end of each experimental run, the reduce software of the ARSST was launched as shown in Figure 3.1d and the XYPlot2 was used to reduce the data in the corresponding experimental run's file. Typical results obtained are shown in Figure 3.1e. It was ascertained that at low phi-factor, the results were closer to adiabatic condition although it failed to separate peaks and at high phi-factor, instrument sensitivity problems at onset.

HG-1 indicates that SH is both complex and autocatalytic which qualitatively is in agreement with DSC data. The obtained results were found to be in agreement with those obtained by the DSC shown on the last page of Appendix D.

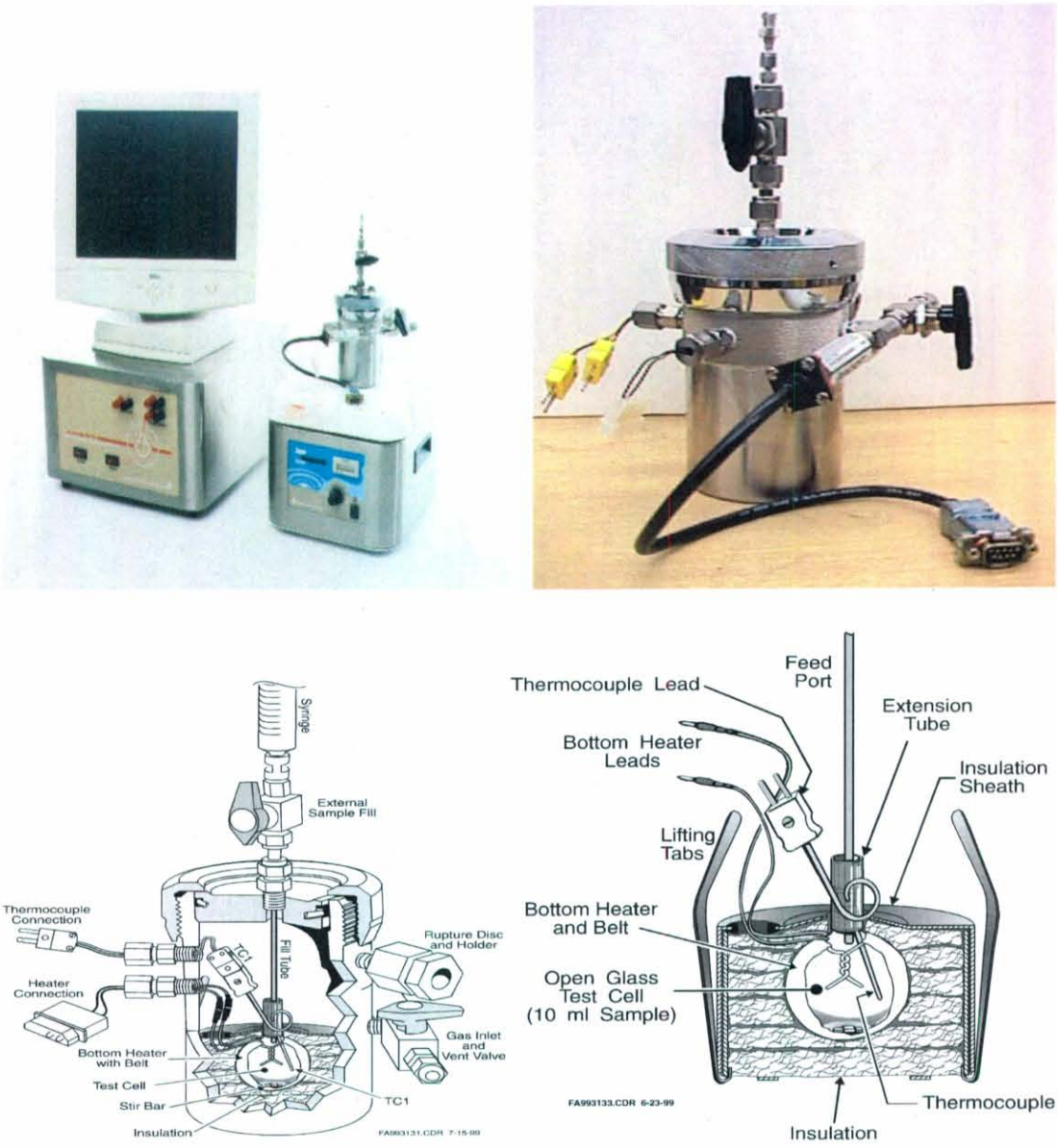

Fig 3.1c: Typical ARSST Experimental Set-up for the Ores

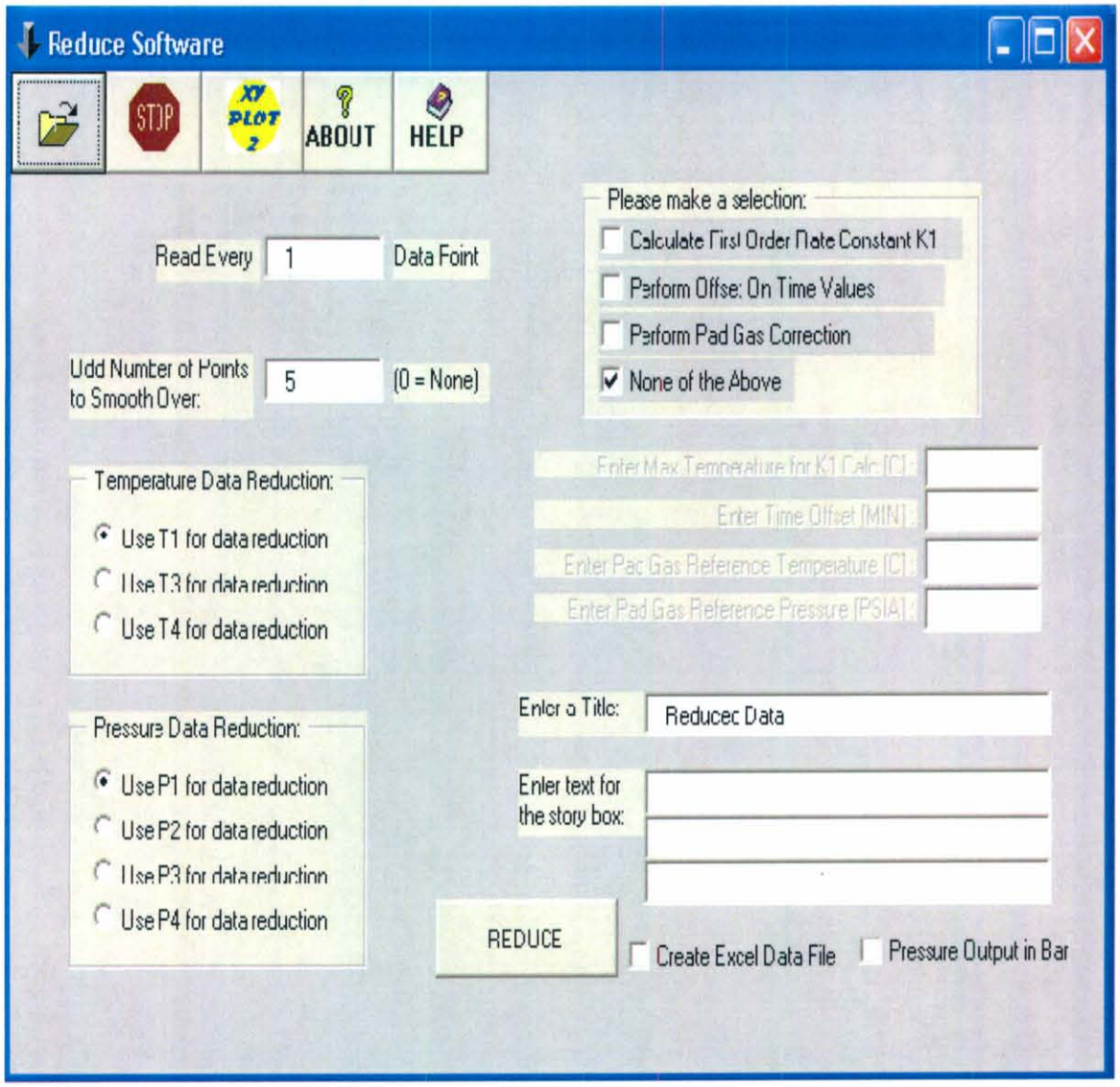

Figure 3.1d: GUI of the Reduce Software of the ARSST Instrument

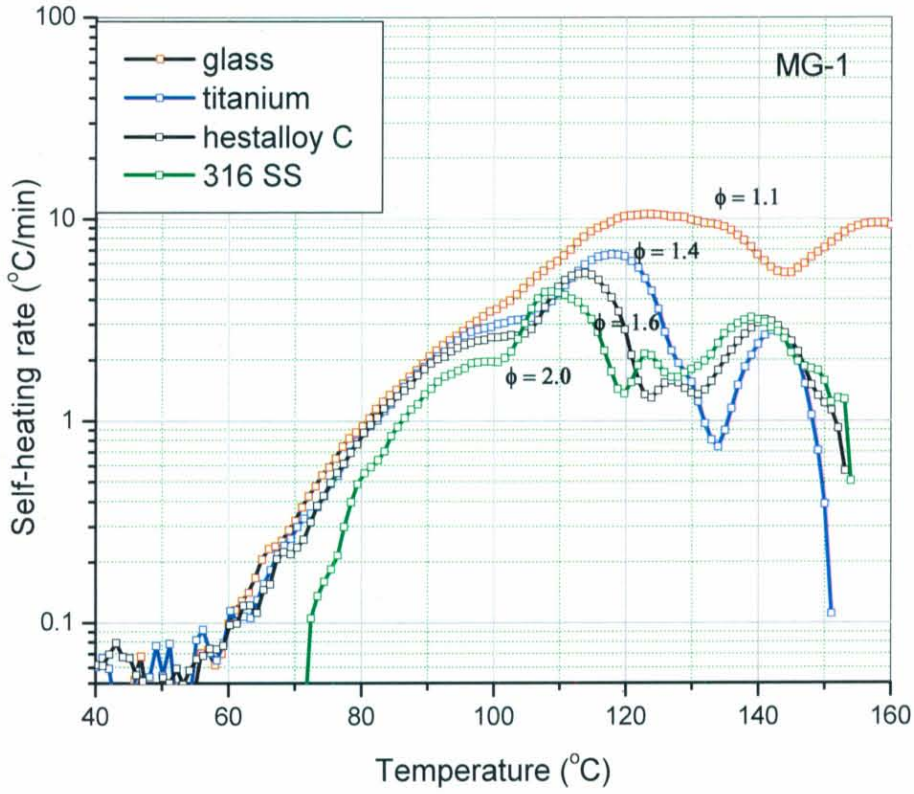

Figure 3.1e: Typical ARSST Result for the Thermal Hazardous Ore.

3.2 Consequences Assessment

The sequences of what can lead to unwanted hazards (accidents) are best described using safety pyramids (Figure 3.2). Severity in the accidents increases from D to A. Heinrich, (1959) asserts that the four layers are interconnected as they aggregate in numbers and occurrences and can lead to or rather influence one another from bottom to top. The attached numerals indicate that about 4000 near misses lead to a minor injury. About 300 minor injuries lead to a major injury and finally, 29 major injuries lead to one fatality.

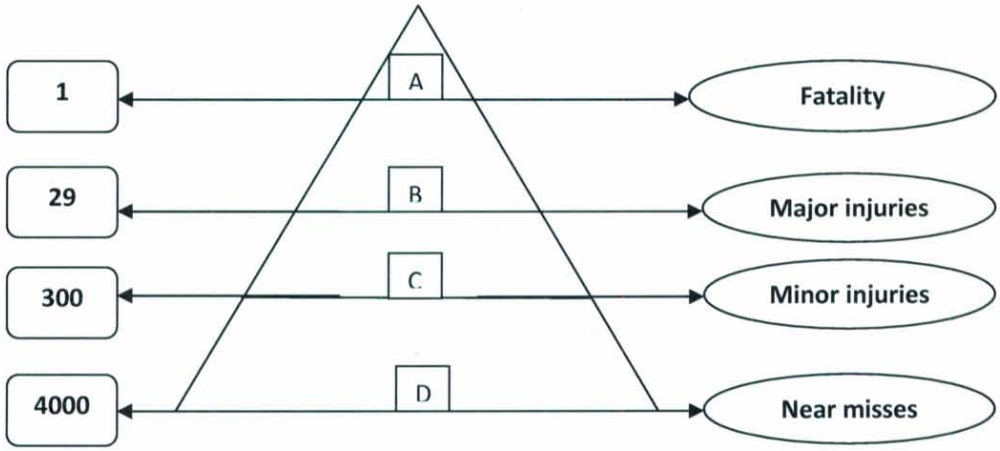

Figure 3.2: Safety Pyramid Denoting Frequency of Occurrence of Events Causing Accidents

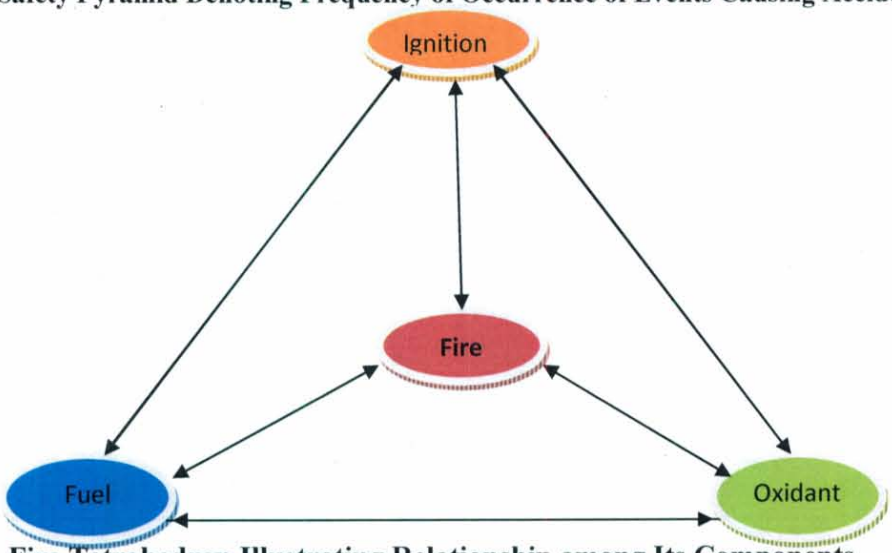

Figure 3.3: Fire Tetrahedron Illustrating Relationship among Its Components

Effective consequences assessment of thermal hazards need sound understanding of interactions between events that can later culminate into hazards. For the case of chemically oriented thermal hazards, the reactions are highly interdependent. In addition, thermal hazards are controlled by availability of sources of ignition e.g. hot spots, surfaces, electric charges, etc. (Kuznetsov and Strizhak, 2009), availability of fuel and oxidants Glassman (1977), localized storage containers and improper designs. Figure 3.3 (Perry, 1999) illustrates the relationships between fuel, oxidants and sources of ignition on released or

generated gases due to pressure build up during chemical reactions which can lead to fire and explosion.

Basically, the overall consequences assessment can be represented by Figure 3.4. Undesired or uncontrolled side reactions are typically more hazardous than the desired reactions. Simplified consequence diagram for solids with thermal hazards is presented in Figure 3.5 for runaway reactions (e.g. Self-Heating Sulfide Mineral Ores and other reactive solids). The basis of the diagrams is rooted in the heat confinement and localized heat generation at the surface and interior of these materials during chemical reactions, storage and transportation (Hu et al, 2006; Chevrier et al, 2006; Chirita et al, 2008; Murphy and Strongin, 2009; Korkin et al, 1999; Janzen et al, 2000 and Mitchell and Akan-Etuk, 2002). This makes it for legislations to be put in place for all chemical industries.

3.2.1 *Effect of Gas and Heat Evolution*

A hazardous gas released is characterized by its chemical and physical properties (density, compressibility, solubility, lower and upper flammable limits, etc.), state before ignition (e.g. boiling liquid expanding vapour cloud (BLEVE), unconfined expanding vapour cloud, etc). For released liquids, the trajectory path, pressure, temperature, boiling and bubble points and flash point are equally important in addition to other properties mentioned for gas. All in all, exposure indices of these fluids must be accurately determined.

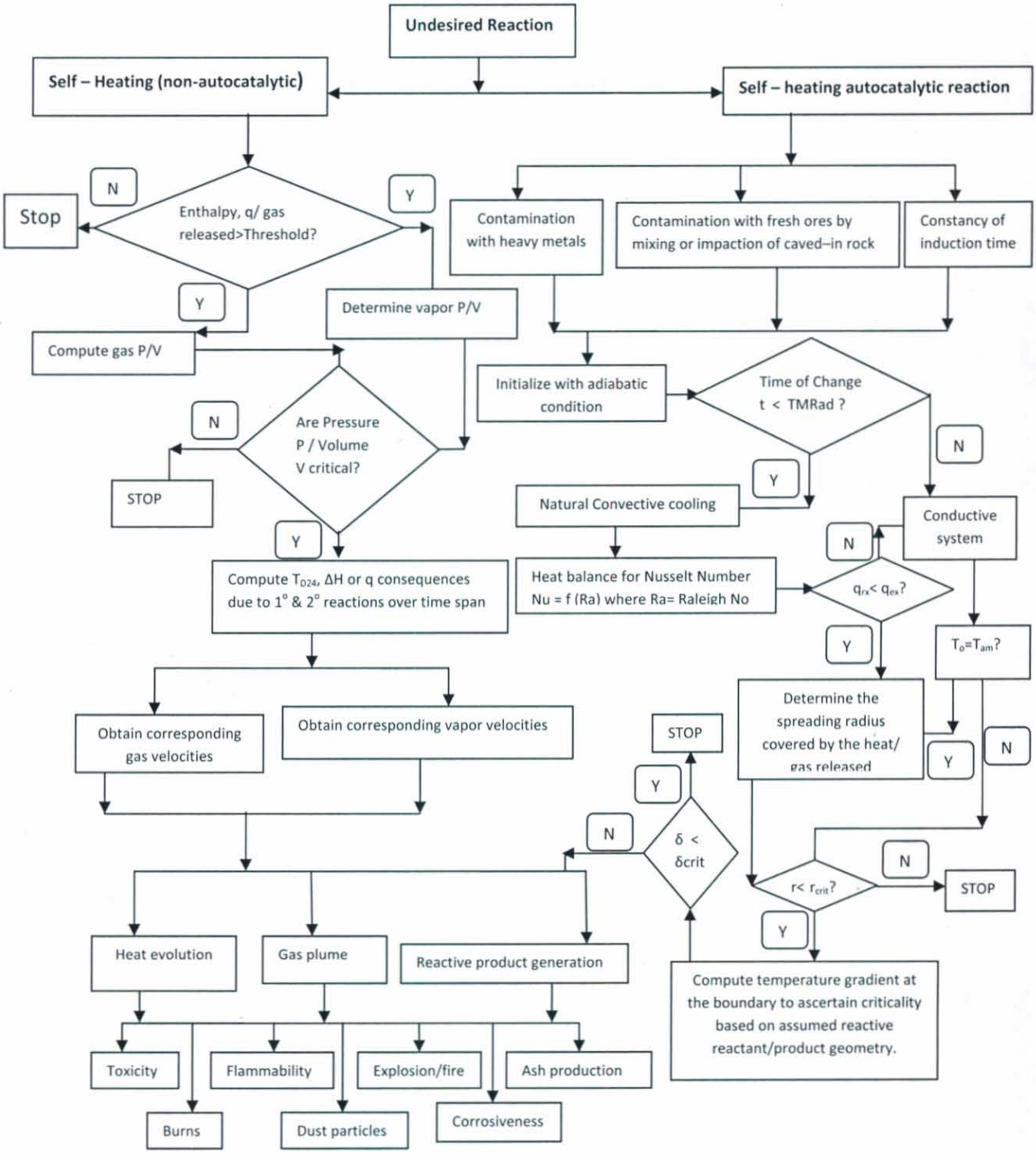

q_{rx} = Enthalpy released rate of Reaction, r = spreading radius of gas plume/heat, δ = Form factor, δ_{crit} = Set limit for critical form factor , q_{ex}= Cooling rate @ boundary/interior, r_{crit} = Set limit for critical radius of gas plume/heat, T_o= Reaction temperature, T_{am}= Prevailing ambient temperature at the peripheral of the reactive solid, TMRad= Time to maximum under adiabatic heating condition, N= No & Y= Yes.

Figure 3.4: Overall Diagram of the consequences Assessment

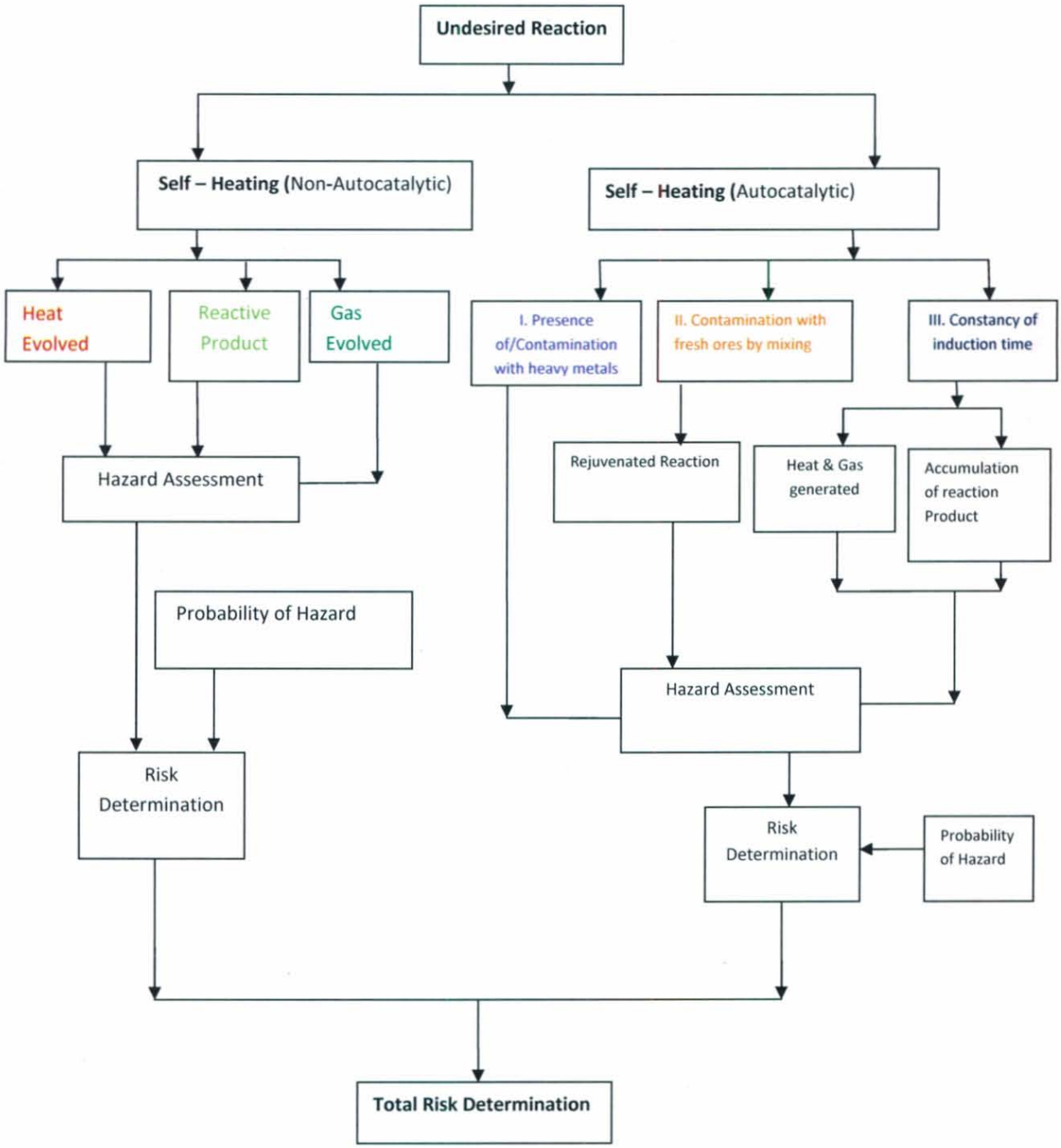

Figure 3.5: Simplified Consequence Assessment Diagram for Self-Heating Thermal Runaway Reaction

The dispersion model of the released gas or vapour is vital to determining impact and risk. These models require downwind speed, concentration, flow rate, cross-wind direction, etc. Quantity of heat released along with fluid is used to determine the severity, intensity and types of inferno (pool, flash and jet fire as well as fire balls). The detailed consequences of the released gas and energy are shown in Figure 3.6. The released gas (acidic and basic in origin) can react with moisture to form acids and bases that can be flammable, toxic or detonate in the presence of ignition sources. These can cause injury and fatality to plant and personnel and degrade or damage equipment. Thermal stress, fatigue, injury and death can be caused by the released heat too.

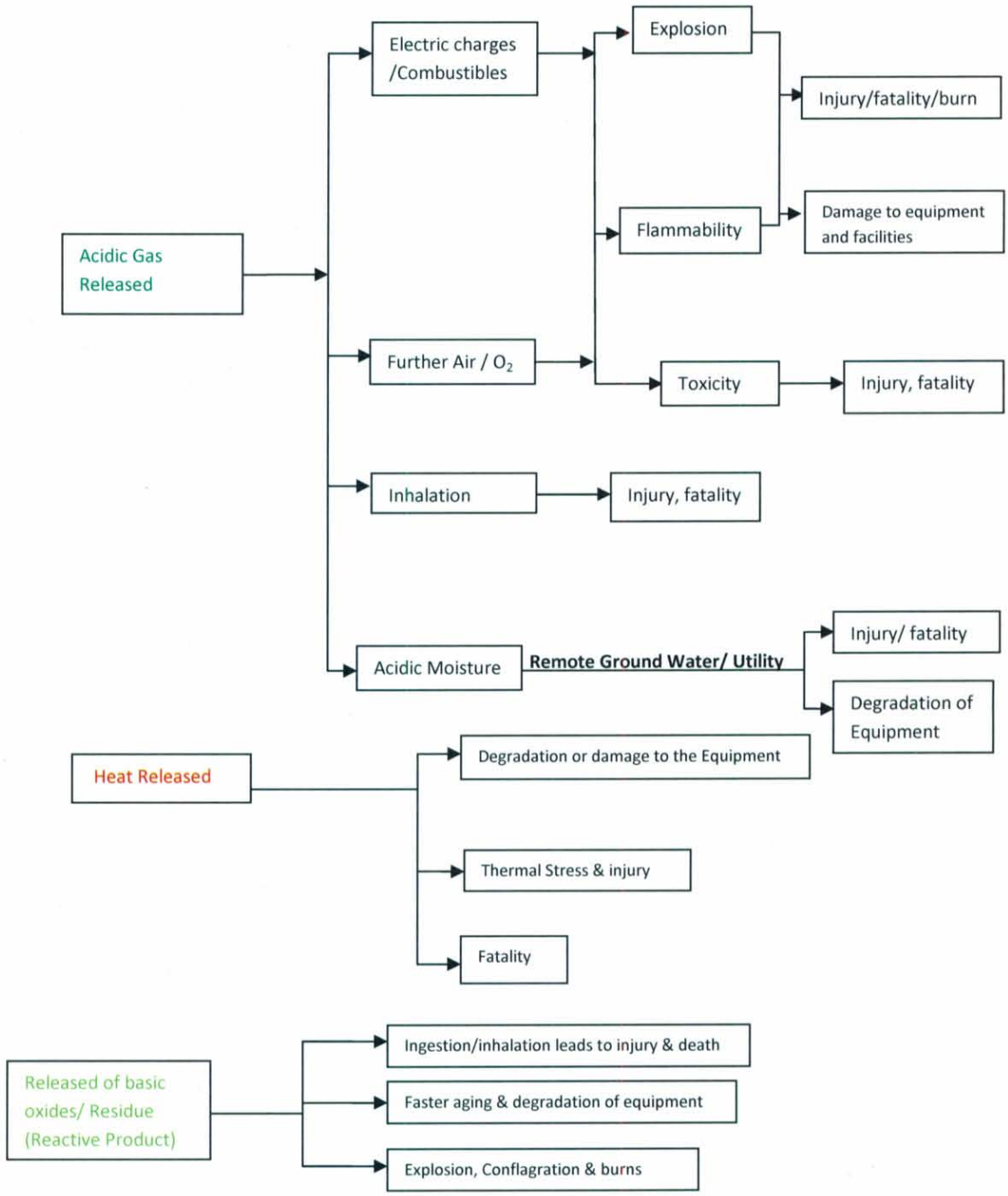

Figure 3.6: Consequence Assessment Diagram for Gas & Heat Evolution Due to Non-Autocatalytic Self-Heating Reaction

3.2.2 Effect of Presence of Heavy Metal and Inert Materials

Metals and other contaminants impact the rate of reaction and reaction pathways. Heavy metals are very reactive and have catalytic properties. Inert materials constitute bulk of the resident heat accumulation in a system and slow down reactivity, waste energy and quench or dampen reactive systems. To assess the contribution of these inert and heavy metals is to execute pilot test on a smaller scale for their inclusion in the production operation before scaling up to an industrial scale. Simulation can also be used based on the obtained results from the experiments to quantify the effects.

Figure 3.7 illustrates the detailed consequences of the presence of metals in the reacting mixtures. Metals can be oxidized to their gaseous forms with huge released of heat energy. In the presence of combustibles, moisture, air or oxygen, the released gas may ignite to cause inferno, explosion, severe burns, injury and death. Heavy metals in samples can enhance catalysis of the reacting systems, speeding up the reaction and generating more gases with high evolution of heat energy.

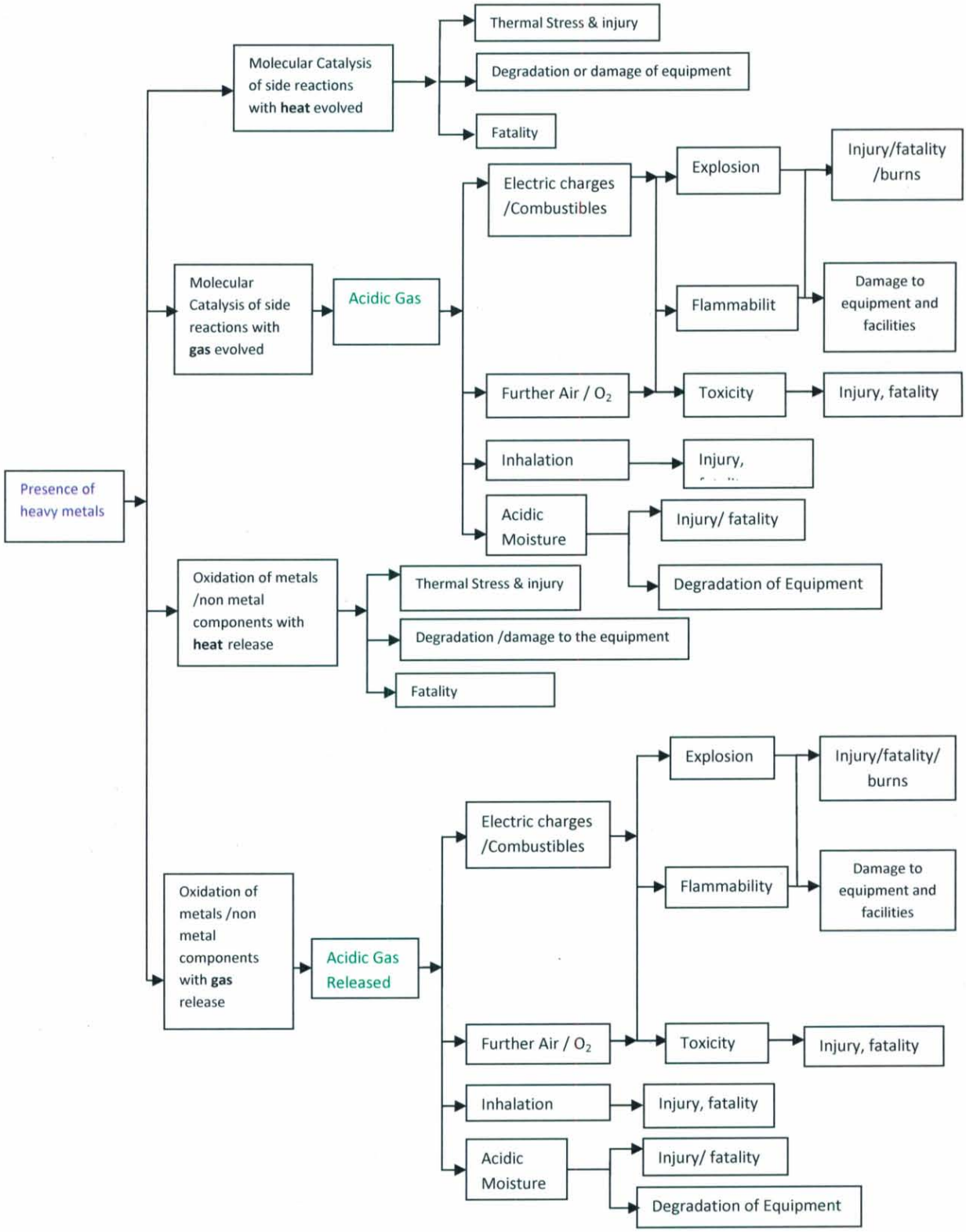

Figure 3.7: Consequence Assessment Diagram for Presence of Heavy Metal Due to Autocatalytic Self-Heating Reaction

3.2.3 Effect of Recycling Materials with Fresh Feed

Recycling is advantageous in terms of industrial practices due to economics. However, properties variations between fresh feeds and recycled materials may result in unanticipated hazards. For example, effective energy utilization is important in control of auto-thermal reactors where products heat stream is employed to pre-heat the fresh feed. However, should the product temperature fall outside a set range, unwanted reaction in the reactor can occur resulting in a runaway reaction. A simple flow diagram of Figure 3.8 reveals the effect of the recycle on feed. The product formed often rejuvenates the reaction in some cases thereby constituting runaway reaction due to uncontrolled heat evolution.

3.2.4 *Effect of Induction Time*

Induction or delayed time is the time it takes at a given initial temperature to evolve from stability to runaway reaction. Most controllers are designed for routine operations and have no time to adjust to the sudden offset. The response to this is to attempt to mitigate the hazard by using curtailment. Induction time for thermal hazard is normally estimated roughly using the Vant Hoff expression given below:

$$\frac{\Delta T}{\Delta t} \approx \frac{dT}{dt} = \frac{Q(T)}{C_p}$$

The consequences of induction time are so great and can be summarized as shown in Figure 3.9 due to their sudden manifestation. The latent nature of induction time leads to high thermal hazards yielding unexpected consequences. Therefore, reactions with induction time should be avoided by first executing pilot laboratory tests to prevent unwanted scenario.

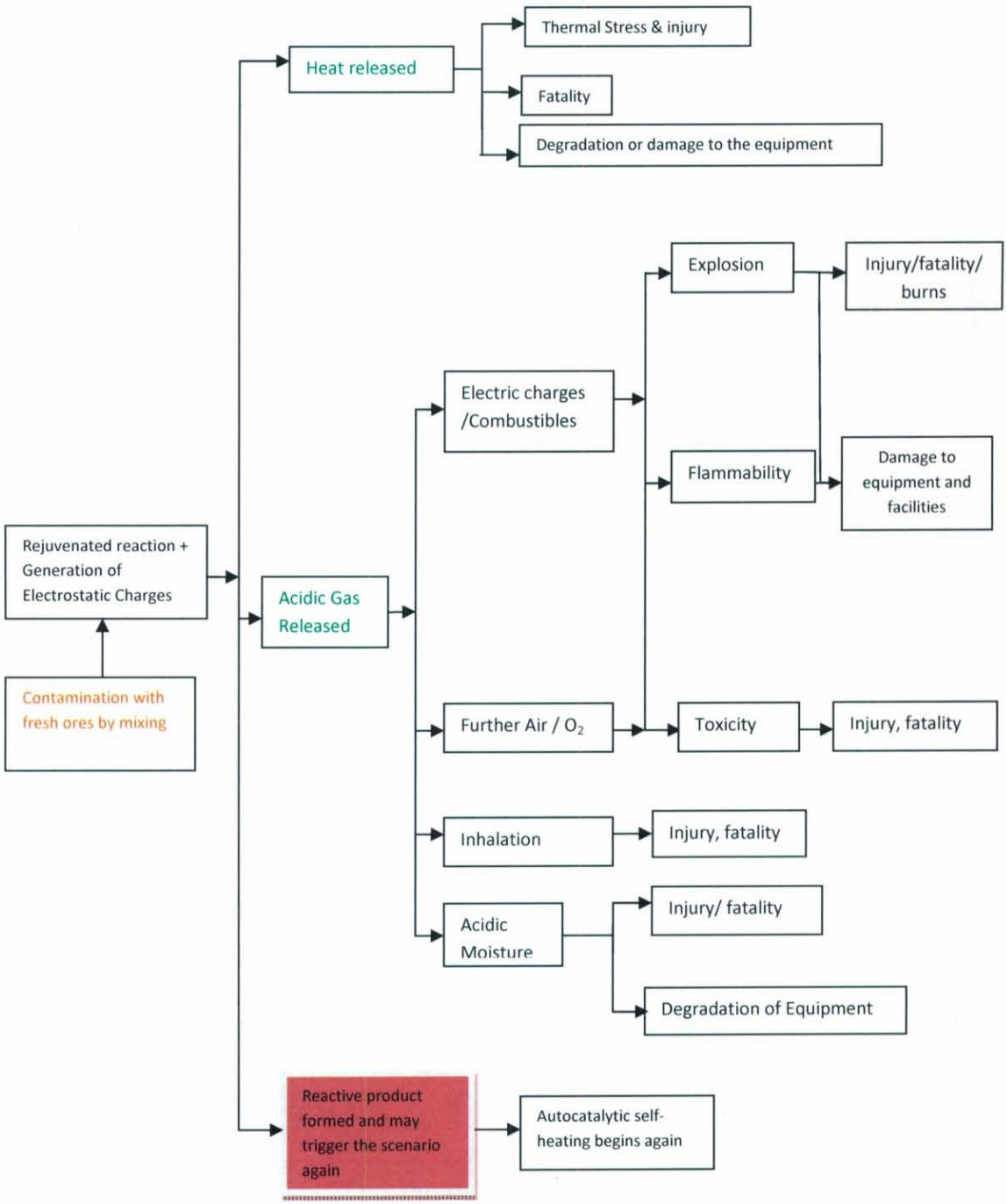

Figure 3.8: Consequence Assessment Diagram for Fresh Feed Contamination by Recycling Due to Autocatalytic Self-Heating Reaction

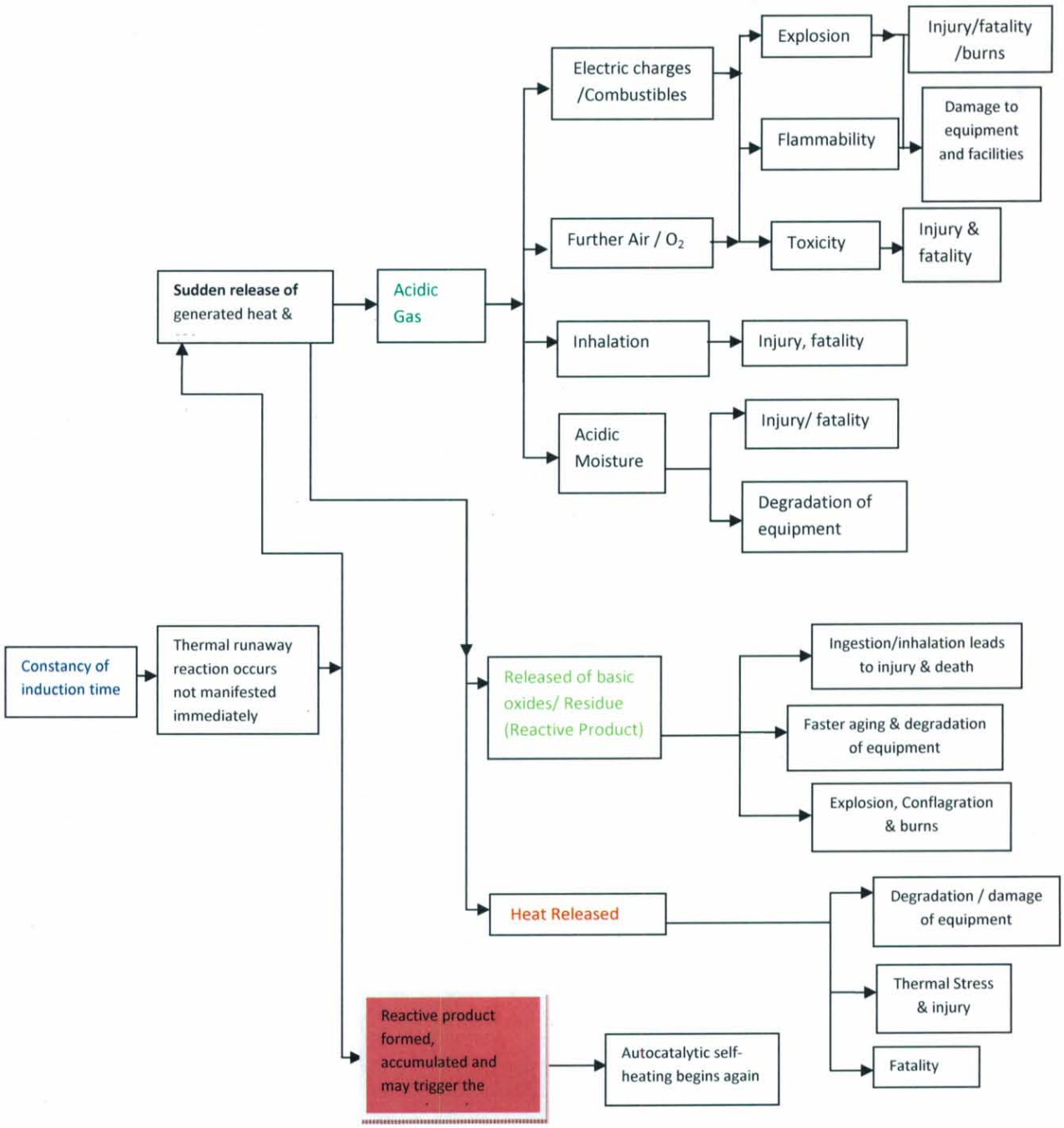

Figure 3.9: Consequence Assessment Diagram for Constant Induction Time Due to Autocatalytic Self-Heating Reaction

3.3 Severity Determination

The severity of thermal hazardous reactions is quantified by the heat (enthalpy) of reactions as it is a measure of the runaway or hazardous nature of the material or reaction (Stoessel, 2008). Therefore, the consequence of any thermal hazard can be determined using:

$$\text{Severity, } \beta = \frac{\textit{Enthalpy of specific reaction material in question}}{\textit{Enthalpy of referenced reaction or material}}$$

$$= \frac{\Delta H_{R\ \text{specific reaction}}}{\Delta H_{R\ \text{referenced reaction/ material}}} \qquad \textbf{3.22}$$

Well studied thermally hazardous materials are used as referenced materials in equation 3.22 as the criticality of the hazard can easily be considered on any scale by varying the referenced material so that the behaviour across board for easy comparison can be easily monitored. Stoessel (2008) proposed that associated ΔT_{ad} with such reactions could be used alongside with their enthalpies to corroborate the above facts and gave a qualitative table to support this i.e. Table 3.1:

How severe a thermal hazard is, can also be assessed by the TMR_{ad}. It is well noted that chance of occurrence is high if TMR_{ad} is less than 8hr i.e. one work shift hours, intermediate if it is between 8-24hr and low or negligible should it be greater than 64hr. The properties of referenced materials used for severity determination are as depicted in Table 3.2.

In applying this approach, the four referenced chemicals were selected with each being a representative of each class of severity or risk. Any new material whose risk is to be quantified is compared with these materials independently to ascertain the numerical value under each class. The values obtained are then compared with standard values on the predefined scale for its proper classification.

Table 3.1: Severity of Thermally Hazardous Reactions based on ΔT_{ad} (K)

Simplified	Extended	ΔT_{ad} (K)	Order of Magnitude of Q (kJ/kg)
High	Catastrophic	□400	□800
	Critical	200-400	400-800
Medium	Medium	50-100	100-400
Low	Negligible	□50	□100

Table 3.2: Referenced Material Used for Severity Determination of Thermal Hazardous Runaway Reaction

Risk Class	Referenced Material Used	Molecular Weight (g/mol)	Onset Temperature, T_o (^oC)	ΔH_R, Reaction Enthalpy (J/g)	TMR_{ad} (min)
Class 1	2-Amino-4-Chlorophenol	144	164	201	100
Class 2	Di-tert-butyl Peroxide	146	162	557	107
Class 3	2,6-dichlorobenzoyl chloride	209	229	2906	98
Class 4	Trinitrotoluene, TNT	227	314	5388	124

Source: Thermal Risk Assessment & Rankings for Reaction Hazards in Process Safety (2009).

3.4 Probability Model Methodology

Probability is the likelihood of occurrence of an event and is used in the quantification of uncertainties in parameter based on their randomized sample. Probability models can be discrete or continuous and are based on the use of probability density mass and functions (PDF). Be it conditional or unconditional probabilities, mathematical models (popularly referred to as probability functions) are employed in obtaining numerical values of the chance of occurrence of any events.

To accurately model thermal hazards, continuous PDF are preferred to the discrete ones among others. PDF includes: Gaussian, Beta, Gamma, Weibull distributions, etc. In this work, Gaussian or normal distribution will be employed for simplicity and conservativeness. The normal probability distribution function is of the form:

$$f(x) = \frac{1}{\sigma\sqrt{2\pi}} e^{-\left(\frac{x-\mu}{\sigma}\right)^2} \qquad 3.23$$

Where the variable x (normal variate) can assume all values from $-\infty \; to \; +\infty$. μ and σ are the parameters of the distribution called mean and standard deviation of the distribution respectively and $-\infty < \mu < +\infty$, with $\sigma > 0$. $f(x)$ is the probability density function with the following properties (Zill & Wright, 2011 and Stroud, 2003):

- $f(x) \geq 0$
- $\int_{-\infty}^{\infty} f(x)dx = 1$, indicating that the total area under the normal curve is unity.
- The normal distribution is symmetric about its mean.
- The distribution is a unimodal distribution with mean, median and mode coincides.

To construct a PDF that can capture this variability, a wide range of rate data was included. However, it is impossible to construct PDF to capture all reactions. Therefore, reactions were grouped based on Ea and A as shown in Appendix A. The activation energy data was grouped into four classes: Ea≥400kJ/mol (class A), 100kJ/mol□Ea≤400kJ/mol (class B), 10kJ/mol□Ea≤100kJ/mol (class C) and Ea≤10kJ/mol (class D). Similarly, the Arrhenius' constant data was classified into three classes: $A \geq 10^{10} s^{-1}$ (Class A), $10^{-1} s^{-1}$ □$A \leq 10^{10} s^{-1}$ (class B) and A□$10^{-1} s^{-1}$ (class C). Fits of these classes were then obtained as in Appendix B.

The probability of an event "E" (self-heating behavior or runaway reaction) occurring for thermally hazardous material, can be modeled by using a normal or Gaussian probability function by computing the slope or distance of a variable of the function h(x, u, t, T,…) or the parametric curve defining the functional relationship between the self-heating parameters via:

$$\mathbf{Pr(x = E) = 1 - Pr(}x_i \leq x \leq x_j\mathbf{)} \qquad \mathbf{3.24}$$

Where x can be converted to a standard score or z-score using:

$$\mathbf{Pr}\left(z_i \leq z \leq z_j\right) = \boldsymbol{Pr}\left(\frac{xi-\mu}{\sigma} \leq \frac{x-\mu}{\sigma} \leq \frac{xj-\mu}{\sigma}\right) = \int_{z_1}^{z_2} \boldsymbol{f}(\boldsymbol{z})\boldsymbol{dz} = \boldsymbol{F}(\boldsymbol{z_2})\boldsymbol{F}(\boldsymbol{z_1}) \qquad \mathbf{3.25}$$

Where: $\boldsymbol{F}(\boldsymbol{z}) = \int_{-\infty}^{z} \boldsymbol{f}(\boldsymbol{x})\boldsymbol{dz} = \boldsymbol{Pr}(\boldsymbol{Z} \leq \boldsymbol{z})$

This becomes necessary since the runaway reaction or self-heating (SH) parameters fall between two points (i.e. onset and maximum values) before decreasing again (if it exists at all for hazardous chemical or reaction). In the functional relationship $y = h(x, u, t, T, \Delta H, \ldots)$ having n-parametric variables where the variables can define SH at any point, the probability "E" occurring can be determined quantitatively on knowing the locus of the point P(x, u, ΔH, t, T., …) or plane defining such SH. The parameters that determine the event can be quantified based on the nature of the material being investigated and on their physicochemical properties and thermal history. Accurate experimental data obtained from thermal analysis experiments are required for the analysis.

For runaway reactions, the kinetic parameters (A & E_a), enthalpy of reactions, thermal time constant τ and characteristic temperatures T_{onset} and T are required for the above analysis. Since temperature (T) determines ΔH_R of the reaction, then, modeling the probability of the

hazardous condition from A and E_a of the reaction is sufficient. Obviously, A and Ea are a function of the reacting system at temperature (T). The resulting probability from this approach gives a true resemblance of the likelihood of thermal hazardous reaction occurring. Therefore the probability of any hazardous condition is computed by [3.26] using joint probability rule.

$$\prod \mathbf{Pr}\,(x) \qquad \mathbf{3.26}$$

Where: "x" is a parameter known probability.

3.5 Quantitative Risk Assessment and Ranking

Mathematically, QRA is simply the product of probability and severity i.e.

$$\boldsymbol{Risk = Frequency\ of\ Occurrence\ (probability) \times Severity(consequence, \beta)} \qquad \mathbf{3.27}$$

$$\boldsymbol{= Pr \times \beta}$$

The associated risk with thermal hazard will be computed from both severity and probability as indicated in sections 3.3 and 3.4 respectively. Successful ranking of thermal hazards was done by Wang, et al. (2008) using predefined scales. Hence, the call for predefined scales from which conclusions can be inferred. An overview of the risk determination process is given in Figure 3.10.

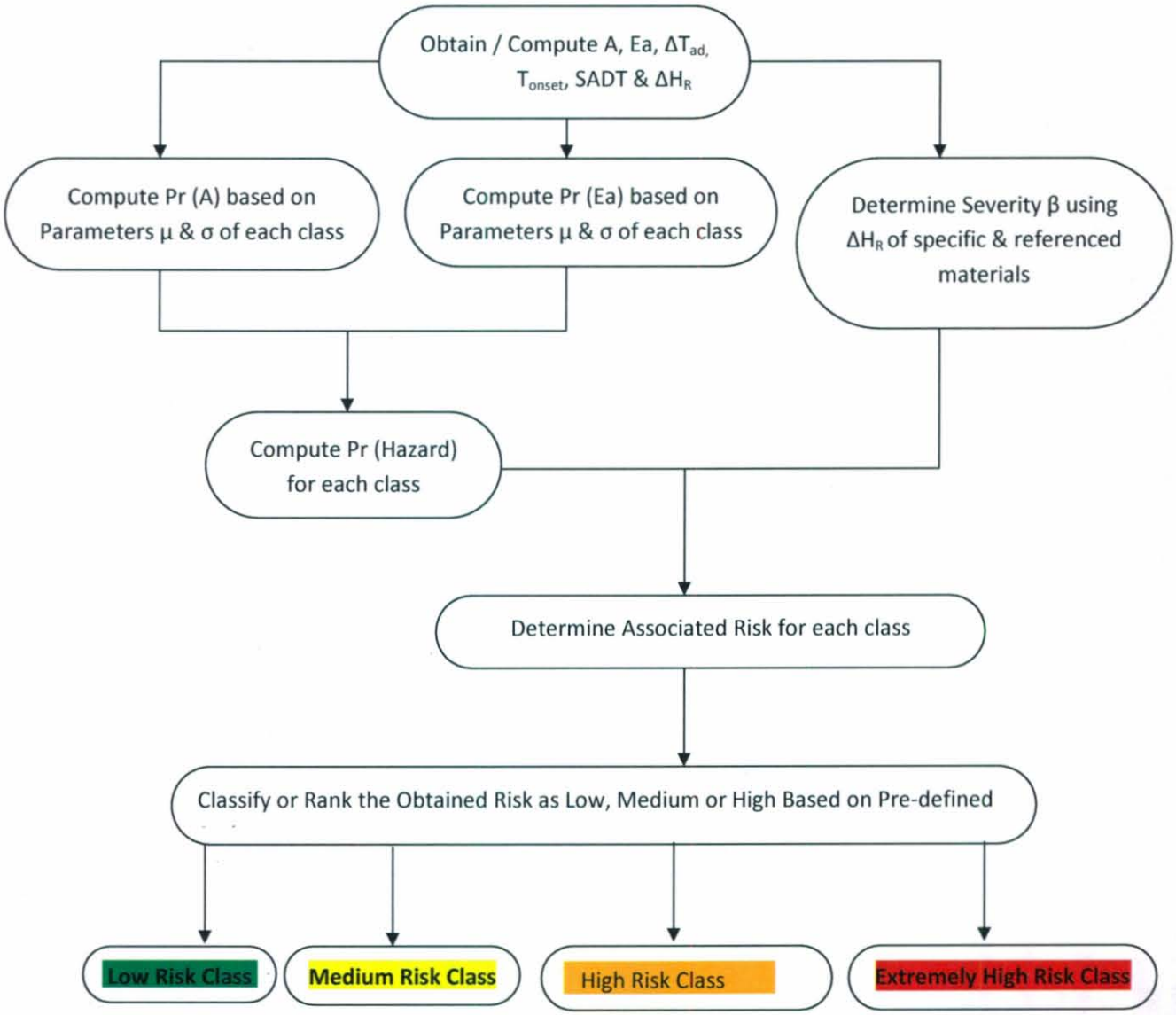

Figure 3.10: Risk Classification Diagram

A predefined scale for quantifying risk is as depicted in Table 3.3 having tested several materials undergoing thermal hazardous reactions using the presented approach with their ascertained experimental evidences from experimental data obtained from the work of several authors. Any obtained numerical risk value obtained is compared with the range shown on the scale to ascertain the class where the material under investigation falls. No matter under which class the material is examined, its real risk class will always manifest and will be consistent if examined under two or more classes.

Last, quantified risk and ranking are pictorially represented or coded using legend in Table 3.4.

Table 3.3: Predefined Risk Scale

Predefined Risk Scale	Class 1	Class 2	Class 3	Class 4
Low	$< 10^{-3}$	$< 10^{-4}$	$< 10^{-5}$	$< 10^{-8}$
Medium	10^{0} -10^{-3}	2.0×10^{-1} - 10^{-4}	10^{-3} - 10^{-5}	10^{-5} - 10^{-8}
High	1.1×10^{0} – $< 3.0 \times 10^{0}$	10^{0} - $< 2.0 \times 10^{-1}$	10^{-1} - 10^{-3}	1.0×10^{-4} - 10^{-5}
Extremely High	$> 3.0 \times 10^{0}$	$> 10^{0}$	$> 10^{-1}$	$> 1.0 \times 10^{-4}$

Table 3.4: Risk Ranking Legend

Risk Class	Risk Ranking Code
Low	
Medium	
High	
Extremely High	

Chapter 4

Case Study

4.1 Self-Heating Minerals

Self-heating is a runaway hazardous reaction in which chemical material either under storage, transportation or processing undergoes exothermic reactions without any external application of heat energy. It is characteristic of oxidation and decomposition reactions under favorable conditions. Several materials including reactive minerals and ores undergo this self-heating behavior. Gases and heat are often released in uncontrolled manner causing imminent danger. The various hazards associated with self-heating were already discussed in Chapter 3.

4.2 Model Application to Self-Heating Minerals

The methodology discussed is applied to the self-heating minerals (sulphide-containing ores) which had been experimentally tested using DSC and ARSST. The experimental results obtained had been treated with the AKTS software. Parameters such as onset temperature, TMRad, ΔTad, SADT and apparent activation energies are evaluated. Using these parameters, risk assessment can be done utilizing proposed semi-empirical model.

The model is not only relevant to quantify the hazards related to self-heating minerals but also solve the scaling up of thermal hazards on the industrial scale. These self-heating minerals have always constituted menace during mining and mineral processing operations whose economic values depend on the fluctuating free market price at the official London Metal Exchange market. This is due to the fact that smelters and miners are worried about the returns and mitigation against hazards to avoid industrial bankruptcy, folding up and

severe damage to the environment, plant facilities, flora and fauna of the biomes. Quantifying the risk will also help to put mechanisms and technologies in place for minerals and their tailing re-work or re-processing to obtain more ore's *contained metal value* by processing route modifications from the present state and sustainability of the industry to prevent recurrence of the ugly scenarios witnessed in the last century (Wills and Napier-Munn, 2006). It will also ensure efficient handling of the minerals throughout all phases of its usage and treatment. A balance between the set operational standards and practical reality of unexpected shutdowns, inventory control, occasional explosions, smoldering that are normally encountered during mining, ore concentration processing, and milling operations can be actively achieved and managed with fore-knowledge of mineral categorization, characterization and risk analysis. One of the prominent acts usually embarked upon by the smelters is ores storage which has its own advantage of allowing blending of different ores to provide consistent feed to the mill. This portends more inherent dangers for the minerals that undergo self-heating behaviour. Prior risk analysis will forestall these dangers.

4.2.1 Model Validation for Hazardous Reaction Using Experimental Data

The model is validated using experimental data from thermal oxidation of 13 ore samples carried out in the DSC. Attached thus are the raw and treated experimental data (Appendix C). The ores were of various compositions as shown in the data with many oxidation reactions simultaneously going on. The overall reaction going in the self-heating of these ores can be put as:

$$\text{Ore} + O_2 + H_2O \longrightarrow \text{Products} \qquad \Delta H_R = -x \text{ kJ/mol} \qquad 4.1$$

Writing concise mechanism of reactions is not the main focus of this work. Further, simple mechanism cannot be written for the oxidized mixture as the reaction mechanisms are very complex. Hence, the data gave the overall enthalpy, Cps, activation energy and densities for the experimental runs done to ascertain effect of parameters such as mineralogy, moisture content or saturation as well as particle size distributions on the self-heating behavior of the ores (well studied complex runaway reaction). Three sets of data (Friedman, Flying- Ozawa-Wall and ASTM E695 Analysis methods) were obtained and used in this validation. Of all these data set, Friedman data were adjudged to be the best (Iliyas, 2011).

In pursuance to the experimental results obtained simulation were runs in Matlab to ascertain the hazardous nature with the model solved using equation [3.21] i.e.

$$\boldsymbol{T = T_{ref} - \Delta T_{ad}\left[1 - e^{\frac{t}{\tau}}\right]} \qquad \textbf{3.21}$$

The initial concentration of the ore was determined from $\boldsymbol{\Delta T_{ad} = [(-\Delta H_R)C_o x/\rho C_p]}$ using data from Appendix C as conversion was at maximum at the end of each experiment i.e. critical temperature. Also, the first commencement of exothermicity signals the beginning of self-heating. The rate of reaction was simulated using τ-expression having known the concentration:

$$\boldsymbol{r_p = \frac{xC_o}{\tau}} \qquad \textbf{4.2}$$

Similarly, the self-heat rate was simulated using equation [3.14] i.e.

$$\boldsymbol{\frac{dT}{dt} = \frac{1}{\tau}\left[\left(T - T_{ref}\right) + \left(\Delta T_{ad}\right)\right]} \qquad \textbf{3.14}$$

Specimen of these calculations is shown here for Ore 03-601(207m) using its experimental data:

Given: ΔTad=393K (i.e.393°C), T_{ref}=20°C, τ = 5556s,

ΔH_R=-36627J/mol, ρ=4369kg/m^3 Cp=601.3J/kgK

Basis: 1hr (3600s)

- $T = T_{ref} - \Delta T_{ad}\left[1 - e^{\frac{t}{\tau}}\right]$ 3.21

  $= [20 - 393\ [1 - e^{(3600/5556)}]\ ]^{o}C$

  $=$ 378.26°C

- $C_o = \frac{\Delta T_{ad}\rho C_p}{-\Delta H_R x} = \frac{393 \times 4369 \times 601.3}{1 \times 36627}\ mol/_{m^3}$ 2.4

  $=2.82 \times 10^3\ mol/_{m^3}$

- $r_p = \frac{xC_o}{\tau} = \frac{1 \times 28188\ mol/_{m^3}}{5556s}$ 4.2

  $= 5.07\ mol/_{m^3 s}$

- $\frac{dT}{dt} = \frac{1}{\tau}[(T - T_{ref}) + (\Delta T_{ad})]$ 3.14

  $= \frac{1}{5556s}[378.26 - 20 + 393]\frac{^oC}{s} = 0.135\frac{^oC}{s}$

The results obtained for other duration and concentrations for the various ores are as shown in Figures 4.1-4.12 for the different experimental runs based on Freidman Analysis data. The results are as shown here for the different ores to illustrate the effects of mineralogy, particle size distribution and moisture contents or saturation. The rate of reaction was found

to be increasing with increasing fractional conversion at the maximum fixed concentration for each ore. Other analysis results (Flynn-Ozawa-Wall and ASTM E698) are the same. Parameter "τ" can be determined as indicated in Appendix E. "τ" is fixed in this work for consistency although its effect (variation) has been tested over a defined range (5556s □ $\tau \leq$ 555556s) by scale factors of 10 and 100 above the computed value. "τ" = 5556s is the least value used in this work indicating processing or residence time of 1.5hr. Values in the order of 1-2days were recorded by AKTS software. This value is typical for the behaviour of the minerals ores. Hence, it necessitates testing the sensitivity of this model using various values of τ. This is reported in Chapter 5. The results obtained are similar in trend under all conditions except that they differ by these scale factors in decreasing the self-heat rate by these scale factors too. Detailed discussion on parameters sensitivity of the model is given in Chapter 5.

Figures 4.1-4.4 show that the rate of reaction and self-heating rate with respect to mineralogy. The reaction rate for the ore 03-601 (207m) is the maximum value based on determining the expected ΔTad for all the ores experimental data with respect to effect of mineralogy (Table C12b in Appendix C). The expected ΔTad values obtained are 225K, 393K, 182K and 90K for ores 03-601(199m), 03-601(207m), 03-601(217m) and 05-658(207m) respectively indicating that the relative least reactive of the four ores is 05-658(207m) using equation [2.4] at full fractional conversion of unity. Therefore, the higher pyrrhotite in the ores governs this observable trend (the higher the pyrrhotite content, the higher the reactivity or self-heating).

Similarly, Figures 4.5-4.8 revealed that the fine particle sizes of <75μm are the most reactive based on the measured experimental data.

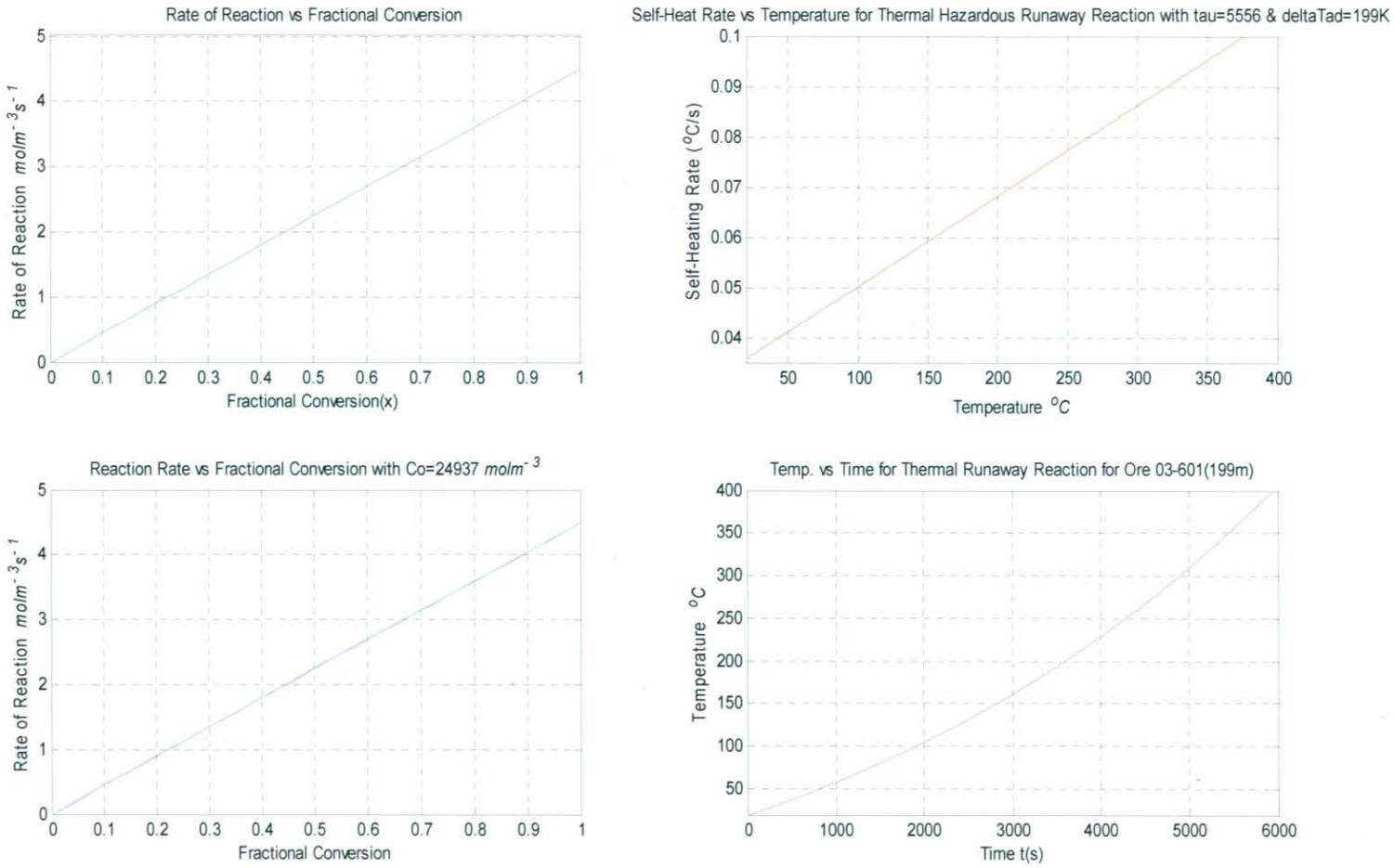

Figure 4.1: Simulated Plot for Ore 03-601 (199m) Experimental Data [Friedman Analysis Data] Mineralogy

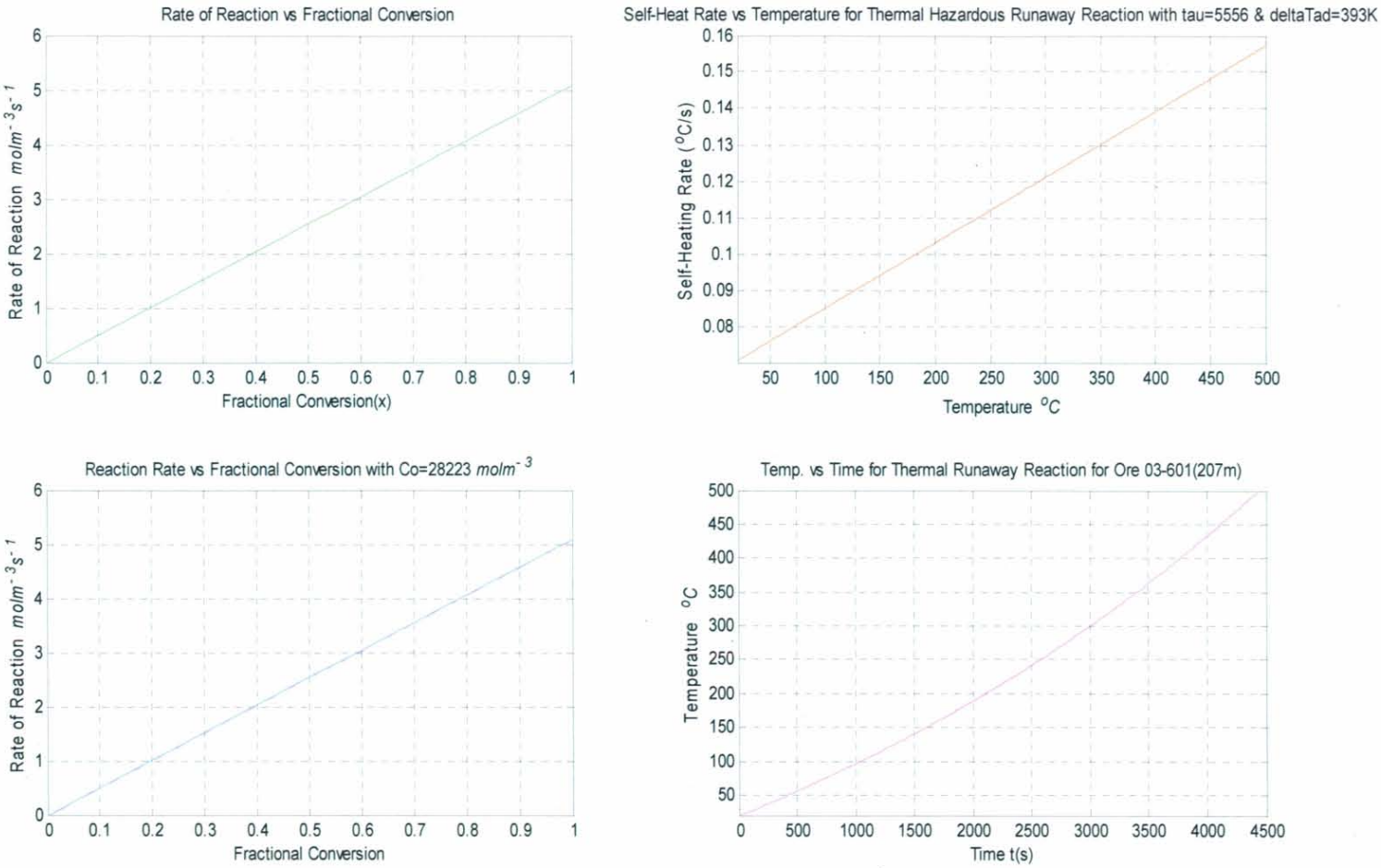

Figure 4.2: Simulated Plot for Ore 03-601 (207m) Experimental Data [Friedman Analysis Data] Mineralogy

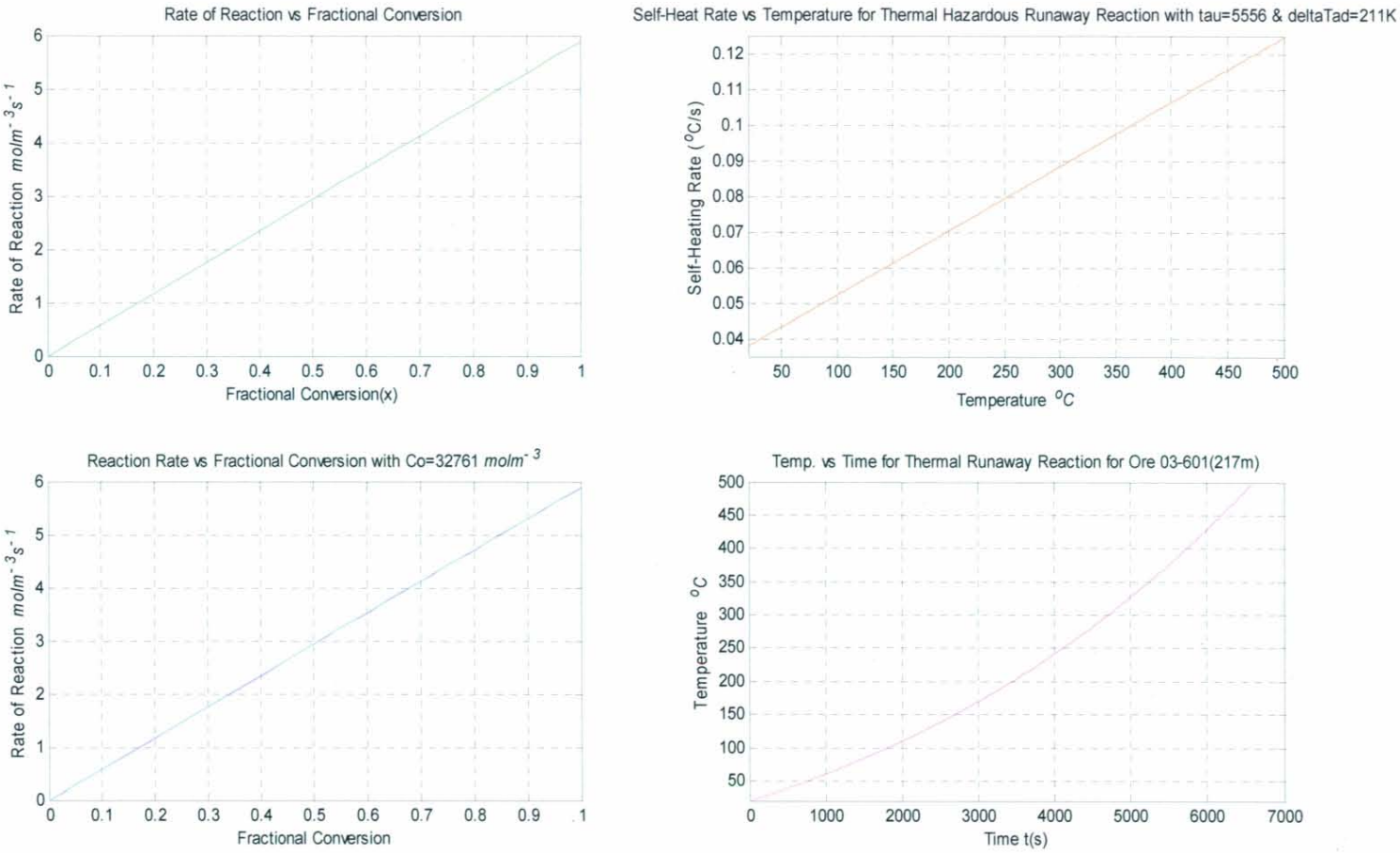

Figure 4.3: Simulated Plot for Ore 03-601 (217m) Experimental Data [Friedman Analysis Data] Mineralogy

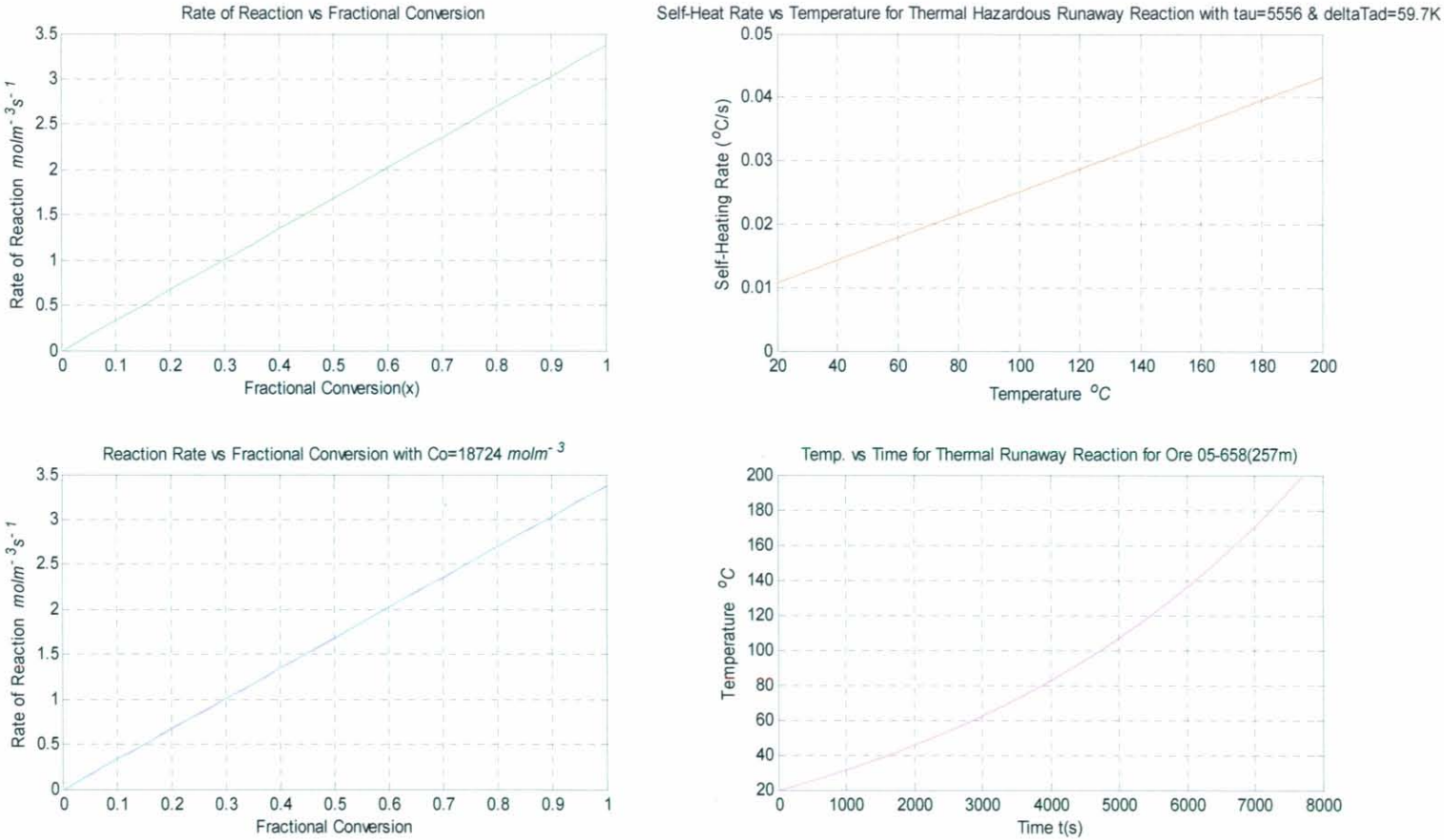

Figure 4.4: Simulated Plot for Ore 05-658 (257m) Experimental Data [Friedman Analysis Data] Mineralogy

The computed "expected experimental ΔTad" using equation [2.4] on the same basis of constant "fixed concentration" across board for a particular investigated parameter is shown in Table C14b (Appendix C). The obtained ΔTad values for <75μm, 75-180μm, >180μm and mixed particles are 59.0K, 4.03K, 1.60K and 45.97K respectively This trend indicates that the order of reactivity of the ores in term of particle size distribution with [<75μm particles] > [mixed particles] > [75-180μm particles]> [>180μm particles]. Therefore, the higher the surface area available for reaction, the higher the reactivity of the particles present in the ores. Although these particles were isolated and tested experimentally, yet, they existed in conglomerated form as an aggregate in each ore type but not segregated class. It can be inferred that the effect of particle size distribution is well represented by the mixed particles.

Figures 4.9-4.12 shows the effect of moisture content on the measured experimental data. The obtained results indicate that there is an optimal moisture content that aids reactivity after which reaction progress decreases. The computed "expected ΔTad trend" which is not a measured trend is 61K, 103K, 89K and 144K for 3%, 8%, 15% and 25% moisture content respectively (Table C16b, Appendix C). Although the computed "expected ΔTad trend" for the effect of moisture content indicates that 25% moisture content is expected to be the most reactive but this is not true as the computed value suggested. This is simply because the effect of the advancing reacting gas front was not captured in this regard. Excessive moisture will inhibit the motion of the advancing gas front thereby slowing down the rate of reaction. Only measured experimental values at the same fixed concentration will reveal the real trend of the moisture effect. Fluid phase interaction in different media was well explained by Smith et al. (2001), McCabe & Harriott (2005), Richardson & Coulson Volume 2 (2002) and Foust (1980) on this aspect.

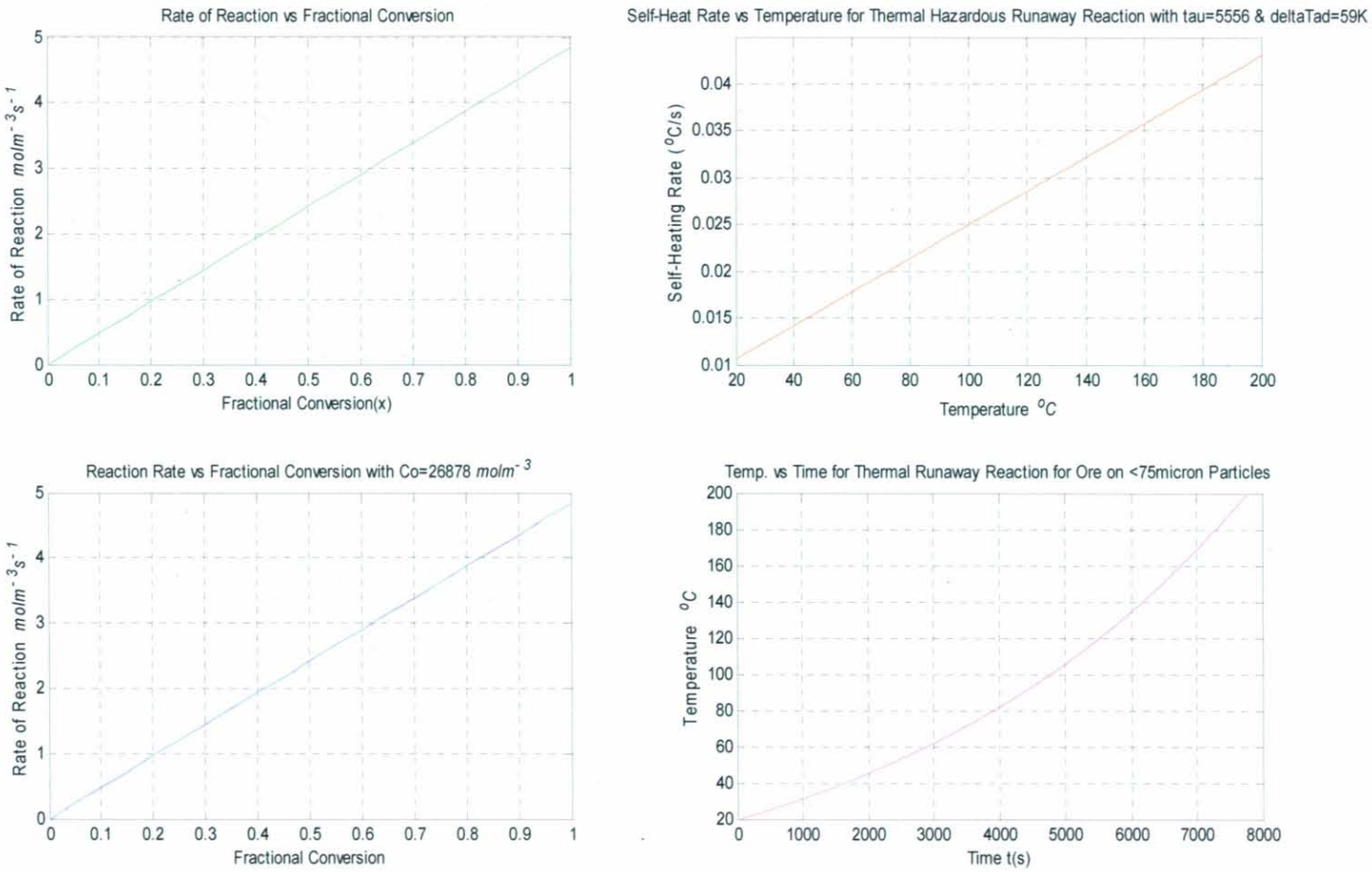

Figure 4.5: Simulated Plot for Ore 05-658(257m) Experimental Data [Friedman Analysis Data] ⍰ 75µm Particles

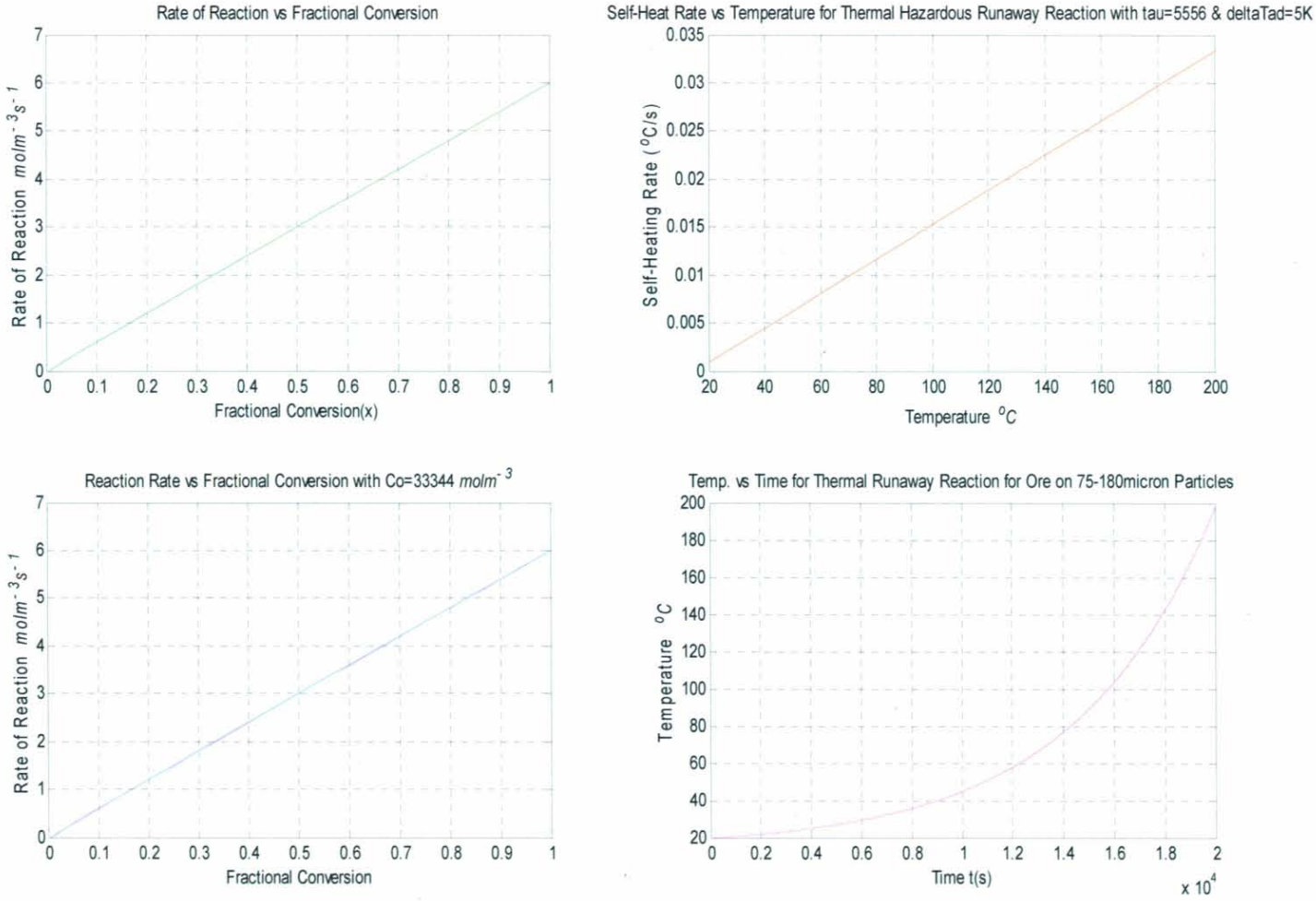

Figure 4.6: Simulated Plot for Ore 05-658(257m) Experimental Data [Friedman Analysis Data] 75-180µm Particles

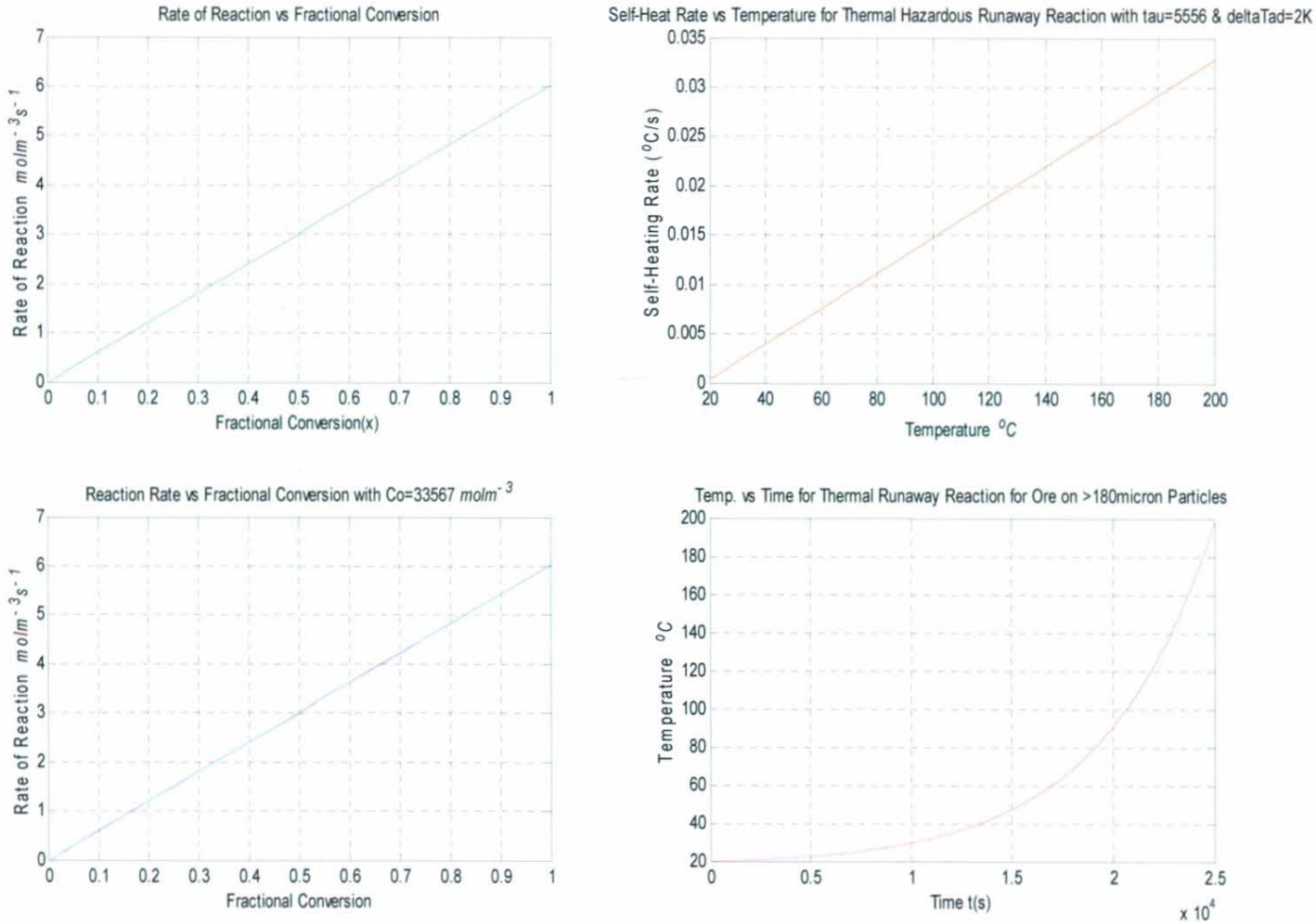

Figure 4.7: Simulated Plot for Ore 05-658 (257m) Experimental Data [Friedman Analysis Data] 180µm Particles

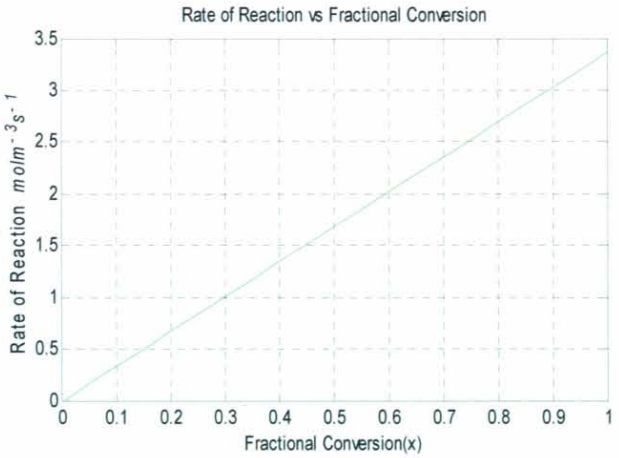

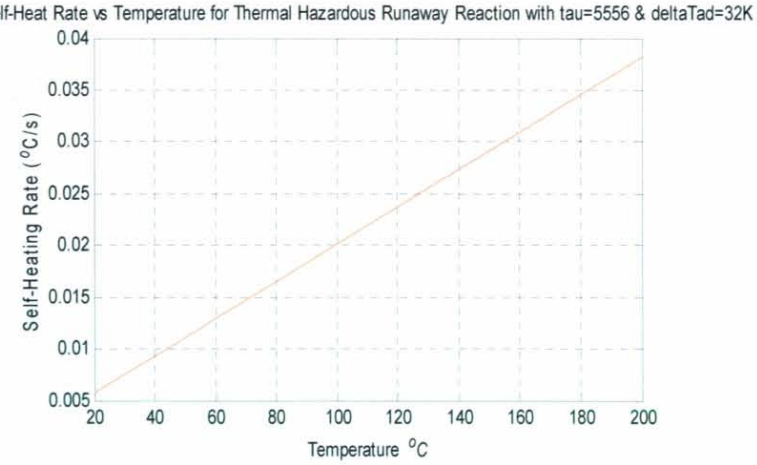

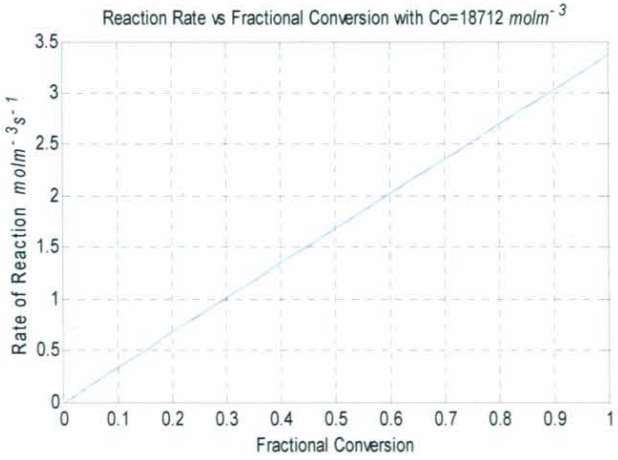

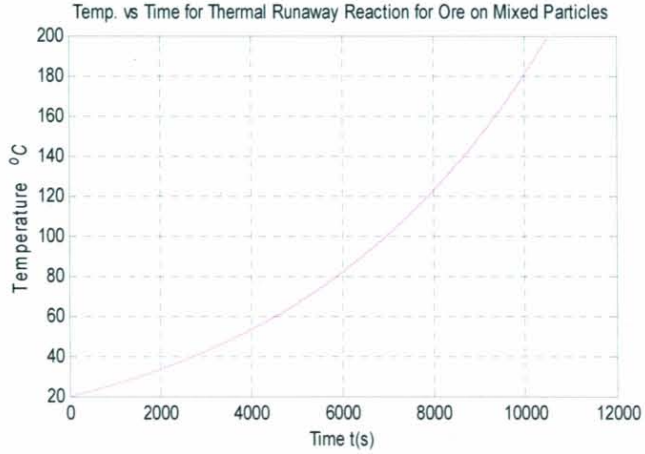

Figure 4.8: Simulated Plot for Ore 05-658 (257m) Experimental Data [Friedman Analysis Data] Mixed Particles

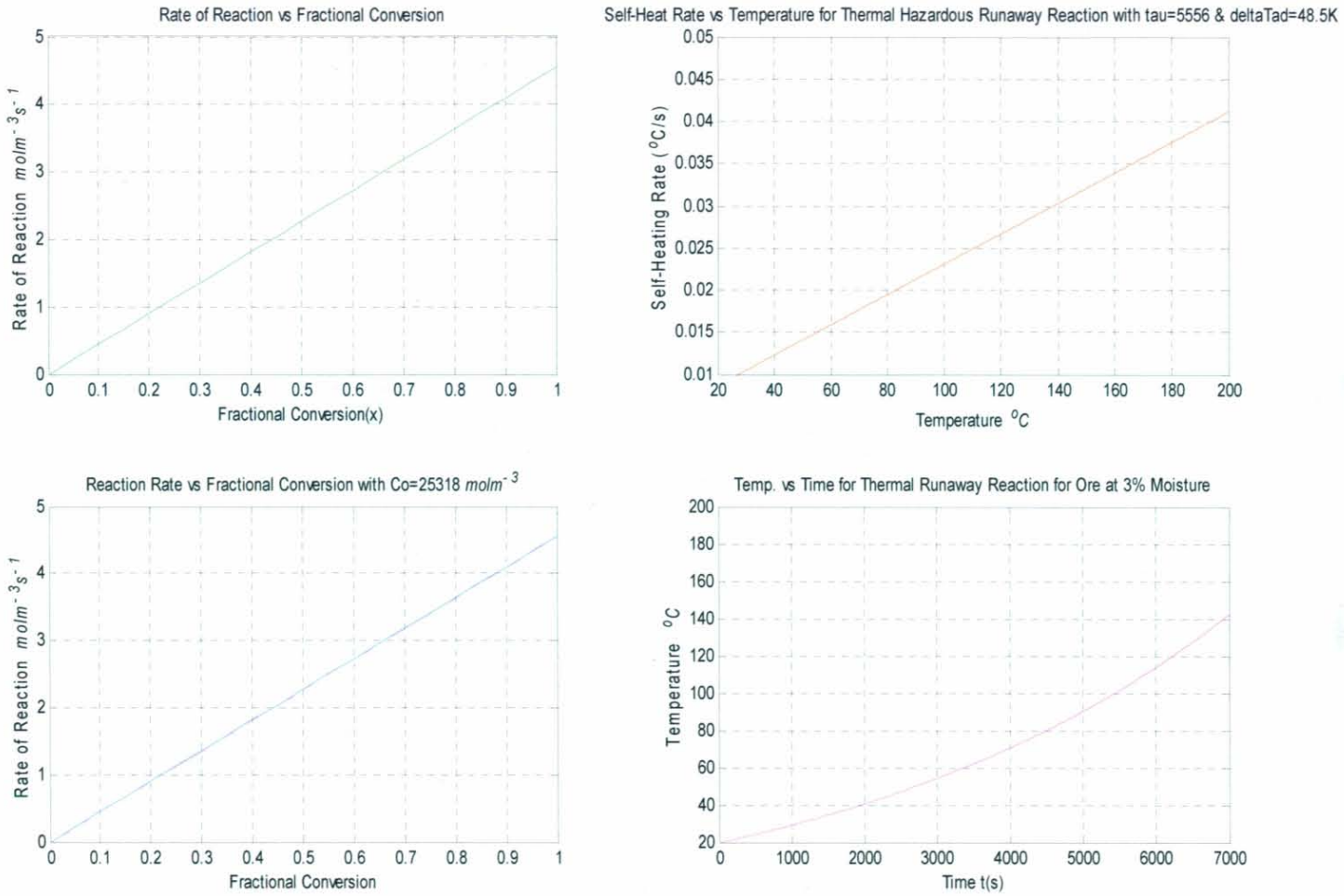

Figure 4.9: Simulated Plot for Ore 03-601 (207m) Experimental Data [Friedman Analysis Data] 3% Moisture

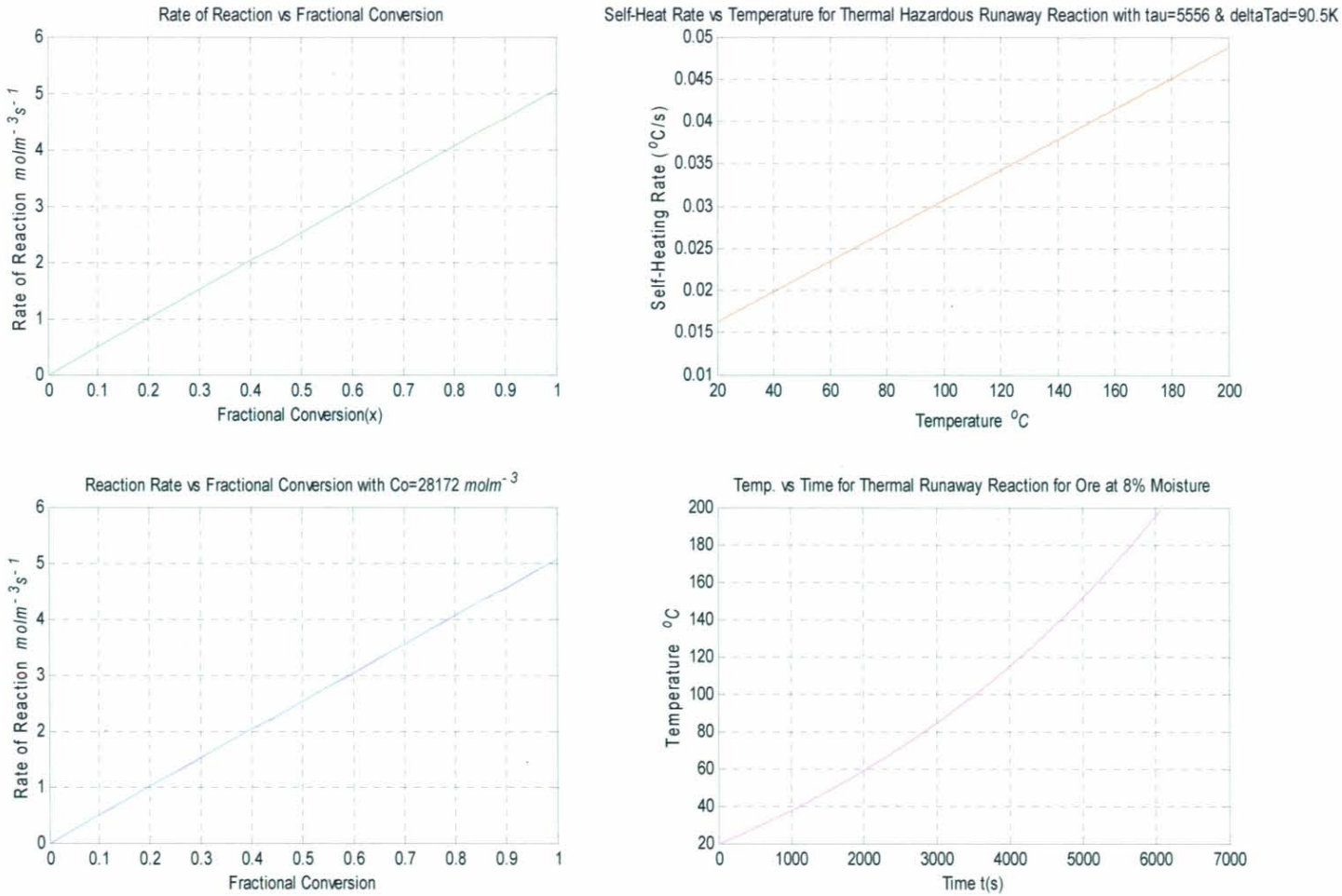

Figure 4.10: Simulated Plot for Ore 03-601 (207m) Experimental Data [Friedman Analysis Data] 8% Moisture

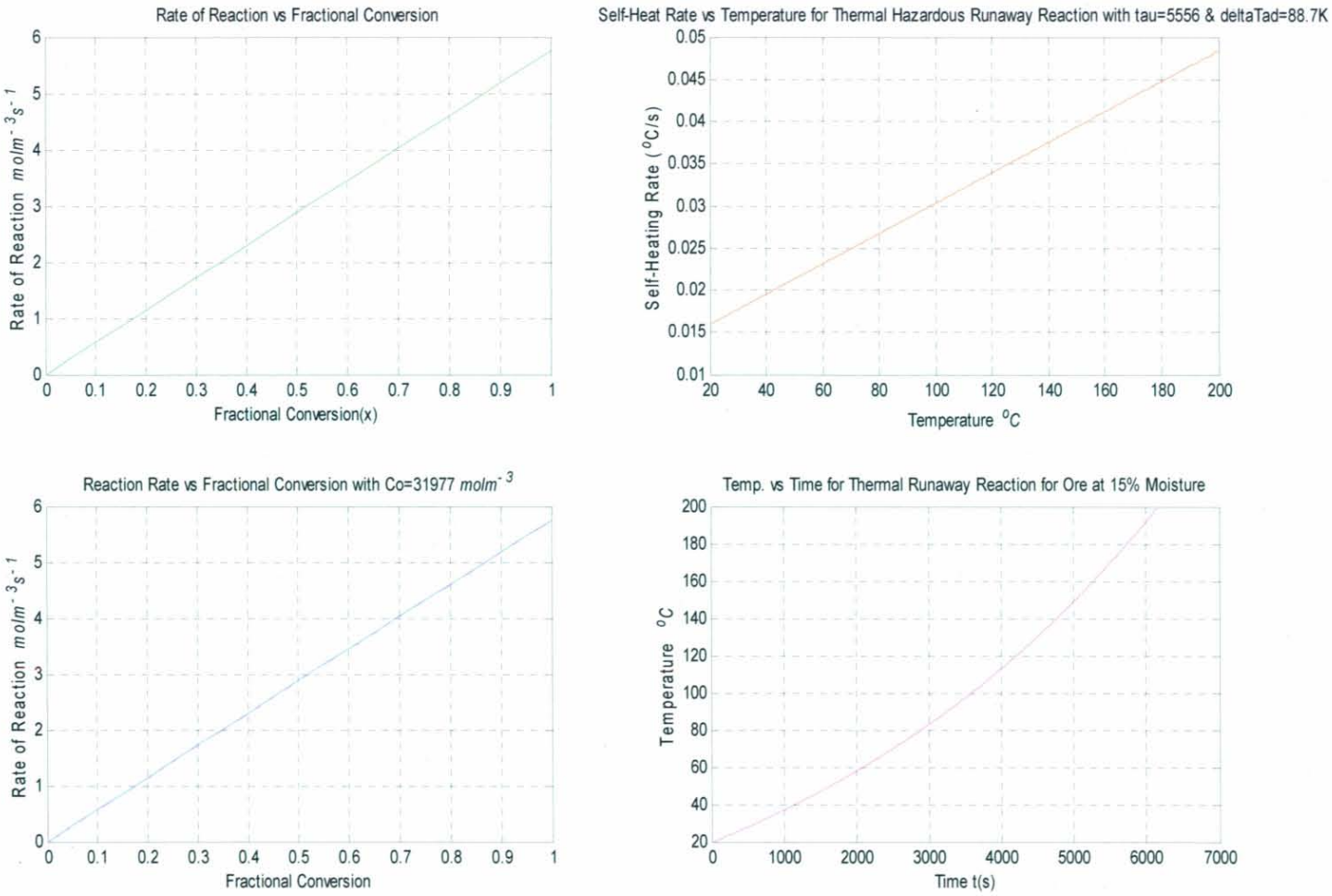

Figure 4.11: Simulated Plot for Ore 03-601 (207m) Experimental Data [Friedman Analysis Data] 15% Moisture

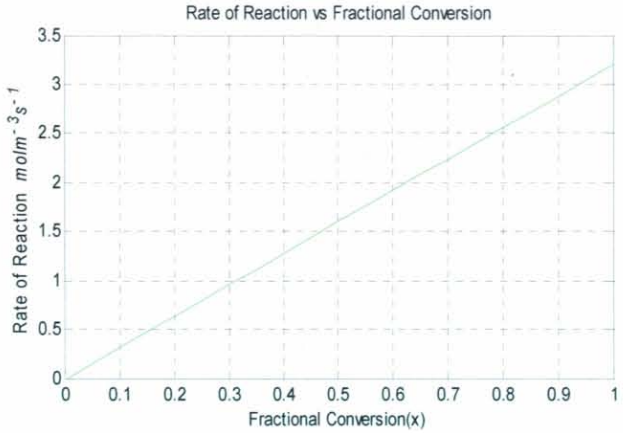

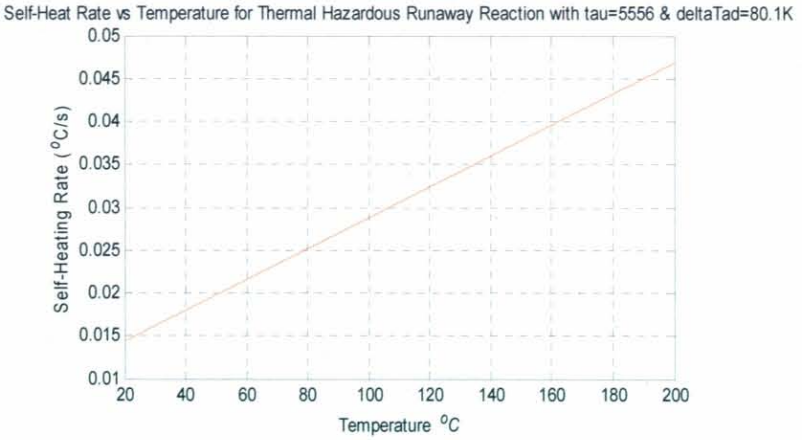

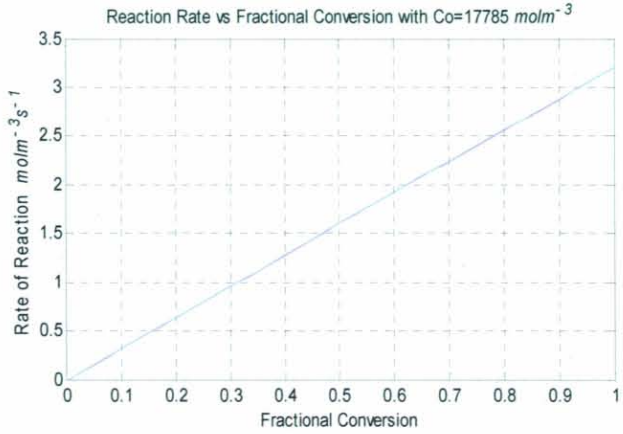

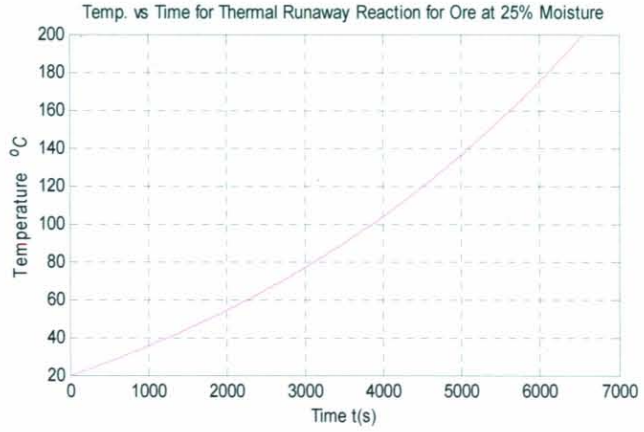

Figure 4.12: Simulated Plot for Ore 03-601 (199m) Experimental Data [Friedman Analysis Data] 25% Moisture

4.2.2 Probability Determination for Thermal Hazardous Reaction Using Ores' Experimental Data

The Arrhenius' constant is first determined for each ore (Appendix E) having known Ea. Gaussian distribution is now used to compute the hazard's probability for each class of Ea and A. Specimen calculation is shown below with the results for other ores computed under different classes are attached in Appendix F. Sensitivity of the results is included in chapter 5 for individual ore indicating the risk classification.

Ore Name: 03-601 (198m) with Mineralogy Effect

The activation energy, Ea, and Arrhenius' constant, A, are 70kJ/mol and 6.337 x $10^{12}s^{-1}$ (ln A= $29.4774s^{-1}$) respectively using TST approach. Arrhenius' constant data is first converted into logarithms form before fitting the data into normal distribution (Appendix B). The thermal hazard probability is computed as:

- Class A (Ea□ 400kJ/mol, μ=570kJ/mol and σ=147.4)59kJ/mol (Tables B1 & B2)

For the activation energy, this becomes:

$$\Pr(z < z_j) = Pr\left(\frac{x-\mu}{\sigma} < \frac{70-570}{147.459}\right)$$

$$= \Pr(z < -3.3908)$$

$$= 0.000348$$

For the Arrhenius' Constant, the expression reduces to:

$$\Pr(z < z_j) = Pr\left(\frac{29.4774-33.4633}{5.12236} < \frac{x-\mu}{\sigma}\right)$$

$$= \Pr(-0.77813 < z)$$

$$= \Pr(z < 0.77813) \text{ by symmetry property}$$

$$= 0.218247 = \mathbf{0.2182}$$

Therefore, the probability of ore self-heating (thermal hazardous reaction) is the joint probability of the individual value (i.e. the product of the two values). This is computed as:

$$\text{Pr (thermal hazard)} = \prod Pr\,(x) = 0.2182 \times 0.000348 = \mathbf{0.00008}$$

- Class B (100 □ Ea ≤ 400kJ/mol, μ=191.461kJ/mol and σ=82.1525kJ/mol)

$$\text{For Ea, Pr}\,(z < z_j) = Pr\left(\frac{x-\mu}{\sigma} < \frac{70-191.461}{82.1525}\right)$$

$$= \text{Pr}\,(z < -1.8785)$$
$$= \text{Pr}\,(z < 1.8785) \quad \text{By symmetry property}$$
$$= 0.0696$$

For the Arrhenius' Constant, the expression reduces to:

$$\text{Pr}\,(z < z_j) = Pr\left(\frac{29.4774-33.4633}{5.12236} < \frac{x-\mu}{\sigma}\right)$$
$$= \text{Pr}\,(-0.77813 < z)$$
$$= \text{Pr}\,(z < 0.77813) \text{ by symmetry property}$$
$$= 0.218247 = \mathbf{0.2182}$$

$$\text{Pr (thermal hazard)} = \prod Pr\,(x) = 0.2182 \times 0.0696 = \mathbf{0.01520}$$

- Class C (10 □ Ea ≤ 100kJ/mol, μ=46.8474kJ/mol and σ=27.03kJ/mol)

$$\text{For Ea, Pr}\,(z < z_j) = Pr\left(\frac{x-\mu}{\sigma} < \frac{70-46.8474}{27.03}\right)$$
$$= \text{Pr}\,(z < 0.8566)$$
$$= 0.8042$$

For **A**, the expression becomes:

$$\text{Pr}\,(z < z_j) = Pr\left(\frac{29.4774-33.4633}{5.12236} < \frac{x-\mu}{\sigma}\right)$$
$$= \text{Pr}\,(-0.77813 < z)$$
$$= \text{Pr}\,(z < 0.77813) \text{ by symmetry properties}$$

$$= 0.218247$$

$$= 0.2182$$

$$\text{Pr (thermal hazard)} = \prod Pr\,(x) = 0.8042 \times 0.2182 = \mathbf{0.1755}$$

- Class D (Ea □ 10kJ/mol, μ=7.702kJ/mol and σ=2.4104kJ/mol)

$$\text{For Ea, Pr}\,(z < z_j) = Pr\left(\frac{x-\mu}{\sigma} < \frac{70-7.702}{2.4104}\right)$$
$$= \text{Pr}\,(z < 25.8456)$$
$$= 1.0$$

For **A**, the expression becomes:

$$\text{Pr}\,(z < z_j) = Pr\left(\frac{29.4774-33.4633}{5.12236} < \frac{x-\mu}{\sigma}\right)$$
$$= \text{Pr}\,(-0.77813 < z)$$
$$= \text{Pr}\,(z < 0.77813) \text{ by symmetry properties}$$
$$= 0.218247$$
$$=0.2182$$
$$\text{Pr (thermal hazard)} = \prod Pr\,(x) = 1.0 \text{ x} 0.2182 = \mathbf{0.2182}$$

All the above is done in MS-Excel by employing two-line commands of standard normal distribution which is used for the spreadsheet results of the Appendix F i.e. "=STANDARDIZE(x, mean, standard_dev)" and " =NORMDIST(x, mean, standard_dev, cumulative)".

The above routine is repeated for each of the ores under the investigated properties of mineralogy, particle size distribution and moisture content. Comprehensive results are presented in Appendix F.

4.2.3 Severity Determination for Thermal Hazardous Reaction Using Ore Experimental Data

The severity of each ore is evaluated using equation [3.22] with enthalpy of the four referenced materials in Table 3.2. Specimen computation is shown here for the above ore sample under effect of mineralogy with details of the others shown in Appendix F.

$$\beta = \frac{\Delta H_{R\ \text{specific reaction}}}{\Delta H_{R\ \text{referenced reaction/ material}}} \qquad 3.22$$

- Ore Severity Based on Referenced Material in Class 1

$$\beta = \frac{\Delta H_{R,ore}}{\Delta H_{R,2-\text{Amino}-4-\text{Chlorophenol}}} \quad \text{Error! Bookmark not defined.}$$

$$= \frac{119.8\ ^{J}/_{g}}{201\ ^{J}/_{g}} = 0.5961 \qquad 3.22$$

- Ore Severity Based on Referenced Material in Class 2

$$\beta = \frac{\Delta H_{R,ore}}{\Delta H_{R,DTBP}} \qquad 3.22$$

$$= \frac{119.8\ ^{J}/_{g}}{557\ ^{J}/_{g}} = 0.21514$$

- Ore Severity Based on Referenced Material in Class 3

$$\beta = \frac{\Delta H_{R,ore}}{\Delta H_{R,2,6-\text{dichlorobenzoyl chloride}}} \qquad 3.22$$

$$= \frac{119.8\ ^{J}/_{g}}{2906\ ^{J}/_{g}} = 0.04123$$

- Ore Severity Based on Referenced Material in Class 4

$$\beta = \frac{\Delta H_{R,ore}}{\Delta H_{R,TNT}} \qquad 3.22$$

$$= \frac{119.8\ ^{J}/_{g}}{5388\ ^{J}/_{g}} = 0.02223$$

4.2.4 Risk Determination for Thermal Hazardous Reaction Using Ore Experimental Data

Risk associated with each ore is computed using equation [3.27] by multiplying the computed probability of hazard with the corresponding severity for each risk class i.e.

$$Risk = Frequency\ of\ Occurrence\ (probability) \times Severity(consequence, \beta) \qquad 3.27$$

$$= Pr \times \beta$$

For the ore 03-601 (198m) treated above, the associated risk under each class is:

- Low Risk Class (Class 1)

$$Risk_{low} = 0.21825 \times 0.59612$$
$$= 0.1301$$

- Medium Risk Class (Class 2)

$$Risk_{medium} = 0.1755 \times 0.2151$$
$$= 0.03776$$

- High Risk Class (Class 3)

$$Risk_{high} = 0.01520 \times 0.04123$$
$$= 0.000627$$

- Extremely High Risk Class (Class 4)

$$Risk_{extremely\ high} = 0.0008 \times 0.022233$$
$$= 1.69 \times 10^{-6}$$

4.2.5 Risk Ranking for Thermal Hazardous Reaction Using Ore Experimental Data

The computed risk for the ore sample with respect to the investigated property is compared with the values on the pre-defined risk scale of Table 3.3 and ranked as belonging to one of the four classes. For the ore 03-601 used in above example, it was found that it belong to medium risk class. This is shown in the Table below:

Table 4.1: Risk Categorization for Thermal Hazard for Ore 03-601(198m) Mineralogy Effect

Parameter	*Risk Class 1*	*Risk Class 2*	*Risk Class 3*	*Risk Class 4*
Hazard Probability	0.2183	0.1755	0.0152	0.00008
Severity, β	0.5961	0.2151	0.0412	0.0222
Associated Risk	0.1301	0.0378	6.27×10^{-4}	1.69×10^{-6}
Risk Ranking Range	10^{0}-10^{-3}	2.0×10^{-1} - 10^{-4}	10^{-3} - 10^{-5}	10^{-5} – 10^{-8}
Equivalent Risk Colour Code				

Inference: The associated risk with respect to the investigated parameter belongs to medium risk class.

Chapter 5

Results and Discussion

5.1 Sensitivity Analysis of Results

The proposed model has two important parameters that are critical to the reliability and correctness of the results: "ΔTad" and "τ". The effect of "τ" is briefly discussed in chapter 4. The adiabatic temperature, ΔTad must be accurately determined during the experiment as it is crucial to the determination of other parameters like time to maximum rate under adiabatic condition and induction time as well as self-heat rate. High τ-value implies high inventory and feed rate in terms of material stockpile or accumulation during processing and cooling failure. This is important as intensification is taken over in most processing operations.

Any error in its determination of "ΔTad" and "τ" will translate to high magnitude of errors in other dependent parameters. Therefore, accuracy of the results depends majorly on these two parameters. This is why correct base line must be obtained for the DSC signals during evaluation of the experimental results. ΔTad is a measure of the drift of runaway reaction from safety zone. The larger the ΔTad value, the higher the enthalpy and severity of the reaction and the more cooling system required. This means that enthalpy of reaction is very high with high ΔTad value.

Effect of Varying Only ΔTad Value with Investigated Parameters on Self-Heating

Semenov diagram illustrates the characteristic operating points for the balance between enthalpy of reaction and cooling to quantify the effect of simple drift of operating points from the intersection of the curves representing these two parameters. These intersection

points govern the operating zones or safety boundaries for prevention of runaway reactions. The importance of variation of "ΔTad" at constant τ is illustrated by the two useful plots of SH vs. Temperature and Temperature vs. Time displayed in Figures 5.1-5.12. The two upper curves in each figure illustrate the anticipated behaviour over longer duration and higher temperature regions (exaggeration) while the lower ones show the same behaviour in lower temperature regions. In each case, the self-heating rate is between 0.005°C/s to 0.075°C/s for temperature range of 20°C□T≤50°C for all the ore samples.

Effect of Varying Parameters τ, ΔTad and Moisture Contents on Self-Heating

The effect of τ is critically observed by fixing the varying concentration, C_o, at their respective values used for the experiment and varying τ for the ore 03-601(207m) with various moisture content and simulate the experiment again. The results are as shown in Figures 5.13-5.24 for τ= 5556s, 5.6 x10^4s and 5.6 x 10^5s at the various levels of measured ΔTad. This is done to assess the combined effects of most reactive fine particles of size 75μm, varying concentration, changing ΔTad and moisture content at the fractional conversion 0-1.0 so that meaningful conclusions can be drawn. Also, presence of moisture enhances reactivity of the ores and gaseous diffusion.

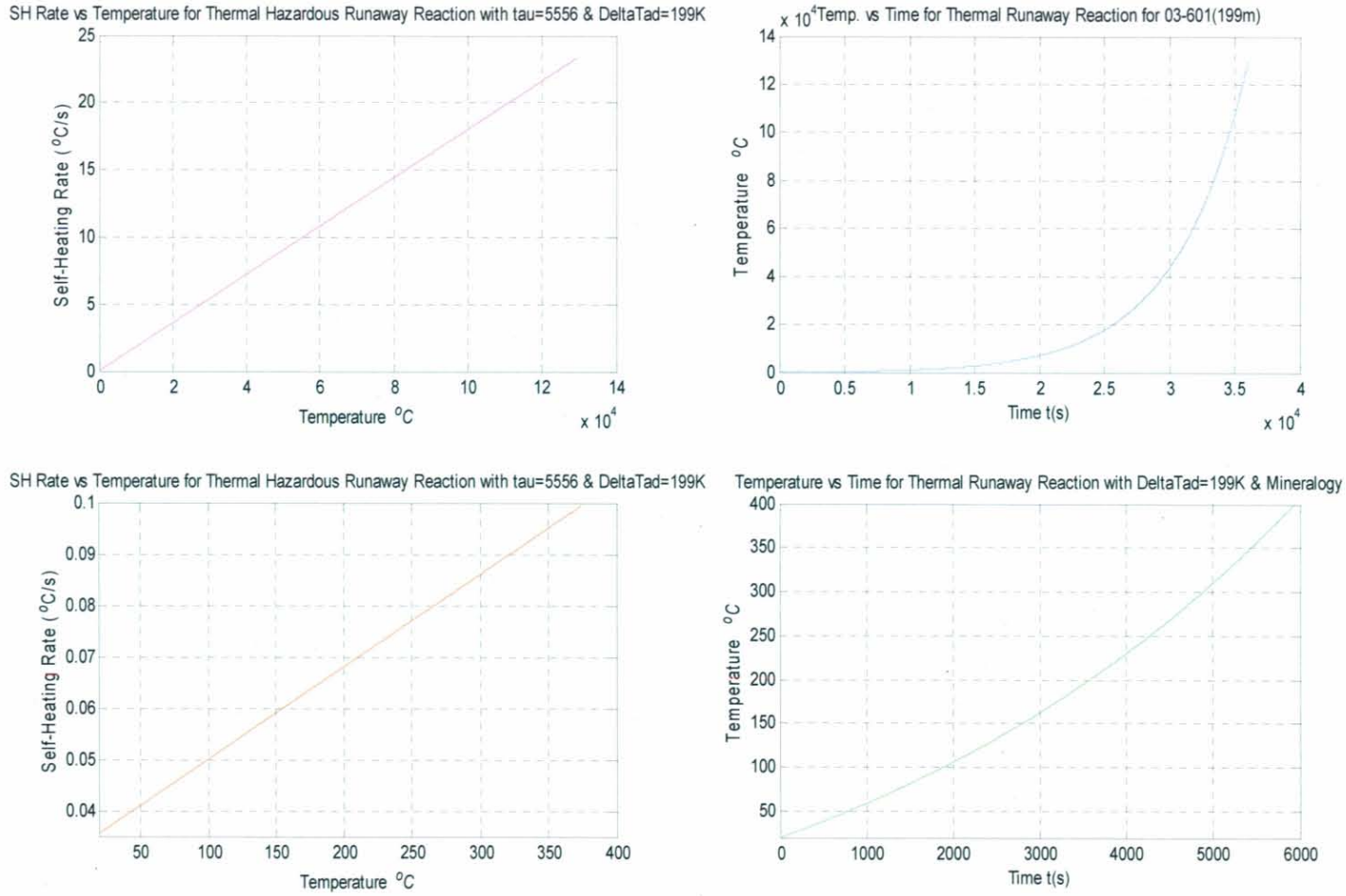

Figure 5.1: SH Rate vs. Temperature and Temperature-Time Plots for Thermal Hazardous Ore 03-601(199m) Mineralogy

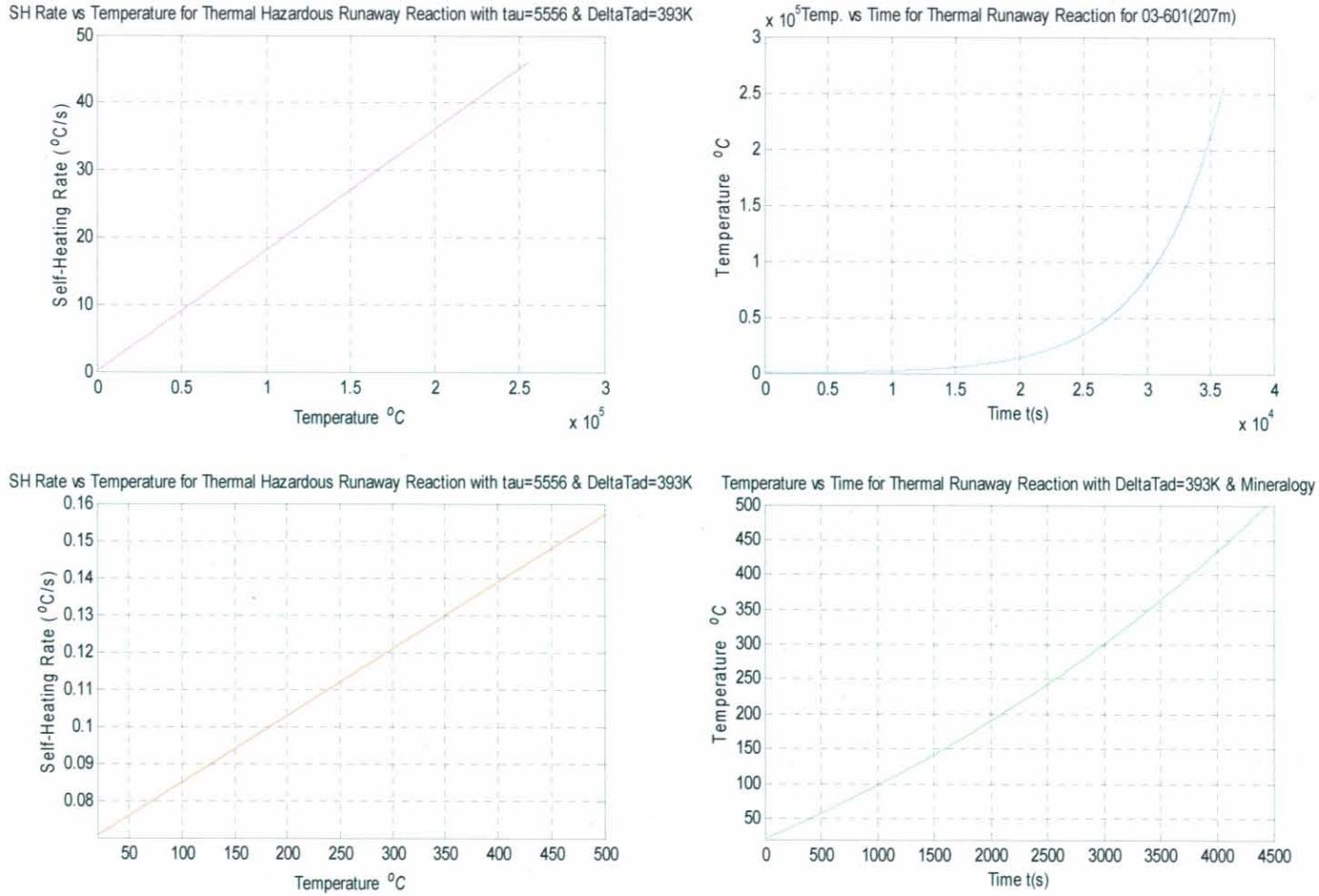

Figure 5.2: SH Rate vs. Temperature-Time Plots for Thermal Hazardous Ore 03-601(207m) Mineralogy

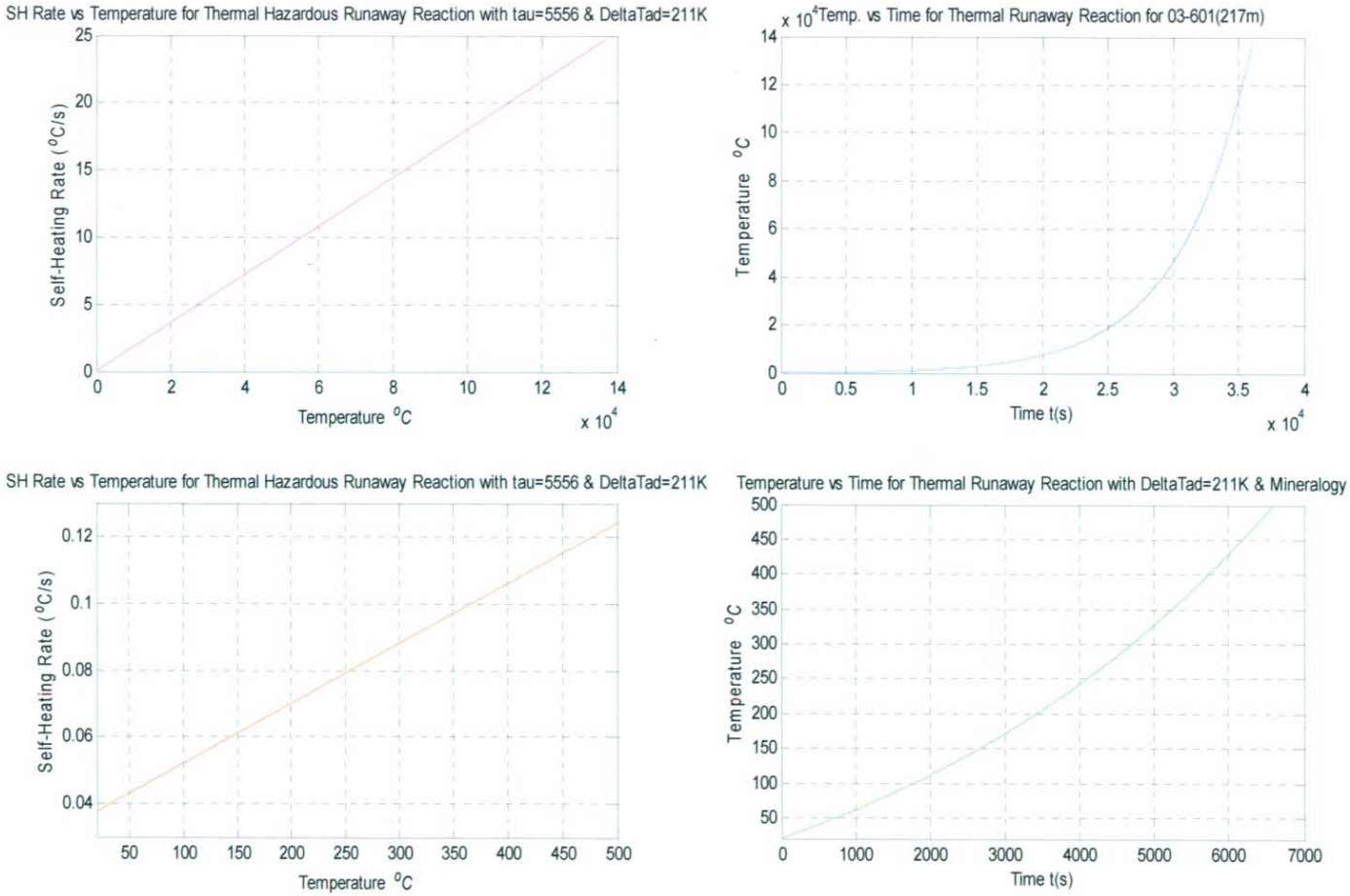

Figure 5.3: SH Rate vs. Temperature-Time Plots for Thermal Hazardous Ore 03-601(217m) Mineralogy

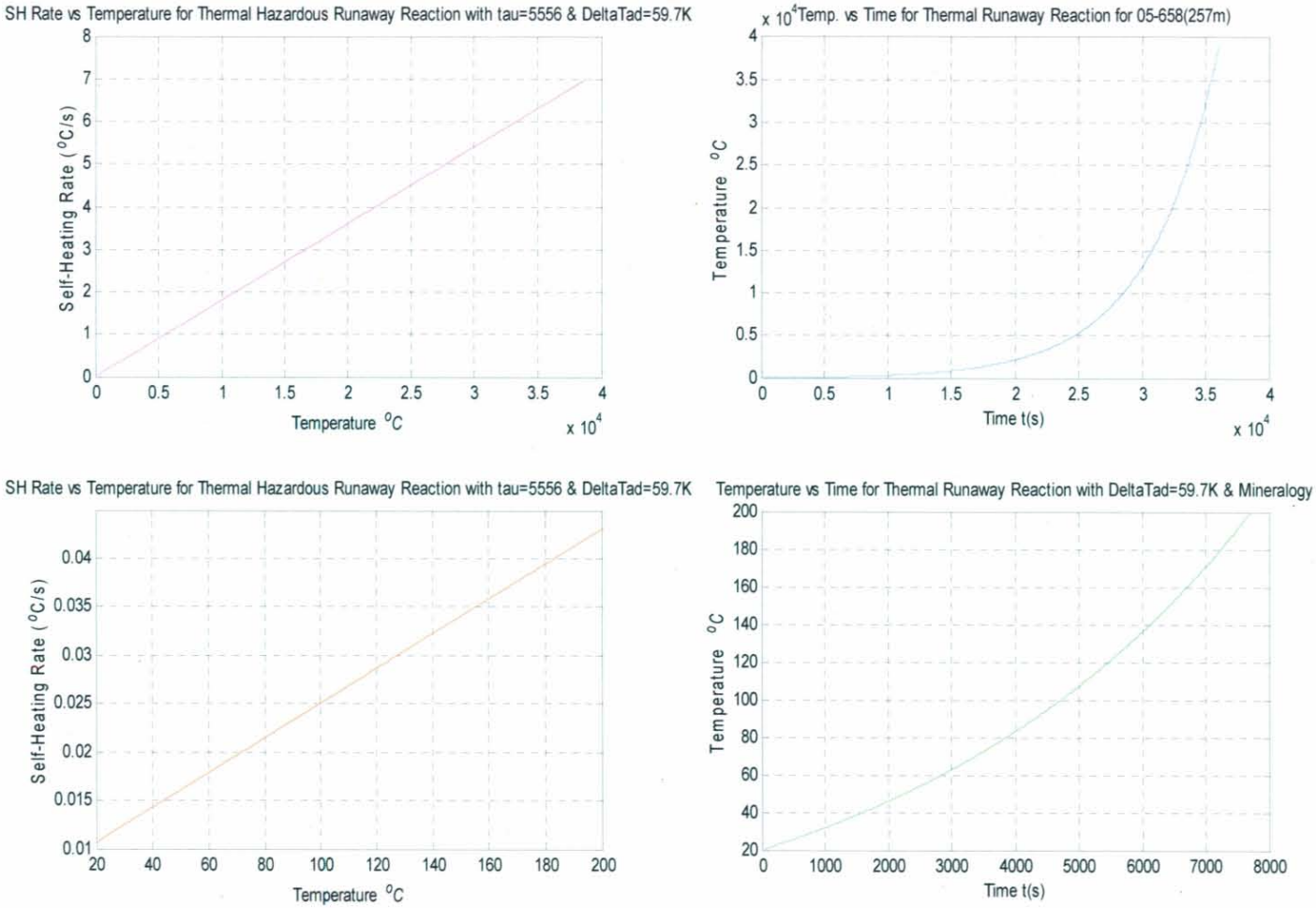

Figure 5.4: SH Rate vs. Temperature-Time Plots for Thermal Hazardous Ore 05-658(257m) Mineralogy

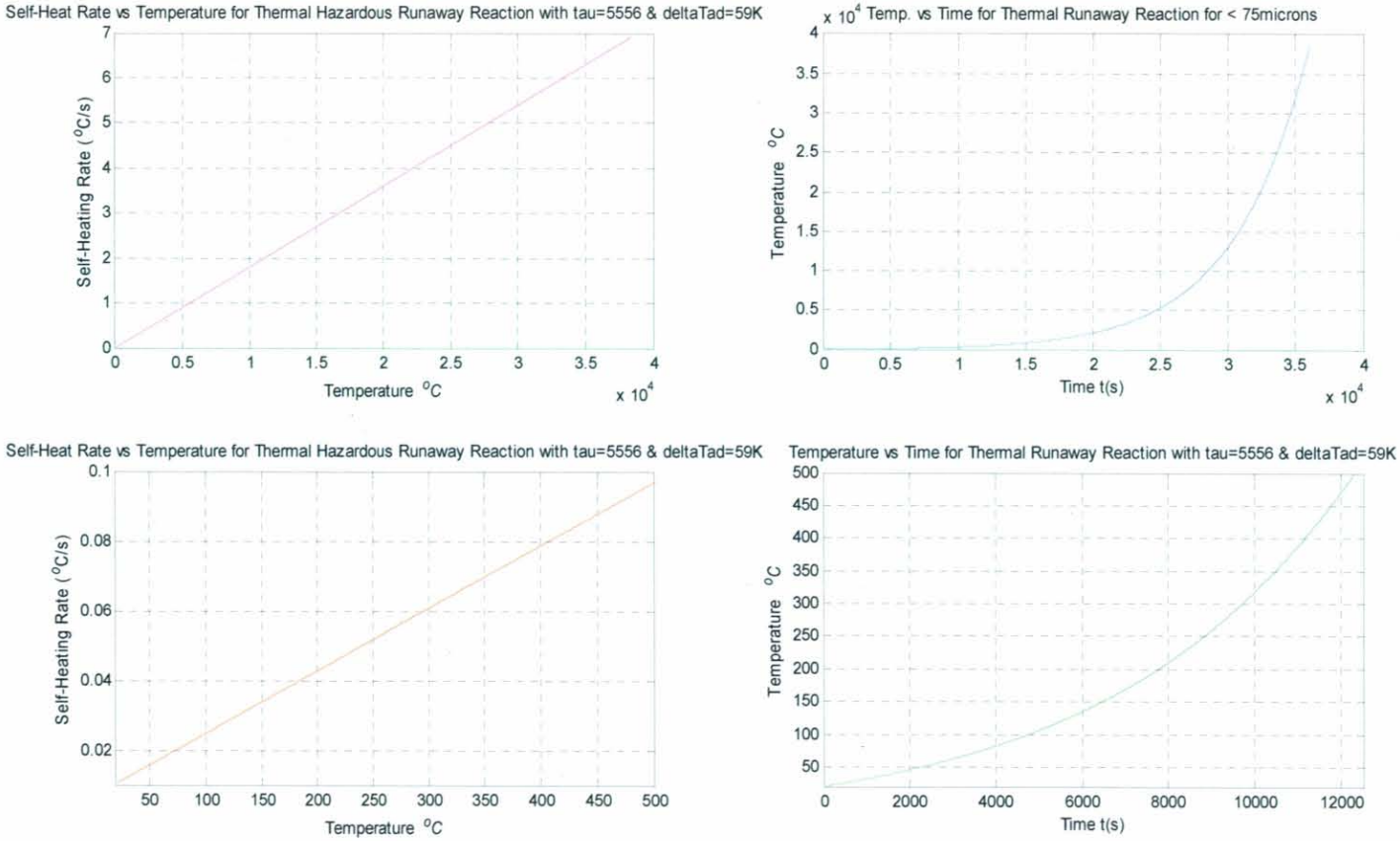

Figure 5.5: SH Rate vs. Temperature-Time Plots for Thermal Hazardous Ore 05-658(257m) □75µm Particles

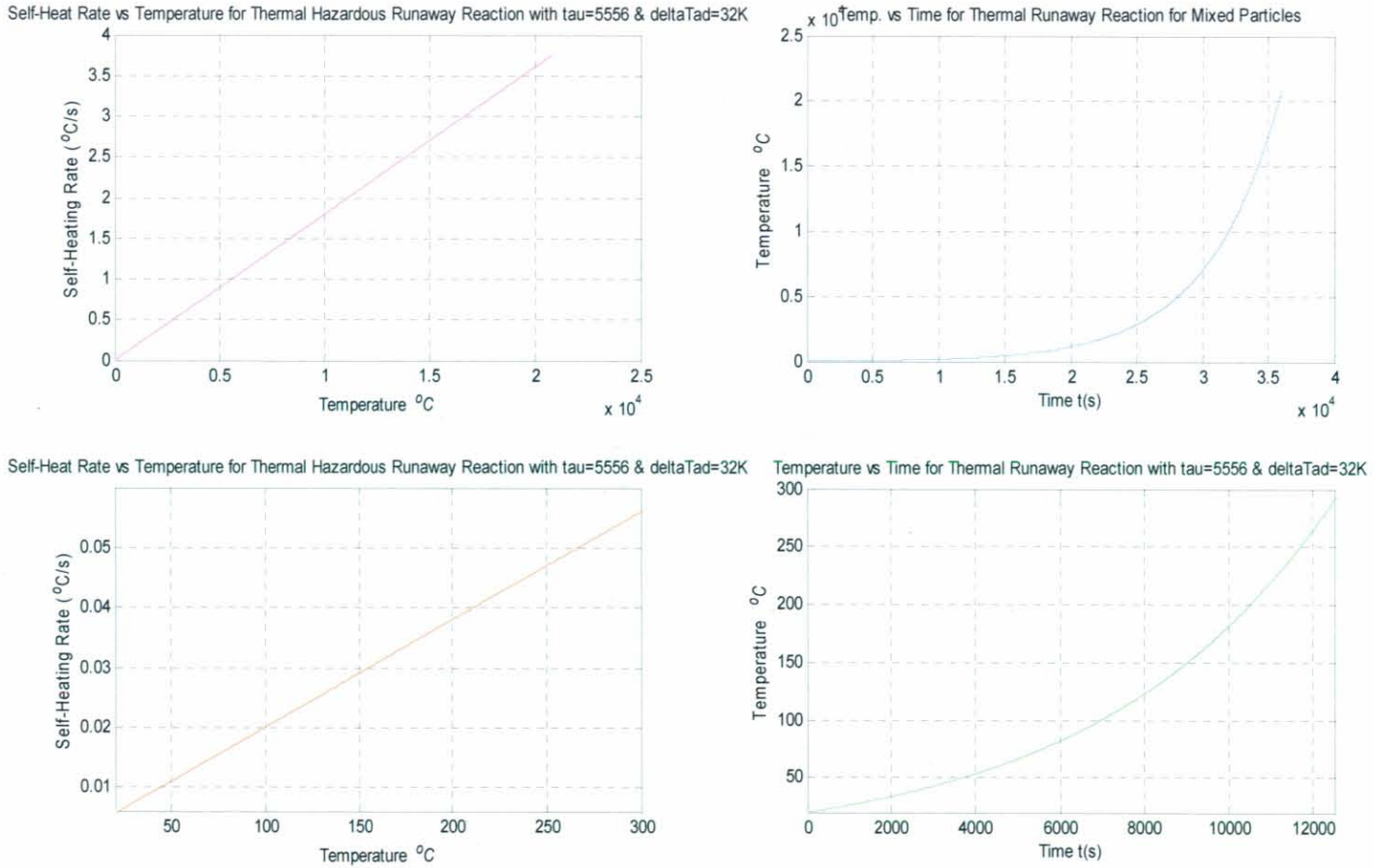

Figure 5.6: SH Rate vs. Temperature-Time Plots for Thermal Hazardous Ore 05-658(257m) Mixed Particles

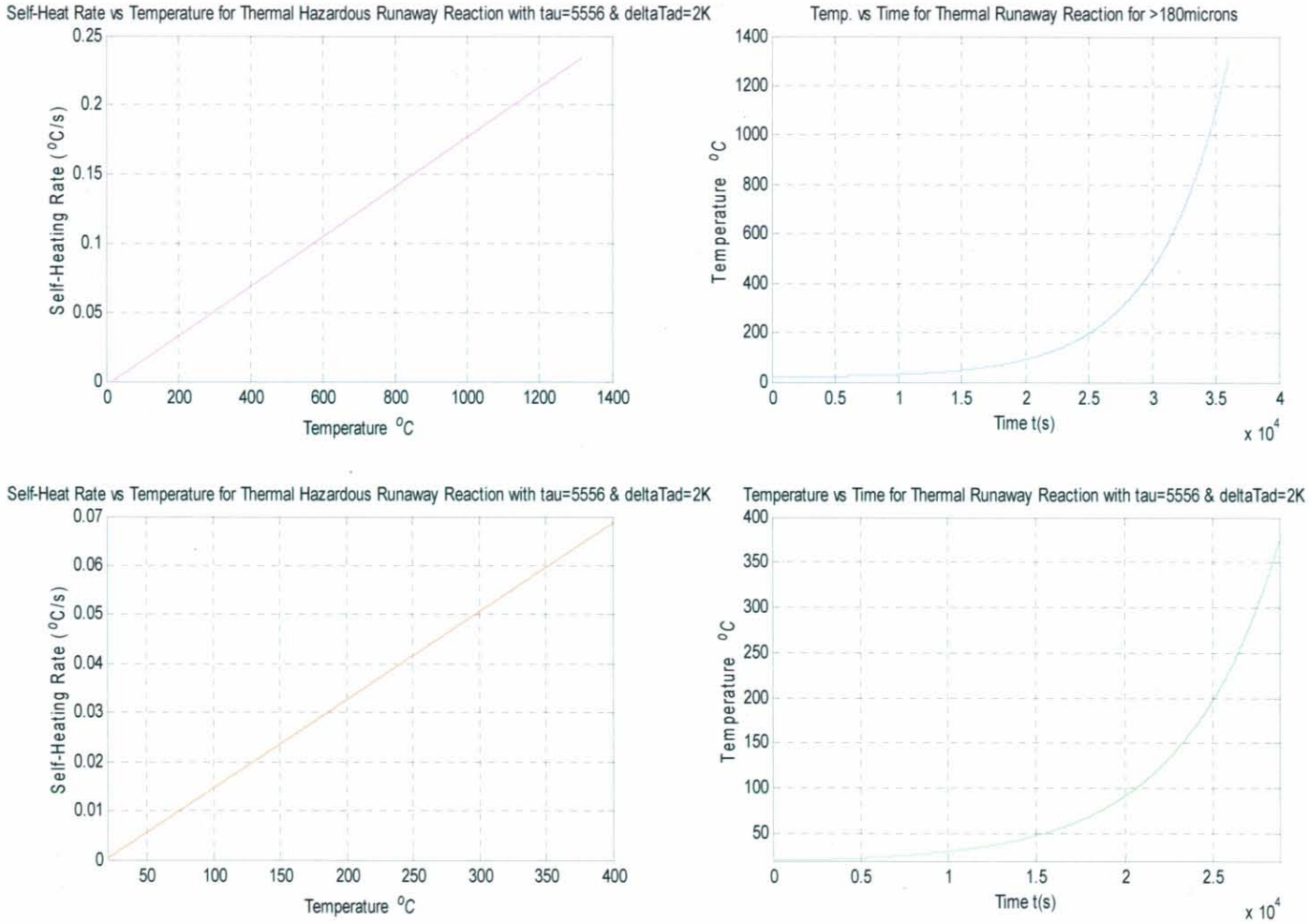

Figure 5.7: SH Rate vs.Temperature-Time Plots for Thermal Hazardous Ore 05-658(257m) □180μm Particles

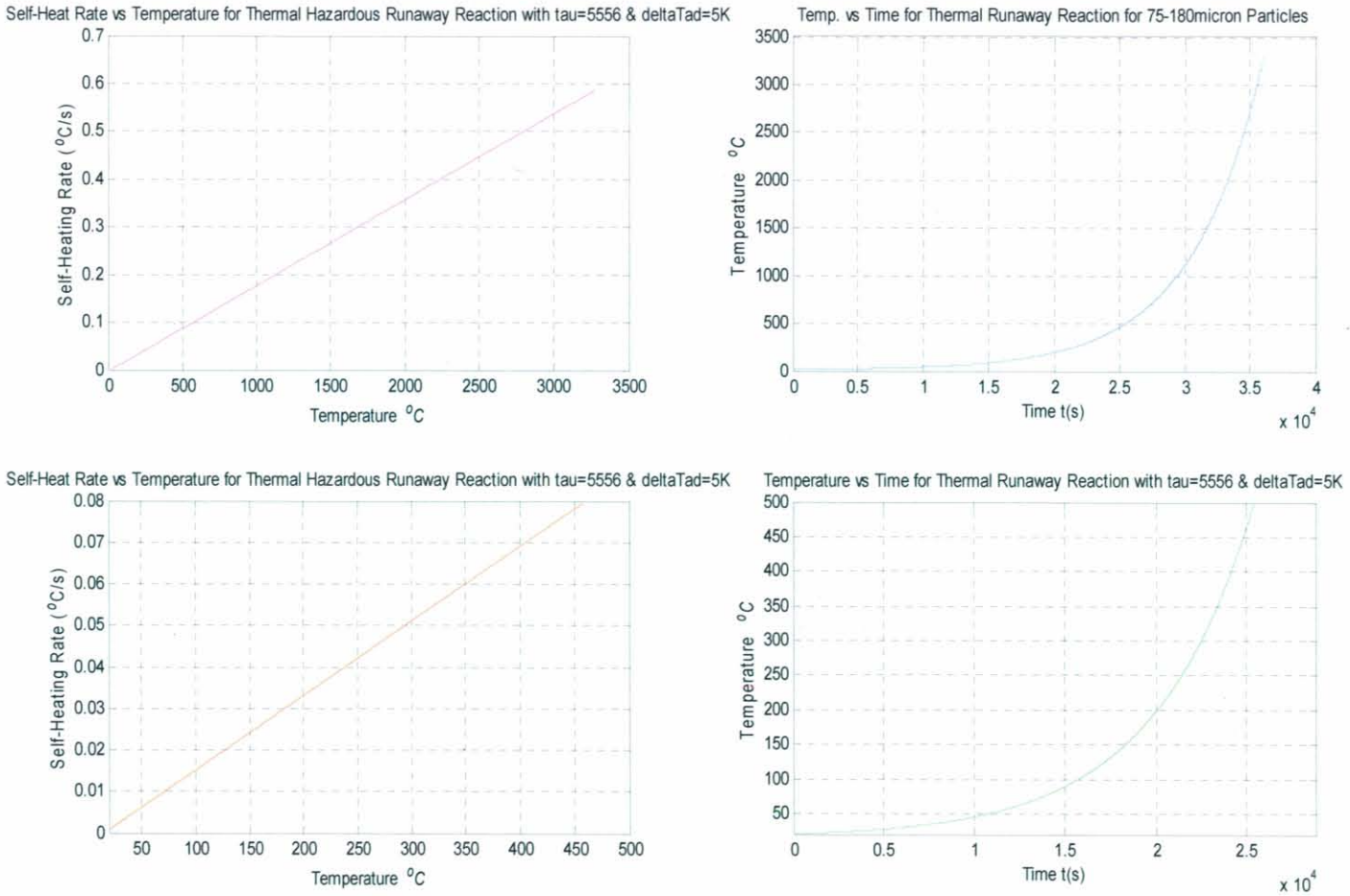

Figure 5.8: SH Rate vs. Temperature-Time Plots for Thermal Hazardous Ore 05-658(257m) 75-180µm Particle

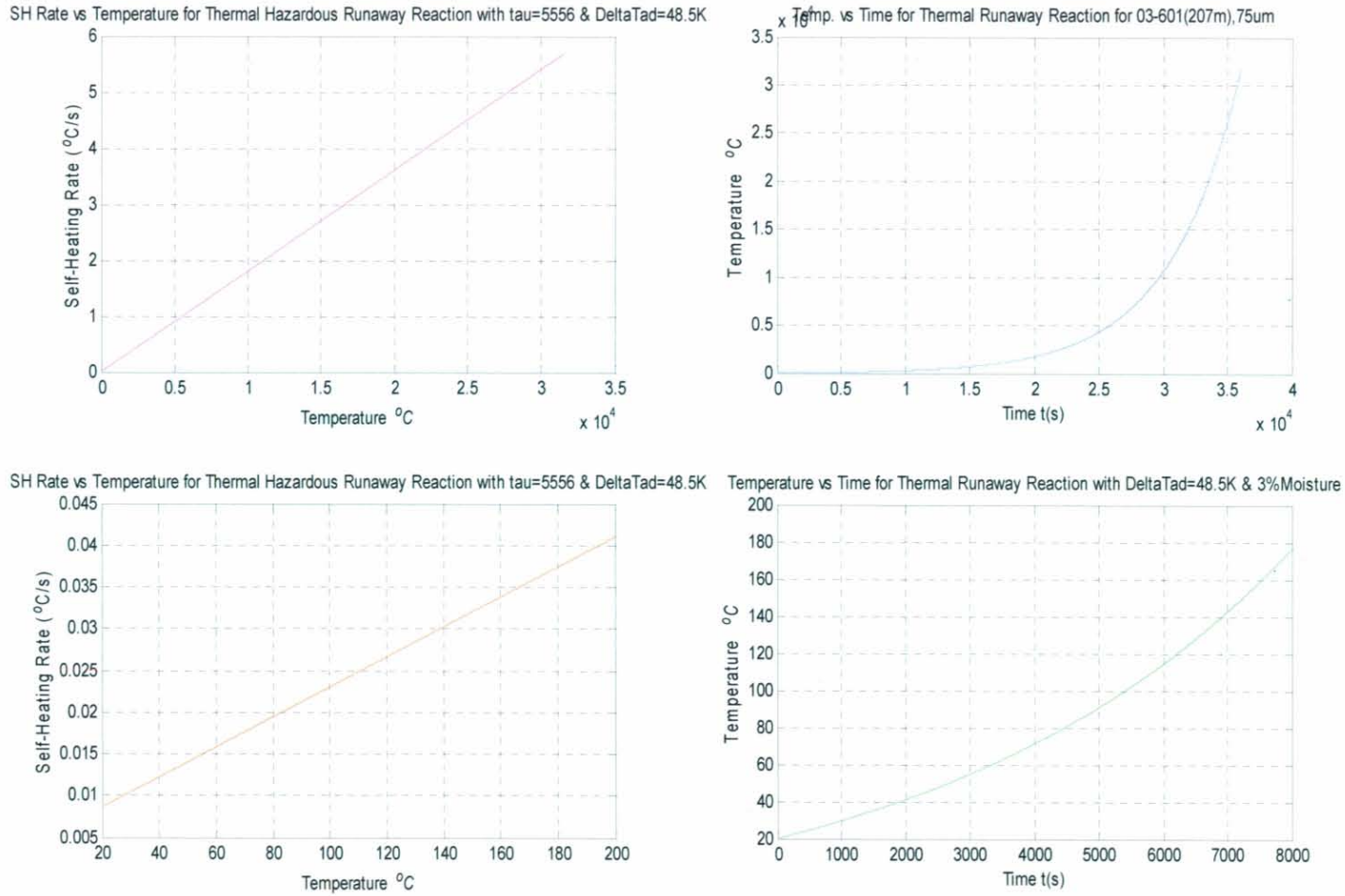

Figure 5.9: SH Rate vs. Temperature-Time Plots for Thermal Hazardous Ore 03-601(207m) 3% Moisture

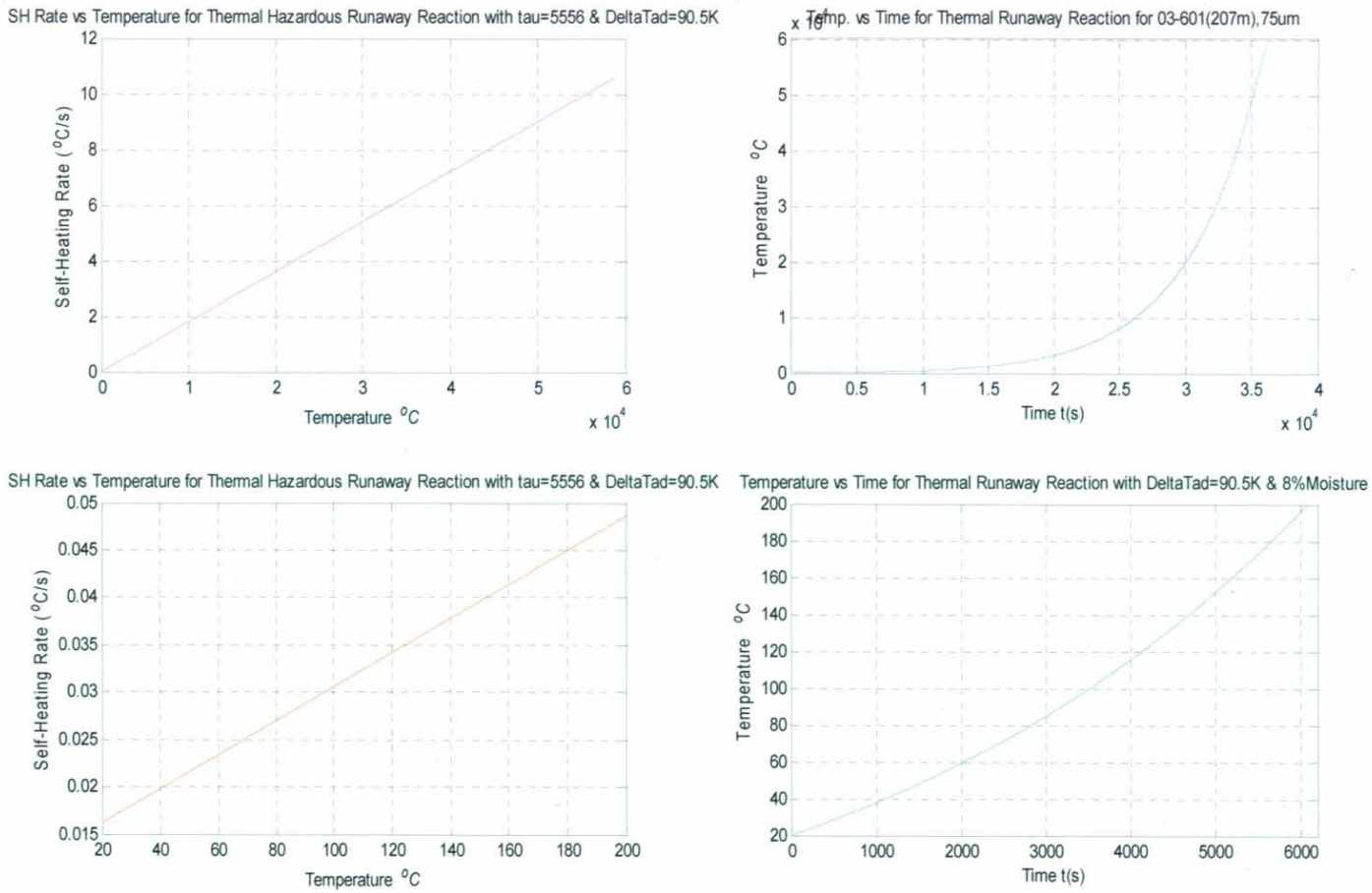

Figure 5.10: SH Rate vs. Temperature-Time Plots for Thermal Hazardous Ore 03-601(207m) 8% Moisture

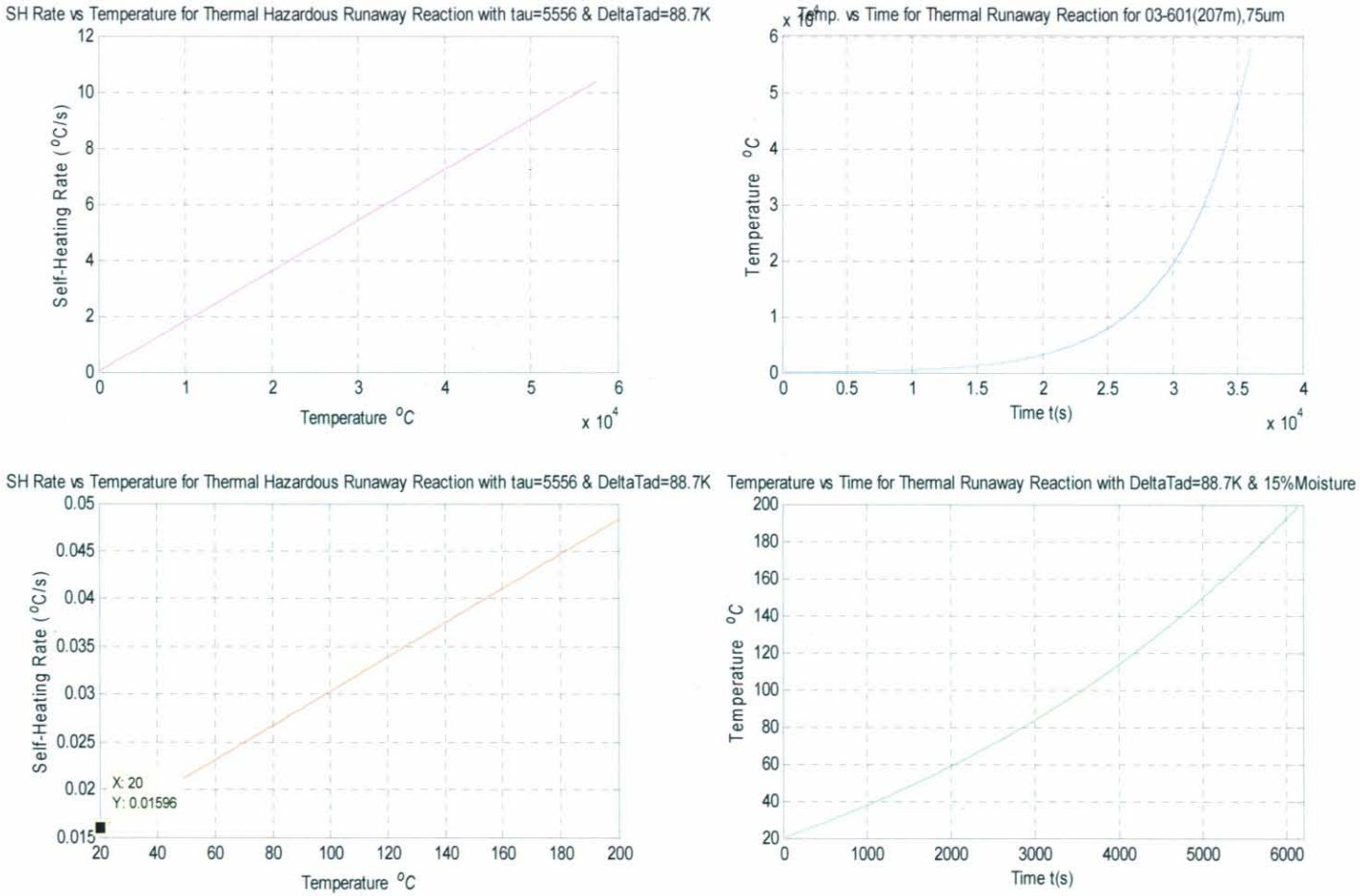

Figure 5.11: SH Rate vs.Temperature-Time Plots for Thermal Hazardous Ore 03-601(207m) 15% Moisture

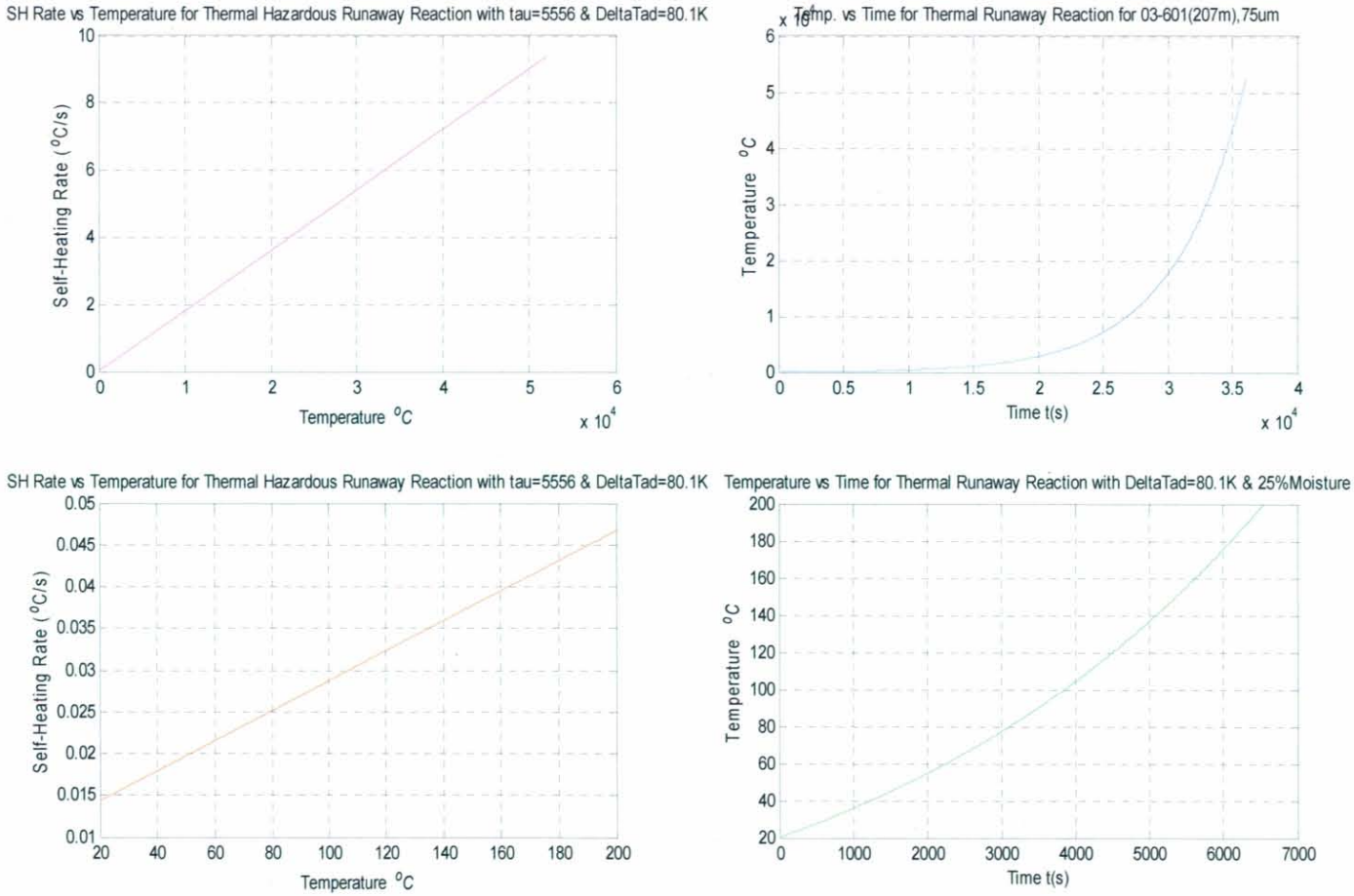

Figure 5.12: SH Rate vs. Temperature-Time Plots for Thermal Hazardous Ore 03-601(207m) 25% Moisture

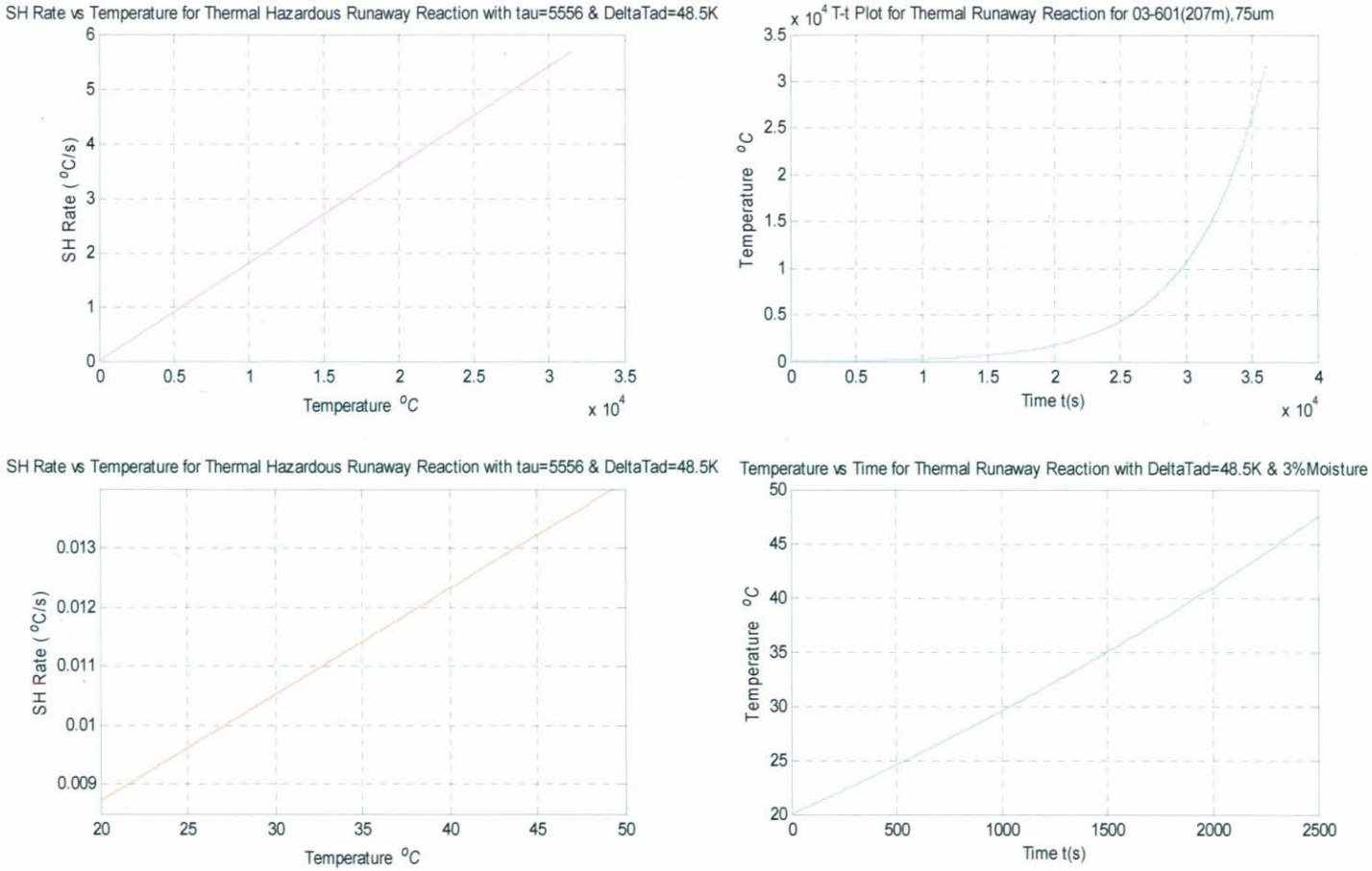

Figure 5.13: SH Rate vs. Temperature and Temperature-Time Plots for Thermal Hazardous Ore 03-601(207m) at 3% Moisture & *Tau= 5556s*

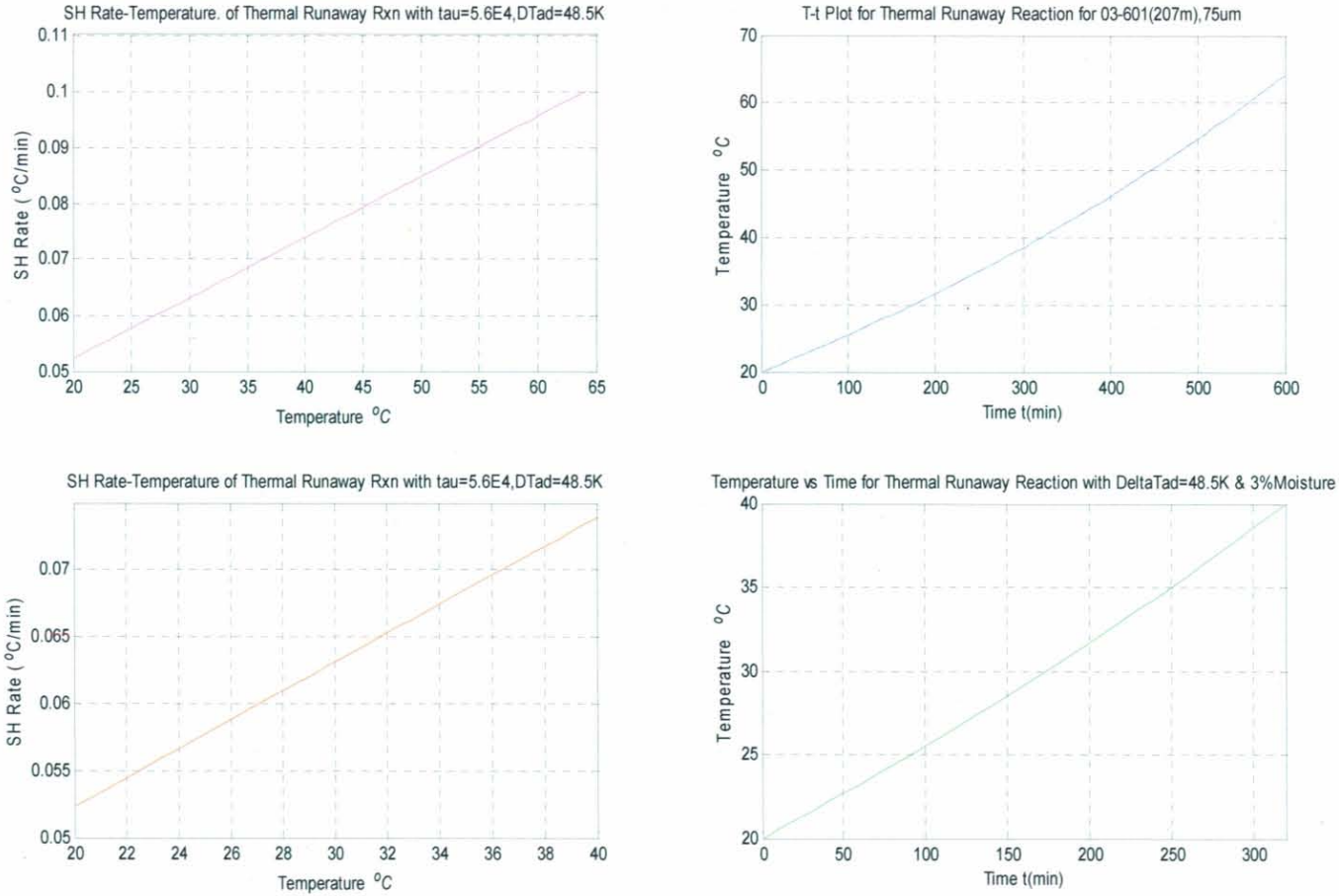

Figure 5.14: SH Rate vs. Temperature and Temperature-Time Plots for Thermal Hazardous Ore 03-601(207m) at 3% Moisture & *Tau= 55556s*

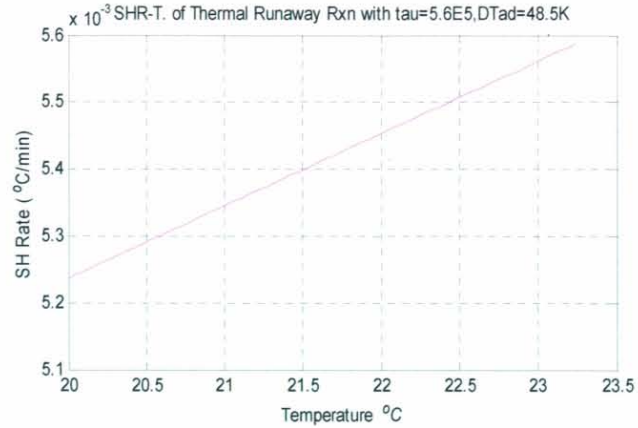

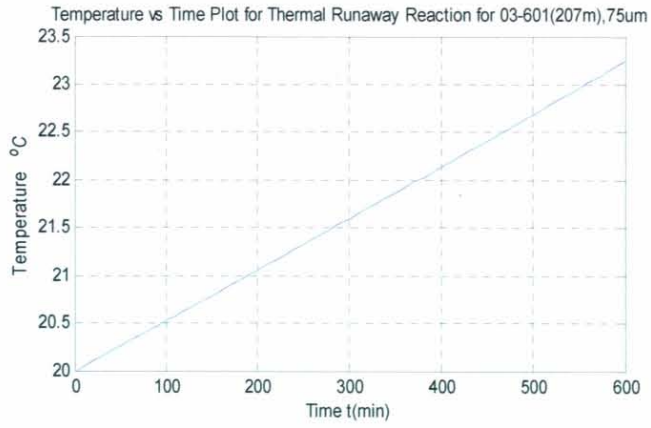

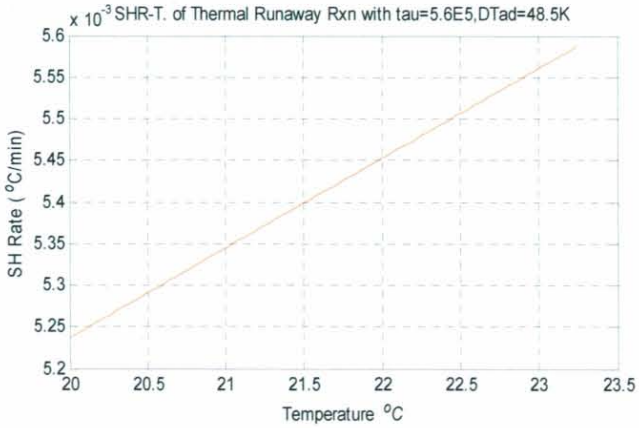

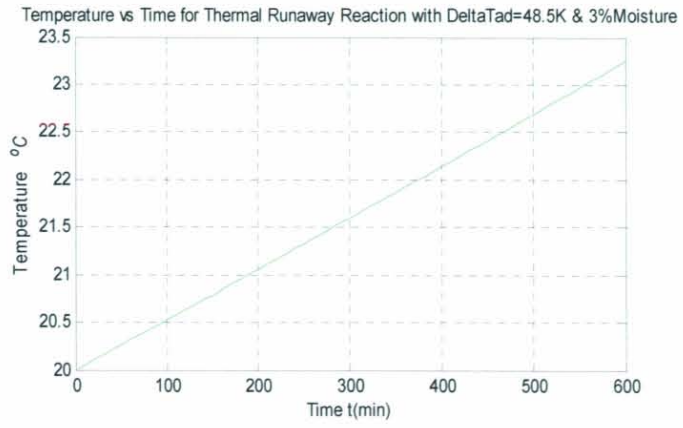

Figure 5.15: SH Rate vs. Temperature and Temperature-Time Plots for Thermal Hazardous Ore 03-601(207m) at 3% Moisture & *Tau= 555556s*

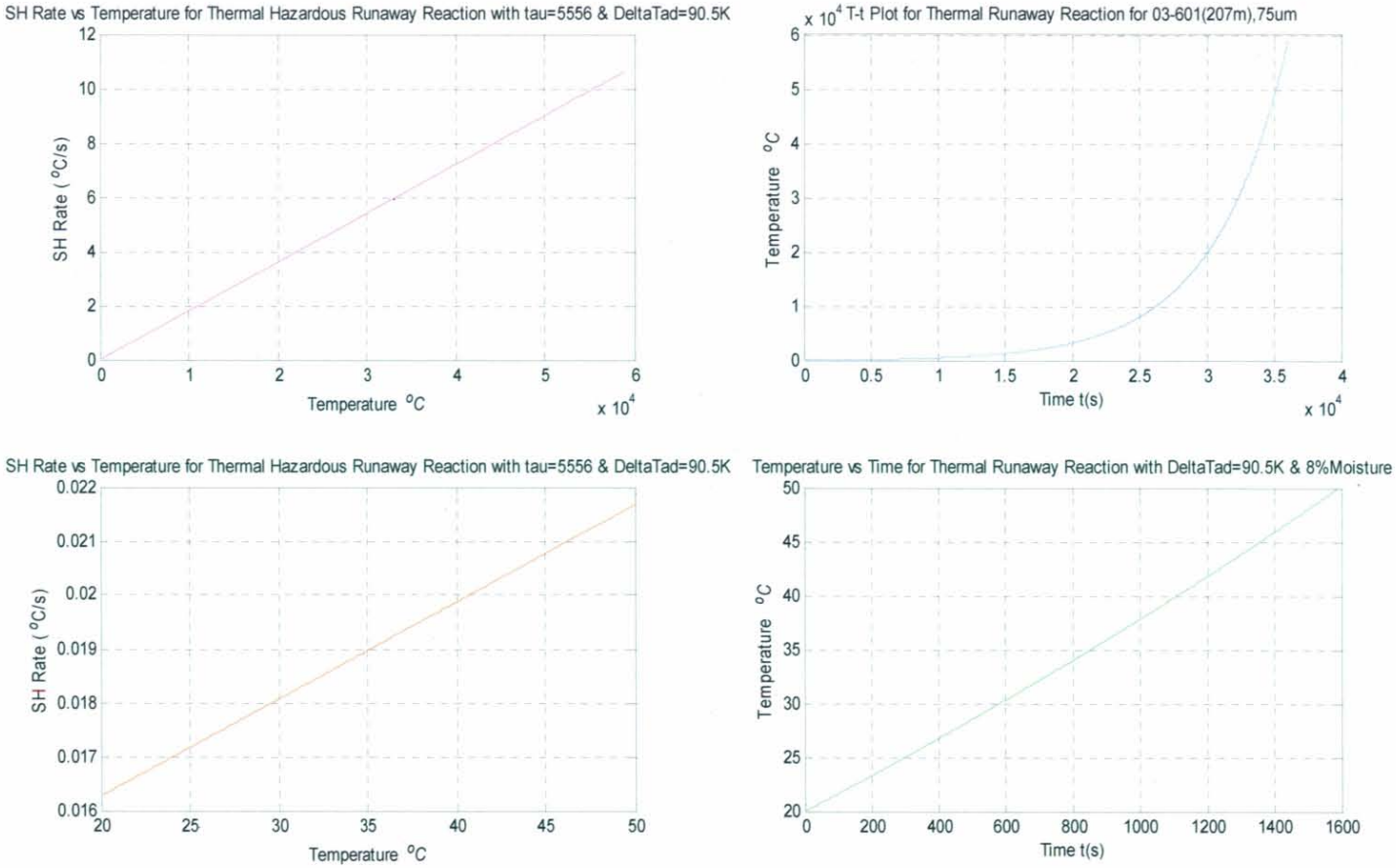

Figure 5.16: SH Rate vs. Temperature and Temperature-Time Plots for Thermal Hazardous Ore 03-601(207m) at 8% Moisture & *Tau= 5556s*

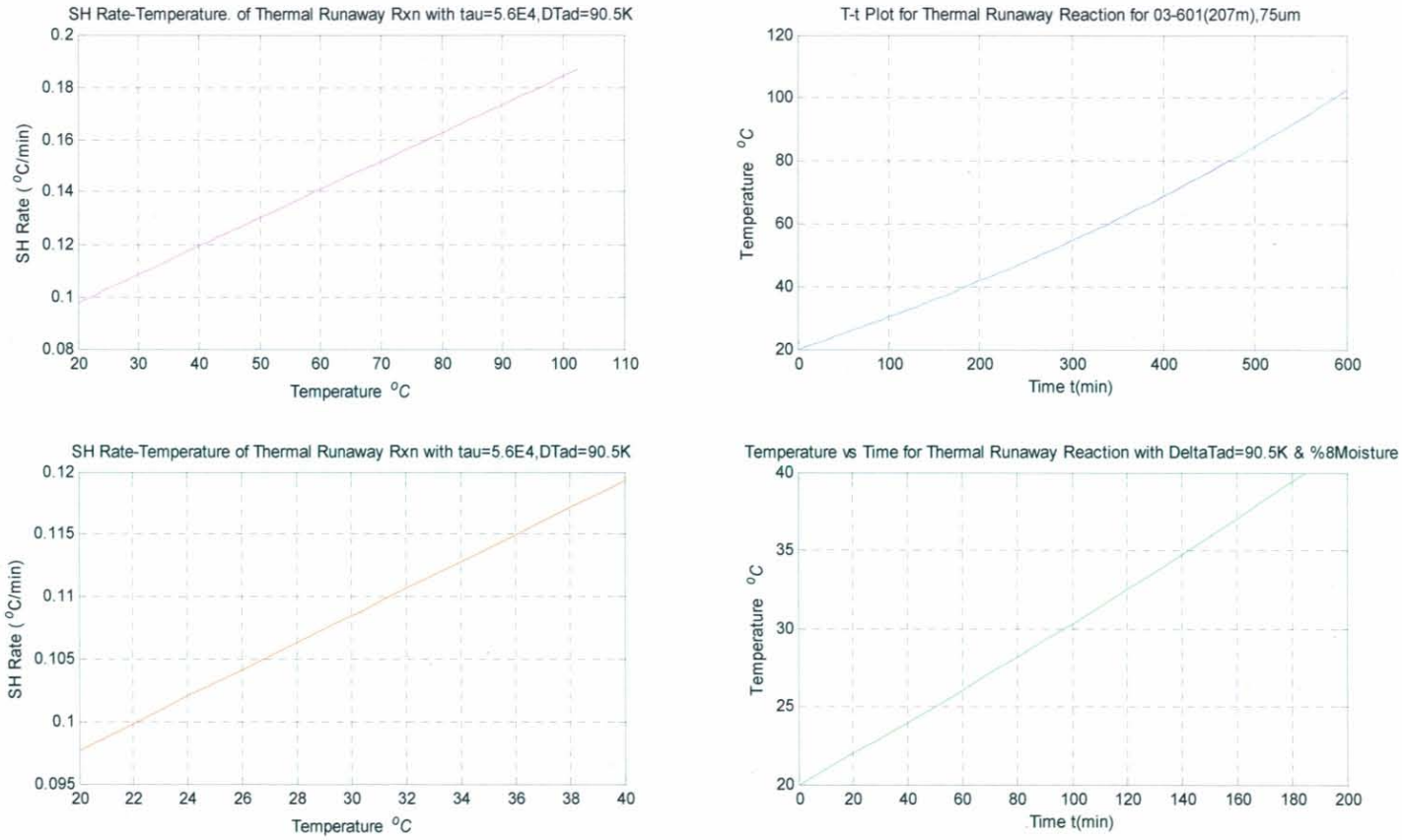

Figure 5.17: SH Rate vs. Temperature and Temperature-Time Plots for Thermal Hazardous Ore 03-601(207m) at 8% Moisture & *Tau= 55556s*

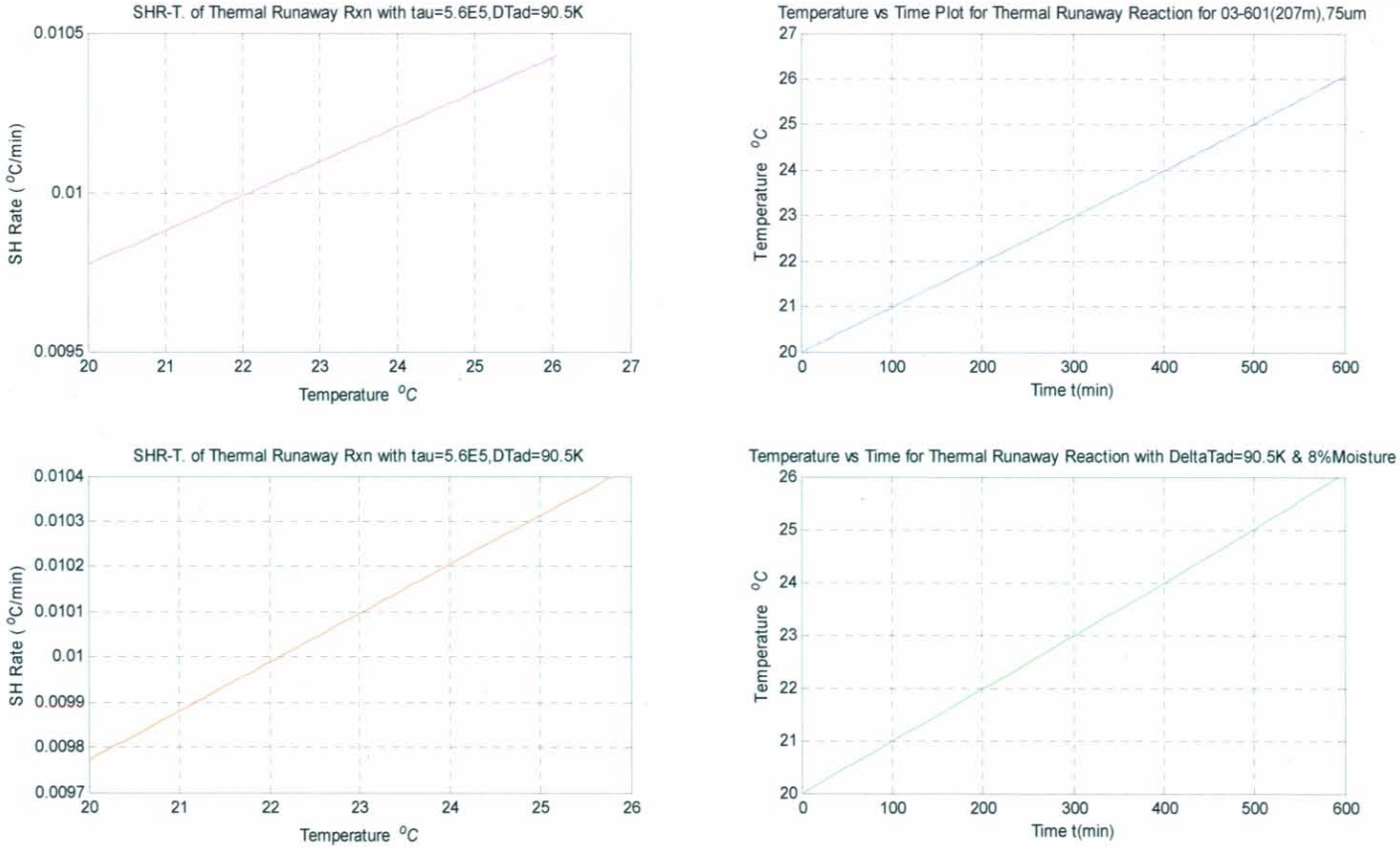

Figure 5.18: SH Rate vs. Temperature and Temperature-Time Plots for Thermal Hazardous Ore 03-601(207m) at 8% Moisture & *Tau= 555556s*

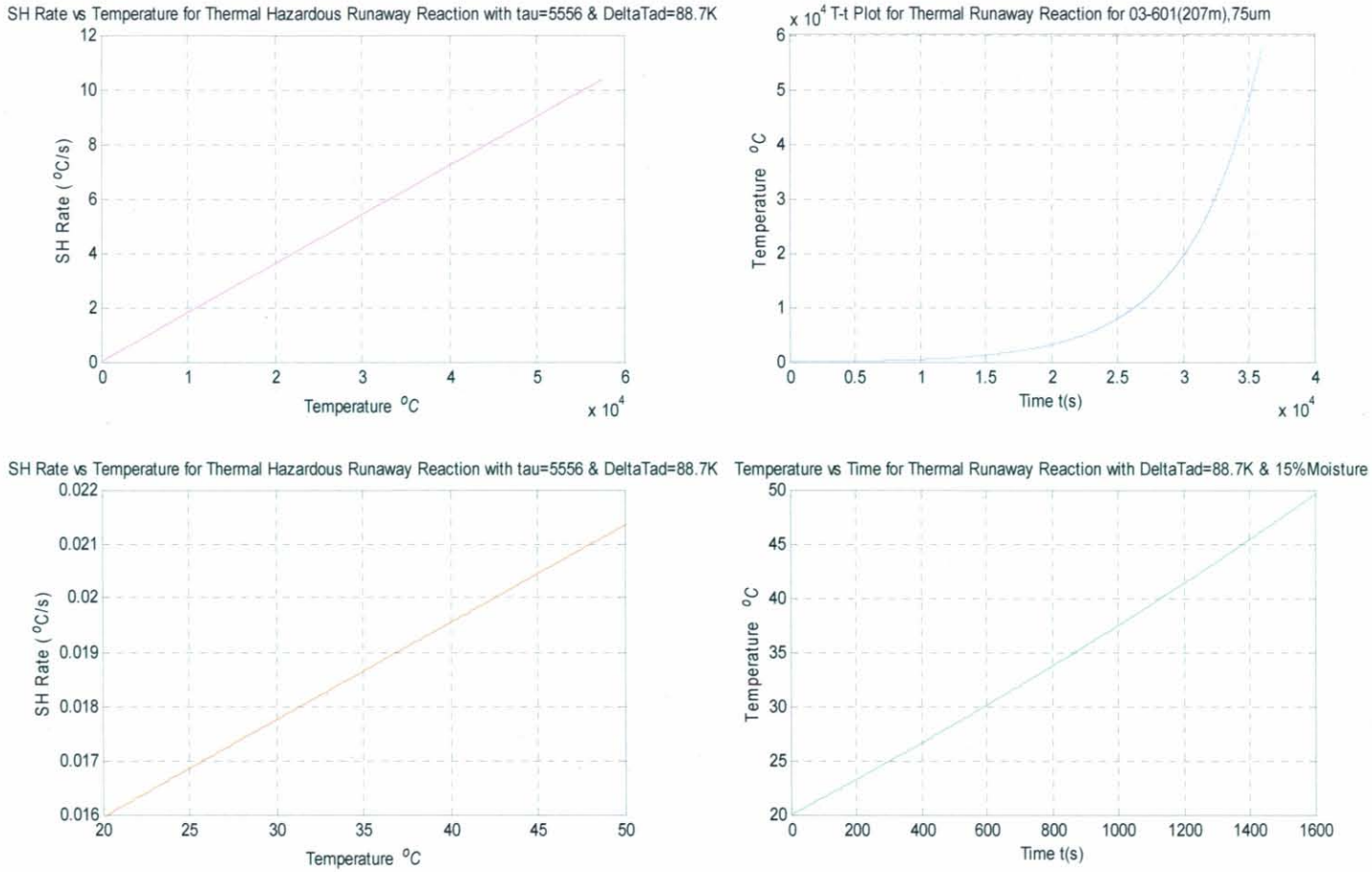

Figure 5.19: SH Rate vs. Temperature and Temperature-Time Plots for Thermal Hazardous Ore 03-601(207m) at 15% Moisture & *Tau= 5556s*

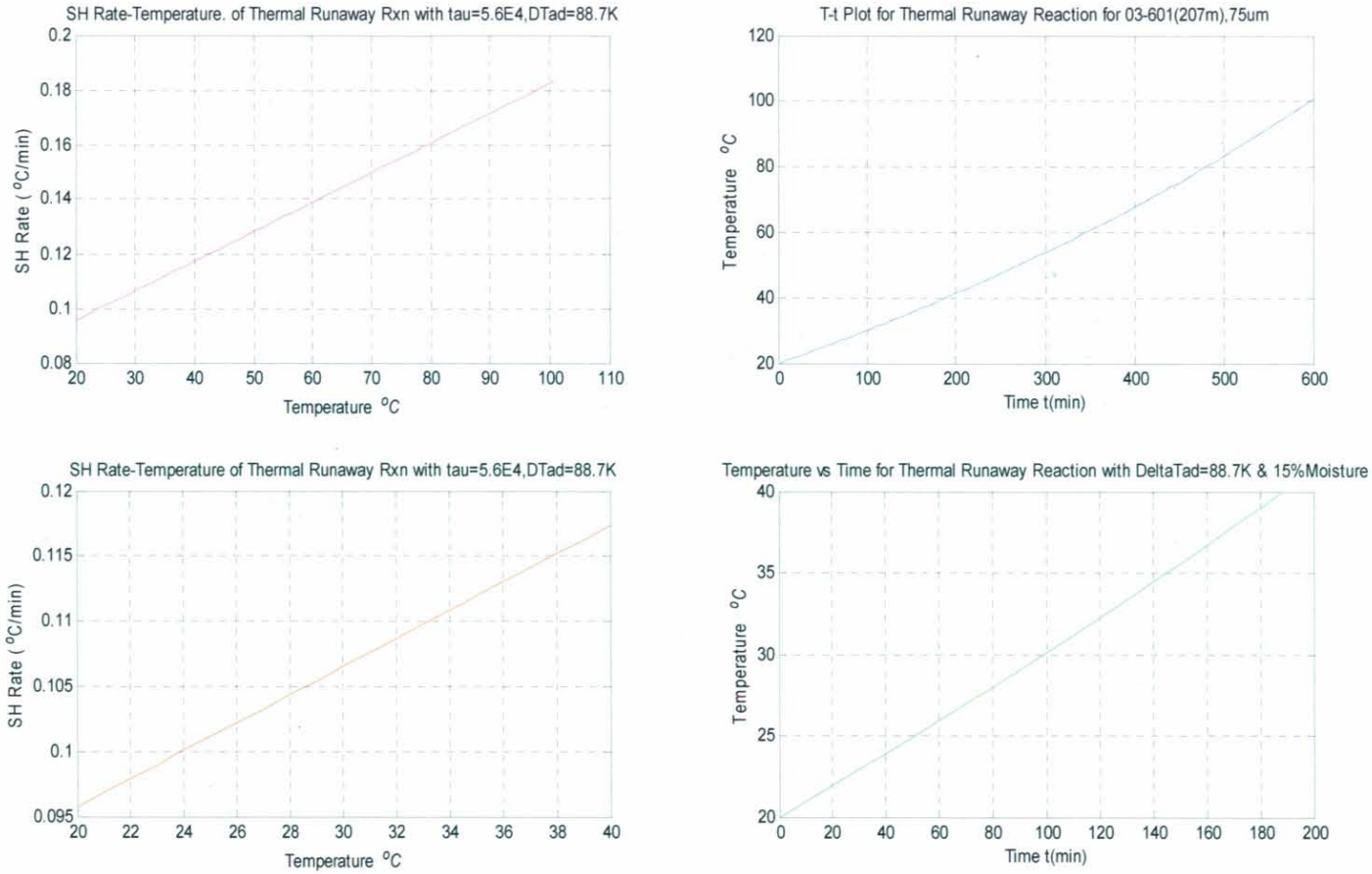

Figure 5.20: SH Rate vs. Temperature and Temperature-Time Plots for Thermal Hazardous Ore 03-601(207m) at 15% Moisture & *Tau= 55556s*

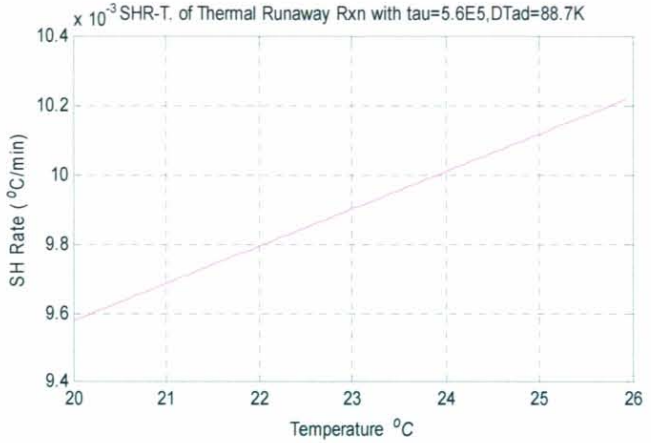

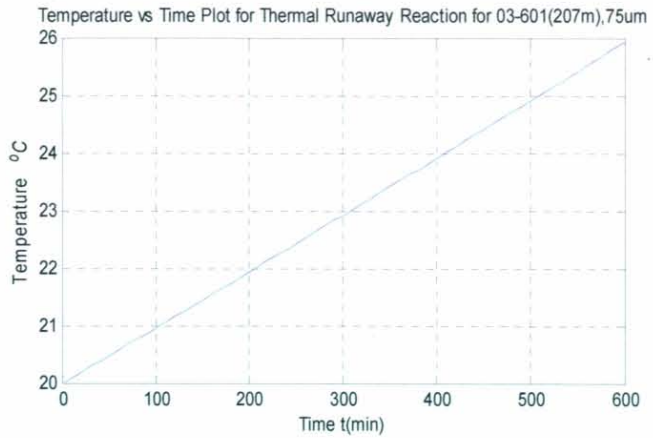

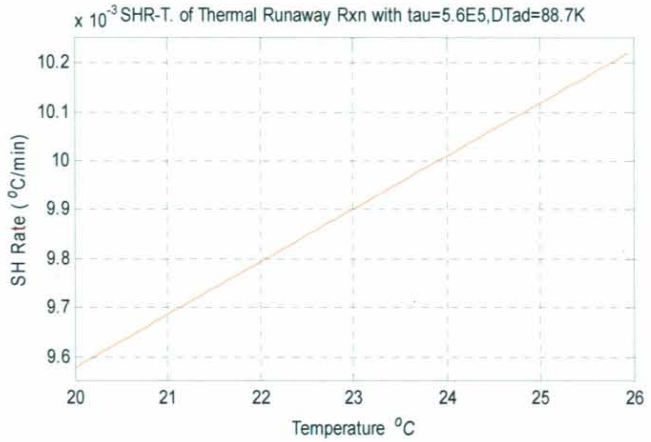

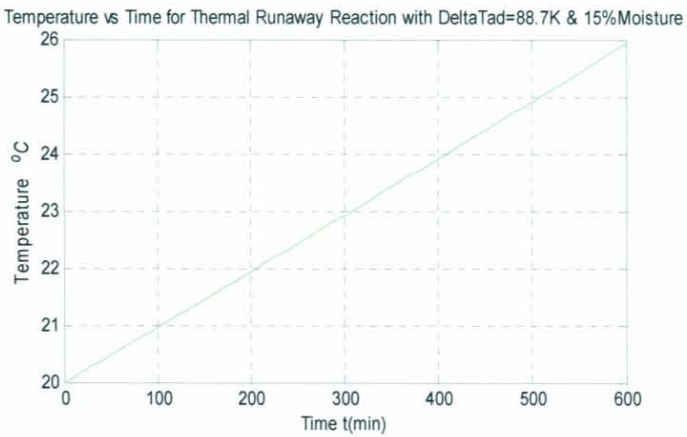

Figure 5.21: SH Rate vs. Temperature and Temperature-Time Plots for Thermal Hazardous Ore 03-601(207m) at 15% Moisture & *Tau= 555556s*

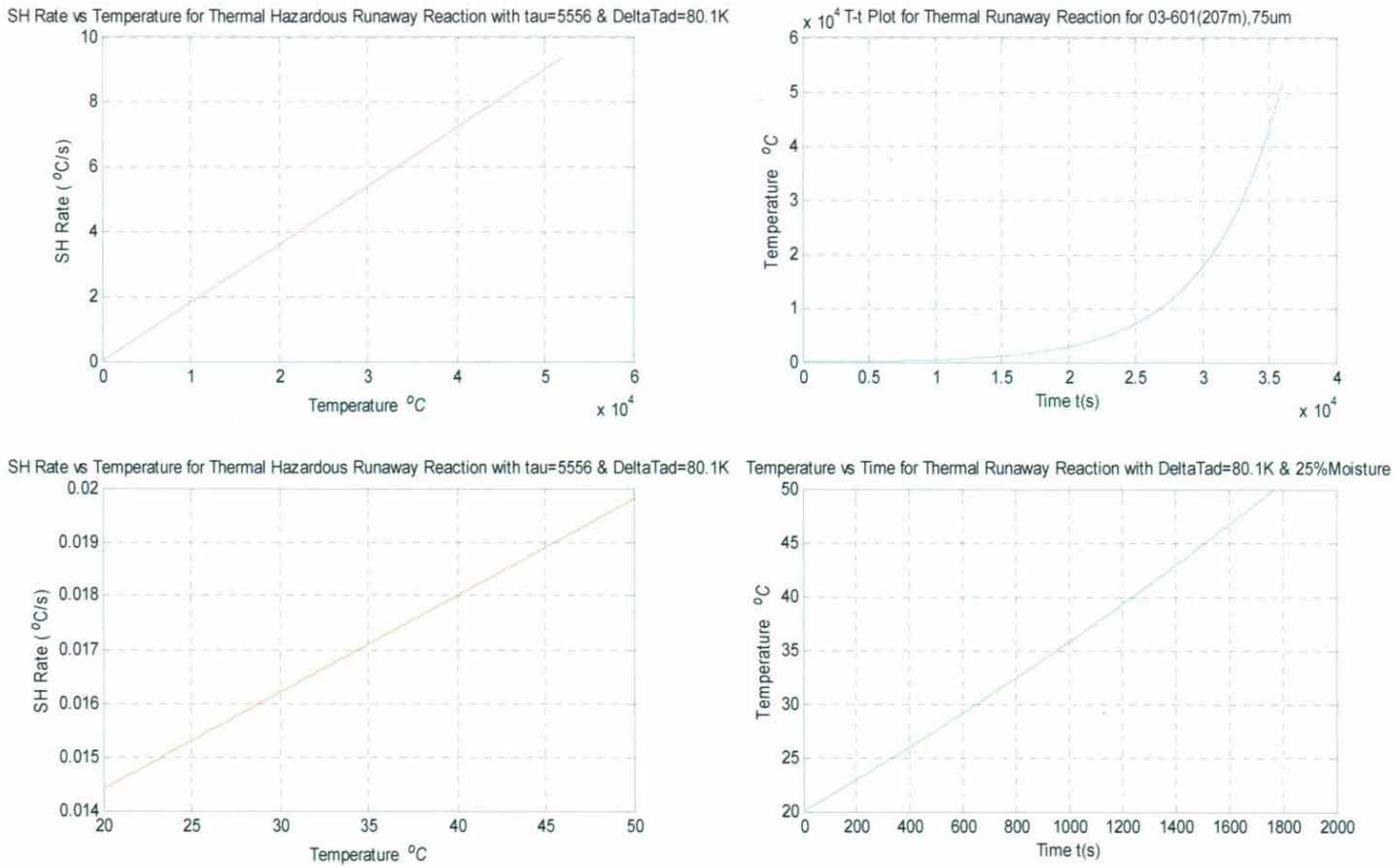

Figure 5.22: SH Rate vs. Temperature and Temperature-Time Plots for Thermal Hazardous Ore 03-601(207m) at 25% Moisture & *Tau= 5556s*

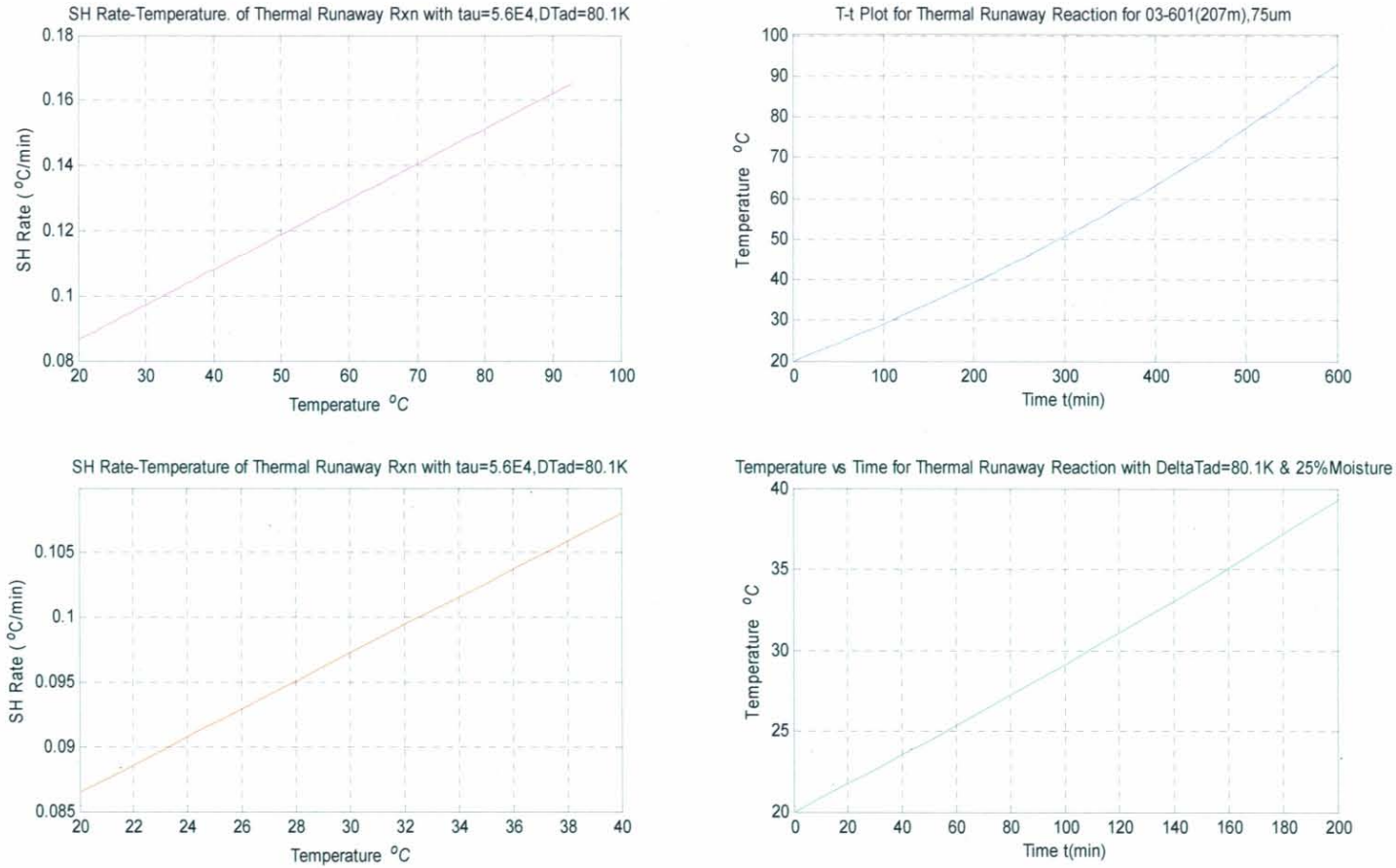

Figure 5.23: SH Rate vs. Temperature and Temperature-Time Plots for Thermal Hazardous Ore 03-601(207m) at 25% Moisture & *Tau= 55556s*

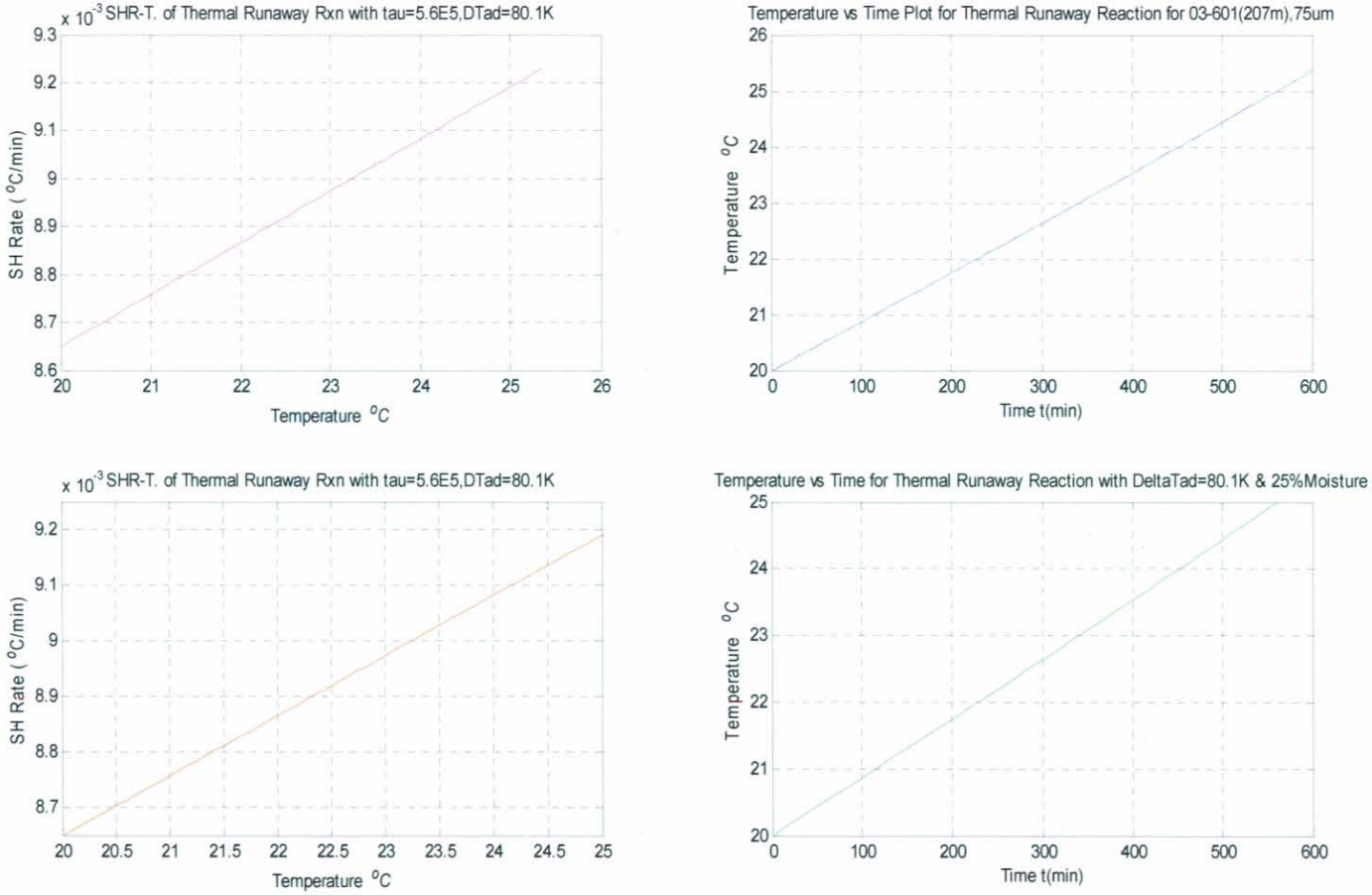

Figure 5.24: SH Rate vs. Temperature and Temperature-Time Plots for Thermal Hazardous Ore 03-601(207m) at 25% Moisture & *Tau= 555556s*

For the chance of occurrence of thermal hazards, both Arrhenius' Constants and activation energy of the reactions are crucial in its determination. A small off-set in the correct determination of these values corresponds to large error in the computed probability even if lognormal distribution is used. The higher the Ea, the lower the chance of occurrence of the runaway reaction as few molecules will possess the kinetic energy required to cross the energy barrier called activation complex and which reacts to cause the self-heating behaviour.

Having explained the parametric sensitivity of the model and methodology, the computed risks for the ore samples with investigated parameters are as shown in Tables 5.1-5.12 for Friedman Analysis data. Other results for Flynn-Ozawa-Wall and ASTM E658 data are presented in Appendix F.

Quantified Risk for Effect of Mineralogy

- Ore 03-601 (207m)

Table 5.1: Risk Categorization for Thermal Hazard for Ore 03-601(207m) Mineralogy Effect

Parameter	*Risk Class 1*	*Risk Class 2*	*Risk Class 3*	*Risk Class 4*
Hazard Probability	0.2177	0.2078	0.0249	0.0001
Severity, β	1.1758	0.4244	0.0813	0.0439
Associated Risk	0.2560	0.0882	0.0020	5.74×10^{-6}
Risk Ranking Range	10^{0}-10^{-3}	2.0×10^{-1} - 10^{-4}	10^{-3} - 10^{-5}	10^{-5} – 10^{-8}
Equivalent Risk Colour Code				

Inference: The associated risk with respect to the investigated parameter belongs to medium risk class.

- Ore 03-601 (217m)

Table 5.2: Risk Categorization for Thermal Hazard for Ore 03-601(217m) Mineralogy Effect

Parameter	*Risk Class 1*	*Risk Class 2*	*Risk Class 3*	*Risk Class 4*
Hazard Probability	0.2177	0.2095	0.0262	0.0001
Severity, β	0.6310	0.2277	0.0436	0.0235
Associated Risk	0.1373	0.0477	1.14×10^{-3}	3.27×10^{-6}
Risk Ranking Range	10^{0}-10^{-3}	2.0×10^{-1} - 10^{-4}	10^{-3} - 10^{-5}	10^{-5} – 10^{-8}
Equivalent Risk Colour Code				

Inference: The associated risk with respect to the investigated parameter belongs to medium risk class.

- Ore 06-658 (257)m

Table 5.3: Risk Categorization for Thermal Hazard for Ore 06-658(257m) Mineralogy Effect

Parameter	*Risk Class 1*	*Risk Class 2*	*Risk Class 3*	*Risk Class 4*
Hazard Probability	0.2174	0.2161	0.0383	0.0002
Severity, β	0.1781	0.0643	0.0123	0.0066
Associated Risk	0.0387	0.0139	4.71×10^{-4}	1.47×10^{-6}
Risk Ranking Range	10^{0}-10^{-3}	2.0×10^{-1} - 10^{-4}	10^{-3} - 10^{-5}	10^{-5} – 10^{-8}
Equivalent Risk Colour Code				

Inference: The associated risk with respect to the investigated parameter belongs to medium risk class.

Quantified Risk for the Effect of Particle Size Distribution

- Ore 05-658 (257m) Fine Grain Size

Table 5.4: Risk Categorization for Thermal Hazard for Ore 06-658 (257m) □75µm Particle Size

Parameter	*Risk Class 1*	*Risk Class 2*	*Risk Class 3*	*Risk Class 4*
Hazard Probability	0.2174	0.2156	0.0366	0.0002
Severity, β	0.1781	0.0643	0.0123	0.0066
Associated Risk	0.0387	0.0139	4.51×10^{-4}	1.39×10^{-6}
Risk Ranking Range	10^{0}-10^{-3}	2.0×10^{-1} - 10^{-4}	10^{-3} - 10^{-5}	10^{-5} – 10^{-8}
Equivalent Risk Colour Code				

Inference: The associated risk with respect to the investigated parameter belongs to medium risk class.

- Ore 05-658 (257m) Intermediate Grain Size

Table 5.5: Risk Categorization for Thermal Hazard for Ore 05-658(257m) 75-180µm Particles

Parameter	*Risk Class 1*	*Risk Class 2*	*Risk Class 3*	*Risk Class 4*
Hazard Probability	0.2177	0.2078	0.0249	0.00013
Severity, β	0.0159	0.0057	0.0011	0.000594
Associated Risk	0.0035	0.0012	2.74×10^{-5}	7.78×10^{-6}
Risk Ranking Range	10^{0}-10^{-3}	2.0×10^{-1} - 10^{-4}	10^{-3} - 10^{-5}	10^{-5} – 10^{-8}
Equivalent Risk Colour Code				

Inference: The associated risk with respect to the investigated parameter belongs to medium risk class.

➢ Ore 05-658 (257m) Coarse Grain Size

Table 5.6: Risk Categorization for Thermal Hazard for Ore 05-658(257m) □ 180µm Particles

Parameter	*Risk Class 1*	*Risk Class 2*	*Risk Class 3*	*Risk Class 4*
Hazard Probability	0.2175	0.2148	0.0334	0.0002
Severity, β	0.0065	0.0023	0.00045	0.00024
Associated Risk	0.0014	0.0005	1.49×10^{-5}	4.49×10^{-6}
Risk Ranking Range	10^{0}-10^{-3}	2.0×10^{-1} - 10^{-4}	10^{-3} - 10^{-5}	10^{-5} – 10^{-8}
Equivalent Risk Colour Code				

Inference: The associated risk with respect to the investigated parameter belongs to medium risk class.

➢ Ore 05-658 (257m) Aggregate Grain Size

Table 5.7: Risk Categorization for Thermal Hazard for Ore 03-601 Mixed Particles

Parameter	*Risk Class 1*	*Risk Class 2*	*Risk Class 3*	*Risk Class 4*
Hazard Probability	0.2182	0.1808	0.0161	0.00008
Severity, β	0.0955	0.0345	0.0066	0.0036
Associated Risk	0.0208	0.0062	1.06×10^{-4}	2.88×10^{-7}
Risk Ranking Range	10^{0}-10^{-3}	2.0×10^{-1} - 10^{-4}	10^{-3} - 10^{-5}	10^{-5} – 10^{-8}
Equivalent Risk Colour Code				

Inference: The associated risk with respect to the investigated parameter belongs to medium risk class.

Quantitative Risk for the Effect of Moisture Content

- Ore 03-601 (207m) with Addition of **3%** w/w Water

Table 5.8: Risk Categorization for Thermal Hazard for Ore 03-601(207m), 3% Moisture Content

Parameter	*Risk Class 1*	*Risk Class 2*	*Risk Class 3*	*Risk Class 4*
Hazard Probability	0.2174	0.2156	0.0366	0.00021
Severity, β	0.2359	0.0851	0.0163	0.0088
Associated Risk	0.0513	0.0184	5.97×10^{-4}	1.83×10^{-6}
Risk Ranking Range	10^{0}-10^{-3}	2.0×10^{-1} - 10^{-4}	10^{-3} - 10^{-5}	10^{-5} – 10^{-8}
Equivalent Risk Colour Code				

Inference: The associated risk with respect to the investigated parameter belongs to medium risk class.

- Ore 03-601 (207m) with Addition of **8%** w/w Water

Table 5.9: Risk Categorization for Thermal Hazard for Ore 03-601(207m), 8% Moisture Content

Parameter	*Risk Class 1*	*Risk Class 2*	*Risk Class 3*	*Risk Class 4*
Hazard Probability	0.2192	0.1198	0.0093	0.00005
Severity, β	0.2702	0.0975	0.0187	0.0101
Associated Risk	0.0592	0.0117	1.74×10^{-4}	4.65×10^{-7}
Risk Ranking Range	10^{0}-10^{-3}	2.0×10^{-1} - 10^{-4}	10^{-3} - 10^{-5}	10^{-5} – 10^{-8}
Equivalent Risk Colour Code				

Inference: The associated risk with respect to the investigated parameter belongs to medium risk class.

- Ore 03-601 (207m) with Addition of **15%** w/w Water

Table 5.10: Risk Categorization for Thermal Hazard for Ore 03-601(257m), 15% Moisture Content

Parameter	*Risk Class 1*	*Risk Class 2*	*Risk Class 3*	*Risk Class 4*
Hazard Probability	0.2179	0.1975	0.0201	0.0001
Severity, β	0.3423	0.1236	0.0237	0.0128
Associated Risk	0.0746	0.0244	4.77×10^{-4}	1.32×10^{-6}
Risk Ranking Range	10^{0}-10^{-3}	2.0×10^{-1} - 10^{-4}	10^{-3} - 10^{-5}	10^{-5} – 10^{-8}
Equivalent Risk Colour Code				

Inference: The associated risk with respect to the investigated parameter belongs to medium risk class.

- Ore 03-601 (207m) with Addition of **25%** w/w Water

Table 5.11: Risk Categorization for Thermal Hazard for Ore 03-601(257m), 25% Moisture Content

Parameter	*Risk Class 1*	*Risk Class 2*	*Risk Class 3*	*Risk Class 4*
Hazard Probability	0.2175	0.2148	0.0334	0.00019
Severity, β	0.3209	0.1158	0.0222	0.0120
Associated Risk	0.0698	0.0249	7.41×10^{-4}	2.23×10^{-6}
Risk Ranking Range	10^{0}-10^{-3}	2.0×10^{-1} - 10^{-4}	10^{-3} - 10^{-5}	10^{-5} – 10^{-8}
Equivalent Risk Colour Code				

Inference: The associated risk with respect to the investigated parameter belongs to medium risk class.

5.2 Discussion of Results

Closer look at Figures 4.1-4.12 reveals that the ore will self-heat under favourable condition without any additional external heat energy at the rate ranging 0.12°C/min to 4.5°C/min at lower temperature. This is exactly what was observed on the field in terms of oxidation characteristic (Table C2 of Appendix C) and during experiments. Individual result indicates that Ore 03-601(207m) is the most oxidative or self-heated one with characteristic SHR of 4.2°C/min-4.5°C/min within 1min over 20°C-50°C temperature range. Similarly, its maximum rate of reaction (5.07 mol/m^3s) at full conversion is the highest if the same concentration of 28223mol/m^3 were to be used for all the ores alongside with the corresponding ΔTad (a fact that is hidden from the plots but obvious from Table C12b of Appendix C). The computed associated risk (0.2560-low risk, 0.0882-medium risk, 0.0020-high risk & 5.74 x 10^{-6}-extremely high risk) values corroborate this fact. This is the observable trend across board irrespective of the analysis data-type used. Therefore, presence of high percentage pyrrhotite content corresponds to severe thermal hazard. This assertion was also made by Thomas et al, 1998; Thomas et al, 2001; Mikhlin et al, 2002; Miller et al, 2005; Wills and Napier-Munn, 2006; Nakamura et al. (1994), Iliyas, (2011) and Peek et al, 2011.

Finer particle size (<75μm) in the ore has higher risk values than other particle size distribution. This is true because the larger the surface area of particles taking part in chemical reaction, the higher the rate of reaction. On the other hand, it is highly otiose to see this finer size particles distribution alone as aggregate particles of all sizes react together during reaction. This is why the risk values (i.e. 0.0208 under class 1, 0.0062 under class 2, 0.000106 under class 3 and 2.88E-7 under class 4 for ore 03-601(207m)) obtained for the

mixed particles are the true representative governing the effect of particle size distribution. Their own values are next to the values (e.g. 0.0387 under class 1, 0.0139 under class 2, 0.000451 under class 3 and 1.39E-6 under class 4) obtained for the finer particles. The same is observed on the SHR values obtained (field study, experiments and simulation). Several authors observed this effect (Nakamura et al.1994, Ahonen and Tuovinen, 1991, Belzile et al. 2004 and Janzen et al. 2000).

Although moisture presence in the ore accelerates rate of reaction, yet, its effect is masked by the inhibition of gas front during diffusion of air or oxygen as the stoichiometry of reaction shows that it is solid-gas phase reaction. This is why the computed values for the associated risks increase from 3% moisture (0.0512) to 15% moisture (0.0746) before decreasing again at 25% moisture content. Computed risks follow this trend irrespective of the source of the data (Appendix F). This gives an indication of optimum saturation level for the reaction to proceed optimally to prevent ore solvation or coating. From this, it can be inferred that too much moisture will hamper self-heating. This is why these ores and their tailings are covered or stored under water to prevent rapid oxidation.

Globally, the associated risks with self-heating behaviour of these mineral ores indicate that the ores are of medium risk class on the conservative safety margin. Varying parameter τ shows that the self-heat rate is decreasing as τ increases suggesting that conversion is rapid. Also, the corresponding temperature variation with the increment in τ-value is small. This is due to the varnishing of the exponential term.

5.3 Usability of the Model

The derived model is a semi-empirical model that can be used for any thermal hazardous reaction. This model is independent of the order of reaction in its final form but depends on feed rate as it has been derived for general kinetic reaction undergoing runaway reactions. The limitations of the model include need for experiments to be run to unravel the unknown parameters such as onset temperature, SADT, ΔTad, etc. before it can be applied. If temperature T is plotted against ($e^{t/\tau}$ - 1), the slope of such line will represent ΔTad with intercept representing the referenced temperature. This is not a valid approach to obtain experimental ΔTad prior to the execution of experiments as ΔTad depends on the chemical nature of the material under investigation. This is why the model is an empirical one that relies heavily on experimental runs. The model should not be used this way without running experiments on the sample to be assessed otherwise, many materials with different values of experimental ΔTad will have the same behaviour if this warning is not heeded.

Chapter 6

Conclusions and Recommendations

6.1 Conclusions

The mineral ores (03-601(199m), 03-601(207m), 03-601(217m) and 05-658(217m)) portend intermediate risk of self-heating thermal runaway reaction that can be managed effectively. Processing, storage and transportation of these ores constitute moderate thermal hazard as their self-heating rates are tolerable under the cold climate where temperatures are generally in the lowest ebbs. Mineral composition plays significant roles in this observable SH behavior. The global minimum and maximum SH rates were found to influence the quantified risk values as the accompanied enthalpy and activation energy of each particular ore vary accordingly. Rapid oxidation of the ores occurs due to high reactivity of oxygen on the pyrrhotite content alongside with other reactive minerals contents such as: pentlandite, magnetite, chlorite and chalcopyrite with chalcopyrite oxidation reactivity trailing that of pyrrhotite ahead of other components.

The mineralogy in the ores revealed that the self-heat rate increases with increase of % pyrrhotite, % moisture content and increase of fine particles. The particle size distribution of the ores affect the SH as the quantified risk values (0.03873 under class1, 0.01387 under class 2, 0.00045 under class 3 and 1.4 $x10^{-6}$ under class 4 for the fine particles) associated with the effect of fine particle size distribution which are the highest values under each category confirms that fine particles react vigorously than other particle types. Hence, the higher the proportion of these fine particles in an ore sample, the higher the tendency to self-heat to cause potential hazards.

Presence of extra much moisture impedes self-heating reaction by inhibiting the advancing diffusing gaseous reactant. At moisture content greater than 15% by weight, the self-heat rates were found to be optimal after which excess moisture beyond this inhibits the reactivity. This is why the ores and their tailings are stored under excess water to mitigate the hazards temporarily as acid mine drainage is another potential hazards in industries and environment if there is a leakage to the ground water bodies (Thomas et al, 2001 and Toner et al, 2009). Masking of the oxide coating of the ores after surface oxidation of the ores does not reduce the SH rate as their reactivity follows the shrinking unreacted core model with continuous diffusion of gaseous reactants through the ash layer formed. This is why SH increases with time as the reactions progress. The reactions are governed by the combined effect of diffusion, ash-layer and chemical controlled reaction at both microscopic and macroscopic levels. Therefore, the formed ash layer on the ores prevents effective cooling of the reacted ores but rather promotes internal heat generation rate.

The various ores investigated was found to be self-heating at different rate covering the entire range of the quantified medium risk range on the predefined risk scale. Finally, the parameters involved in the semi-empirical model need to be determined accurately during experiments to get meaningful results. Further, an uncertainty analysis of the parameters and assessed risk is useful. The proposed approach of risk ranking of thermal hazards accounts for uncertainty in assessing risk and assigning risk rank.

6.2 Recommendations

- The work can be extended by investigating the combined effect of different parameters under various classes of the Arrhenius' Constant.

- The probability assessment can be revised by adopting conditional probability such as: Bayes' Theorem.
- This work could further be enhanced by testing the model and methodology on other minerals and fine chemicals.
- The risk ranking proposed in this work though broad to capture wide range of chemicals, this needs to be tested and verified.
- The consequences model used in the risk assessment could further be improved.

References

Ahonen, L. (1992). Bacterial Oxidation of Sulfide Minerals in Column Leaching Experiments at Suboptimal Temperatures. *Applied Environmental Microbiology, 58*(2), 600-606.

Ando, T., Fujimoto, Y., & Morisaki, S. (1991). Analysis of Differential Scanning Calorimetric Data for Reactive Chemicals. *Journal of Hazardous Materials, 28*(3), 251-280.doi: 10.1016/0304-3894(91)87079-H

Asaki, Z., Tosa, M., Tanabe, T., & Kondo, Y. (1984). Oxidation Kinetics of Mixed Copper-Iron Sulfide At 1173 K. *Transactions of the Japan Institute of Metals, 25*(7), 487-496.

Asay, B. (2010). The Chemical Kinetics of Solid Thermal Explosions. *Shock Wave Science and Technology Reference Library, Vol. 5 Non-Shock Initiation of Explosives, 5*, 45-128. doi:10.1007/978-3-540-87953-4_3

Aylward, G and Findlay, T. (1971). SI Chemical Data. Australia: John Wiley & Sons Australasia Ltd.

Baba, A. A., & Adekola, F. A. (2010). Hydrometallurgical Processing of a Nigerian Sphalerite in Hydrochloric Acid: Characterization and Dissolution Kinetics. *Hydrometallurgy, 101*(1-2), 69-75.

Bach, W., & Edwards, K. J. (2003). Iron and Sulfide Oxidation within the Basaltic Ocean Crust: Implications for Chemolithoautotrophic Microbial Biomass Production. *Geochimica Et Cosmochimica Acta, 67*(20), 3871-3887. doi:DOI: 10.1016/S0016-7037(03)00304-1

Barton, J. & Rogers, R. (1997). *Chemical Reaction Hazards: A Guide to Safety* (Second ed.). Houston Texas: Gulf Publishing Company.

Belzile, N., Chen, Y., Cai, M., & Li, Y. (2004). A Review on Pyrrhotite Oxidation. *Journal of Geochemical Exploration, 84*(2), 65-76.

Bowles, M. W., Samarkin, V. A., Bowles, K. M., & Joye, S. B. (2011). Weak Coupling between Sulfate Reduction and the Anaerobic Oxidation of Methane in Methane-rich Seafloor Sediments During Ex Situ Incubation. *Geochimica Et Cosmochimica Acta, 75*(2), 500-519. doi: 10.1016/j.gca.2010.09.043

Bretherick's Handbook of Reactive Chemical Hazards volume 2 (2007). In Urben P. G. (Ed.), (Sixth ed.). Oxford: Academic Press.

Burelbach, J. P. (1999). Advanced Reactive System Screening Tool (ARSST).

Carreto-Vazquez, V., Wjcik, A. K., Liu, Y. -., Bukur, D. B., & Mannan, M. S. (2010). Miniaturized Calorimeter for Thermal Screening of Energetic Materials. *Microelectronics Journal, 41*(12), 874-881.

Chevrier, V., Mathé, P. -., Rochette, P., Grauby, O., Bourrié, G., & Trolard, F. (2006). Iron Weathering Products in a CO2 + (H2O or H2O2) Atmosphere: Implications for Weathering Processes on the Surface of Mars. *Geochimica Et Cosmochimica Acta, 70*(16), 4295-4317. doi:DOI: 10.1016/j.gca.2006.06.1368

Chirita, P., Descostes, M., & Schlegel, M. L. (2008). Oxidation of FeS by Oxygen-Bearing Acidic Solutions. *Journal of Colloid and Interface Science, 321*(1), 84-95. Retrieved from http://dx.doi.org/10.1016/j.jcis.2008.01.024

CMPT. (1999). A Guide to Quantitative Risk Assessment for Offshore Installations. The Centre for Marine and Petroleum Technology. Publication 99/100a.

Covello, V. T., & Merkhofer, M. W. (1993). Risk Assessment Methods: Approaches *for Assessing Health and Environmental Risks*. New York, USA: Plenum Press.

Daubert, T. & Danner, P. (1985). Data Compilation Tables of Properties of Pure Compounds. New York, USA: Design Institute for Physical Property Data, American Institute of Chemical Engineers.

Egidijus, R. V. & Virmantas, J. (2008). Sustainable Development and Major Industrial Accidents: The Beneficial Role of Risk-Oriented Structural Engineering. *Technological and Economic Development of Economy, 14*(4), 612-613-627.

Fisher, H. G., Forrest, H. S., & Grossel, S. S. Emergency Relief System Design using DIERS Technology - The Design Institute for Emergency Relief Systems (DIERS) Project Manual Design Institute for Physical Property Research/AIChE. http://www.knovel.com.qe2a-proxy.mun.ca/web/portal/browse/display?_EXT_KNOVEL_DISPLAY_bookid=1079

Foust, A. S., Wenzel, L. A., Clump, C. W., Maus, L., & Anderson, L. B. (1980). Principles of Unit Operations (2nd ed.). India: John Willey&Sons.

Garrick, B. J., Stetkar, J. W., & Bembia, P. J. (2010). Quantitative Risk Assessment of the New York State Operated West Valley Radioactive Waste Disposal Area. *Risk Analysis, 30*(8), 1219-1230. Retrieved from http://dx.doi.org/10.1111/j.1539-6924.2010.01418.x

Glassman, I. (1977). Combustion. New York, USA: Academic Press.

Green, D. and Perry, R. (Ed.). (2008). Perry's Chemical Engineers' Handbook (Eighth ed.). New York, USA: McGraw-Hill.

Gunawan, R., & Zhang, D. (2009). Thermal Stability and Kinetics of Decomposition of Ammonium Nitrate in the Presence of Pyrite. *Journal of Hazardous Materials, 165*(1-3), 751-758. Retrieved from http://dx.doi.org/10.1016/j.jhazmat.2008.10.054

Hauptmanns, U. (2004). Semi-Quantitative Fault Tree Analysis for Process Plant Safety using Frequency and Probability Ranges. *Journal of Loss Prevention in the Process Industries, 17*(5), 339-345. Retrieved from http://dx.doi.org/10.1016/j.jlp.2004.06.004

Heinrich, H. (1959). Industrial Accident Prevention: A scientific Approach (4th ed.). New York, USA: McGraw-Hill.

Herman, F. C. (1968). The preexponential Factors for Solid-State Thermal Decomposition. *The Journal of Physical Chemistry, 72*(6), 2185-2186-2189. doi:10.1021/j100852a052

Hu, G., Dam-Johansen, K., Wedel, S., & Hansen, J. P. (2006). Decomposition and Oxidation of Pyrite. *Progress in Energy and Combustion Science, 32*(3), 295-314. Retrieved from http://dx.doi.org/10.1016/j.pecs.2005.11.004

Iliyas, A., Hawboldt, K., & Khan, F. (2011). Kinetics and Safety Analysis of Sulfide Mineral Self-Heating Part 1. Effect of Mineralogy. *Journal of Thermal Analysis and Calorimetry,* doi:10.1007/s10973-011-1621-7

Janzen, M. P., Nicholson, R. V., & Scharer, J. M. (2000). Pyrrhotite Reaction Kinetics: Reaction Rates for oxidation by Oxygen, Ferric Iron, and for Nonoxidative Dissolution. *Geochimica Et Cosmochimica Acta, 64*(9), 1511-1522. doi:DOI: 10.1016/S0016-7037(99)00421-4

Jeong, H. Y., Han, Y., Park, S. W., & Hayes, K. F. (2010). Aerobic Oxidation of Mackinawite (FeS) and its Environmental Implication for Arsenic Mobilization. *Geochimica Et Cosmochimica Acta, 74*(11), 3182-3198. doi:DOI: 10.1016/j.gca.2010.03.012

Kaplan, S. and Garrick, B. J. (2006). On the Quantitative Definition of Risk. *Risk Analysis, 1*(1), 11-12-27. doi:10.1111/j.1539-6924.1981.tb01350.x

Khan, F. I., & Abbasi, S. A. (1998). Techniques and Methodologies for Risk Analysis in Chemical Process Industries. *Journal of Loss Prevention in the Process Industries, 11*(4), 261-277. doi:DOI: 10.1016/S0950-4230(97)00051-X

Khan, F. I., Husain, T., & Abbasi, S. A. (2002). Design and Evaluation of Safety Measures using a Newly Proposed Methodology "SCAP". *Journal of Loss Prevention in the Process Industries, 15*(2), 129-146. Retrieved from http://dx.doi.org/10.1016/S0950-4230(01)00026-2

Kohlbrand, H. T. (1984). Use of Reactive Chemical Screening in Pilot Plant Safety. Paper Presented at the *1984 Annual Meeting - American Institute of Chemical Engineers.* AIChE, New York, NY, USA.

Korkin, A. A., Cole, J. V., Sengupta, D., & Adams, J. B. (1999). On the Mechanism of Silicon Nitride Chemical Vapor Deposition from Dichlorosilane and Ammonia. *Journal of the Electrochemical Society, 146*(11), 4203-4212. Retrieved from http://dx.doi.org/10.1149/1.1392615

Kumpinsky, E. (2008). Lumped kinetics of Self-Heating Runaway Reactions: A Statistical Treatment. *Industrial and Engineering Chemistry Research, 47*(20), 7570-7579. Retrieved from http://dx.doi.org/10.1021/ie0714201

Kuznetsov, G.V. and Strizhak, P.A. (2009). Numerical Solution of the Problem of Ignition of a Combustible Liquid by a Single Hot Particle. *Combustion, Explosion, and Shock Waves, 45*(5), 543-544-550. doi:10.1007/s10573-009-0066-9

Lengke, M. F., & Tempel, R. N. (2001). Kinetic Rates of Amorphous As_2S_3 Oxidation at 25 to 40°C and Initial pH of 7.3 to 9.4. *Geochimica Et Cosmochimica Acta, 65*(14), 2241-2255. doi:DOI: 10.1016/S0016-7037(01)00592-0

Lengke, M. F., & Tempel, R. N. (2005). Geochemical Modeling of Arsenic Sulfide Oxidation Kinetics in a Mining Environment. *Geochimica Et Cosmochimica Acta, 69*(2), 341-356. doi:DOI: 10.1016/j.gca.2004.06.032

Levenspiel, O. (1999). Chemical Reaction Engineering (Third ed.). New York, USA: John Wiley & Sons, Inc.

Markowski, A. S., Mannan, M. S., Kotynia (Bigoszewska), A., & Siuta, D. (2010). Uncertainty Aspects in Process Safety Analysis. *Journal of Loss Prevention in the Process Industries, 23*(3), 446-454. Retrieved from http://dx.doi.org/10.1016/j.jlp.2010.02.005

McCabe, W. L., & Smith, J. C. and Harriott, P. (2005). Unit Operations of Chemical Engineering (7th ed.). New York, USA: McGraw-Hill.

McIntosh, R. D., & Waldram, S. P. (2003). Obtaining More, and Better Information from Simple Ramped Temperature Screening Tests. *Journal of Thermal Analysis and Calorimetry, 73*(1), 35-52. Retrieved from http://dx.doi.org/10.1023/A:1025169121312

Mikhlin, Y. L., Kuklinskiy, A. V., Pavlenko, N. I., Varnek, V. A., Asanov, I. P., Okotrub, A. V., . . . Solovyev, L. A. (2002). Spectroscopic and XRD Studies of the Air Degradation of Acid-reacted Pyrrhotites. *Geochimica Et Cosmochimica Acta, 66*(23), 4057-4067. doi: 10.1016/S0016-7037(02)00989-4

Miller, J. D., Li, J., Davidtz, J. C., & Vos, F. (2005). A Review of Pyrrhotite Flotation Chemistry in the Processing of PGM Ores. Paper presented at the , *18*(8) 855-865. Retrieved from http://dx.doi.org/10.1016/j.mineng.2005.02.011

Mitchell R.E. and Akan-Etuk. (2002). Mechanisms of Pyrite Oxidation to Non-slagging Species , Final Report Submitted to the United States Department for Energy for the Work done under Grant DE-FG22-94PC94205.

Murphy, R., & Strongin, D. R. (2009). Surface Reactivity of Pyrite and Related Sulfides. *Surface Science Reports, 64*(1), 1-45. Retrieved from http://dx.doi.org/10.1016/j.surfrep.2008.09.002

Nakamura, H., Sato, S., & Hara, Y. (1994). The Oxidation of Pyrite. *Journal of Hazardous Materials, 37*(2), 253-263. Retrieved from http://dx.doi.org/10.1016/0304-3894(93)E0095-J

Nandi, A. K., Sutar, V. B., & Bhattacharyya, S. C. (2004). Thermal Hazards Evaluation for Sym-TCB Nitration Reaction using Thermal Screening Unit (TSU). *Journal of Thermal Analysis and Calorimetry, 76*(3), 895-901. Retrieved from http://dx.doi.org/10.1023/B:JTAN.0000032273.27765.00

Nolan, D. P. (1996). Risk Analysis. In D. P. Nolan (Ed.), *Handbook of |Fire and Explosion Protection Engineering Principles for Oil, Gas, Chemical, and Related Facilities* (pp. 87-94). Westwood, N.J., U.S.A.: Noyes Publications.

Oba, M.: Mita, H and Shimoyama, A. (2002). Determination of Activation Energy and Pre-exponential Factor for Individual Compounds on Release from Kerogen by a Laboratory Heating Experiment.*36*, 51-52-60.

Ottaway, M. (2004). Calorimetric Screening of Exothermic Reactions and Materials. Paper Presented at the *Progress in Safety Science and Technology Volume 4: Proceedings of the 2004 International Symposium on Safety Science and Technology, October 25, 2004 - October 28,* 2707-2712.

Ozog, H., & Bendixen, L. M. (1987). Hazard Identification and Quantification. *Chemical Engineering Progress, 83*(4), 55-64.

Peek, E., Barnes, A., & Tuzun, A. (2011). Nickeliferous Pyrrhotite - "Waste or Resource?". *Minerals Engineering, 24*(7), 625-637. Retrieved from http://dx.doi.org/10.1016/j.mineng.2010.10.004

Pitblado, R. M., Williams, J. C., & Slater, D. H. (1990). Quantitative Assessment of Process Safety Programs. *Plant/operations Progress, 9*(3), 169-175. Retrieved from http://dx.doi.org/10.1002/prsb.720090317

Richardson, J. F., Harker, J. H., & Backhurst, J. R. (2002). Coulson and Richardson's Chemical Engineering Volume 2 - Particle Technology and Separation Processes (5th ed.). Oxford, UK: Butterworth Heinemann.

Roduit, B. Guillaume, P. Wilker, S. Folly, P. Sarbach, A. Berger, B. Mathieu, J. Ramin , M. and Vogelsanger, B. Advanced Simulation of the lifetime of Energetic Materials Based on HFC Signals

Roduit, B.,. (2005). The Prediction of Thermal Stability of Self-Reactive Chemicals: from Milligrams to Tons. *Journal of Thermal Analysis and Calorimetry, 80*(1), 91-102.

Roduit, B., Dermaut, W., Lunghi, A., Folly, P., Berger, B., & Sarbach, A. (2008). Advanced Kinetics-based Simulation of Time to Maximum Rate under Adiabatic Conditions. *93*(1) 163-173. Retrieved from http://dx.doi.org/10.1007/s10973-007-8866-1

Roduit, B., Folly, P., Berger, B., Mathieu, J., Sarbach, A., Andres, H., . . . Vogelsanger, B. (2008). Evaluating SADT by Advanced Kinetics-based Simulation Approach. *93*(1) 153-161. Retrieved from http://dx.doi.org/10.1007/s10973-007-8865-2

Roduit, B., Xia, L., Folly, P., Berger, B., Mathieu, J., Sarbach, A., . . . Dilhan, D. (2008). The Simulation of the Thermal Behavior of Energetic Materials Based on DSC and HFC signals. *93*(1) 143-152. Retrieved from http://dx.doi.org/10.1007/s10973-007-8864-3

Safety, C. f. C. P. (1995). Guidelines for Chemical Reactivity Evaluation and Application to Process Design. Center for Chemical Process Safety/AIChE. Retrieved from http://www.knovel.com.qe2a-proxy.mun.ca/web/portal/browse/display?_EXT_KNOVEL_DISPLAY_bookid=840

Safety, C. f. C. P. (2000). Guidelines for Chemical Process Quantitative Risk Analysis (2nd edition). Center for Chemical Process Safety/AIChE. Retrieved from http://www.knovel.com.qe2a-proxy.mun.ca/web/portal/browse/display?_EXT_KNOVEL_DISPLAY_bookid=677

Sanchirico, R. (2011). Model Selection and Parameters Estimation in Kinetic Thermal Evaluations using Semi-Empirical Models. *AIChE Journal,* doi:10.1002/aic.12711

Sarma, H. K., Yazawa, N., Moore, R. G., Mehta, S. A., Okazawa, N. E., Ferguson, H., & Ursenbach, M. G. (2002). Screening of Three Light-Oil Reservoirs for Application of Air Injection Process by Accelerating Rate Calorimetric and TG/PDSC Tests. *Journal of Canadian Petroleum Technology, 41*(3), 50-61.

Schmidt, L. (2005). The Engineering of Chemical Reactions (Second ed.). New York, USA: Oxford University Press.

Sears, P. (2006). Thermal Hazards in the Chemical Industry.

Shah, S., Fischer, U., & Hungerbuhler, K. (2003). A Hierarchical Approach for the Evaluation of Chemical Process Aspects from the Perspective of Inherent Safety. *Process Safety and Environmental Protection: Transactions of the Institution of Chemical Engineers, Part B, 81*(6), 430-443. Retrieved from http://dx.doi.org/10.1205/095758203770866601

Shah, S., Fischer, U., & Hungerbuhler, K. (2005). Assessment of Chemical Process Hazards in Early Design Stages. Paper Presented at the *Selected Papers Presented at the International Conference on Bhopal Gas Tragedy and its Effects on Process Safety, , 18*(4-6) 335-352. Retrieved from http://dx.doi.org/10.1016/j.jlp.2005.06.016

Shen, L., & Wang, X. (2005). Thermal Stability Assessment of Anti-Explosive Ammonium Nitrate. *Journal of University of Science and Technology Beijing: Mineral Metallurgy Materials (Eng Ed), 12*(1), 12-15.

Smart, R. S. (1991). Surface Layers in Base Metal Sulphide Flotation. *Minerals Engineering, 4*(7-11), 891-909.

Smith, J. C., Van Ness, H., & Abbott, M. (2001). Introduction to Chemical Engineering Thermodynamics (7th ed.). New York, USA: McGraw-Hill's.

Srinivasan, R., & Nhan, N. T. (2008). A Statistical Approach for Evaluating Inherent Benign-ness of Chemical Process Routes in Early Design Stages. *Process Safety and Environmental Protection, 86*(3), 163-174. Retrieved from http://dx.doi.org/10.1016/j.psep.2007.10.011

Stoessel, F. (2008). Thermal Safety of Chemical Processes: Risk Assessment and Process Design. Federal Republic of Germany: John Wiley-VCH Verlag GmbH & Co. KGaA.

Stroud, K. A. (2003). Advanced Engineering Mathematics with Addition by Dexter J. Booth (Fourth ed.). Hounsmills, Basingstokes, Hampshire, New York, USA: Palgrave Macmillan.

Thomas, J. E., Jones, C. F., Skinner, W. M., & Smart, R. S. C. (1998). The Role of Surface Sulfur Species in the Inhibition of Pyrrhotite Dissolution in Acid Conditions. *Geochimica Et Cosmochimica Acta, 62*(9), 1555-1565. doi: 10.1016/S0016-7037(98)00087-8

Thomas, J. E., Skinner, W. M., & Smart, R. S. C. (2001). A Mechanism to Explain Sudden Changes in Rates and Products for Pyrrhotite Dissolution in Acid Solution. *Geochimica Et Cosmochimica Acta, 65*(1), 1-12. doi: 10.1016/S0016-7037(00)00503-2

Toner, B. M., Santelli, C. M., Marcus, M. A., Wirth, R., Chan, C. S., McCollom, T., . . . Edwards, K. J. (2009). Biogenic Iron Oxyhydroxide Formation at Mid-ocean Ridge Hydrothermal Vents: Juan de Fuca Ridge. *Geochimica Et Cosmochimica Acta, 73*(2), 388-403. doi: 10.1016/j.gca.2008.09.035

Venugopal, B., & Kohn, D. Y. (2005). Chemical Reactivity Hazards and Inherently Safer Technology. Paper Presented at the *2005 AIChE Spring National Meeting, April 10, 2005 - April 14,* 3717-3724.

Wang, Q., Rogers, W. J., & Mannan, M. S. (2009). Thermal Risk Assessment and Rankings for Reaction Hazards in Process Safety. *Journal of Thermal Analysis and Calorimetry, 98*(1), 225-233. Retrieved from http://dx.doi.org/10.1007/s10973-009-0135-z

Zhang, P. Peng, J., Shen, X. Han, Z. Tian, A. Pang, H. Sha, J.Chen, Y.and Zhu, M. (2009). A Twofold Interpenetrating Framework Based on the α-Metatungstates. *Journal of Solid State Chemistry, 182*(12), 3399-3400-3405.

Zill, G. and Wright, S. (2011). Advanced Engineering Mathematics (Fourth ed.). Boston, USA: Jones and Barttlett Publishers International Series in Mathematics.

Appendix A

Activation Energy and Arrhenius' Constants

The activation energy and Arrhenius Constants of some first order reactions are as given in the table below with the validity of the range of operating conditions for 10 reactions:

Table A1: Class A of Activation Energy (Ea □ 400kJ/mol)

Reaction Type	Activation Energy(kJ/mol)	kt expression/rate expression/ Controlling mechanism	Temperature / Pressure Range	Reacting Species
Reduction of Metallic Oxide:$MnFe_2O_4$ using H_2	572	Diffusion control, x=0-0.3	800-900°C	$MnFe_2O_4$ & CH_4
Sintering of high density ThO_2-UO_2 Pellet (powder metallurgy)	500	Solid State dissolution of metals	1000-1500°C	ThO_2, U_3O_8 and UO_2
Evaporation of forsterite under isotopic fractionation	628	Solution of Metals	1500-1800°C	Forsterite
Elevated temperature Deformation of Fe-39.8Al & Fe-3.6Mn-39.4Al	410	Diffusion Controlled	1000-1500°C	Fe-39.8Al & Fe-3.6Mn-39.4Al
Sintering of Si_3N_4 with rare earth metal: La	677	Chemical Reaction Controlled	1700-1850°C	Si_3N_4, SiO_2, alkali earth oxide and rare earth metal
Sintering of Si_3N_4 with rare earth metal: Nd	546	Chemical Reaction Controlled	1700-1850°C	Si_3N_4, SiO_2, alkali earth oxide and rare earth metal
Sintering of Si_3N_4 with rare earth metal: Gd	487	Chemical Reaction Controlled	1700-1850°C	Si_3N_4, SiO_2, alkali earth oxide and rare earth metal
Sintering of Si_3N_4 with rare earth metal: Yb	424	Chemical Reaction Controlled	1700-1850°C	Si_3N_4, SiO_2, alkali earth oxide and rare earth metal
Crystallization of Meso-phase transition of thermotropic Co-Polyester	886	Diffusion Controlled	120-150°C	Thermotropic Co-Polyester

Note: The operating conditions of the experiments are as tabulated as shown with emphasis placed on temperature.

Table A2: Class B of Activation Energy (100kJ/mol □ Ea ≤ 400kJ/mol)

Reaction Type	Activation Energy(kJ/mol)	kt expression/rate expression/ Controlling mechanism	Temperature / Pressure Range	Reacting Species
Surface Pyrolysis/ Thermal Decomposition	120	Surface/ Chemical controlled	0-550°C, $2x10^{-7}$torr	$As(N(CH_3)_2)_n$ - TDMAA, Langmuir Adsorption on GaAs
Oxidation of Pyrite (particle size:147-295μm)	370	$1-(1-x)^{\frac{1}{3}}$	450-700°C	FeS_2 &O_2
Oxidation of Alex	219+/- 7		30-400	Nanometre size Aluminium powder
Thermal Decomposition of PTFE in the presence of Si	287.5		750-850°C	PTFE and Si
Thermal Decomposition of PTFE in the presence of Ca_2Si	356.6		770-850°C	PTFE & Ca_2Si
Thermal Decomposition	190+/- 6		25-200°C	KDNBF, Potassium-4,6-dinitrobenzofurazan
Oxidation of Pyrite (particle size:74-104μm)	199	$1-3(1-x)^{\frac{2}{3}}+2(1-x)$	450-700°C	FeS_2 &O_2
Decomposition of pure NH_4NO_3	102.6	Chemical Reaction Controlled	25-350°C	NH_4NO_3
Decomposition of pure NH_4NO_3 pyrite	101.8	Chemical Reaction Controlled	25-350°C	NH_4NO_3 & Pyrite
Reduction of Metallic Oxide:Fe_2O_3 using CH_4	271	Diffusion control	800-900°C	Fe_2O_3 & CH_4
Reduction of Metallic Oxide:$MnFe_2O_4$ using CH_4	139	Diffusion control, x=0-0.3	800-900°C	$MnFe_2O_4$ & CH_4
Reduction of Metallic Oxide:$ZnFe_2O_4$ using CH_4	272	Random nucleation control, x=0-0.3		$ZnFe_2O_4$ & CH_4
Reduction of Metallic Oxide:Fe_2O_3 using CO	104	Chemical reaction control, x=0-0.3	700-900°C	Fe_2O_3 & CO
Reduction of Metallic Oxide:$NiFe_2O_4$ using H_2	117	Chemical reaction control, x=0-1.0	340-420°C	$NiFe_2O_4$ & H_2
Reduction of Metallic Oxide:NiO+$MgAl_2O_4$ using CH_4	114	Chemical reaction control, x=0-1.0	800-1000°C	NiO, $MgAl_2O_4$ & H_2
Oxidation of Metallic oxides: $MnFe_2O_4$ using $H_2O(g)$	109.7	Diffusion reaction Control, x=0-1.0	500-900°C	$MnFe_2O_4$ & H_2O
Oxidation of Metallic oxides: $ZnFe_2O_4$ using $H_2O(g)$	102.3	Diffusion reaction Control only, x=0-1.0	500-700°C	$ZnFe_2O_4$ & H_2O
Decomposition of Nitrous oxide over Cu-ZSM-5	100	Chemical reaction control	≤200°C	N_2O & Cu-ZSM-5

Table A2: Class B of Activation Energy (100kJ/mol □ Ea ≤ 400kJ/mol) Cont'd

DME formation via Partial auto thermal Methanol Decomposition	117(±2%)	Surface adsorption reaction	245°C	CH_3OH & metallic catalyst
Decomposition of Kerogen to produce Benzene	227	Chemical Reaction	20-800°C	Kerogen
Decomposition of Kerogen to produce Hexane	244	Chemical Reaction	20-800°C	Kerogen
Decomposition of Kerogen to produce Toluene	242	Chemical Reaction	20-800°C	Kerogen
Decomposition of Kerogen to produce Phenol	255	Chemical Reaction	20-800°C	Kerogen
Decomposition of Kerogen to produce Heptane	233	Chemical Reaction	20-800°C	Kerogen
Decomposition of Kerogen to produce Indene	230	Chemical Reaction	20-800°C	Kerogen
Thermal Decomposition (Pyrolitic reaction) of $[Cu(bbi)_5H[H_2W_{12}O_{40}]]$ where bbi = 1,1'-(1,4-butanediyl)bis(Imidazole))	154.49±17.90	Pyrolitic Chemical Reaction	25-600°C with major reaction occurring btw 260-600°C	$[Cu(bbi)=H[H_2W_{12}O_{40}]]$ where bbi = 1,1'-(1,4-butanediyl)bis(Imidazole))

Note: The operating conditions of the experiments are as tabulated as shown with emphasis placed on temperature.

Table A3: Class C of Activation Energy (10kJ/mol □ Ea ≤ 100kJ/mol)

Reaction Type	Activation Energy(kJ/mol)	kt expression/rate expression/ Controlling mechanism	Temperature / Pressure Range	Reacting Species
Methanol Decomposition (autothermal partial oxidation to produce H2 for fuel)	76(±4%)	1st order reaction,	250-400°C	CH_3OH
Roasting of Chromium Oxide with $NaNO_3$	22.7	Ash-layer Control	100-500°C	Cr_2O_3 & $NaNO_3$
Oxidation of Pyrite (particle size:≤43μm)	97	$1-3(1-x)^{\frac{2}{3}}+2(1-x)$	450-700°C	FeS_2 &O_2
Adsorption of Arsenate on synthetic Geothite	20-43	$\frac{dx}{dt}=kf(x)$, diffusion controlled	----------	$Fe^{3+}O(OH)$ & AsO_4^{3-}
Adsorption of Arsenate on synthetic Geothite	22-45	$\frac{dx}{dt}=kf(x)$, chemical reaction controlled	----------	$Fe^{3+}O(OH)$ & AsO_4^{3-}
Leaching of metals from spent hydrate Sulphurization, Mo	31 ± 2	$1-(1-x)^{\frac{1}{2}}$	30-70°C	Mo, $H_2C_2O_4$, H_2O_2
Desulphurization in presence of oxidant	11.81	Surface/Chemical reaction Controlled	25°C	Coal/CH_3CO_3H

Table A3: Class C of Activation Energy (10kJ/mol □ Ea ≤ 100kJ/mol) Cont'd

Desulphurization in presence of oxidant	10.95	Surface reaction mechanism	25°C	Coal/CH_3CO_3H/Cu+
Photocatalytic decomposition of Methylene Blue	36.23	Chain reaction controlled	Ambient temperature	TiO + dye/ TiO-Dye
Steam Reforming of Methanol	81(±7%)	Chemical Reaction Controlled	700-1100°C	CH_3OH & steam
Leaching of metals from spent hydrate Sulphurization, Ni	36 ± 4	$1-(1-x)^{\frac{1}{2}}$	30-70°C	Ni, $H_2C_2O_4$, H_2O_2
Leaching of metals from spent hydrate Sulphurization, V	30 ± 4	$1-(1-x)^{\frac{1}{2}}$	30-70°C	V, $H_2C_2O_4$, H_2O_2
Leaching of metals from spent hydrate Sulphurization, Al	57 ± 3	$1-(1-x)^{\frac{1}{2}}$	30-70°C	Al, $H_2C_2O_4$, H_2O_2
Reduction of Metallic Oxide: NiO/YSZ using H_2	82	Chemical reaction/diffusion control, x=0-1.0	800-1000°C	NiO & H_2
Reduction of Metallic Oxide:Fe_2O_3 using H_2	23.9	Chemical reaction control, x=0-0.3	700-900°C	Fe_2O_3 & H_2
Reduction of Metallic Oxide:$CuO+Al_2O_3$ using CH_4&H_2O	60	Chemical reaction control, x=0-1.0	500-800°C	CuO, Al_2O_3, CH_4 & H_2O
Oxidation of Metallic oxides: Fe_2O_3 using H_2O(g)	77.9	Diffusion Control, x=0-0.3	500-900oC	Fe_2O_3 & H_2O(g)
Oxidation of Metallic oxides: $MnFe_2O_4$	57.4	Diffusion Control, x=0-1.0	500-900°C	$MnFe_2O_4$ & H_2O(g)
Oxidation of Metallic oxides: Ni/Bentonite using O_2	31	Diffusion Control, x=0-1.0	900-1000°C	Ni, Bentonite & O_2
Oxidation of Metallic oxides: NiO/$MgAl_2O_4$ using O_2	40	Chemical reaction Control, x=0-1.0	800-1000°C	NiO, $MgAl_2O_4$ & O_2
Oxidation of Metallic oxides: NiO/YSZ using O_2	17-56	Chemical reaction+ diffusion Control, x=0-1.0	600-800°C	NiO & O_2
Oxidation of Metallic oxides: CuO/Al_2O_3 using O_2	15	Chemical reaction Control, x=0-1.0	500-900°C	CuO, Al_2O_3 & O_2
Water gas Shift Reaction	99.1(±25%), varies with conditions.	Surface reaction (Adsorption/ Desorption) cum Chemical Reaction controlled	75-1000°C depending on catalyst used and routes	CO, H_2O and metallic Catalysts such as Cu, Pd, Fe, etc.

Note: The operating conditions of the experiments are as tabulated as shown with emphasis placed on temperature.

Table A4: Class D of Activation Energy (Ea ≤10kJ/mol)

Reaction Type	Activation Energy(kJ/mol)	kt expression/rate expression/ Controlling mechanism	Temperature / Pressure Range	Reacting Species
Diffusion of water in Silicalite	1.8	Diffusion Controlled	25-125°C	Water & Silicalite e.g.$Mg_2Al_2Si_5O_{18}$
Diffusion of water in Human Cell	10	Diffusion Controlled	32-42°C	Water And Cell/ Tissues
Gas Phase Reaction between NO & O_3	10	Light Controlled	Ambient Temperature	NO & O_3
Alkali Silica Reactivity of Concrete with 1.0N NaOH: Opal mineral	7.0	Thermal Chemical reaction/ expansion	60-80°C	NaOH, water and Opal ($SiO_2.nH_2O$)
Alkali Silica Reactivity of Concrete with 1.0N NaOH: Jasper mineral	8.0	Thermal Chemical reaction/ expansion	60-80°C	NaOH, water and Jasper (quartz coloured by oxides of Iron.)
Alkali Silica Reactivity of Concrete with 1.0N NaOH: Chalcedony mineral	8.1	Thermal Chemical reaction/ expansion	60-80°C	NaOH, water and Chalcedony (quartz, air and water)
Alkali Silica Reactivity of Concrete with 1.0N NaOH: Flint mineral	8.5	Thermal Chemical reaction/ expansion	60-80°C	NaOH, water and Flint (microcrystalline and cryptocrystalline silica)
Alkali Silica Reactivity of Concrete with 1.0N NaOH: Rhyolite mineral	9.1	Thermal Chemical reaction/ expansion	60-80°C	NaOH, water and Rhyolite.
Desulphurization in presence of oxidant	8.52	Adsorption/ Chemical reaction Controlled	25°C	Coal/CH_3CO_3H/Pd_{2+}
Thermal Decomposition of Gases Ammonium Nitrate(Zero-order rxn)	6.00	Diffusion Controlled	25°C-930°C, 5-6.2torr	$HNO_3+(B_2O_3/SiO_2)$ → OH + NO_2 + (B_2O_3/SiO_2)

Note: The operating conditions of the experiments are as tabulated as shown with emphasis placed on temperature.

Classification of Arrhenius' Constants or Pre-Exponential Factors

Table A5: Class A of Arrhenius's Constant (A □ $10^{10}s^{-1}$)

Reaction Type	Arrhenius Constant (s^{-1})	Temperature / Pressure Range	Reacting Species
Decomposition of Kerogen to produce Hexane	$1.88x10^{15}$	20-800°C	Kerogen
Decomposition of Kerogen to produce Phenol	$1.21x10^{16}$	20-800°C	Kerogen
Oxidation of Alex	$3.0x10^{13}$	30-400	Nanometre size Aluminium powder
Thermal Decomposition of PTFE in the presence of Si	$2.3x10^{13}$	750-850°C	PTFE and Si
Thermal Decomposition of PTFE in the presence of Ca_2Si	$5.94x10^{19}$	770-850°C	PTFE & Ca_2Si
Thermal Decomposition	$4.81x10^{16}$	25-200°C	KDNBF, Potassium-4,6-dinitrobenzofurazan
Decomposition of Kerogen to produce Benzene	$9.35x10^{13}$	20-800°C	Kerogen
Decomposition of Kerogen to produce Heptane	$4.13x10^{14}$	20-800°C	Kerogen
Decomposition of Kerogen to produce Indene	$1.64x10^{14}$	20-800°C	Kerogen
Decomposition of Kerogen to produce Toluene	$1.20x10^{15}$	20-800°C	Kerogen
Vapor Phase Decomposition of SiH_2Cl_2	$2.00x10^{13}$	700°C	SiH_2Cl_2
Vapor Phase Synthesis of $SiHCl_2NH_2$	$3.98x10^{10}$	700°C	NH_3 & SiH_2Cl_2
Thermal Decomposition of Dicumyl peroxide	$3.124x10^{12}$	25-600°C	Dicumyl Peroxide

Note: The operating conditions of the experiments are as tabulated as shown with emphasis placed on temperature.

Table A6: Class B of Arrhenius's Constant ($10^{-1}s^{-1} \square A \leq 10^{10}s^{-1}$)

Reaction Type	Arrhenius Constant (s^{-1})	Temperature / Pressure Range	Reacting Species
Thermal Decomposition (Pyrolitic reaction) of $[Cu(bbi)_3H[H_2W_{12}O_{40}]]$ where bbi = 1,1'-(1,4-butanediyl)bis(Imidazole))	$9.045x10^3$	25-600°C with major reaction occurring btw 260-600°C	$[Cu(bbi)=H[H_2W_{12}O_{40}]]$ where bbi = 1,1'-(1,4-butanediyl)bis(Imidazole))
Synthesis of complex by Silylene insertion	$5.01x10^9$	700°C	SiH_2Cl_2 & $SiCl_2$
Decomposition of pure NH_4NO_3	$4.55x10^7$	25-350°C	NH_4NO_3
Decomposition of pure NH_4NO_3 pyrite	$2.57x10^9$	25-350°C	NH_4NO_3 & Pyrite
Thermal Decomposition of Gaseous Ammonium Nitrate(Zero-order rxn)	7.91×10^7	25°C-930°C, 5-6.2torr	$HNO_3+(B_2O_3/SiO_2) \rightarrow OH + NO_2 + (B_2O_3/SiO_2)$

Note: The operating conditions of the experiments are as tabulated as shown with emphasis placed on temperature.

Table A7: Class C of Arrhenius's Constant ($A \leq 10^{-1}s^{-1}$) and Lower

Reaction Type	Arrhenius Constant (s^{-1})	Temperature / Pressure Range	Reacting Species
Roasting of Chromium Oxide with $NaNO_3$	$3.04x10^{-3}$	100-500°C	Cr_2O_3 & $NaNO_3$
Desulphurization in presence of oxidant	$11.30x10^{-3}$	25°C	$Coal/CH_3CO_3H$
Desulphurization in presence of oxidant	$1.64x10^{-3}$	25°C	$Coal/CH_3CO_3H/Cu^+$
Desulphurization in presence of oxidant	$2.01x10^{-3}$	25°C	$Coal/CH_3CO_3H/Pd^{2+}$
Thermal Decomposition of 1,1-dimethylhydrazine	$(6.14\pm 3.84)x10^{-3}$	600-730°C	1,1-dimethylhydrazine
Surface Pyrolysis/ Thermal Decomposition	$6x10^{-14}$	0-550°C, $2x10^{-7}$torr	$As(N(CH_3)_2)_n$ - TDMAA, Langmuir Adsorption on GaAs

Note: The operating conditions of the experiments are as tabulated as shown with emphasis placed on temperature.

APPENDIX B

Normal PDF and CDF for Thermal Hazardous Reactions

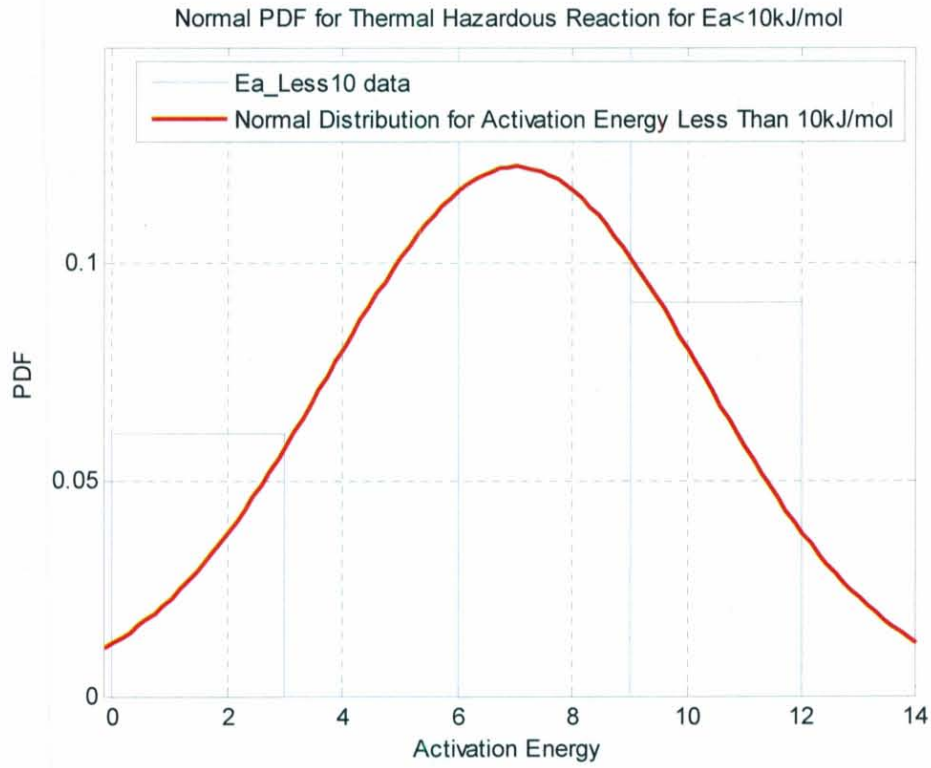

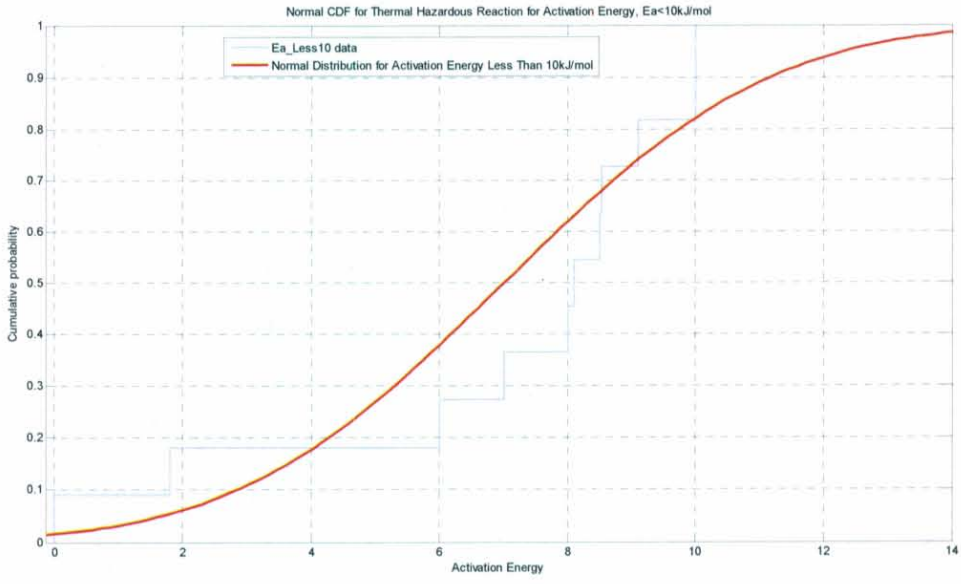

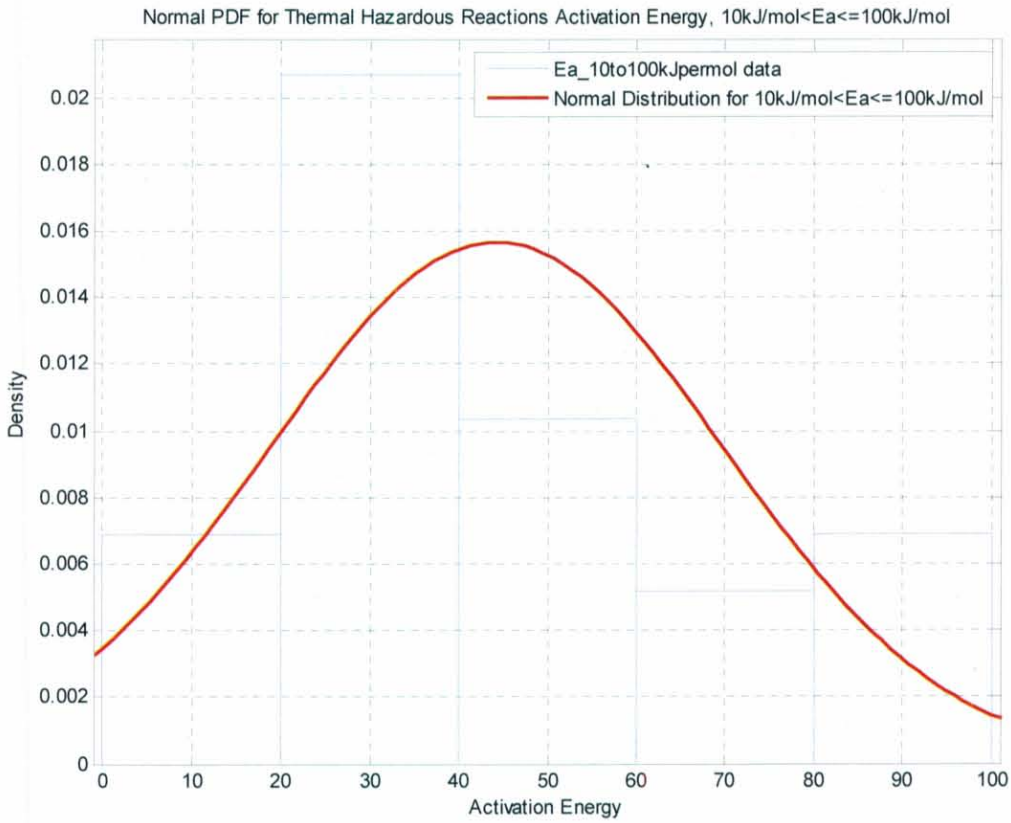
Normal PDF for Thermal Hazardous Reactions Activation Energy, 10kJ/mol<Ea<=100kJ/mol
Ea_10to100kJpermol data
Normal Distribution for 10kJ/mol<Ea<=100kJ/mol
Density
0.02
0.018
0.016
0.014
0.012
0.01
0.008
0.006
0.004
0.002
0
0
10
20
30
40
50
60
70
80
90
100
Activation Energy

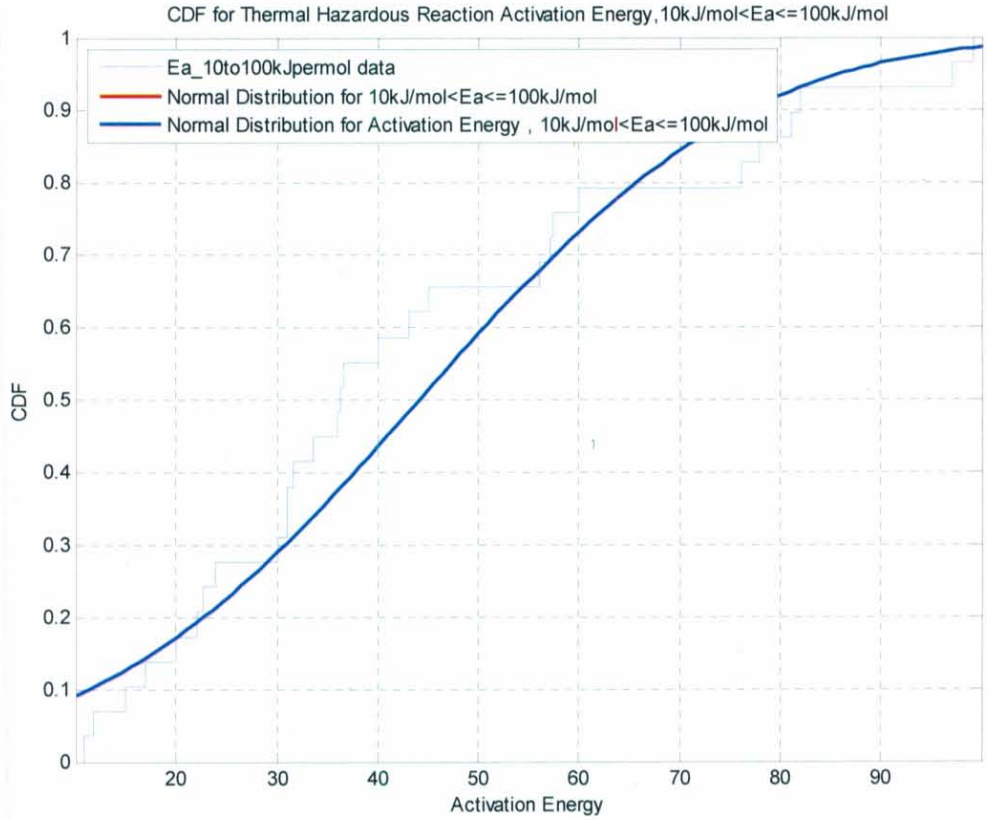
CDF for Thermal Hazardous Reaction Activation Energy,10kJ/mol<Ea<=100kJ/mol
Ea_10to100kJpermol data
Normal Distribution for 10kJ/mol<Ea<=100kJ/mol
Normal Distribution for Activation Energy , 10kJ/mol<Ea<=100kJ/mol
CDF
Activation Energy
0
0.1
0.2
0.3
0.4
0.5
0.6
0.7
0.8
0.9
1
20
30
40
50
60
70
80
90

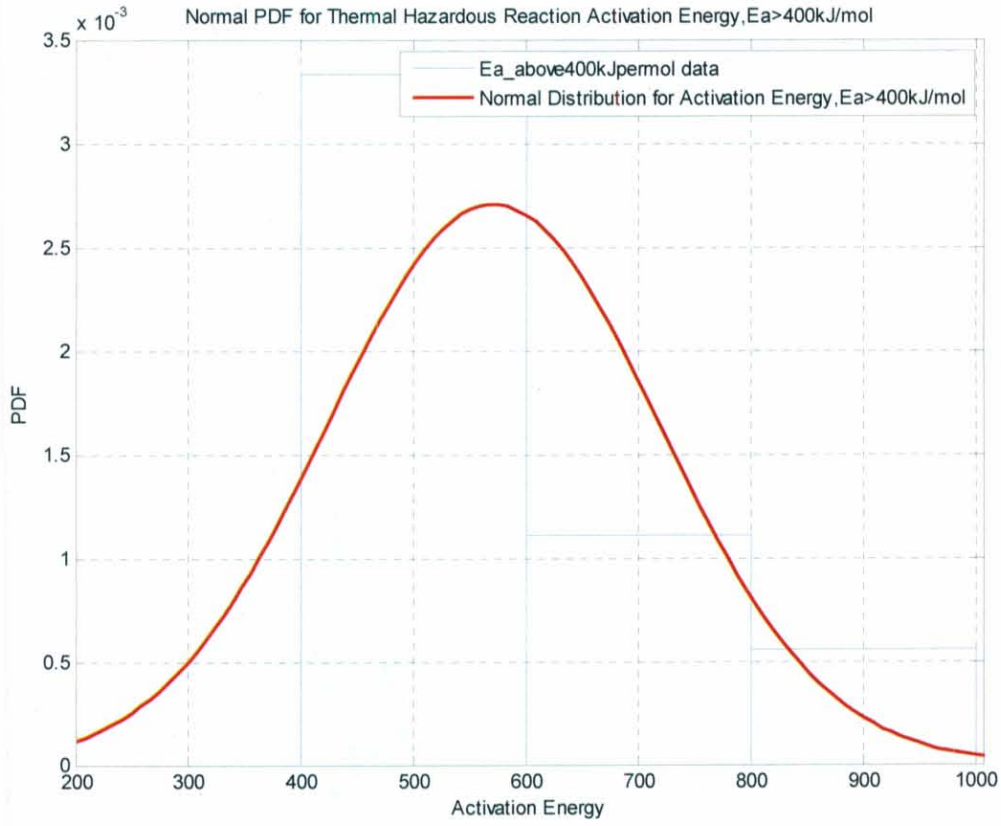
Normal PDF for Thermal Hazardous Reaction Activation Energy,Ea>400kJ/mol
x 10^-3
3.5
3
2.5
2
1.5
1
0.5
0
PDF
200
300
400
500
600
700
800
900
1000
Activation Energy
Ea_above400kJpermol data
Normal Distribution for Activation Energy,Ea>400kJ/mol

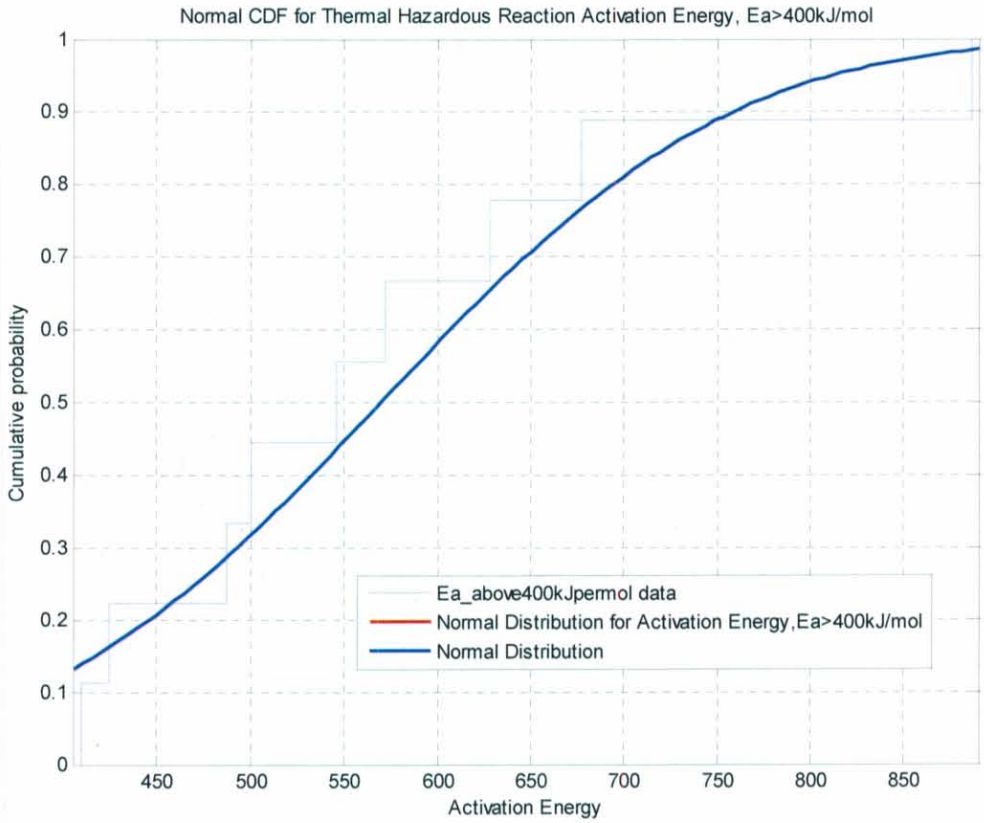
Normal CDF for Thermal Hazardous Reaction Activation Energy, Ea>400kJ/mol
Cumulative probability
Activation Energy
0
0.1
0.2
0.3
0.4
0.5
0.6
0.7
0.8
0.9
1
450
500
550
600
650
700
750
800
850
Ea_above400kJpermol data
Normal Distribution for Activation Energy,Ea>400kJ/mol
Normal Distribution

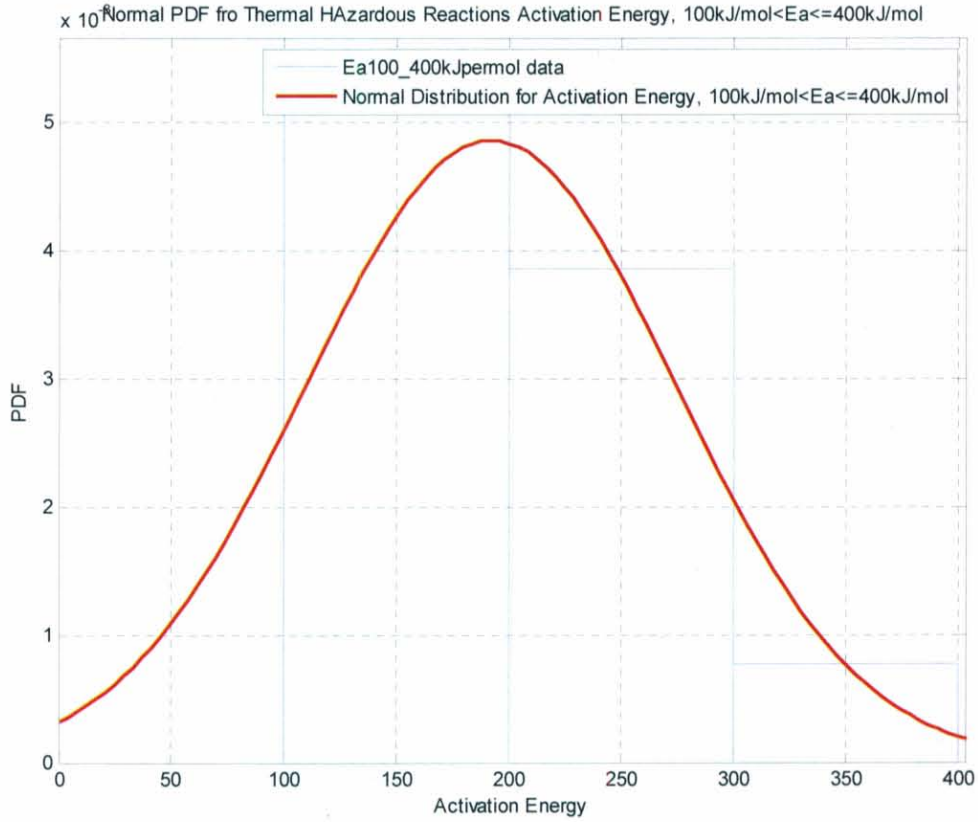
Normal PDF fro Thermal HAzardous Reactions Activation Energy, 100kJ/mol<Ea<=400kJ/mol
x 10^-3
Ea100_400kJpermol data
Normal Distribution for Activation Energy, 100kJ/mol<Ea<=400kJ/mol
PDF
Activation Energy
0
1
2
3
4
5
0
50
100
150
200
250
300
350
400

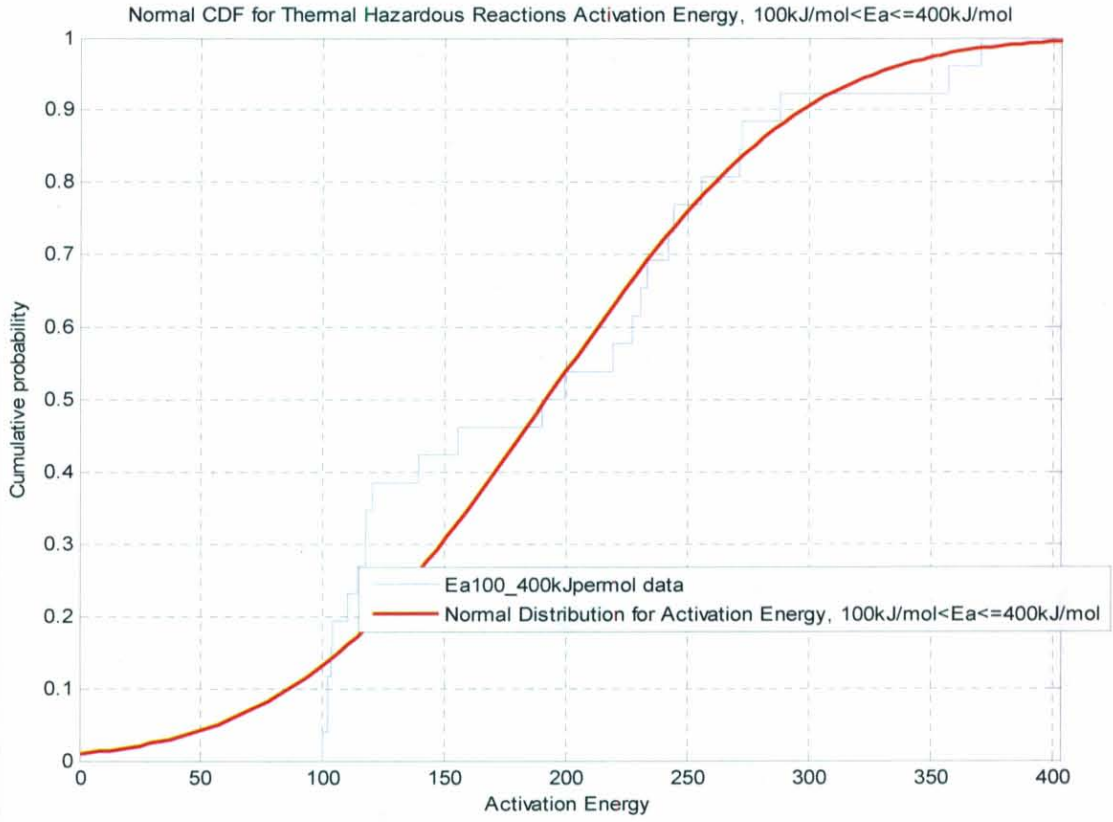
Normal CDF for Thermal Hazardous Reactions Activation Energy, 100kJ/mol<Ea<=400kJ/mol
Cumulative probability
Activation Energy
Ea100_400kJpermol data
Normal Distribution for Activation Energy, 100kJ/mol<Ea<=400kJ/mol
0
0.1
0.2
0.3
0.4
0.5
0.6
0.7
0.8
0.9
1
0
50
100
150
200
250
300
350
400

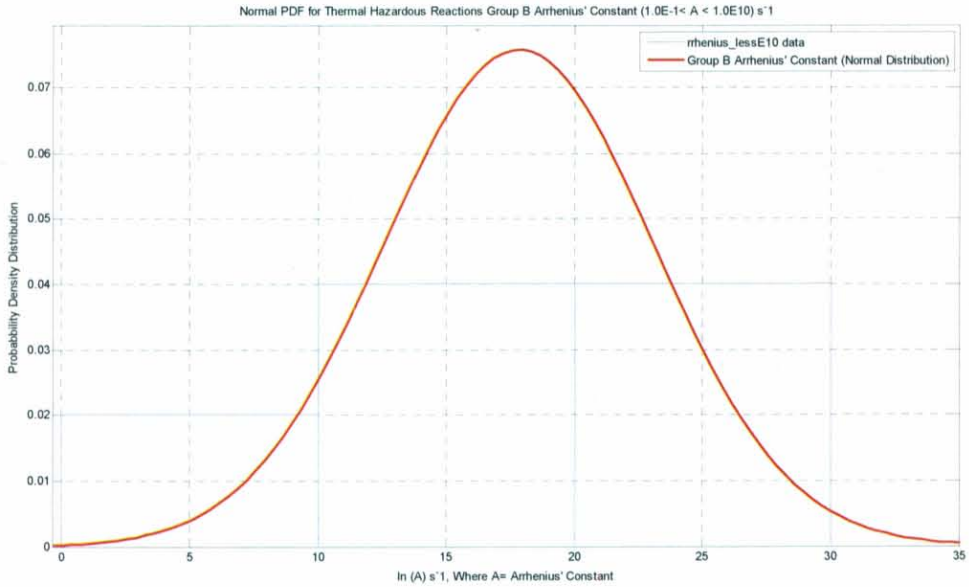
Normal PDF for Thermal Hazardous Reactions Group B Arrhenius' Constant (1.0E-1< A < 1.0E10) s^1
rrhenius_lessE10 data
Group B Arrhenius' Constant (Normal Distribution)
Probability Density Distribution
0.07
0.06
0.05
0.04
0.03
0.02
0.01
0
0
5
10
15
20
25
30
35
ln (A) s^1, Where A= Arrhenius' Constant

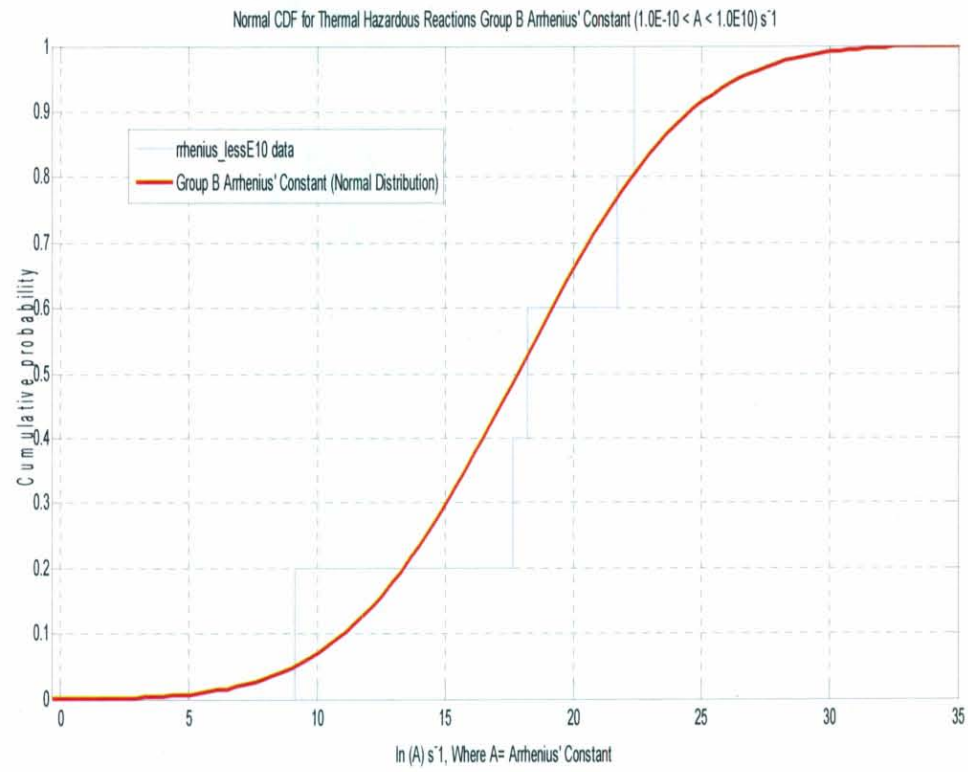
Normal CDF for Thermal Hazardous Reactions Group B Arrhenius' Constant (1.0E-10 < A < 1.0E10) s^1
rrhenius_lessE10 data
Group B Arrhenius' Constant (Normal Distribution)
Cumulative probability
1
0.9
0.8
0.7
0.6
0.5
0.4
0.3
0.2
0.1
0
0
5
10
15
20
25
30
35
ln (A) s^1, Where A= Arrhenius' Constant

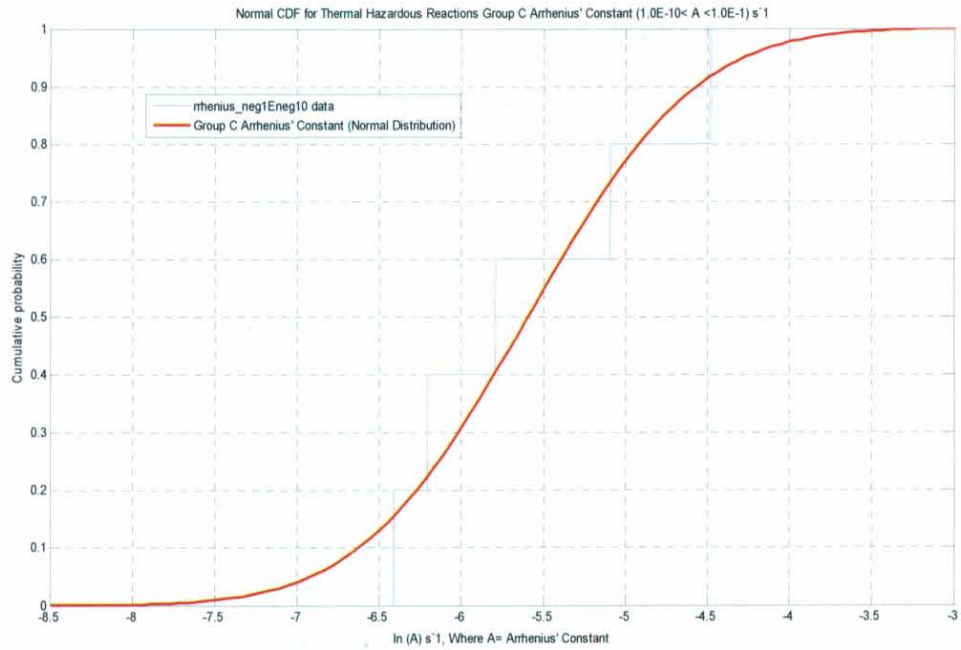
Normal CDF for Thermal Hazardous Reactions Group C Arrhenius' Constant (1.0E-10< A <1.0E-1) s^1
rrhenius_neg1Eneg10 data
Group C Arrhenius' Constant (Normal Distribution)
Cumulative probability
ln (A) s^1, Where A= Arrhenius' Constant

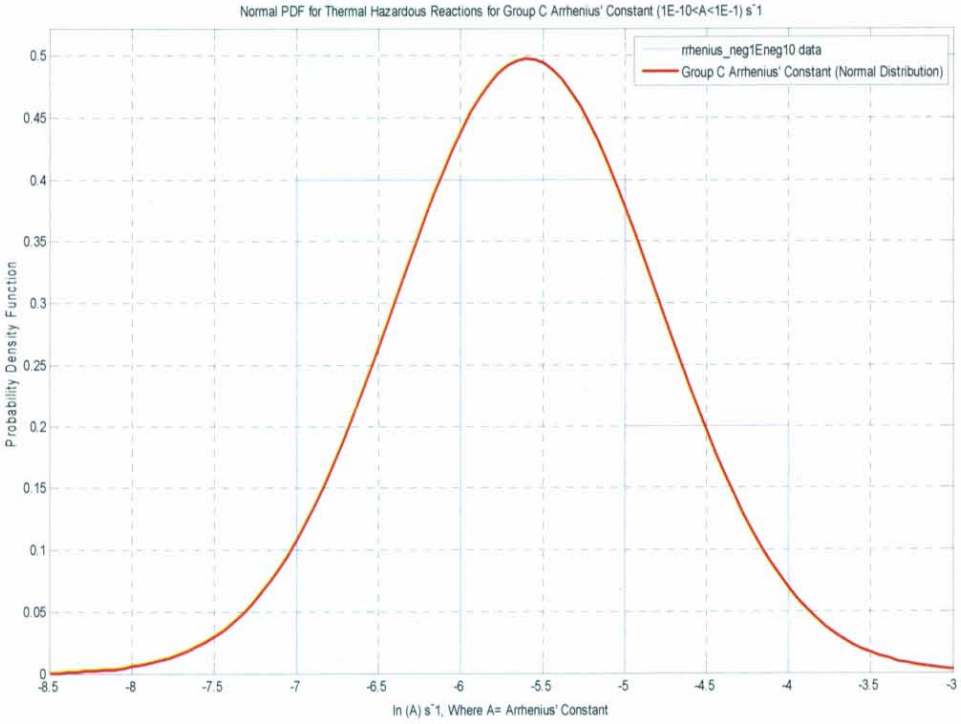
Normal PDF for Thermal Hazardous Reactions for Group C Arrhenius' Constant (1E-10<A<1E-1) s^1
rrhenius_neg1Eneg10 data
Group C Arrhenius' Constant (Normal Distribution)
Probability Density Function
ln (A) s^1, Where A= Arrhenius' Constant

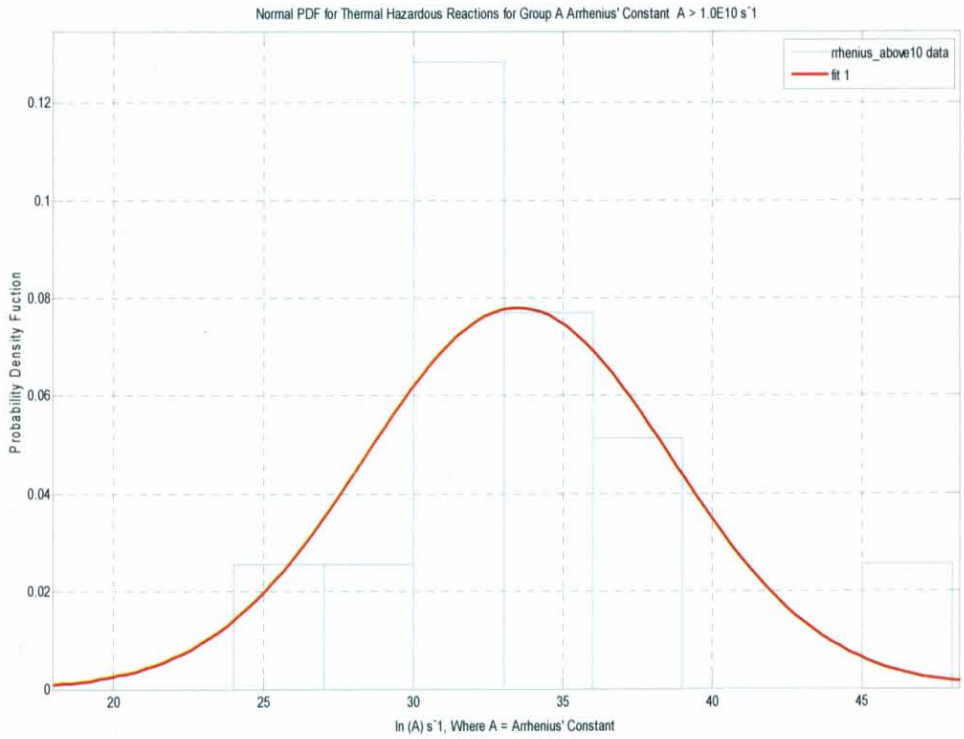
Normal PDF for Thermal Hazardous Reactions for Group A Arrhenius' Constant A > 1.0E10 s^1
rrhenius_above10 data
fit 1
Probability Density Fuction
0.12
0.1
0.08
0.06
0.04
0.02
0
20
25
30
35
40
45
ln (A) s^1, Where A = Arrhenius' Constant

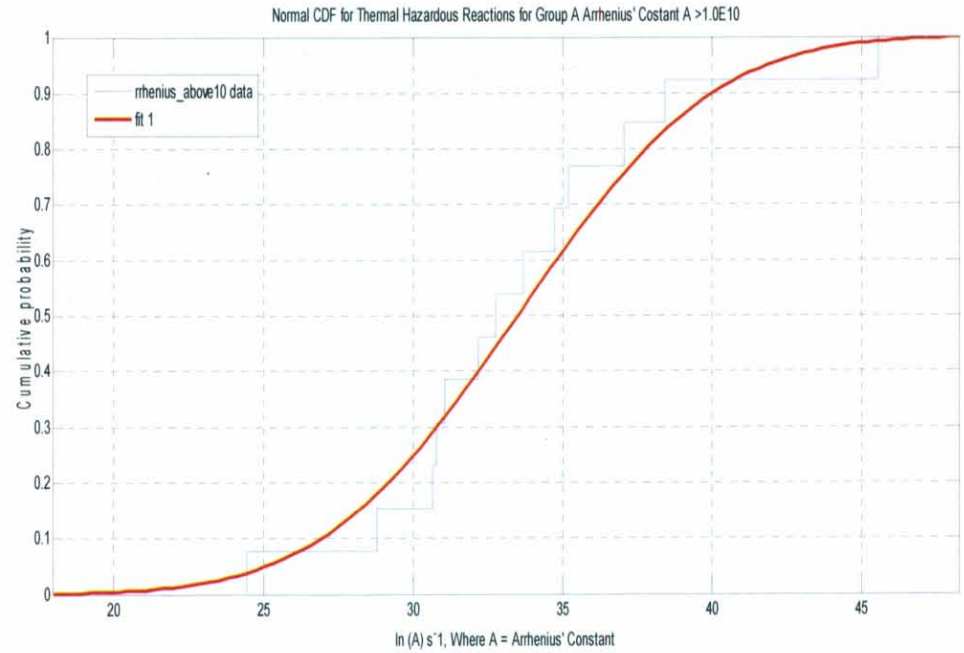
Normal CDF for Thermal Hazardous Reactions for Group A Arrhenius' Costant A >1.0E10
rrhenius_above10 data
fit 1
Cumulative probability
1
0.9
0.8
0.7
0.6
0.5
0.4
0.3
0.2
0.1
0
20
25
30
35
40
45
ln (A) s^1, Where A = Arrhenius' Constant

Table B1: Mean and Standard Deviation of Each Class of the Arrhenius' Constants

Class/ Group	Range of Values of Raw A (s^{-1})	Mean of ln(A), μ	Standard Deviation of ln(A), σ
A	□ 1.0×10^{10}	33.4633	5.12236
B	1.0×10^{-1} □ A ≤ 1.0×10^{10}	17.7863	5.27284
C	≤ 1.0×10^{-1}	-5.59889	0.802494

Table B2: Mean and Standard Deviation of Each Class of the Activation Energies

Class/ Group	Range of Values of Ea (kJ/mol)	Mean of Ea (kJ/mol),μ	Standard Deviation of Ea (kJ/mol), σ
A	□ 400	570	147.459
B	100 □ Ea ≤ 400	191.461	82.1525
C	10 □ Ea ≤ 100	46.8474	27.03
D	≤ 10	7.702	2.4104

Appendix C

Table C1: Raw Data of the Ore Samples Based on their Mineralogy

Sample	Borehole	Depth (m)	Pyrrh	Troil	Pentla	Chalc + Cuba	Magn	Plagio	Biotite	Chlori	% Sum	MW App	ρ(kgm^{-3})
1	03-601	198.60	64.47	0.00	8.47	19.71	3.07	0.00	0.02	0.02	95.76	172.39	4.288
2	03-601	207.00	73.34	0.00	6.89	14.03	3.13	0.00	0.04	0.01	97.44	155.00	4.369
3	03-601	217.20	84.74	0.00	6.28	5.60	1.42	0.00	0.04	0.01	98.09	136.86	4.473
4	07-824	476.50	71.19	18.13	6.58	2.64	0.45	0.15	0.09	0.10	99.33	135.67	4.573
5	07-833	121.00	67.89	14.04	12.06	4.12	1.76	0.00	0.01	0.00	99.88	176.72	4.557
6	07-840	117.00	55.61	15.95	10.86	6.29	1.21	1.27	1.17	2.19	94.55	181.76	4.312
7	05-658	225.00	68.44	19.03	8.83	2.92	0.78	0.00	0.00	0.00	100.00	151.60	4.594
8	05-658	257.00	49.92	15.62	20.39	13.13	0.87	0.00	0.00	0.00	99.93	245.51	4.593
9	07-829	200.00	74.62	11.50	7.62	2.51	1.92	0.00	0.06	1.23	99.46	149.01	4.505
10	07-829	210.00	68.32	15.02	9.21	5.66	1.53	0.00	0.02	0.01	99.77	159.01	4.552
11	05-669	192.00	53.42	12.29	21.61	10.17	2.24	0.00	0.00	0.00	99.73	251.41	4.541
12	05-670	198.00	59.43	12.52	15.27	10.76	1.72	0.00	0.00	0.00	99.70	207.93	4.546
13	06-774	352.00	57.91	14.57	20.21	4.58	2.44	0.00	0.05	0.00	99.76	234.40	4.541
													4.496

NOTE

Apparent molecular weight and density of each ore sample were determined from their constituent mineralogy.

Table C2: Ore Samples Elemental Analysis

Sample	Borehole	Depth (m)	Field Observation	Fe	S	Ni	Cu	Others (wt%)	wt% Sum
1	03-601	198.60	No oxidation noted	54.40	36.32	5.70	4.87	0.00	101.29
2	03-601	207.00	Strong oxidation	56.90	36.72	3.80	1.54	1.04	100.00
3	03-601	217.20	Weak oxidation	56.18	37.66	3.70	1.51	0.96	100.01
4	07-824	476.50	Strong oxidation	50.90	36.10	2.70	0.90	9.40	100.00
5	07-833	121.00	Weak oxidation	51.80	36.90	3.60	1.40	6.20	99.90
6	07-840	117.00	Bronze Colour	50.50	33.40	4.10	2.30	9.60	99.90
7	05-658	225.00	No oxidation	56.28	36.40	3.34	1.04	2.95	100.01
8	05-658	257.00	No oxidation	51.41	34.31	7.20	4.65	2.42	99.99
9	07-829	200.00	Strong oxidation	51.50	34.60	3.30	1.00	9.60	100.00
10	07-829	210.00	Rapid oxidation	51.80	36.20	3.50	1.90	6.60	100.00
11	05-669	192.00	N/A	53.38	34.94	6.46	3.69	1.56	100.03
12	05-670	198.00	N/A	54.52	34.06	3.27	2.06	6.08	99.99
13	06-774	352.00	N/A	54.59	33.54	3.48	1.13	7.26	100.00

Table C3: Raw Experimental Data on Thermal Oxidation of Most Exothermic Ore Samples

Sample	ΔH_r (J/g)	E_a (kJ/mol) [Friedman Analysis]	E_a (kJ/mol) [Ozawa Analysis]	E_a (kJ/mol) [ASTM E698]	dTAD (°C) (φ=1/φ=2)	SADT (°C)
A	-119.8 ± 12.3	40 -100	75-90	78.585	199/99	72.00
B	-236.3 ± 48.1	50 -135	80-170	77.822	393/196	81.00
C	-126.8 ± 39.4	80 -110	85-95	75.123	211/105	63.00
D	-35.8 ± 6.3	80-150	80-110	92.939	59.7/29.8	72.00

NOTE

Sample A = Self-Heating Sulfide containing Iron ore 03-601 taken from depth of 198m

Sample B = Self-Heating Sulfide containing Iron ore 03-601 taken from depth 207m

Sample C = Self-Heating Sulfide containing Iron ore 03-601 taken from 217m

Sample D = Self-Heating Sulfide containing Iron ore 05-658 taken from 257m

Table C4: Calculated Experimental Data Used for the Simulation Based on Most Exothermic Samples

Sample	Cp (J/gK) φ=1	Cp (J/gK) φ=2	Cp (J/gK) Average	E_a (kJ/mol) Average [Friedman Analysis]	E_a (kJ/mol) Average [Ozawa Analysis]	E_a (kJ/mol) [ASTM E698]
A	0.6020	0.6051	0.6035	70.00	82.50	78.585
B	0.6013	0.6028	0.6020	92.50	125.00	77.822
C	0.6009	0.6038	0.6024	95.00	90.00	75.123
D	0.5997	0.6007	0.6002	115.00	95.00	92.939

Sample	ΔCp (J/gK) φ=1, ±	ΔCp (J/gK) φ=2,±	ΔCp (J/gK) AVG (±)
A	0.0618	0.0621	0.1239
B	0.1224	0.1227	0.2451
C	0.1867	0.1876	0.3743
D	0.1055	0.1057	0.2112

Table C5: Calculated Experimental Data Used for the Simulation Based on Most Exothermic Samples (Cont'd)

A (s^{-1})	A (s^{-1})	A (s^{-1})	MW (App)	ρ (g/cm3)	Cp (J/molK)	ΔH_r (J/mol)
[Friedman Analysis]	[Ozawa Analysis]	[ASTM E698]			Average	
6.337E+12	6.300E+12	6.310E+12	172.39	4.288	104.04	-20652
6.278E+12	6.232E+12	6.313E+12	155.00	4.369	93.32	-36627
6.274E+12	6.283E+12	6.320E+12	136.86	4.473	82.44	-17354
6.244E+12	6.274E+12	6.277E+12	245.51	4.593	147.35	-8789

Table C6: Experimental Data of Thermally Oxidized Ore Samples Based on Particle Size Distribution

Particle Size (μm)	ΔH_r (J/g)	E_a (kJ/mol) [Friedman]	E_a (kJ/mol) [ASTM E698]	dTAD(°C) (φ=1/φ=2)	SADT (°C)
<75	-35.8 ± 6.3	80-145	92.939	59/29	72 (34 days)
75-180	-3.2 ±1.5	35-130	93.412	5 & 2	-
>180	-1.3 ± 7.6E-1	75-140	85.514	2 & 1	-
Mixed	-19.2 ± 3.2	35-110	91.632	32/16	69 (32 days)

Table C7: Calculated Experimental Data Used for the Simulation Based on Particle Size Distribution

Particle Size (μm)	Cp (J/gK) φ=1	Cp (J/gK) φ=2	Cp (J/gK) Average	E_a (kJ/mol) Average [Friedman Analysis]	E_a (kJ/mol) [ASTM E698]
<75	0.6068	0.6172	0.6120	112.50	92.939
75-180	0.6400	0.8000	0.7200	92.50	93.412
>180	0.6500	0.6500	0.6500	107.50	85.514
Mixed	0.6000	0.6000	0.6000	72.50	91.632

	ΔCp (J/gK) φ=1	ΔCp (J/gK) φ=2	ΔCp (J/gK) AVG
<75	0.1068	0.1086	0.2154
75-180	0.3000	0.3750	0.6750
>180	0.3047	0.3047	0.6094
Mixed	0.2813	0.2813	0.5625

Table C8: Calculated Experimental Data Used for the Simulation Based on Particle Size Distribution (Cont'd)

A (s^{-1})	A (s^{-1})	MW (App)	ρ (g/cm3)	Cp (J/molK)	ΔH_r (J/mol)	ρ (kg/m3)
[Friedman Analysis]	[ASTM E698]			Average		
6.247E+12	6.277E+12	172.39	4.594	105.50	-6171.56	4594
6.278E+12	6.277E+12	155.00	4.594	111.60	-496.00	4594
6.253E+12	6.293E+12	136.86	4.594	88.96	-177.92	4594
6.329E+12	6.280E+12	245.51	4.594	147.31	-4713.79	4594

Table C9: Experimental Data on Thermal Oxidation of Ore 03-601(207m), 75µm Particles, Based on % Moisture Content

Saturation Levels	ΔH_r (J/g)	E_a (kJ/mol) [Friedman]	E_a (kJ/mol) [Ozawa Analysis]	E_a (kJ/mol) [ASTM E698]	SADT (°C) Self Adiabatic Decomposition Temperature	dTAD(°C) (φ=1/φ=2)
3%	-47.4 ± 8.8	80-145	60-105	98.963	33 (8 days)	48.5/24.3
8%	-54.3± 6.1	25-75	25-75	50.475	40 (8 days)	90.5/45.3
15%	-68.8 ±2.8	35-130	70-77	70.793	52 (9days)	88.7/44.4
25%	-64.5 ± 5.0	75-140	75-80	76.353	53 (8 days)	80.1/40.1

NOTE

The most exothermic ore sample according to mineralogy was used for the moisture saturation test.

Table C10: Calculated Experimental Data Used for the Simulation Based on % Moisture Saturation (Cont'd)

Cp (J/gK) φ=1	Cp (J/gK) φ=2	Cp (J/gK) Average	E_a (kJ/mol) Average [Friedman Analysis]	E_a (kJ/mol) Average [Ozawa Analysis]	E_a (kJ/mol) [ASTM E698]
0.9773	0.9753	0.9763	112.50	82.50	98.963
0.6000	0.5993	0.5997	50.00	50.00	50.475
0.7756	0.7783	0.7770	82.50	73.50	70.793
0.8052	0.8042	0.8047	107.50	77.50	76.353

ΔCp (J/gK) φ=1	ΔCp (J/gK) φ=2	ΔCp (J/gK) AVG
0.1814	0.1811	0.3625
0.0808	0.0673	0.1481
0.0316	0.0317	0.0632
0.0624	0.0623	0.1248

Table C11: Calculated Experimental Data Used for the Simulation Based on % Moisture Saturation (Cont'd)

A (s^{-1}) [Friedman Analysis]	A (s^{-1}) [Ozawa Analysis]	A (s^{-1}) [ASTM E698]	MW (App)	Cp (J/molK) Average	ΔH_r (J/mol)	ρ (g/cm3)
6.247E+12	6.300E+12	6.267E+12	172.39	168.31	-8171.29	4.369
6.439E+12	6.439E+12	6.436E+12	155.00	92.95	-8416.50	4.369
6.300E+12	6.325E+12	6.334E+12	136.86	106.34	-9415.97	4.369
6.253E+12	6.313E+12	6.317E+12	245.51	197.57	-15835.40	4.369

Table C12a: Raw Experimental Data on Thermal Oxidation of Most Exothermic Ore Samples

Sample	ΔHr (J/g)	dTAD (°C)	ρ (kg/m^3)	ΔH_r (J/mol)	Cp (J/kgK)	C_o (mol/m^3)
		(φ=1/φ=2)			Average	
A	-119.8 ± 12.3	199/99	4288	-20652	604	24937
B	-236.3 ± 48.1	393/196	4369	-36627	602	28223
C	-126.8 ± 39.4	211/105	4473	-17354	602	32761
D	-35.8 ± 6.3	59.7/29.8	4593	-8789	600	18724

Table C12b: Expected ΔTad Experimental Data Based on Thermal Oxidation of Most Exothermic Ore Samples'

Sample	ΔH_r (J/mol)	ρ (kg/m^3)	Cp (J/kgK)	Fixed C_o (mol/m^3)	Expected ΔT_{ad}
A	-20652	4288	604	28223	225
B	-36627	4369	602	28223	393
C	-17354	4473	602	28223	182
D	-8789	4593	600	28223	90

Note:

The values obtained in Table C12b are based on fixing all concentration of the samples to 28223mol/dm^3
This is done to know the equivalent ΔTad.

Table C13: Calculated Experimental Data Used for the Simulation Based on Most Exothermic Samples

Sample	Cp (J/gK) φ=1	Cp (J/gK) φ=2	Cp (J/gK) Average	E_a (kJ/mol) Average [Friedman Analysis]	E_a (kJ/mol) Average [Ozawa Analysis]	MW (App)	ρ (g/cm3)	Cp (J/molK) Average	ΔHr (J/mol)
A	0.6020	0.6051	0.6035	70.00	82.50	172.39	4.288	104.04	-20652
B	0.6013	0.6028	0.6020	92.50	125.00	155.00	4.369	93.32	-36627
C	0.6009	0.6038	0.6024	95.00	90.00	136.86	4.473	82.44	-17354
D	0.5997	0.6007	0.6002	115.00	95.00	245.51	4.593	147.35	-8789

Sample	ΔCp (J/gK) φ=1, ±	ΔCp (J/gK) φ=2, ±	ΔCp (J/gK) AVG (±)
A		0.0621	0.1239
B	0.1224	0.1227	0.2451
C	0.1867	0.1876	0.3743
D	0.1055	0.1057	0.2112

Table C14a: Experimental Data of Thermal Oxidation of Ore Samples Based on Particle Size Distribution

Particle Size (μm)	ΔHr (J/g)	dTAD(°C) (φ=1/φ=2)	ρ (kg/m^3)	ΔHr (J/mol)	Cp (J/kgK) Average	C_o (mol/m^3)
<75	-35.8 ± 6.3	59/29	4594	-6171.56	612	26878.61
75-180	-3.2 ±1.5	5 & 2	4594	-496.00	720	33343.55
>180	-1.3 ± 7.6E-1	2 & 1	4594	-177.92	650	33567.15
Mixed	-19.2 ± 3.2	32/16	4594	-4713.79	600	18712.07

Table C14b: Expected ΔT_{ad} Experimental Data Based on Thermal Oxidation of Most Exothermic Ore Samples' Concentration

Particle Size (μm)	ΔH_r (J/mol)	ρ (kg/m^3)	Cp (J/kgK)	Fixed C_o (mol/m^3)	Expected ΔT_{ad}
<75	-6171.56	4594	612	26878.61	59.00
75-180	-496.00	4594	720	26878.61	4.03
>180	-177.92	4594	650	26878.61	1.60
Mixed	-4713.79	4594	600	26878.61	45.97

Note:

The values obtained in Table C12b are based on fixing all concentration of the samples to 26878.61mol/dm^3

This is done to know the equivalent ΔTad associated with each particle size distribution at the same concentration.

Table C15: Calculated Experimental Data Used for the Simulation Based on Particle Size Distribution

Particle Size (μm)	Cp (J/gK) ϕ=1	Cp (J/gK) ϕ=2	Cp (J/gK) Average	E_a (kJ/mol) Average [Friedman Analysis]	MW (App)	ρ (g/cm3)	Cp (J/molK) Average	ΔHr (J/mol)	ρ (kg/m3)
<75	0.6068	0.6172	0.6120	112.50	172.39	4594	105.50	-6171.56	4594
75-180	0.6400	0.8000	0.7200	92.50	155.00	4594	111.60	-496.00	4594
>180	0.6500	0.6500	0.6500	107.50	136.86	4594	88.96	-177.92	4594
Mixed	0.6000	0.6000	0.6000	72.50	245.51	4594	147.31	-4713.79	4594

ΔCp (J/gK) ϕ=1	ΔCp (J/gK) ϕ=2	ΔCp (J/gK) AVG
0.1068	0.1086	0.2154
0.3000	0.3750	0.6750
0.3047	0.3047	0.6094
0.2813	0.2813	0.5625

Table C16a: Experimental Data on Thermal Oxidation of Ore 03-601(207m) Based on % Moisture Content

Saturation Levels	ΔHr (J/g)	dTAD(°C) (φ=1/φ=2)	ρ (kg/m³)	ΔHr (J/mol)	Cp (J/kgK) Average	C_o (mol/m³)
3%	-47.4 ± 8.8	48.5/24.3	4369	-8171.29	976.31	25317.62
8%	-54.3± 6.1	90.5/45.3	4369	-8416.50	599.67	28171.54
15%	-68.8 ±2.8	88.7/44.4	4369	-9415.97	776.96	31977.30
25%	-64.5 ± 5.0	80.1/40.1	4369	-15835.40	804.74	17784.51

Table C16b: Expected ΔT_{ad} Experimental Data Based on Thermal Oxidation of Most Exothermic Ore Samples' Concentration

Moisture Content	ΔH_r (J/mol)	ρ (kg/m^3)	Cp (J/kgK)	Fixed C_o (mol/m^3)	Expected ΔT_{ad}
3%	-8171.29	4369	976	31977.30	61.28
8%	-8416.50	4369	600	31977.30	102.67
15%	-9415.97	4369	777	31977.30	88.70
25%	-15835.40	4369	805	31977.30	143.98

Note:

The values obtained in Table C12b are based on fixing all concentration of the samples to 31977.30134mol/dm^3

This is done to know the equivalent ΔTad associated with each particle size distribution at the same concentration.

Table C17: Calculated Experimental Data Used for the Simulation Based on % Moisture Saturation

Cp (J/gK) φ=1	Cp (J/gK) φ=2	Cp (J/gK) Average	E_a (kJ/mol) Average [Friedman Analysis]	E_a (kJ/mol) Average [Ozawa Analysis]	MW (App)	E_a (kJ/mol) [ASTM E698]	Cp (J/molK) Average	ΔHr (J/mol)	ρ (g/cm3)	ρ (kg/m3)
0.9773	0.9753	0.9763	112.50	82.50	172.39	98.963	168.31	-8171.29	4.3693	4369
0.6000	0.5993	0.5997	50.00	50.00	155.00	50.475	92.95	-8416.50	4.369	4369
0.7756	0.7783	0.7770	82.50	73.50	136.86	70.793	106.34	-9415.97	4.369	4369
0.8052	0.8042	0.8047	107.50	77.50	245.51	76.353	197.57	-15835.40	4.369	4369

ΔCp (J/gK) φ=1	ΔCp (J/gK) φ=2	ΔCp (J/gK) AVG
0.1814	0.1811	0.3625
0.0808	0.0673	0.1481
0.0316	0.0317	0.0632
0.0624	0.0623	0.1248

Appendix D

Raw DSC Graphical Experimental Results for Some Ores

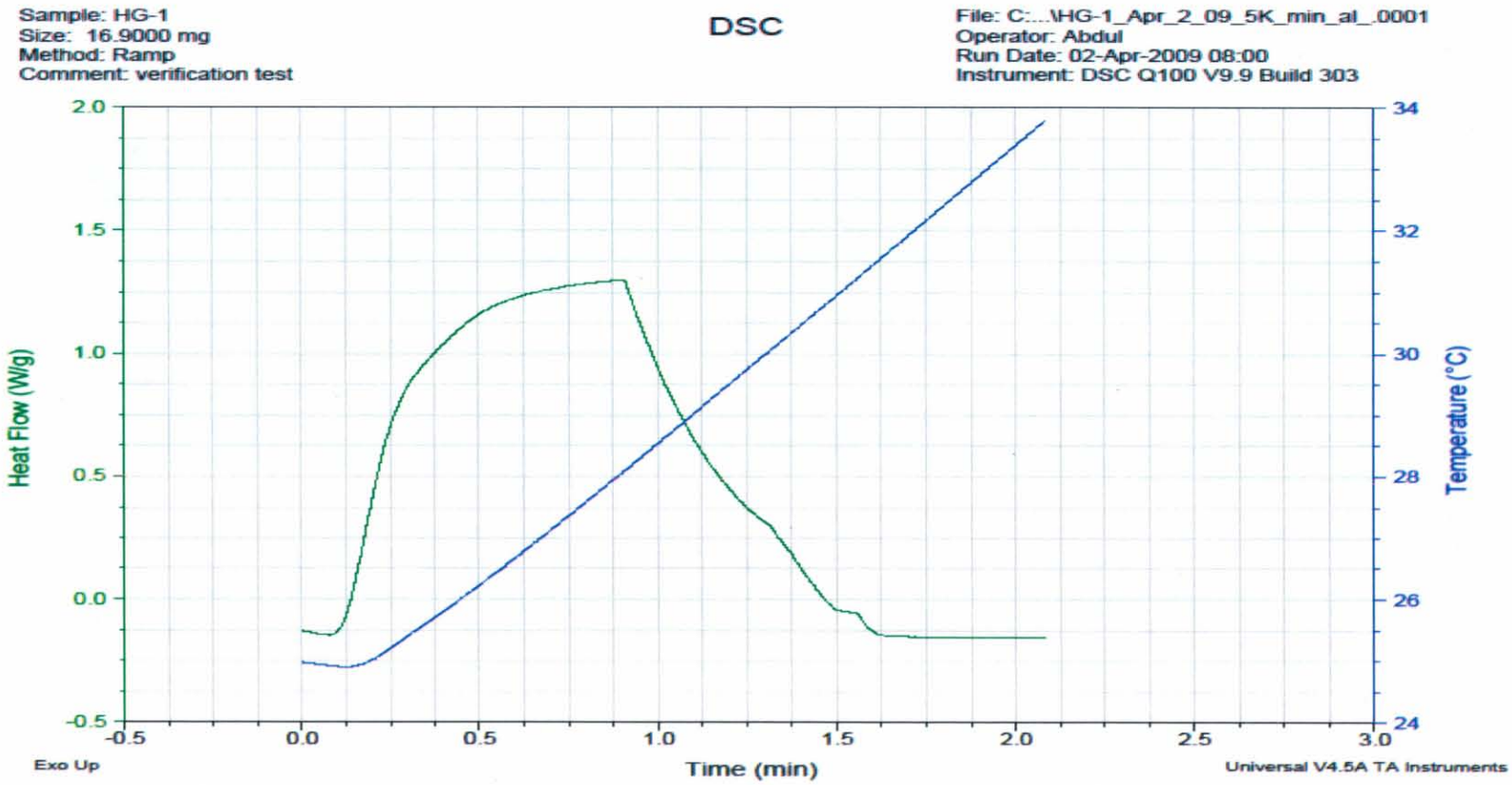

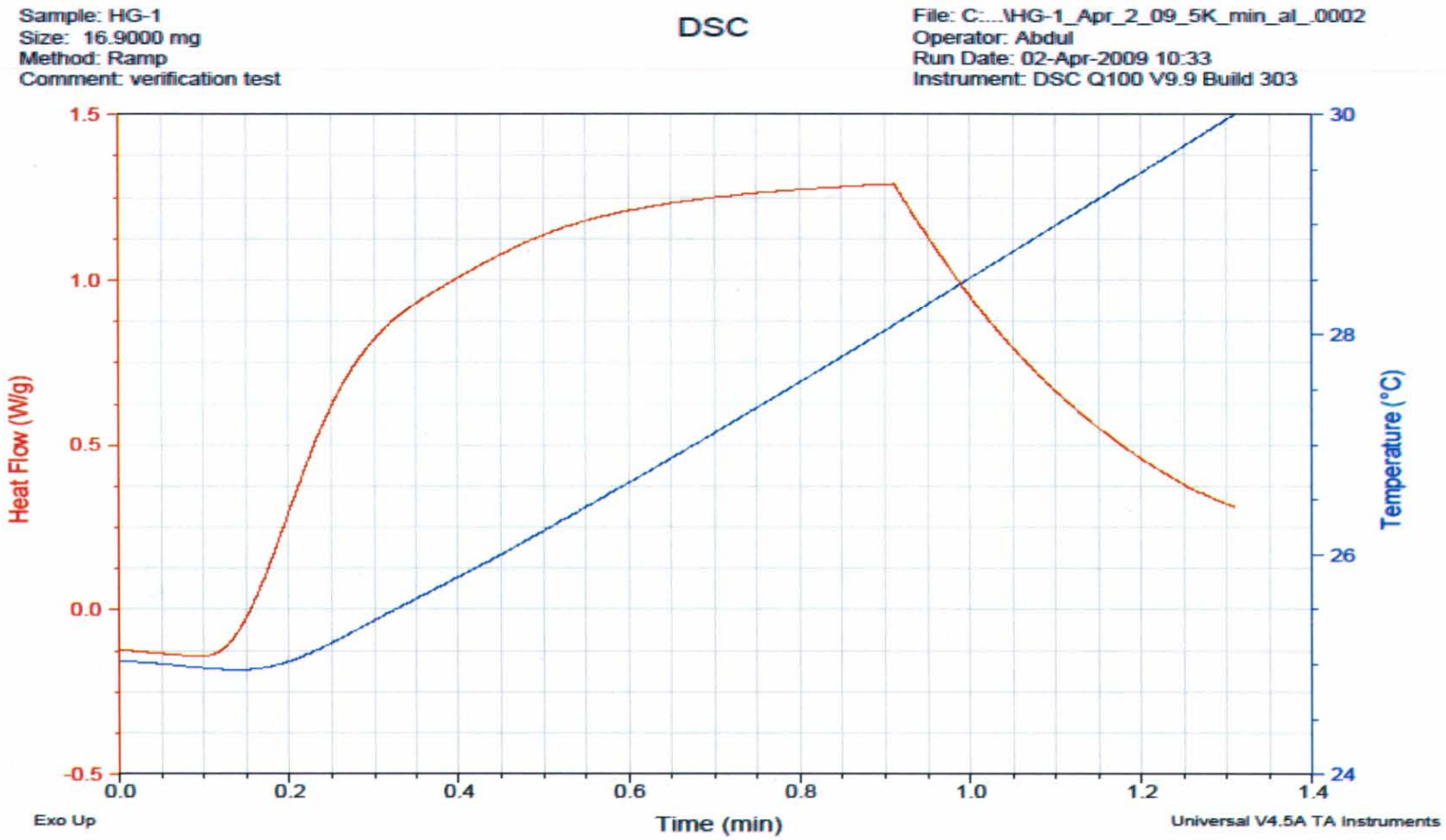
Sample: HG-1
Size: 16.9000 mg
Method: Ramp
Comment: verification test
DSC
File: C:...\HG-1_Apr_2_09_5K_min_al_.0002
Operator: Abdul
Run Date: 02-Apr-2009 10:33
Instrument: DSC Q100 V9.9 Build 303
Heat Flow (W/g)
Temperature (°C)
Time (min)
Exo Up
Universal V4.5A TA Instruments

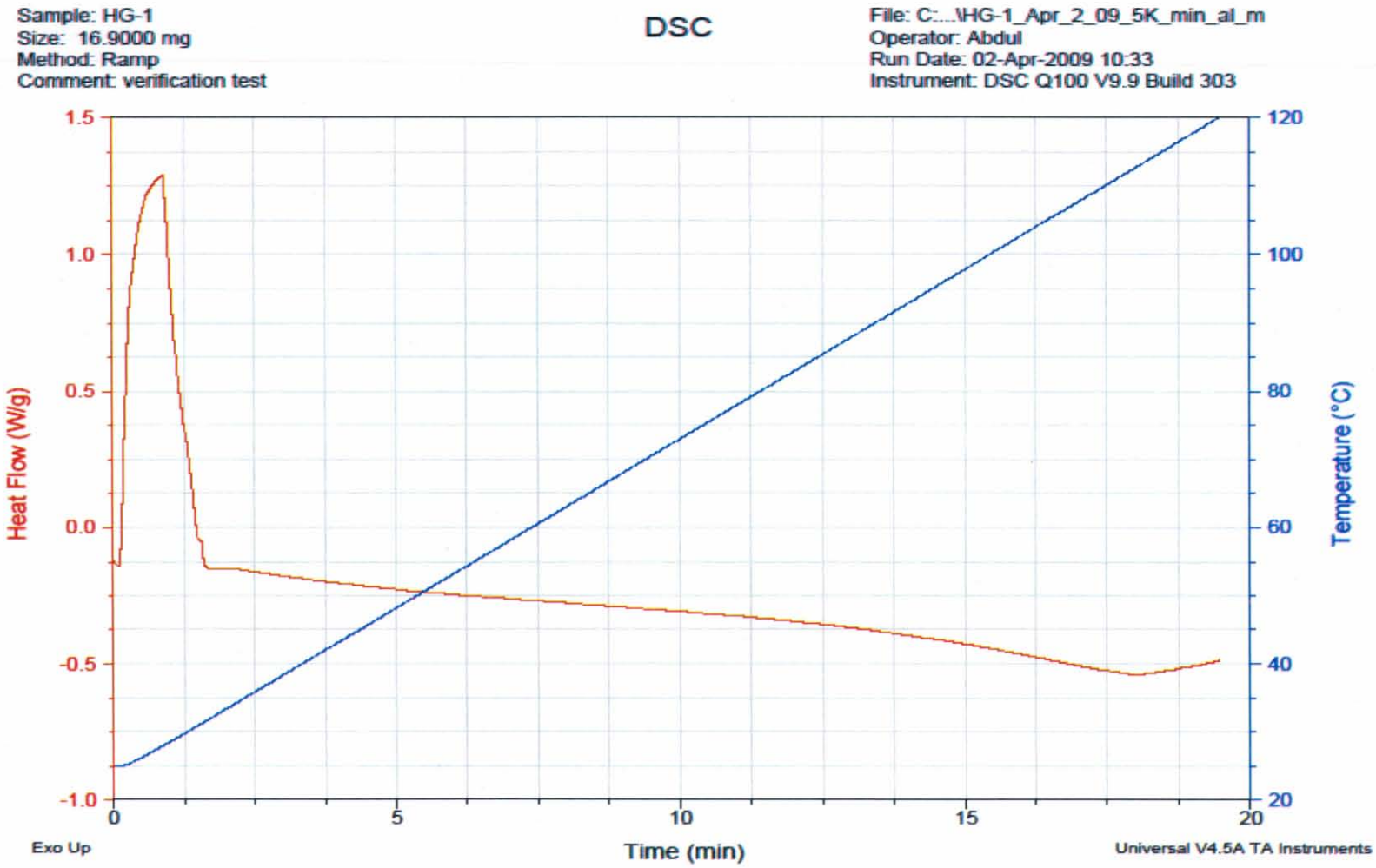
Sample: HG-1
Size: 16.9000 mg
Method: Ramp
Comment: verification test
DSC
File: C:...\HG-1_Apr_2_09_5K_min_al_m
Operator: Abdul
Run Date: 02-Apr-2009 10:33
Instrument: DSC Q100 V9.9 Build 303
Heat Flow (W/g)
Temperature (°C)
Time (min)
Exo Up
Universal V4.5A TA Instruments

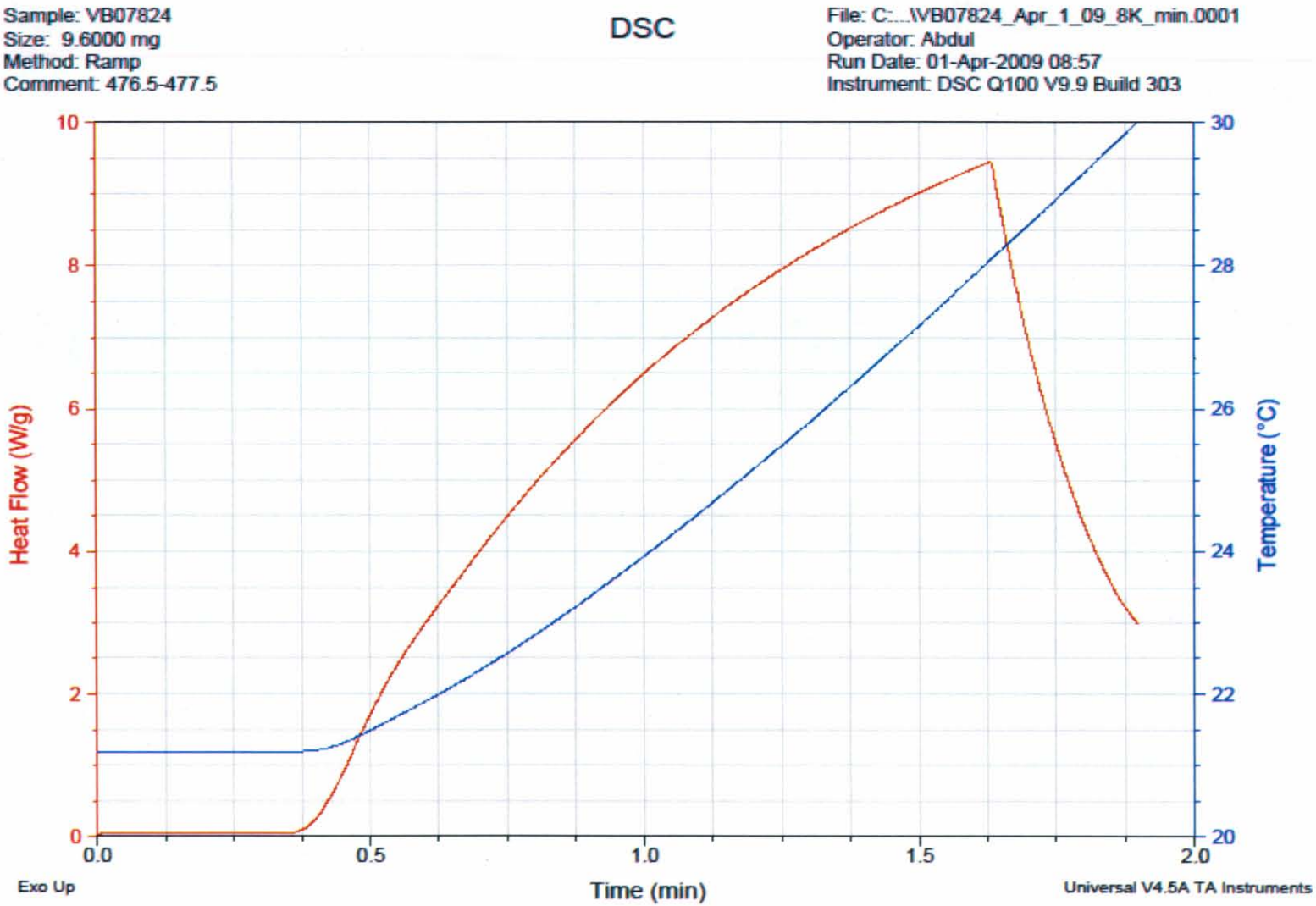
Sample: VB07824
Size: 9.6000 mg
Method: Ramp
Comment: 476.5-477.5
DSC
File: C:...\VB07824_Apr_1_09_8K_min.0001
Operator: Abdul
Run Date: 01-Apr-2009 08:57
Instrument: DSC Q100 V9.9 Build 303
Heat Flow (W/g)
Temperature (°C)
Time (min)
Exo Up
Universal V4.5A TA Instruments

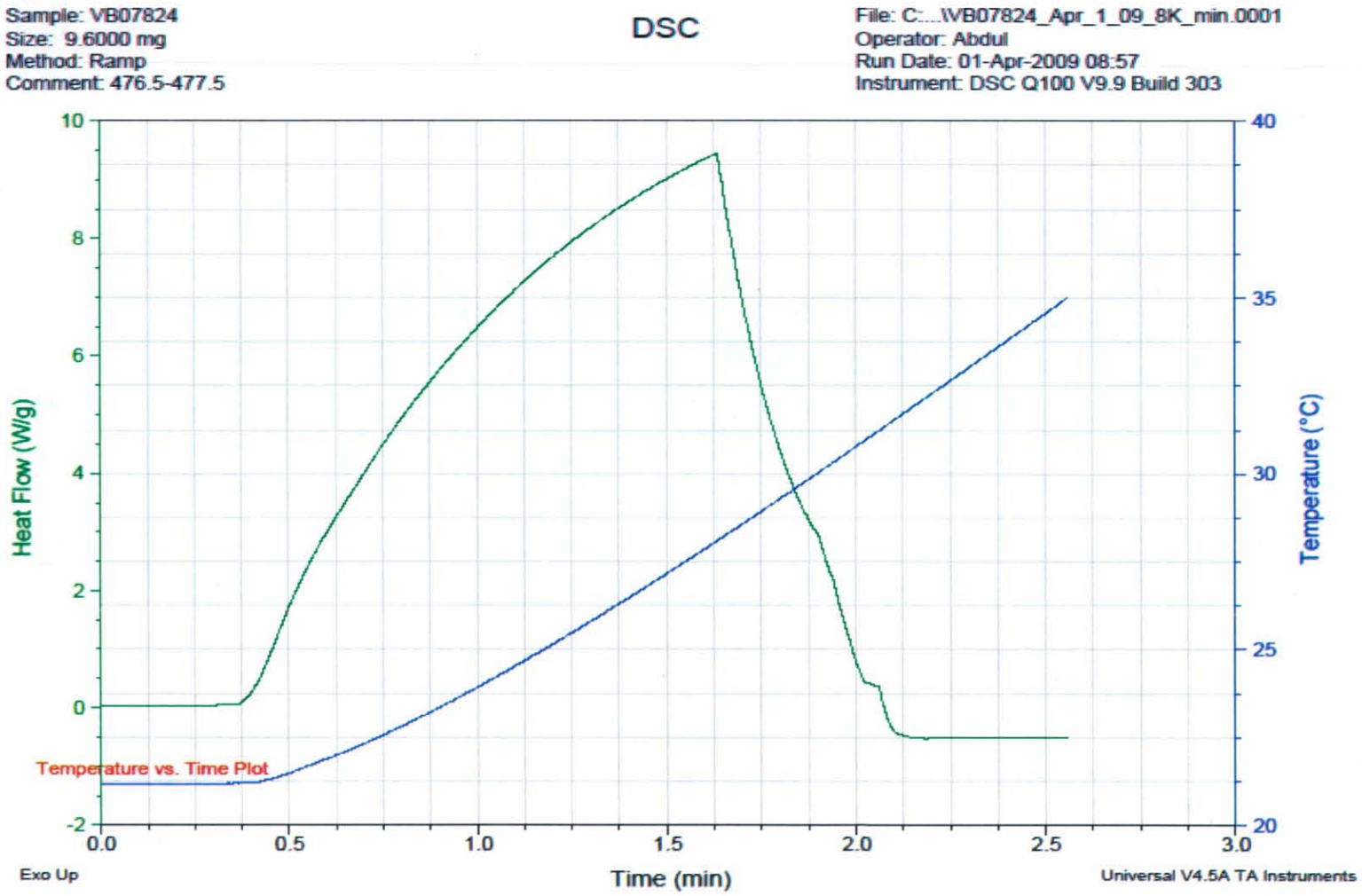
Sample: VB07824
Size: 9.6000 mg
Method: Ramp
Comment: 476.5-477.5
DSC
File: C:...\VB07824_Apr_1_09_8K_min.0001
Operator: Abdul
Run Date: 01-Apr-2009 08:57
Instrument: DSC Q100 V9.9 Build 303
Heat Flow (W/g)
Temperature (°C)
Time (min)
Temperature vs. Time Plot
Exo Up
Universal V4.5A TA Instruments

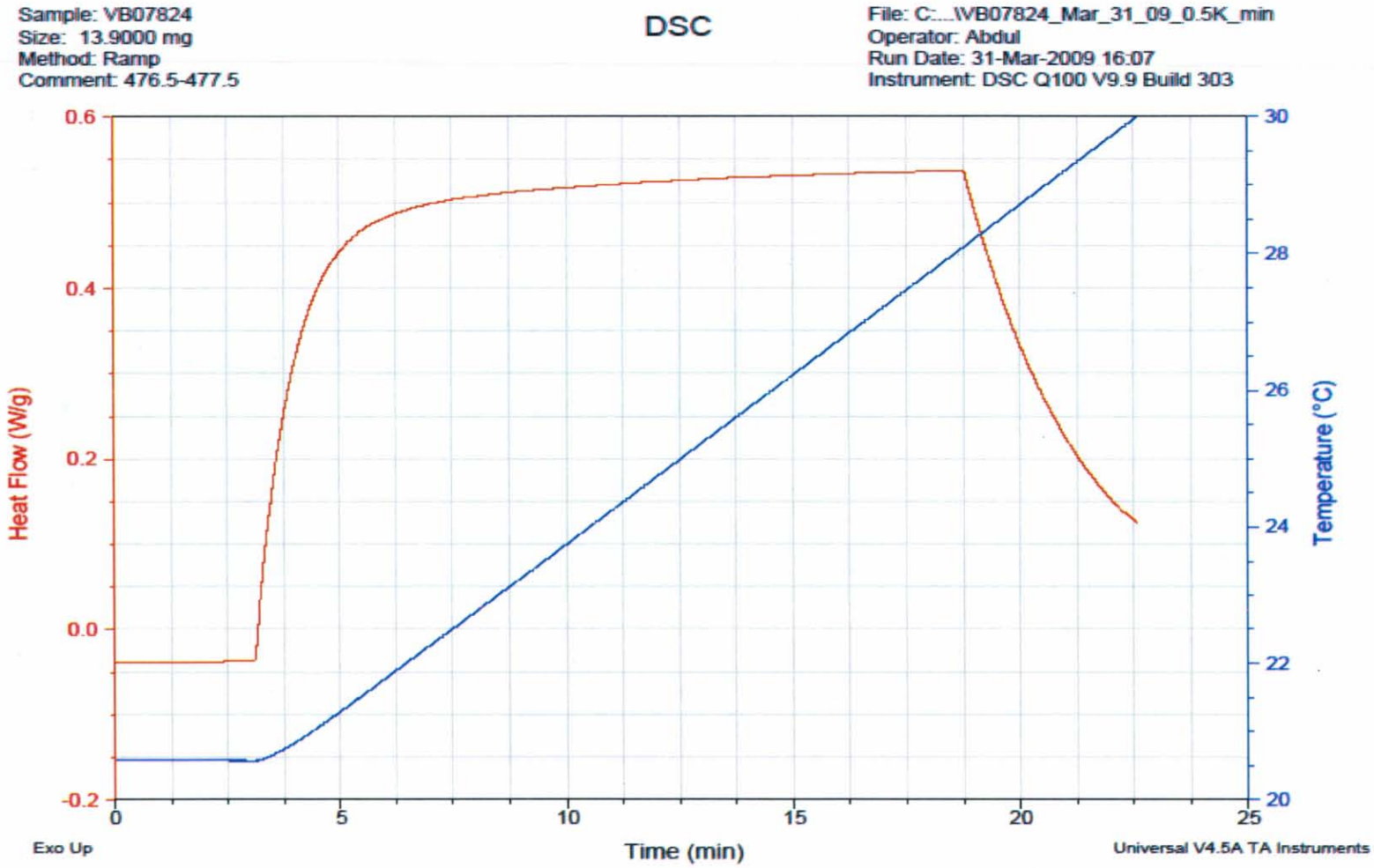
Sample: VB07824
Size: 13.9000 mg
Method: Ramp
Comment: 476.5-477.5
DSC
File: C:...\VB07824_Mar_31_09_0.5K_min
Operator: Abdul
Run Date: 31-Mar-2009 16:07
Instrument: DSC Q100 V9.9 Build 303
Heat Flow (W/g)
Temperature (°C)
Time (min)
Exo Up
Universal V4.5A TA Instruments

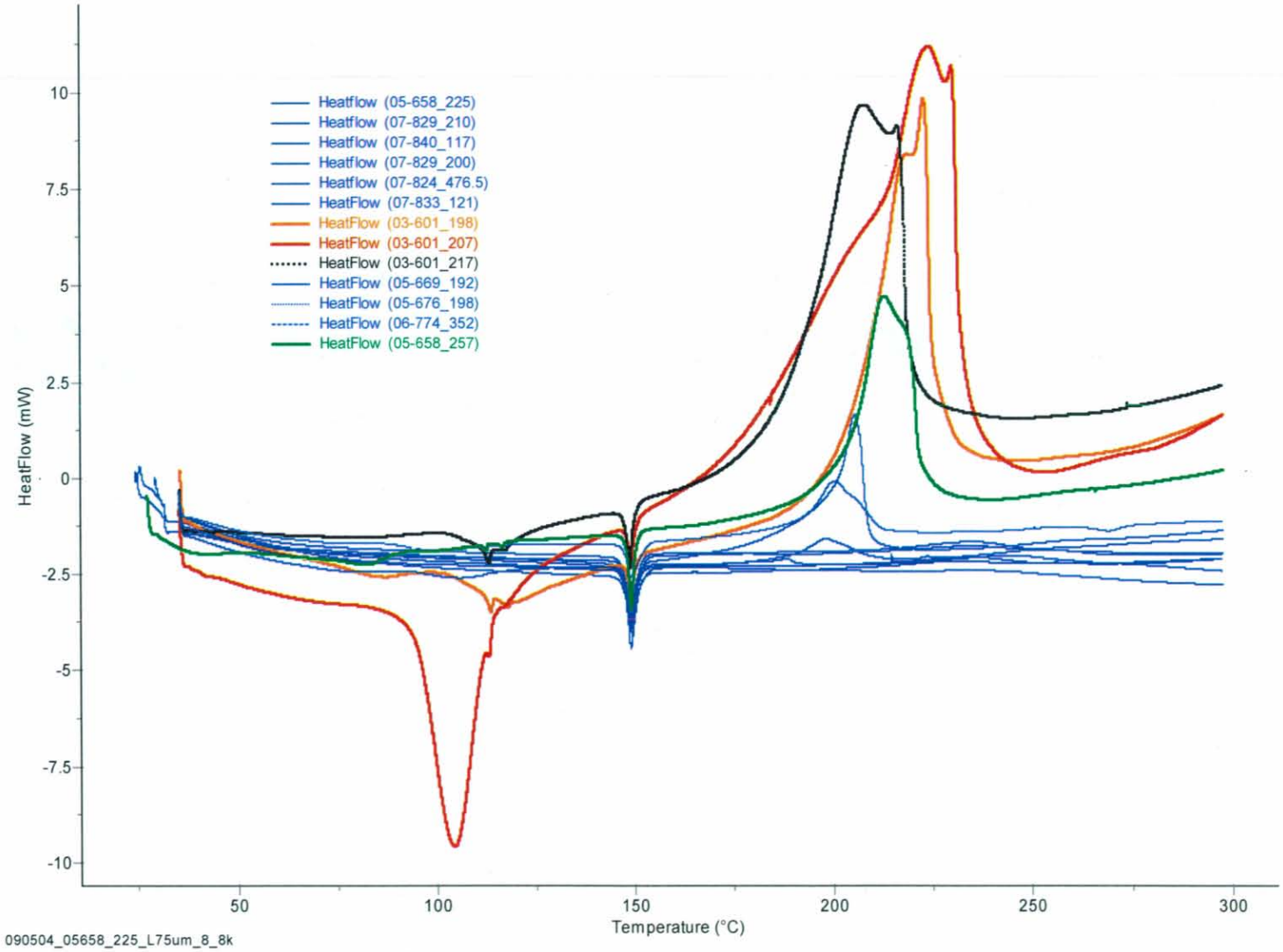
Heatflow (05-658_225)
Heatflow (07-829_210)
Heatflow (07-840_117)
Heatflow (07-829_200)
Heatflow (07-824_476.5)
Heatflow (07-833_121)
HeatFlow (03-601_198)
HeatFlow (03-601_207)
HeatFlow (03-601_217)
HeatFlow (05-669_192)
HeatFlow (05-676_198)
HeatFlow (06-774_352)
HeatFlow (05-658_257)
HeatFlow (mW)
10
7.5
5
2.5
0
-2.5
-5
-7.5
-10
50
100
150
200
250
300
Temperature (°C)
090504_05658_225_L75um_8_8k

Raw ARSST Results

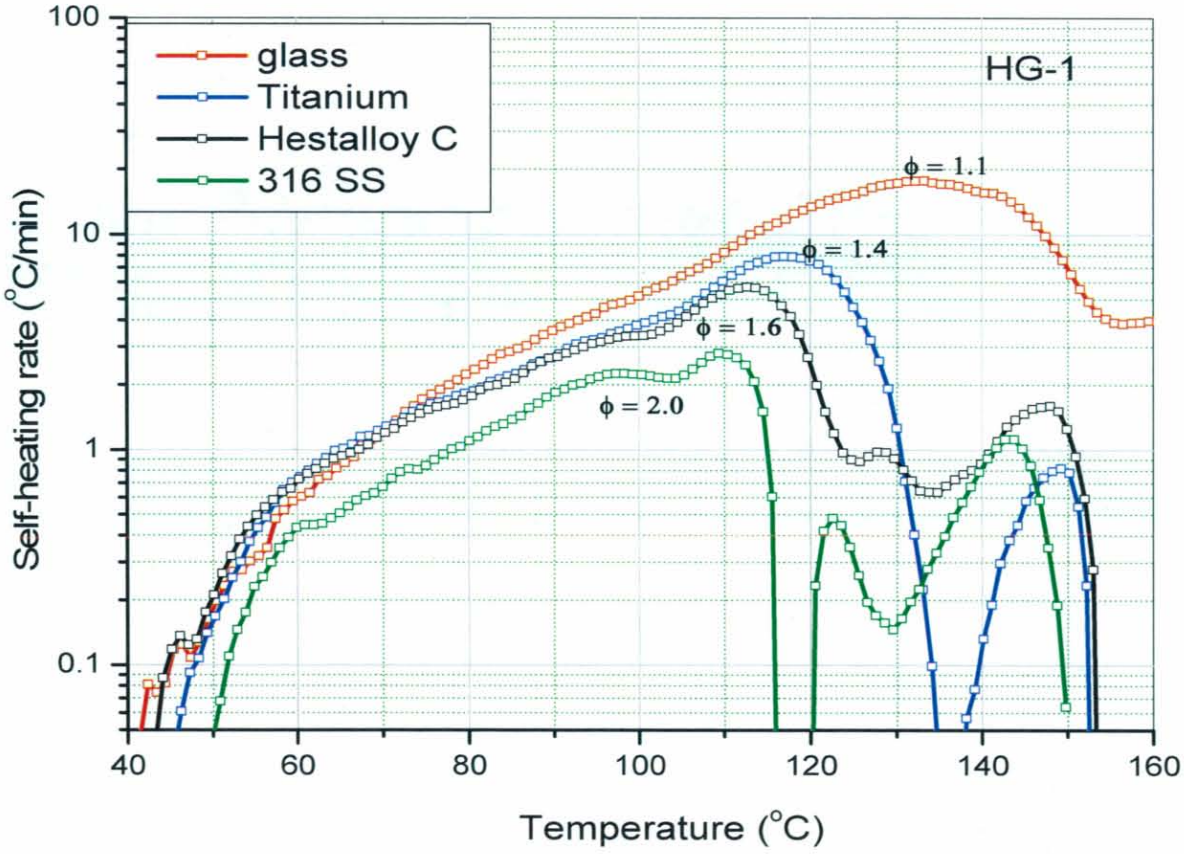

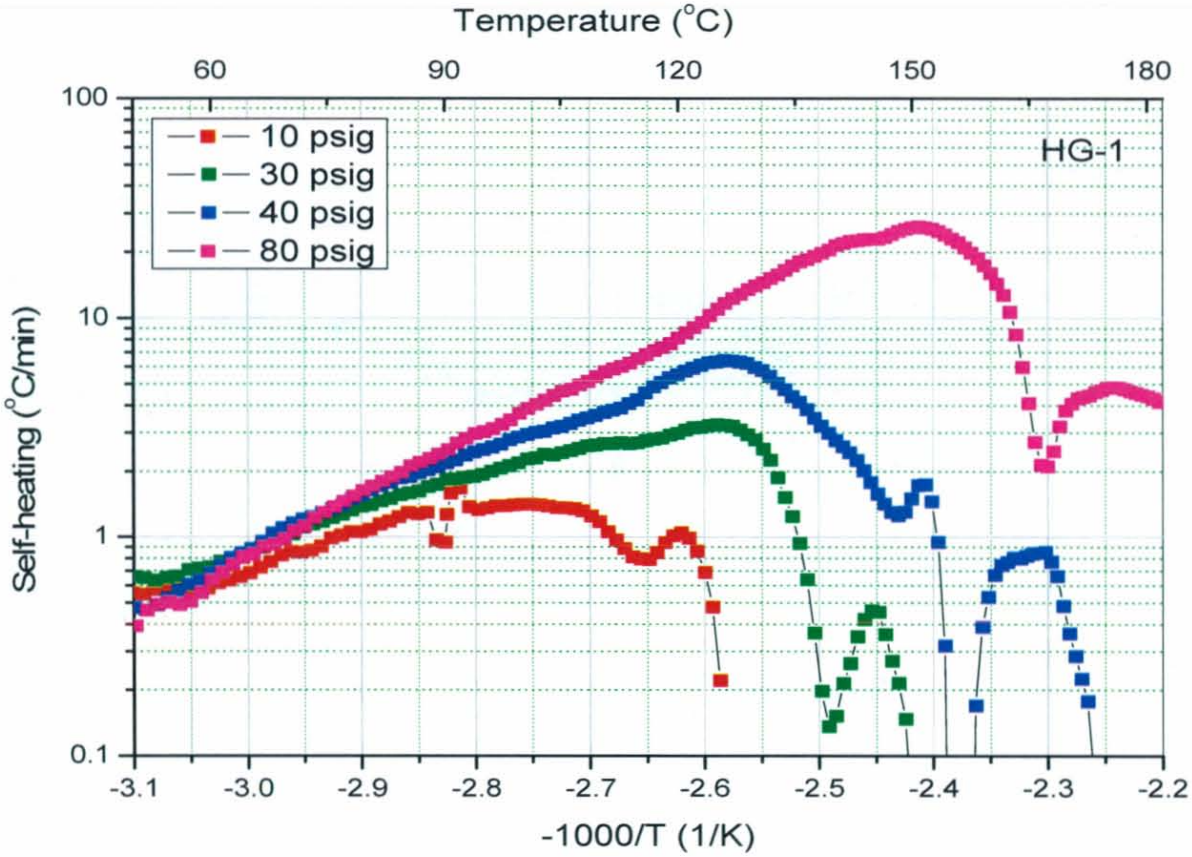

Effect of Oxygen (Air) Partial Pressure

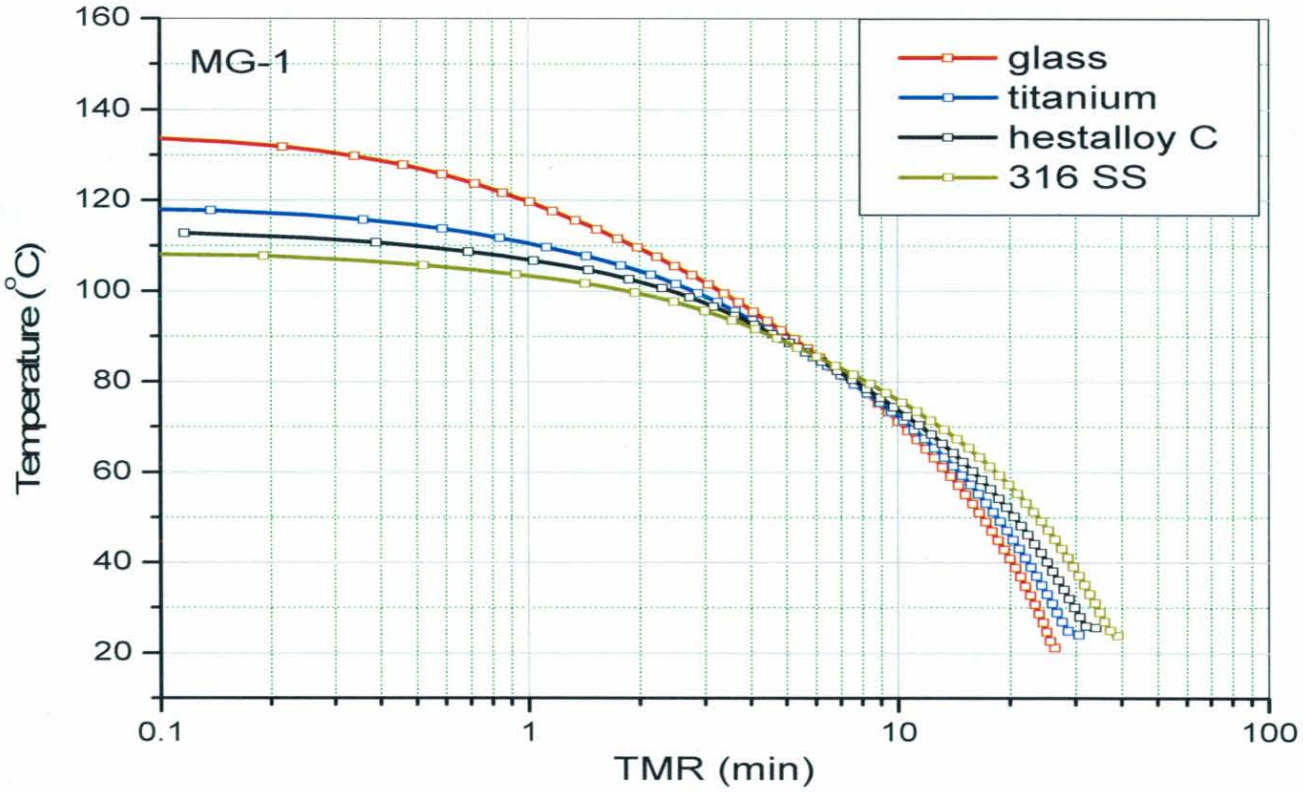
MG-1
glass
titanium
hestalloy C
316 SS
Temperature (°C)
TMR (min)
160
140
120
100
80
60
40
20
0.1
1
10
100

Appendix E

Determination of τ

Parameter "τ" can be determined using representative industrial reactor data on a pilot scale (such as autoclave data used for treating the concentrate and ore). For a typical production where 2200 tons/hr (611.1kg/s) of ore is fed in, the average density of the ores is 4900kg/m^3. Density of pyrrhotite, the major active constituent of the ore causing self-heating, lies between 4800kg/m^3 and 5000kg/m^3. Therefore, the volumetric flow rate for the feed is:

$$v = \frac{Mass\ flow\ rate\ of\ feed}{Average\ dnsity\ of\ feed}$$

$$= \frac{\dot{m}}{\rho} = \frac{611.1\ \text{kgs}^{-1}}{4900\ \text{kgm}^{-3}}$$

$$= \frac{0.125m^3}{s} = \frac{450m^3}{hr}$$

The corresponding autoclave volume is 693m^3 with corresponding working volume of 462m^3 (i.e. two-third of normal reactor volume), Levenspiel (1999) to allow for haulage space and gas build up.

$$\tau = \frac{Autoclave\ or\ reactor\ volume}{Volumetric\ flow\ rate\ of\ feed}$$

$$= \frac{V}{v} = \frac{693\text{m}^3}{0.125m^3/s} = 5556\ s$$

Determination of Arrhenius' Constant

The best approach to obtain Arrhenius' Constant, A, is to obtain it from the self-heating regime from the AKTS software data or ARSST Self-heat Rate vs. Temperature Plot or DSC Temperature vs. Time Plot. The value obtained using this approach is a true representative of what is happening at the onset or any other temperature of the runaway reaction. Another approach to calculate A is that of classical global chemistry/ physics model rooted in Transition State Theory (TST) given as:

$$A = \frac{k_B T_i}{h}$$

Where: k_B = Boltzmann's constant, T_i = critical temperature & h = Planck's constant

$$T_i = \frac{E_a}{2R}\left[1 - \sqrt{\left[1 - \frac{4RT_o}{E_a}\right]}\right] \;\&\; T_o = Referenced\ room\ temperature$$

The precise approach is based on graphical experimental plot of the self-heat rate vs. temperature at the onset temperature using the expression below based on AKTS and instruments software such as: ARSST and ARC with zero-order reaction assumption:

$$A = \left[\frac{dT}{dt}_{@\,T_{onset}}\left[\frac{\rho C_p e^{\frac{E_a}{RT_{onset}}}}{xC_o\Delta H_R}\right]\right] = \left[\frac{dT}{dt}_{@\,T_{onset}}\left[\frac{e^{\frac{E_a}{RT_{onset}}}}{\Delta T_{ad}}\right]\right]$$

This is valid since the first term in equation [3.13] approaches zero or negligible i.e. $\frac{[T-T_{ref}]}{\tau} \approx 0$.

$$\frac{dT}{dt} = \frac{1}{\tau}[\mathrm{T} - T_{ref}] + r_p[(-\Delta H_R)/\rho C_p] \qquad \textbf{3.13}$$

For ore VB07824, a strongly oxidized ore ramped @ 8K/min experimentally with 9.60mg sample and cell constant of 1.3979, the SH at the onset temperature of 21.20°C (294.20K) is determined using (0.39min, 21.20°C) & (1.64min, 28.12) from the Temperature-time Plot of the DSC composite plot of Heat rate vs. Time and Temperature vs. Time as follows:

$$\frac{dT}{dt}_{@\,T_{onset}} = \frac{(28.12 - 21.20)}{(1.64 - 0.39)} \frac{^oC}{min}$$

$$= 5.536 \frac{^oC}{min} = 0.092267 \frac{^oC}{s}$$

The equivalent "ΔTad" measured to the peak of exotherm curve is 6.92°C and activation energy of 82.6kJ/mol. Therefore, using the above formula gives Arrhenius' constant as:

$$A = \left[\frac{dT}{dt}_{@\,T_{onset}} \left[\frac{e^{\frac{E_a}{RT_{onset}}}}{\Delta T_{ad}} \right] \right]$$

$$A = \left[0.092267 \frac{^oC}{s} \times \left[\frac{e^{\left[\frac{82600}{8.314 \times 294.20}\right]}}{6.92 \deg C} \right] \right]$$

$$= 6.18 \times 10^{12} s^{-1}$$

Similarly, using classical method

$$A = \frac{k_B T_i}{h} = \frac{1.3806503 \times 10^{-23} \frac{J}{K} \times 294.20K}{6.626068 \times 10^{-34} Js}$$

$$= 6.13 \times 10^{12}\, s^{-1}$$

These two values agree with experimental uncertainty.

Compositional Balance Modeling

{Initial molar flow rate} = {Converted molar flow rate by reaction +{Final molar flow rate at time t}

$$\frac{n_o}{\tau} = r_p V + \frac{n_t}{\tau}$$

But molar flow rate = Concentration x Volume/ Time = CV/ τ

$$\frac{VC_o}{\tau} = r_p V + \frac{VC_f}{\tau}$$

Also, $C_f = C_o - xC_o = C_o[1 - x]$

Therefore, $\frac{VC_o}{\tau} - \frac{VC_f}{\tau} = r_p V$

$$\frac{V[C_o - C_f]}{\tau} = r_p V$$

$$r_p V = \frac{V[C_o - C_o[1 - x]]}{\tau}$$

$$r_p = \frac{xC_o}{\tau}$$

The above expression for "r_p" was used in equation [3.11] in Chapter 3.

Appendix F

Thermal Hazard Risk Calclation for Self-Heating Sulfide Mineral Ores

Table F1: Standard Z-Score and Probability Calculation for Experimental Data for Class 1 (Low Risk)

Sample	Fdman Ea	Fdman Z-Score	Pr(Ea)	A (s^{-1})	Z-Score of A (s^{-1})	Pr(A (s^{-1}))	Pr(Hzd)	"-ΔHr" (J/g)	Severity,β	Associated Risk
A	70.000	25.846	1.000	6.337E+12	-0.778	0.2182	**0.2182**	119.800	0.5961	0.1301
B	92.500	35.180	1.000	6.278E+12	-0.780	0.2177	**0.2177**	236.300	1.1758	0.2560
C	95.000	36.217	1.000	6.274E+12	-0.780	0.2177	**0.2177**	126.800	0.6310	0.1373
D	115.000	44.515	1.000	6.244E+12	-0.781	0.2174	**0.2174**	35.800	0.1781	0.0387

Particle Size	Fdman Ea	Fdman Z-Score	Pr(Ea)	A (s^{-1})	Z-Score of A (s^{-1})	Pr(A (s^{-1}))	Pr(Hzd)	"-ΔHr" (J/g)	Severity,β	Associated Risk
<75μm	112.500	43.477	1.000	6.247E+12	-0.781	0.2174	**0.2174**	35.800	0.1781	0.0387
75-180μm	92.500	35.180	1.000	6.278E+12	-0.780	0.2177	**0.2177**	3.200	0.0159	0.0035
>180μm	107.500	41.403	1.000	6.253E+12	-0.781	0.2175	**0.2175**	1.300	0.0065	0.0014
Mixed	72.500	26.883	1.000	6.329E+12	-0.778	0.2182	**0.2182**	19.200	0.0955	0.0208

% Moisture	Fdman Ea	Friedman Z-Score	Pr(Ea)	A (s^{-1})	Z-Score of A (s^{-1})	Pr(A (s^{-1}))	Pr(Hzd)	"-ΔHr" (J/g)	Severity,β	Associated Risk
3	112.500	43.477	1.000	6.247E+12	-0.781	0.2174	**0.2174**	47.400	0.2359	0.0513
8	50.000	17.548	1.000	6.439E+12	-0.775	0.2192	**0.2192**	54.300	0.2702	0.0592
15	82.500	31.031	1.000	6.300E+12	-0.779	0.2179	**0.2179**	68.800	0.3423	0.0746
25	107.500	41.403	1.000	6.253E+12	-0.781	0.2175	**0.2175**	64.500	0.3209	0.0698

Fit Parameters Used

ln(A) (s^{-1})	μ (s-1)	σ (s-1)
30.8378	33.463	5.122

NOTE

The bold face figures are the probability of thermal hazards for each experimental data set

Table F1: Standard Z-Score and Probability Calculation for Experimental Data for Class 1 (Low Risk) Cont'd

Sample	Ozawa Ea	Ozawa Z-Score	Pr(Ea)	A (s^{-1})	Z-Score of A (s^{-1})	Pr(A (s^{-1}))	Pr(Hzd)	"-ΔHr" (J/g)	Severity,β	Associated Risk
A	82.500	31.031	1.000	6.300E+12	-0.7793	0.2179	**0.2179**	119.800	0.5961	0.1299
B	125.000	48.663	1.000	6.232E+12	-0.7814	0.2173	**0.2173**	236.300	1.1758	0.2555
C	90.000	34.143	1.000	6.283E+12	-0.7798	0.2178	**0.2178**	126.800	0.6310	0.1374
D	95.000	36.217	1.000	6.274E+12	-0.7801	0.2177	**0.2177**	35.800	0.1781	0.0388

Particle Size	ASTM Ea	ASTM E698 Z-Score	Pr(Ea)	A (s^{-1})	Z-Score of A (s^{-1})	Pr(A (s^{-1}))	Pr(Hzd)	"-ΔHr" (J/g)	Severity,β	Associated Risk
<75μm	92.939	35.362	1.000	6.277E+12	-0.7800	0.2177	**0.2177**	35.800	0.1781	0.0388
75-180μm	93.412	35.558	1.000	6.277E+12	-0.7800	0.2177	**0.2177**	3.200	0.0159	0.0035
>180μm	85.514	32.282	1.000	6.293E+12	-0.7795	0.2178	**0.2178**	1.300	0.0065	0.0014
Mixed	91.632	34.820	1.000	6.280E+12	-0.7799	0.2177	**0.2177**	19.200	0.0955	0.0208

% Moisture	Ozawa Ea	Ozawa Z-Score	Pr(Ea)	A (s^{-1})	Z-Score of A (s^{-1})	Pr(A (s^{-1}))	Pr(Hzd)	"-ΔHr" (J/g)	Severity,β	Associated Risk
3	82.500	31.031	1.000	6.300E+12	-0.7793	0.2179	**0.2179**	47.400	0.2359	0.0514
8	50.000	17.548	1.000	6.439E+12	-0.7750	0.2192	**0.2192**	54.300	0.2702	0.0592
15	73.500	27.298	1.000	6.325E+12	-0.7785	0.2181	**0.2181**	68.800	0.3423	0.0747
25	77.500	28.957	1.000	6.313E+12	-0.7789	0.2180	**0.2180**	64.500	0.3209	0.0700

Table F1: Standard Z-Score and Probability Calculation for Experimental Data for Class 1 (Low Risk) Cont'd

Sample	ASTM Ea	ASTM E698 Z-Score	Pr(Ea)	A (s^{-1})	Z-Score of A (s^{-1})	Pr(A (s^{-1}))	Pr(Hzd)	"-ΔHr" (J/g)	Severity,β	Associated Risk
A	78.585	29.407	1.000	6.310E+12	-0.7790	0.2180	**0.2180**	119.800	0.5961	0.1300
B	77.822	29.091	1.000	6.313E+12	-0.7789	0.2180	**0.2180**	236.300	1.1758	0.2564
C	75.123	27.971	1.000	6.320E+12	-0.7786	0.2181	**0.2181**	126.800	0.6310	0.1376
D	92.939	35.362	1.000	6.277E+12	-0.7800	0.2177	**0.2177**	35.800	0.1781	0.0388

% Moisture	ASTM Ea	ASTM E698 Z-Score	Pr(Ea)	A (s^{-1})	Z-Score of A (s^{-1})	Pr(A (s^{-1}))	Pr(Hzd)	"-ΔHr" (J/g)	Severity,β	Associated Risk
3	98.963	37.861	1.000	6.267E+12	-0.7803	0.2176	**0.2176**	47.400	0.2359	0.0513
8	50.475	17.745	1.000	6.436E+12	-0.7751	0.2191	**0.2191**	54.300	0.2702	0.0592
15	70.793	26.174	1.000	6.334E+12	-0.7782	0.2182	**0.2182**	68.800	0.3423	0.0747
25	76.353	28.481	1.000	6.317E+12	-0.7788	0.2181	**0.2181**	64.500	0.3209	0.0700

Table F2: Standard Z-Score and Probability Calculation for Experimental Data for Class 2 (Medium Risk)

Sample	Fdman Ea	Fdman Z-Score	Pr(Ea)	A (s^{-1})	Z-Score of A (s^{-1})	Pr(A (s^{-1}))	Pr(Hzd)	"-ΔHr" (J/g)	Severity,β	Associated Risk
A	70.000	0.8566	0.8042	6.337E+12	-0.778	0.2182	**0.1755**	119.800	0.2151	0.0378
B	92.500	1.6890	0.9544	6.278E+12	-0.780	0.2177	**0.2078**	236.300	0.4244	0.0882
C	95.000	1.7815	0.9626	6.274E+12	-0.780	0.2177	**0.2095**	126.800	0.2277	0.0477
D	115.000	2.5214	0.9942	6.244E+12	-0.781	0.2174	**0.2161**	35.800	0.0643	0.0139
Particle Size	**Fdman Ea**	**Fdman Z-Score**	**Pr(Ea)**	**A (s^{-1})**	**Z-Score of A (s^{-1})**	**Pr(A (s^{-1}))**	**Pr(Hzd)**	**"-ΔHr" (J/g)**	**Severity,β**	**Associated Risk**
<75μm	112.500	2.4289	0.9924	6.247E+12	-0.781	0.2174	**0.2158**	35.800	0.0643	0.0139
75-180μm	92.500	1.6890	0.9544	6.278E+12	-0.780	0.2177	**0.2078**	3.200	0.0057	0.0012
>180μm	107.500	2.2439	0.9876	6.253E+12	-0.781	0.2175	**0.2148**	1.300	0.0023	0.0005
Mixed	72.500	0.9490	0.8287	6.329E+12	-0.778	0.2182	**0.1808**	19.200	0.0345	0.0062
% Moisture	**Fdman Ea**	**Friedman Z-Score**	**Pr(Ea)**	**A (s^{-1})**	**Z-Score of A (s^{-1})**	**Pr(A (s^{-1}))**	**Pr(Hzd)**	**"-ΔHr" (J/g)**	**Severity,β**	**Associated Risk**
3	112.500	2.4289	0.9924	6.247E+12	-0.781	0.2174	**0.2158**	47.400	0.0851	0.0184
8	50.000	0.1166	0.5464	6.439E+12	-0.775	0.2192	**0.1198**	54.300	0.0975	0.0117
15	82.500	1.3190	0.9064	6.300E+12	-0.779	0.2179	**0.1975**	68.800	0.1236	0.0244
25	107.500	2.2439	0.9876	6.253E+12	-0.781	0.2175	**0.2148**	64.500	0.1158	0.0249

ln(A) (s^{-1})	μ (s-1)	σ (s-1)	Z-Score
30.8378	33.463	5.1224	-0.5126

The bold face figures are the probability of thermal hazards for each experimental data set

Table F2: Standard Z-Score and Probability Calculation for Experimental Data for Class 2 (Medium Risk) (Cont'd)

Sample	Ozawa Ea	Ozawa Z-Score	Pr(Ea)	A (s^{-1})	Z-Score of A (s^{-1})	Pr(A (s^{-1}))	Pr(Hzd)	"-ΔHr" (J/g)	Severity,β	Associated Risk
A	82.500	1.3190	0.9064	6.300E+12	-0.7793	0.2179	**0.1975**	119.800	0.2151	0.0425
B	125.000	2.8913	0.9981	6.232E+12	-0.7814	0.2173	**0.2169**	236.300	0.4244	0.0920
C	90.000	1.5965	0.9448	6.283E+12	-0.7798	0.2178	**0.2057**	126.800	0.2277	0.0468
D	95.000	1.7815	0.9626	6.274E+12	-0.7801	0.2177	**0.2095**	35.800	0.0643	0.0135

Particle Size	ASTM Ea	ASTM E698 Z-Score	Pr(Ea)	A (s^{-1})	Z-Score of A (s^{-1})	Pr(A (s^{-1}))	Pr(Hzd)	"-ΔHr" (J/g)	Severity,β	Associated Risk
<75μm	92.939	1.7052	0.9559	6.277E+12	-0.7800	0.2177	**0.2081**	35.800	0.0643	0.0134
75-180μm	93.412	1.7227	0.9575	6.277E+12	-0.7800	0.2177	**0.2084**	3.200	0.0057	0.0012
>180μm	85.514	1.4305	0.9237	6.293E+12	-0.7795	0.2178	**0.2012**	1.300	0.0023	0.0005
Mixed	91.632	1.6568	0.9512	6.280E+12	-0.7799	0.2177	**0.2071**	19.200	0.0345	0.0071

% Moisture	Ozawa Ea	Ozawa Z-Score	Pr(Ea)	A (s^{-1})	Z-Score of A (s^{-1})	Pr(A (s^{-1}))	Pr(Hzd)	"-ΔHr" (J/g)	Severity,β	Associated Risk
3	82.500	1.3190	0.9064	6.300E+12	-0.7793	0.2179	**0.1975**	47.400	0.0851	0.0168
8	50.000	0.1166	0.5464	6.439E+12	-0.7750	0.2192	**0.1198**	54.300	0.0975	0.0117
15	73.500	0.9860	0.8379	6.325E+12	-0.7785	0.2181	**0.1828**	68.800	0.1236	0.0226
25	77.500	1.1340	0.8716	6.313E+12	-0.7789	0.2180	**0.1900**	64.500	0.1158	0.0220

Table F2: Standard Z-Score and Probability Calculation for Experimental Data for Class 2 (Medium Risk) (Cont'd)

Sample	ASTM Ea	ASTM E698 Z-Score	Pr(Ea)	A (s^{-1})	Z-Score of A (s^{-1})	Pr(A (s^{-1}))	Pr(Hzd)	"-ΔHr" (J/g)	Severity,β	Associated Risk
A	78.585	1.1742	0.880	6.310E+12	-0.7790	0.2180	**0.1918**	119.800	0.2151	0.0413
B	77.822	1.1459	0.874	6.313E+12	-0.7789	0.2180	**0.1906**	236.300	0.4244	0.0809
C	75.123	1.0461	0.852	6.320E+12	-0.7786	0.2181	**0.1859**	126.800	0.2277	0.0423
D	92.939	1.7052	0.956	6.277E+12	-0.7800	0.2177	**0.2081**	35.800	0.0643	0.0134

% Moisture	ASTM Ea	ASTM E698 Z-Score	Pr(Ea)	A (s^{-1})	Z-Score of A (s^{-1})	Pr(A (s^{-1}))	Pr(Hzd)	"-ΔHr" (J/g)	Severity,β	Associated Risk
3	98.963	1.9281	0.973	6.267E+12	-0.7803	0.2176	**0.2117**	47.400	0.0851	0.0180
8	50.475	0.1342	0.553	6.436E+12	-0.7751	0.2191	**0.1213**	54.300	0.0975	0.0118
15	70.793	0.8859	0.812	6.334E+12	-0.7782	0.2182	**0.1772**	68.800	0.1236	0.0219
25	76.353	1.0916	0.862	6.317E+12	-0.7788	0.2181	**0.1881**	64.500	0.1158	0.0218

Table F3: Standard Z-Score and Probability Calculation for Experimental Data for Class 3 (High Risk Class)

Sample	Fdman Ea	Fdman Z-Score	Pr(Ea)	A (s^{-1})	Z-Score of A (s^{-1})	Pr(A (s^{-1}))	Pr(Hzd)	"-ΔHr" (J/g)	Severity,β	Associated Risk
A	70.000	-1.4785	0.0696	6.337E+12	-0.7781	0.2182	**0.0152**	119.800	0.0412	0.00063
B	92.500	1.6890	0.1142	6.278E+12	-0.7799	0.2177	**0.0249**	236.300	0.0813	0.00202
C	95.000	1.7815	0.1202	6.274E+12	-0.7801	0.2177	**0.0262**	126.800	0.0436	0.00114
D	115.000	-0.9307	0.1760	6.244E+12	-0.7810	0.2174	**0.0383**	35.800	0.0123	0.00047
Particle Size	**Fdman Ea**	**Fdman Z-Score**	**Pr(Ea)**	**A (s^{-1})**	**Z-Score of A (s^{-1})**	**Pr(A (s^{-1}))**	**Pr(Hzd)**	**"-ΔHr" (J/g)**	**Severity,β**	**Associated Risk**
<75μm	112.500	-0.9612	0.1682	6.247E+12	-0.7809	0.2174	**0.0366**	35.800	0.0123	0.00045
75-180μm	92.500	-1.2046	0.1142	6.278E+12	-0.7799	0.2177	**0.0249**	3.200	0.0011	0.00003
>180μm	107.500	-1.0220	0.1534	6.253E+12	-0.7807	0.2175	**0.0334**	1.300	0.0004	0.00001
Mixed	72.500	-1.4481	0.0738	6.329E+12	-0.7784	0.2182	**0.0161**	19.200	0.0066	0.00011
% Moisture	**Fdman Ea**	**Friedman Z-Score**	**Pr(Ea)**	**A (s^{-1})**	**Z-Score of A (s^{-1})**	**Pr(A (s^{-1}))**	**Pr(Hzd)**	**"-ΔHr" (J/g)**	**Severity,β**	**Associated Risk**
3	112.500	-0.9612	0.1682	6.247E+12	-0.7809	0.2174	**0.0366**	47.400	0.0163	0.00060
8	50.000	-1.7219	0.0425	6.439E+12	-0.7750	0.2192	**0.0093**	54.300	0.0187	0.00017
15	82.500	-1.3263	0.0924	6.300E+12	-0.7793	0.2179	**0.0201**	68.800	0.0237	0.00048
25	107.500	-1.0220	0.1534	6.253E+12	-0.7807	0.2175	**0.0334**	64.500	0.0222	0.00074
ln(A) (s^{-1})	**μ (s^{-1})**	**σ (s^{-1})**								
30.8378	33.4633	5.12236								

The bold face figures are the probability of thermal hazards for each experimental data set

Table F3: Standard Z-Score and Probability Calculation for Experimental Data for Class 3 (High Risk Class) (Cont'd)

Sample	Ozawa Ea	Ozawa Z-Score	Pr(Ea)	A (s^{-1})	Z-Score of A (s^{-1})	Pr(A (s^{-1}))	Pr(Hzd)	"-ΔHr" (J/g)	Severity,β	Associated Risk
A	82.500	-1.3263	0.0924	6.300E+12	-0.7793	0.2179	**0.0201**	119.800	0.0412	0.00083
B	125.000	-0.8090	0.2093	6.232E+12	-0.7814	0.2173	**0.0455**	236.300	0.0813	0.00370
C	90.000	-1.2350	0.1084	6.283E+12	-0.7798	0.2178	**0.0236**	126.800	0.0436	0.00103
D	95.000	-1.1742	0.1202	6.274E+12	-0.7801	0.2177	**0.0262**	35.800	0.0123	0.00032
Particle Size	**ASTM Ea**	**ASTM E698 Z-Score**	**Pr(Ea)**	**A (s^{-1})**	**Z-Score of A (s^{-1})**	**Pr(A (s^{-1}))**	**Pr(Hzd)**	**"-ΔHr" (J/g)**	**Severity,β**	**Associated Risk**
<75μm	92.939	-1.1993	0.1152	6.277E+12	-0.7800	0.2177	**0.0251**	35.800	0.0123	0.00031
75-180μm	93.412	-1.1935	0.1163	6.277E+12	-0.7800	0.2177	**0.0253**	3.200	0.0011	0.00003
>180μm	85.514	-1.2896	0.0986	6.293E+12	-0.7795	0.2178	**0.0215**	1.300	0.0004	0.00001
Mixed	91.632	-1.2152	0.1122	6.280E+12	-0.7799	0.2177	**0.0244**	19.200	0.0066	0.00016
% Moisture	**Ozawa Ea**	**Ozawa Z-Score**	**Pr(Ea)**	**A (s^{-1})**	**Z-Score of A (s^{-1})**	**Pr(A (s^{-1}))**	**Pr(Hzd)**	**"-ΔHr" (J/g)**	**Severity,β**	**Associated Risk**
3	82.500	-1.3263	0.0924	6.300E+12	-0.7793	0.2179	**0.0201**	47.400	0.0163	0.00033
8	50.000	-1.7219	0.0425	6.439E+12	-0.7750	0.2192	**0.0093**	54.300	0.0187	0.00017
15	73.500	-1.4359	0.0755	6.325E+12	-0.7785	0.2181	**0.0165**	68.800	0.0237	0.00039
25	77.500	-1.3872	0.0827	6.313E+12	-0.7789	0.2180	**0.0180**	64.500	0.0222	0.00040

Table F3: Standard Z-Score and Probability Calculation for Experimental Data for Class 3 (High Risk Class) (Cont'd)

Sample	ASTM Ea	ASTM E698 Z-Score	Pr(Ea)	A (s^{-1})	Z-Score of A (s^{-1})	Pr(A (s^{-1}))	Pr(Hzd)	"-ΔHr" (J/g)	Severity,β	Associated Risk
A	78.585	-1.3740	0.0847	6.310E+12	-0.7790	0.2180	**0.0185**	119.800	0.0412	0.000762
B	77.822	-1.3833	0.0833	6.313E+12	-0.7789	0.2180	**0.0182**	236.300	0.0813	0.001477
C	75.123	-1.4161	0.0784	6.320E+12	-0.7786	0.2181	**0.0171**	126.800	0.0436	0.000746
D	92.939	-1.1993	0.1152	6.277E+12	-0.7800	0.2177	**0.0251**	35.800	0.0123	0.000309

% Moisture	ASTM Ea	ASTM E698 Z-Score	Pr(Ea)	A (s^{-1})	Z-Score of A (s^{-1})	Pr(A (s^{-1}))	Pr(Hzd)	"-ΔHr" (J/g)	Severity,β	Associated Risk
3	98.963	-1.1259	0.1301	6.267E+12	-0.7803	0.2176	**0.0283**	47.400	0.0163	0.000462
8	50.475	-1.7161	0.0431	6.436E+12	-0.7751	0.2191	**0.0094**	54.300	0.0187	0.000176
15	70.793	-1.4688	0.0709	6.334E+12	-0.7782	0.2182	**0.0155**	68.800	0.0237	0.000367
25	76.353	-1.4012	0.0806	6.317E+12	-0.7788	0.2181	**0.0176**	64.500	0.0222	0.000390

Table F4: Standard Z-Score and Probability Calculation for Experimental Data for Class 4 (Extremely High Risk)

Sample	Fdman Ea	Fdman Z-Score	Pr(Ea)	A (s^{-1})	Z-Score of A (s^{-1})	Pr(A (s^{-1}))	Pr(Hzd)	"-ΔHr" (J/g)	Severity,β	Associated Risk
A	70.000	-3.391	0.0003	6.337E+12	-0.778	0.2182	**0.00008**	119.800	0.0222	1.6909E-06
B	92.500	-3.238	0.0006	6.278E+12	-0.780	0.2177	**0.00013**	236.300	0.0439	5.7423E-06
C	95.000	-3.221	0.0006	6.274E+12	-0.780	0.2177	**0.00014**	126.800	0.0235	3.2689E-06
D	115.000	-3.086	0.0010	6.244E+12	-0.781	0.2174	**0.00022**	35.800	0.0066	1.4670E-06

Particle Size	Fdman Ea	Fdman Z-Score	Pr(Ea)	A (s^{-1})	Z-Score of A (s^{-1})	Pr(A (s^{-1}))	Pr(Hzd)	"-ΔHr" (J/g)	Severity,β	Associated Risk
<75μm	112.500	-3.103	0.0010	6.247E+12	-0.781	0.2174	**0.00021**	35.800	0.0066	1.3857E-06
75-180μm	92.500	-3.238	0.0006	6.278E+12	-0.780	0.2177	**0.00013**	3.200	0.0006	7.7763E-08
>180μm	107.500	-3.136	0.0009	6.253E+12	-0.781	0.2175	**0.00019**	1.300	0.0002	4.4861E-08
Mixed	72.500	-3.374	0.0004	6.329E+12	-0.778	0.2182	**0.00008**	19.200	0.0036	2.8815E-07

% Moisture	Fdman Ea	Friedman Z-Score	Pr(Ea)	A (s^{-1})	Z-Score of A (s^{-1})	Pr(A (s^{-1}))	Pr(Hzd)	"-ΔHr" (J/g)	Severity,β	Associated Risk
3	112.500	-3.103	0.0010	6.247E+12	-0.781	0.2174	**0.00021**	47.400	0.0088	1.8347E-06
8	50.000	-3.526	0.0002	6.439E+12	-0.775	0.2192	**0.00005**	54.300	0.0101	4.6518E-07
15	82.500	-3.306	0.0005	6.300E+12	-0.779	0.2179	**0.00010**	68.800	0.0128	1.3165E-06
25	107.500	-3.136	0.0009	6.253E+12	-0.781	0.2175	**0.00019**	64.500	0.0120	2.2258E-06

ln(A) (s^{-1})	μ (s^{-1})	σ (s^{-1})
30.8378	33.463	5.122

The bold face figures are the probability of thermal hazards for each experimental data set

Table F4: Standard Z-Score and Probability Calculation for Experimental Data for Class 4 (Extremely High Risk) Cont'd

Sample	Ozawa Ea	Ozawa Z-Score	Pr(Ea)	A (s^{-1})	Z-Score of A (s^{-1})	Pr(A (s^{-1}))	Pr(Hzd)	"-ΔHr" (J/g)	Severity,β	Associated Risk
A	82.500	-3.306	0.0005	6.300E+12	-0.7793	0.2179	**0.0001**	119.800	0.0222	2.2925E-06
B	125.000	-3.018	0.0013	6.232E+12	-0.7814	0.2173	**0.0003**	236.300	0.0439	1.2131E-05
C	90.000	-3.255	0.0006	6.283E+12	-0.7798	0.2178	**0.0001**	126.800	0.0235	2.9038E-06
D	95.000	-3.221	0.0006	6.274E+12	-0.7801	0.2177	**0.0001**	35.800	0.0066	9.2293E-07

Particle Size	ASTM Ea	ASTM E698 Z-Score	Pr(Ea)	A (s^{-1})	Z-Score of A (s^{-1})	Pr(A (s^{-1}))	Pr(Hzd)	"-ΔHr" (J/g)	Severity,β	Associated Risk
<75μm	92.939	-3.235	0.0006	6.277E+12	-0.7800	0.2177	**0.0001**	35.800	0.0066	8.7906E-07
75-180μm	93.412	-3.232	0.0006	6.277E+12	-0.7800	0.2177	**0.0001**	3.200	0.0006	7.9460E-08
>180μm	85.514	-3.286	0.0005	6.293E+12	-0.7795	0.2178	**0.0001**	1.300	0.0002	2.6746E-08
Mixed	91.632	-3.244	0.0006	6.280E+12	-0.7799	0.2177	**0.0001**	19.200	0.0036	4.5707E-07

% Moisture	Ozawa Ea	Ozawa Z-Score	Pr(Ea)	A (s^{-1})	Z-Score of A (s^{-1})	Pr(A (s^{-1}))	Pr(Hzd)	"-ΔHr" (J/g)	Severity,β	Associated Risk
3	82.500	-3.306	0.0005	6.300E+12	-0.7793	0.2179	**0.0001**	47.400	0.0088	9.0704E-07
8	50.000	-3.526	0.0002	6.439E+12	-0.7750	0.2192	**0.0000**	54.300	0.0101	4.6518E-07
15	73.500	-3.367	0.0004	6.325E+12	-0.7785	0.2181	**0.0001**	68.800	0.0128	1.0581E-06
25	77.500	-3.340	0.0004	6.313E+12	-0.7789	0.2180	**0.0001**	64.500	0.0120	1.0936E-06

Table F4: Standard Z-Score and Probability Calculation for Experimental Data for Class 4 (Extremely High Risk) Cont'd

Sample	ASTM Ea	ASTM Z-Score	Pr(Ea)	A (s^{-1})	Z-Score of A (s^{-1})	Pr(A (s^{-1}))	Pr(Hzd)	"-ΔHr" (J/g)	Severity,β	Associated Risk
A	78.585	-3.333	0.0004	6.310E+12	-0.779	0.2180	**0.00009**	119.800	0.0222	2.0854E-06
B	77.822	-3.338	0.0004	6.313E+12	-0.779	0.2180	**0.00009**	236.300	0.0439	4.0379E-06
C	75.123	-3.356	0.0004	6.320E+12	-0.779	0.2181	**0.00009**	126.800	0.0235	2.0290E-06
D	92.939	-3.235	0.0006	6.277E+12	-0.780	0.2177	**0.00013**	35.800	0.0066	8.7906E-07

% Moisture	ASTM Ea	ASTM Z-Score	Pr(Ea)	A (s^{-1})	Z-Score of A (s^{-1})	Pr(A (s^{-1}))	Pr(Hzd)	"-ΔHr" (J/g)	Severity,β	Associated Risk
3	98.963	-3.194	0.0007	6.267E+12	-0.780	0.2176	**0.00015**	47.400	0.0088	1.3413E-06
8	50.475	-3.523	0.0002	6.436E+12	-0.775	0.2191	**0.00005**	54.300	0.0101	4.7080E-07
15	70.793	-3.385	0.0004	6.334E+12	-0.778	0.2182	**0.00008**	68.800	0.0128	9.9019E-07
25	76.353	-3.348	0.0004	6.317E+12	-0.779	0.2181	**0.00009**	64.500	0.0120	1.0635E-06